INTEGRATED MODELLING STUDIES OF SOLUTE TRANSPORT IN RIVER BASIN SYSTEMS

Anthony Osei-Twumasi

A thesis submitted to Cardiff University as partial fulfilment of requirements for a PhD

Division of Civil Engineering, Cardiff School of Engineering
Cardiff University

August, 2010

ProQuest LLC
789 East Eisenhower Parkway
P.O. Box 1346
Ann Arbor, MI 48106-1346

DECLARATION

This work has not previously been accepted in substance for any degree and is not concurrently submitted in candidature for any degree.

Signed.....(A. Osei-Twumasi) Date.23/08/10

STATEMENT 1

This thesis is being submitted in partial fulfilment of the requirements for the degree of PhD.

Signed.....(A. Osei-Twumasi) Date.23/08/10

STATEMENT 2

This thesis is the result of my own independent work/investigation, except where otherwise stated. Other sources are acknowledged by explicit references.

Signed.....(A. Osei-Twumasi) Date.23/08/10

STATEMENT 3

I hereby give consent for my thesis, if accepted, to be available for photocopying and for inter-library loan, and for the title and summary to be made available to outside organisations.

Signed.....(A. Osei-Twumasi) Date.23/08/10

ACKNOWLEDGEMENTS

Whilst I acknowledge that I may not be able to express my gratitude to a whole lot of people that have helped bring the curtain down on this long journey, the following, however, deserve to be recognised and acknowledged.

My first gratitude goes to my supervisors, Professor Roger Alexander Falconer and Dr. Bettina Bockelmann-Evans for their support and constructive engagement throughout the entire research period.

I would like to acknowledge the initial support from the Dutch organisation, NUFFIC and Kumasi Polytechnic, Ghana for arranging for me to get this training.

I also hold a debt of gratitude to my colleagues at Cardiff University who in various ways helped in my laborious laboratory work and other technical matters. In this particular case, I take the opportunity to thank specially Messrs Reza Ahmadian and Florian Schaeffer for the wonderful contribution they made to my work.

I would also want to express my appreciation to the secretarial staff of the Engineering Research Office especially Mrs Chris Lee for their magnificent support and dedication. I do appreciate that.

In this occasion, I would also acknowledge the support and encouragement I had received from my mother and all my siblings' throughout the research period.

Finally, I would like to say thank you to my immediate family for their continuous love and support especially my wife Gladys for keeping this large family together at home whilst I was studying in the United Kingdom. I am really grateful.

DEDICATION

To my wife, Gladys and all the children

Portia, Nana, Adelaide, Adwoa and Akua

ABSTRACT

Surface water and groundwater systems are linked dynamically in reality as the one generally impacts directly on the other. Traditionally, however, these two water bodies have more often than not been treated as different entities by water managers and other professionals. The issue of the compartmentality of these two resources is the main focus of the study described herein. In this study, an existing 1D-2D hydro-environmental surface water model that includes a groundwater model (DIVAST-SG) has been extended to 2-D and refined through testing against three laboratory studies.

A surface water–groundwater system model using foam to replicate groundwater material was created in the laboratory and the results of the hydrodynamic processes (i.e. water elevations and flowpaths) were compared with the numerical model predictions. On the whole the comparisons showed good agreement. However, dye studies for replicating pollutant transport did not show such good agreement and this discrepancy was thought to be due to a number of reasons.

In the second series of studies, the groundwater material was then replaced with the more traditional sand embankment and again results for both hydrodynamic and solute transport processes (by way of dye studies) from the laboratory set up were compared with the numerical predictions which were in almost perfect agreement.

In the same tidal basin, a Severn Estuary model was then designed and set up. Although there were differences from the prototype owing to space and scaling difficulties, the results showed good agreement for both tidal amplitudes and tidal currents with the predictions from the numerical model and particularly the tidal amplitudes were found to compare favourably with field studies. Tracer results from the physical model also showed consistency with simulations from previous researchers in the main estuary.

Overall, the purpose of this study, which was to investigate the manner in which flow and solute (conservative tracer) fluxes interacted between surface and sub-surface flows, for simulated riverine and tidal conditions, has been achieved. These experiments and the corresponding datasets are thought to be unique.

TABLE OF CONTENTS

Content **Page**

LIST OF FIGURES

LIST OF TABLES

CHAPTER 1 INTRODUCTION

1.1 General

Environmental water degradation has become a challenge to governments, engineers, scientists and managers, with many challenges to government agencies and water professionals. Wherever relatively large populations have existed they have tended to destabilise the environmental regime or the local aquatic conditions. Wastewater has been generated with the corresponding consequence in terms of pollution of the aquatic environment. Environmental degradation of river basins has permeated the entire life of communities to varying degrees and has created the environment for slums in many cities and towns, especially in developing countries.

In general, water bodies in the form of rivers and estuaries have borne the brunt of receiving often enormous loads of contaminants, generally in the liquid or solid form. The impact on rivers and estuaries affects the adjacent groundwater resources and vice versa. As the problems of rivers and other surface waters are compounded, so too are the groundwaters. Seawater intrusion into adjacent groundwaters has been well documented. Oceans adjacent to large urban areas are often the final repositories of pollutants from a myriad of point and non-point sources of human waste (Culliton, 1998; Ahn et al., 2005). Human activity has therefore often been the bane of these natural resources. The health of rivers, estuaries and indeed all water bodies has generally declined steadily as a result of these inputs.

What has often ensued out of these epidemics are water–borne diseases such as cholera, enteric fevers etc. in both developing countries and some developed countries. Outbreaks of waterborne disease via public water supplies continue to be reported even in developed countries (Payment et al., 1997; Gibson et al., 1998; Howe et al., 2002; all cited in Brookes et al., 2004). In low income countries the global burden of disease and mortality (estimated to be 2.1 million deaths in the year 2000) result from unsafe water supplies and inadequate hygiene (Taylor et al., 2004). As can be seen in Figure 1.1, pollution in water bodies is widespread where in this particular stream in a rural setting in a developing country, washing of clothes, swimming, and wading all are taking place simultaneously, whilst people downstream use the river as a source of drinking water.

Figure 1.1: A flowing stream in a rural setting in a developing country, showing some of the sources of water pollution.

Recent research has demonstrated a positive relationship between community hygiene and, in particular, access to sanitation facilities and the bacteriological quality of

groundwater in the tropics (Taylor et al., 2004). The result has been an increase in water borne disease, especially amongst people in developing countries. It is therefore not surprising that rivers have been most studied amongst various environmental groups (Thomann and Mueller, 1987). Apart from the degeneration of the hydro-environmental system as a result of anthropogenic changes, the quantity of water has also been influenced as a result.

The overall cost to national economies of water pollution is rarely known (Ongley and Booty, 1999). In his studies, however, Smil (1996) found that in 1991 the cost of water pollution to the Chinese national economy was approximately 0.5% of GDP or, in dollar terms, equal to the value of Chinese exports for that entire year.

It is therefore not just a coincidence that over the last two to three decades, professionals in the field have been looking for ways of managing water resources, both in terms of supply and pollution. One important aspect is the use of state-of-the-art models to address the issues discussed earlier and thereby ameliorate the enormity of the challenge. These models have come in the form of computational or numerical models, particularly with the use of modern day cheap computers. The benefits of numerical modelling are clear: numerical methods may be used to improve our understanding of and simulate key processes in providing two- or three-dimensional prediction fields, which can provide considerable insight into the distribution of processes within water basins or catchments (Lane, 1998). Lin and Falconer (2001) highlight the use of water quality models by engineers in the design of hydraulic structures that are related to water quality problems.

In terms of legislation, the European Union Water Framework Directive (2000/60/EC) for example sets standards for member countries to comply with for both inland and coastal waters. To address the concerns in case of possible violation or impairment, mathematical models have been used by water managers to develop remediation strategies (Auer and Niehas, 1993).

The scope for using such models is considerable. However, caution must be exercised in their use. One of the key problems with numerical models is whether the numerical formulations of such models accurately represent the field or physical situation and whether the users of the models understand the model being used. Ongley and Booty (1999) therefore sounded a note of caution for developing countries: "Mathematical modelling, as a means of determining remediation options, is the usual method of choice in data-rich developed countries and requires substantial investment in reliable data, scientific capacity and sophisticated management culture that generally are not found in developing countries". If geomorphologists and hydrologists and for that matter all professionals are to use these models effectively, often without specific training in computational fluid dynamics, then it is critical that they are aware of the physical basis of the models they use, and of the inherent limitations of the assumptions made during model development (Lane, 1998). Henriksen and Hojberg (2008) emphasised that during the last decade a lack of credibility of modelling results among end-users have been identified. They attribute this phenomenon to ambiguous terminology, lack of reliable data, insufficient process knowledge, and overselling model capabilities as some of the reasons for this situation. The credibility of the model must therefore be evaluated through a solid confirmation of the conceptual

model, through proper verification of the model code and through a rigorous calibration and validation of site specific models (Refsgaard and Henriksen, 2003). With the dwindling resources of nations and the risks associated with embarking on continuous and regular field data collection, the appearance of such models in water resources management has been very significant. They have been helpful in tackling the many and varied water environmental challenges.

1.2 Objectives of this study

The focus of this study has been the investigation of flow and solute transport interaction between rivers, estuaries and groundwater systems. The main objectives of this study are therefore:

- Refine an existing 1-D and 2-D hydro-environmental modelling predicting elevations, currents and dye tracer concentration distributions in rivers, estuaries and to include groundwater.
- Carry out detail laboratory studies using both foam and sand as groundwater materials separately.
- Calibrate and verify the models against data from foam and sand embankment laboratory studies.
- Apply the model to idealised and distorted practical study specifically to Severn Estuary physical model.

1.3 Structure of thesis

Chapter 2 reviews the work done in this field by previous researchers. Emphasis has been placed in the coupling of surface water-groundwater models and how decay, diffusion and dispersion affect solute transport in this system. Mention is also made of the impact of diffuse source inputs from catchments on the surface water-groundwater system.

In chapter 3, the governing equations for hydrodynamic and solute transport processes in free surface and subsurface flows are outlined and how the equations in the two systems are coupled.

Chapter 4 treats the discretisation procedures used for the numerical models. Also the boundary conditions are discussed.

In chapter 5, the laboratory studies are fully detailed for two idealised studies, namely foam and sand embankment studies together with details being given of the studies undertaken for a distorted Severn Estuary model.

In chapter 6, the numerical model predictions have been verified by comparing results with the laboratory model studies and with the computer results being used to refine the model coefficients etc.

Chapter 7 draws some useful conclusions from the study and makes some recommendations for future work.

CHAPTER 2 LITERATURE REVIEW

2.1 River basin systems: state-of-the-art in river/estuary and groundwater models

This review is going to highlight a few of the river, estuary and groundwater models that have been used in this field whiles more emphasis is going to be laid on coupled models which is the basis of this study.

2.1.1 Surface Water Models

One dimensional (1-D) numerical models have been widely used in modelling the flow and solute transport processes in rivers and open channels (Lin and Falconer, 2005). Most of these models basically solve the St Venant equations of motion. These models are computationally efficient in dealing with large and complex river or channel systems.

Numerical hydro-environmental models have proved to be a valuable tool for predicting the flow and water quality distribution in estuarine and coastal basins and they have been increasingly used in environmental impact assessment studies (Kashefipour et al., 2006). The state of the art hydrodynamic and ecological models provide extra decision support by predictive modelling of stratification, riverine inflow and pathogen transport (Brookes et al., 2004).

DIVAST (Falconer, 1977) is two-dimensional depth averaged surface water model. It simulates hydrodynamics and solute transport in shallow water bodies especially estuarine and coastal waters.

BRANCH (Schaffranek et al, 1981) is used to simulate steady or unsteady flow in a single open-channel reach (branch) or throughout a system of branches (network) connected in a dendritic or looped pattern. BRANCH is applicable to wide range of hydrologic situations wherein flow and transport are governed by time-dependent forcing functions. BRANCH is particularly suitable for simulation of flow in complex geometric configurations involving regular or irregular cross sections of channels having multiple interconnections, but can be easily used to simulate flow in a single, uniform open-channel reach. Time-varying water levels, flow discharges, velocities, and volumes can be computed at any location within the open-channel network.

DR3M (Alley and Smith, 1982) is a watershed model for routing storm runoff through branched system of pipes and (or) natural channels using rainfall as input. DR3M provides detailed simulation of storm-runoff periods selected by the user. There is daily soil-moisture accounting between storms. A drainage basin is represented as a set of overland-flow, channel, and reservoir segments, which jointly describe the drainage features of the basin. This model is usually used to simulate small urban basins. Interflow and base flows are not simulated. Snow accumulation and snowmelt are not simulated.

DAFLOW (Jobson, 1989) is a diffusive form of the Saint Venant equations is used for streamflow routing. The flow model is designed to provide reasonable predictions of discharge and transport velocity using a minimum of field data and calibration.

FESWMS-2DH (Froehlich, 1989) is a modular set of computer programs that simulates two- dimensional, depth-integrated, surface-water flows. FESWMS-2DH consists of an input data preparation program (DINMOD (1)), flow model (FLOMOD (1)), simulation output analysis program (ANOMOD (1)), and graphics conversion program (HPPLOT (1)). The programs have been developed to analyze flow at bridge crossings where complicated hydraulic conditions exist, although they may be applied to many types of steady or unsteady flow problems. Shallow rivers, flood plains, estuaries, and coastal seas are examples of surface-water bodies in which flows may be essentially two-dimensional in the horizontal plane.

WSPRO (Shearman, 1990) computes water-surface profiles for subcritical, critical, or supercritical flow as long as the flow can be reasonably classified as one-dimensional, gradually-varied, steady flow.

MIKE 11 (Havnø et al., 1995) is a hydraulic modelling system that simulates flow and water level, water quality and sediment transport in rivers, flood plains, irrigation canals, reservoirs and other inland water bodies.

MIKE 21(DHI, 1995) simulates flows, waves, sediments and ecology in rivers, lakes, estuaries, bays, coastal areas and seas in two dimensions.

HEC-RAS (USACE, 1995). The basic computational procedure of HEC-RAS for steady flow is based on the solution of the one-dimensional energy equation. Energy losses are evaluated by friction and contraction / expansion. The momentum equation may be used in situations where the water surface profile is rapidly varied. These situations include hydraulic jumps, hydraulics of bridges, and evaluating profiles at river confluences.

For unsteady flow, HEC-RAS solves the full, dynamic, Saint-Venant equation using an implicit, finite difference method. HEC-RAS is equipped to model a network of channels, a dendritic system or a single river reach. Certain simplifications must be made in order to model some complex flow situations using the HEC-RAS one-dimensional approach. It is capable of modelling subcritical, supercritical, and mixed flow regime flow along with the effects of bridges, culverts, weirs, and structures

SWIM (Verburg et al., 1996) is based on a numerical solution of the Richards' equation and the advection-dispersion equation. It can be used to simulate runoff, infiltration, redistribution, solute transport and redistribution of solutes, plant uptake and transpiration, soil evaporation, deep drainage and leaching. Soil water and solute transport properties, initial conditions, and time dependent boundary conditions (e.g., precipitation, evaporative demand, solute input) need to be supplied by the user in order to run the model.

Surface water models mainly tend to consist of river and estuary models.

In addition to the above models, there are a number of surface water catchment models which are often linked to the river and estuary models cited above and the most common of these are briefly outlined below as examples:

(1) MIKE SHE (Refsgaard and Storm, 1995), a major development in this direction, is a comprehensive deterministic, distributed and physically based modelling system capable of simulating all major hydrological processes in the land phase of the hydrological cycle. Detail of its other capabilities can be found in section 2.1.3.

(2) HSPF (Bicknell et al., 1997) simulates for extended periods of time the hydrologic (e.g. surface runoff) and associated water quality (e.g. faecal coliforms), processes on pervious and impervious land surfaces and in streams and well-mixed impoundments.

(3) E2 (Argent et al. 2006) is a node-link model designed for whole-of-catchment modelling of flow and constituent load. E2 represents the catchment using sub-catchments or 'functional units', nodes and links. Functional units may comprise a rainfall-runoff model, a constituent generation model and a filter mode

2.1.2 Subsurface Water (Groundwater) Models

Cooper and Rorabaugh (1963) derived an analytical solution for changes in groundwater heads, groundwater flow and bank storage that occurred as the result of a flood-wave stage oscillation. That assumption for this analysis was that the stream elevation changes only as a function of time and that the horizontal groundwater flow occurred only normal to the stream.

Realising some limitations to the approach used by Cooper and Rorabaugh (1963), Pinder and Sauer (1971) developed a more complex modelling approach to simulating flood wave modification due to the effects of bank storage. The approach was to use a one-dimensional unsteady channel flow to describe the stream elevation, and a two-dimensional groundwater model to describe the aquifer flow. Darcy's law was used to couple the two models in an iterative manner. The two zones were treated separately in this approach.

PLASM (Prickett and Lonnquist, 1971) is a program package that simulates 2-D non-steady flow of groundwater in heterogeneous anisotropic aquifers under water table, non-leaky and leaky confined situations.

MODFLOW (McDonald and Harbaugh, 1988) is a modular finite difference program that simulates three-dimensional saturated flow. The code's structure is such that there is a main program and other packages that handle different features of the hydrological system. MODFLOW is a three-dimensional finite-difference ground-water model that was first published in 1984. It has a modular structure that allows it to be easily modified to adapt the code for a particular application. Many new capabilities have been added to the original model.

FLOWNET (van Elburg et al., 1993) is used for the modelling of two-dimensional steady state flow in a rectangular anisotropic aquifer.

GFLOW (Haitjema 1995) is a program based on the analytic element method. It models steady-state flow in a single heterogeneous aquifer using the Dupuit-

Forchheimer assumption. While GFLOW supports some local transient and three-dimensional flow modelling, it is particularly suitable for modelling regional horizontal flow. To facilitate detailed local flow modelling, GFLOW supports a MODFLOW-extract option to automatically generate MODFLOW files in a user-defined area with aquifer properties and boundary conditions provided by the GFLOW analytic element model. GFLOW also supports conjunctive surface water and groundwater modelling using stream networks with calculated base flow.

HYDRUS-2D (Šimůnek et al. 1999) is a finite element program for simulating flow and transport in variably saturated media. The unstructured finite element mesh generator is a versatile tool for better representation of complex geometries. Flow may be simulated in three different types, vertical flow, axi-symmetric flow, and horizontal flow. The latter option simulates steady state, saturated flow in a single layered aquifer of any areal shape. The output pressure heads can be imported into a contouring package to produce a steady state three-dimensional groundwater table. The 'vertical flow' option in HYDRUS-2D models variably saturated flow with a range of boundary conditions such as a time-varying constant –head boundary, which simulates a stream. The advantage here is the full flexibility of the code to handle the extent of stream penetration including the option of modelling an unsaturated zone below the stream. It is also possible to explicitly model a stream of any shape and its full interaction with the aquifer by assuming it as a material with porosity equal to unity and having a high hydraulic conductivity. However, due to the complexity of the code, there are spatial limitations in terms of the size of the domain that can be modelled; HYDRUS-2D is usually used on a plot-scale.

MODFLOW 2000 (Harbaugh et al., 2000) is an update of the original MODFLOW.

VS2DI (Hsieh, 2000) is a graphical software package for simulating flow and transport in variably saturated porous media. This software package consists of three components:

- VS2DTI, for simulating fluid flow and solute transport,
- VS2DHI, for simulating fluid flow and energy (heat) transport,
- a standalone postprocessor, for viewing results saved from previous simulation runs.

Both VS2DTI and VS2DHI combine a graphical user interface with numerical model to create an integrated, window-based modelling environment. Users can easily specify or change the model domain, hydraulic and transport properties, initial and boundary conditions, grid spacing, and other model parameters

MODFLOW 2005 (Harbaugh, 2005) documents a general update to MODFLOW, which is called MODFLOW-2005 in order to distinguish it from earlier versions.

2.1.3 Coupled surface-subsurface models

Traditionally, the surface water and subsurface water systems have been treated separately as two different compartments in any evaluation scheme. The interaction between them is usually taken into account as a boundary condition in groundwater modelling, while it is ignored in surface water modelling (Spanoudaki et al., 2005). However, there are many water resources problems that require a more realistic linkage between surface water and groundwater. Indeed, despite the fact that aquifer

and surface water are hydraulically interconnected, they are often modelled as two separate systems and analysed independently (Liang et al, 2007).

Nearly all surface-water features (streams, lakes, reservoirs, wetlands, and estuaries) interact with groundwater. Figure 2.1 shows the hydrological cycle and it can be seen that part of precipitation enters the sea directly and part percolates into the groundwater system where there is an exchange between subsurface flow and the ocean. At the same time, there is seepage from aquifer to the river and vice versa which is combination of a number of exchanges between the various components of the cycle. The interrelation between various aspects of the hydrological cycle is very complex and poorly understood. For a full understanding, the cycle must be considered in its entirety, taking into account the relative magnitudes of the individual processes. Interactions between groundwater and surface water play a critical role in the functioning of riparian ecosystems. In the context of sustainable river basin management it is crucial to understand and quantify exchange processes between groundwater and surface water.

The exchange can be described in principle by two cases, the effluent and the influent condition (Schmalz et al., 2008). When the groundwater level is higher than the water level in the river, flows are directed to the river resulting in effluent flow (exfiltration) (Winter et al., 1998; Schmalz et al., 2008). In areas where hydraulic gradients are small, this results in small flow velocities, although groundwater exchange can still be significant, depending on the size of the interaction zone (Schmalz et al., 2008).

When the water level in the river is higher than the groundwater level, river water flows into the groundwater causing influent conditions (Winter et al., 1998; Schmalz et al., 2008). Influent conditions exist likewise, when the groundwater body is separated from the river bed by an unsaturated zone ((Winter et al., 1998; Schmalz et al., 2008). Where river and groundwater levels are the same, groundwater flows parallel to the river (Sophocleous, 2002; Schmalz et al., 2008).

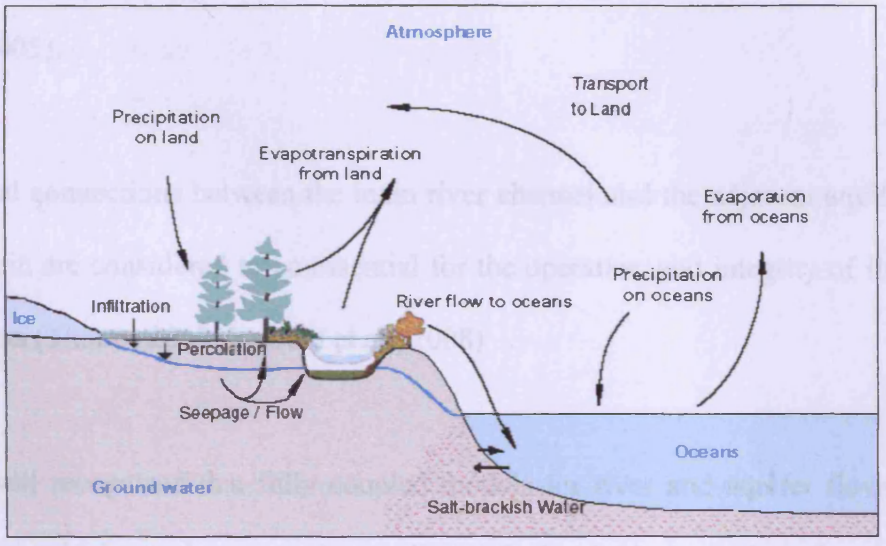

Figure 2.1: The Hydrological Cycle

Conditions of low river flows are usually characterised by effluent conditions, i.e. groundwater discharge, whereas influent conditions, i.e. infiltration of river water into groundwater, occur during flooding periods (Schmalz et al., 2008).Some rivers exhibit effluent flows in some sections and influent flows in other sections (Winter et al., 1998; Schmalz et al., 2008). Sections of alternating effluent and influent conditions (i.e. changing flow directions) can also occur, in particular in smaller rivers which are more strongly controlled by local groundwater systems and seasonal influences (Winter et al., 1998; Sophocleous, 2002; Kalbus et al., 2006; Schmalz et al., 2008).

Contamination of groundwater can impact nearby surface water bodies where groundwater discharges to surface water. An estimated 75% of hazardous waste sites related to the US national Superfund program are located within 0.5 miles of surface water bodies and 50% of all Superfund sites have impacted surface water (US EPA, 2000). Quantity and quality of surface water has also impacted groundwater in areas where surface water recharges groundwater, such as playas in the Southern High Plains (Scanlon and Goldsmith, 1997; Fryar et al., 2000; Bureau of Economic Geology, 2005).

Hydrological connections between the main river channel and the adjacent aquifer in the floodplain are considered to be essential for the operation and integrity of fluvial hydrosystems (Thoms, 2003; Peyrard et al., 2008)

It is now well recognised that fully coupled models for river and aquifer flows are necessary to obtain a better understanding of the hydrological pathways in hydrosystems (Panday and Huyakorn, 2004; Gunduz and Aral, 2005; Peyrard et al., 2008). Typical groundwater evaluations may treat surface water interactions simplistically or be neglected altogether because the area of the interface between the two is typically small relative to the spatial scale of the groundwater system being evaluated (Peyrard et al., 2008). Conversely, surface water evaluations often disregard exchanges with the local groundwater system because the amount of water that flows across the interface is usually small relative to that which originates from other routes.

In watersheds with high permeability soils, interaction between surface and subsurface flow components becomes important especially during overland flow initiation (Morita and Yen, 2002).

Coupled modelling of surface and sub-surface flows can be classified according to the number of spatial dimensions considered for the two flow components (Morita and Yen, 2002). This spatial dimensional grouping is to consider how the surface and subsurface components are coupled mathematically.

The idea of integrated modelling approach to surface water groundwater interactions may not have come before the early 1970's. Although authors have had such thoughts for more than three decades it is only in the last decade or so that much effort is being used to address the issues.

Smith and Woolhiser (1971) developed a model describing infiltration and overland flow based on the soil moisture properties. Based on this approach, Freeze (1972) described numerical solutions to couple 3-D, transient and variably saturated subsurface flow, and a 1-D, gradually varied unsteady channel flow based on Saint Venant equations in an iterative manner. The entry velocity of the surface flow was assumed to be negligible compared to the stream velocity. This model allowed rainfall events to be predicted, together with their effects on a stream via a baseflow input.

MODBRANCH (Swain and Wexler, 1996) is a coupled model using a one-dimensional stream flow Branch model and the three-dimensional saturated groundwater flow model, MODFLOW. In this iterative coupling approach, multiple steps of the surface water code are carried out for each time step in the groundwater

code. This is based on the fact that time steps used for the simulation of surface water are usually of the order of seconds, minutes or hours, but groundwater takes hours, days, months or even years.

MIKE SHE / MIKE 11 (Sørensen et al.1996; Refsgaard and Sørensen, 1997).
River links are only established for those reaches within the hydraulic model that are specified as coupled reaches. Whereas MIKE 11 uses the complete river model, MIKE SHE will only exchange water with these coupled reaches. During a simulation, water levels within the coupled reaches are transferred from MIKE 11 H-points (points along the river model for which water levels are calculated) to adjacent MIKE SHE river links. In turn MIKE SHE calculates the overland flow to each river link from neighbouring grid squares and the river-aquifer exchange. These terms are fed back to the corresponding MIKE 11 H-points as lateral inflows or outflows for the next computational time step. The MIKE SHE/MIKE 11 coupling also enables the simulation of inundation from the MIKE 11 river model onto MIKE SHE grid squares.

MOGROW (Querner, 1997) was developed by combining two models SIMGRO (SIMulation of GROundwater flow and surface water levels) and SIMWAT (SIMulation of WATer networks). SIMGRO models the saturated zone of the subsurface as a quasi three dimensional flow and the unsaturated zone as a one-dimensional flow (according to land use and soil characteristics). SIMWAT models major water courses explicitly as a network of sections. The model is an approximation to the 1-D diffusive waveform of the Saint Venant equations. MOGROW is an iterative integration of these two models. The bed levels from the

surface water system are transferred to the groundwater module, followed by the fluxes and water levels as the time steps proceed.

FHM (Ross et al., 1997) model links two public-domain models: HSPF and MODFLOW. FHM was developed to simulate the interaction of surface water and ground water in shallow water table systems. GIS was incorporated into the integrated model for data preparation, storage and presentation. Either the surface water model (HSPF) or the groundwater model (MODFLOW) can run independently or an integrated combination of the two models can be run.

Typically, the sequence would consist of separate calibrations of the surface water and groundwater models followed by integrated modelling. The model code first uses HSPF to calculate runoff, infiltration, recharge, surface evapotranspiration and storage on an hourly basis. The code then uses MODFLOW to calculate groundwater flow for a daily time step. This sequence is repeated until the simulation time is completed.

Wetland MODFLOW Module (Restrepo et al., 1998) couples a 2-D overland flow to the 3-D saturated groundwater model (MODFLOW). The model attempts to simulate wetland hydrodynamics and the interaction with the underlying aquifer. It allows for wetting and drying of the wetland, evapotranspiration and vertical and horizontal flux components of the wetland aquifer interaction. The coupling method is by simultaneous solution of both the groundwater and surface equations.

Bradford and Katopes (1998) also integrate a 2-D surface flow which is an approximation to the vertical turbulent Navier–Stokes equations and a 2-D vertical and variably saturated groundwater flow. They use an iterative method approach.

DAFLOW-MODFLOW (Jobson and Harbaugh, 1999) couple the one-dimensional diffusive wave channel flow model (DAFLOW) with the 3-D MODFLOW model. The coupled model allows multiple time steps of DAFLOW within a MODFLOW time step acknowledging that appropriate time steps for groundwater and surface water calculations may differ greatly. Like the MODBRANCH, the equations are solved iteratively.

In his work, Vanderkwaak (1999) uses 1-D stream flow and 2-D overland flow diffusion wave approximation to the Saint Venant equation for the surface water and then couple with a 3-D variably saturated subsurface flow to solve the equations simultaneously.

SWATMOD (Sophocleous *et al.*, 1999) links the catchment model SWAT with the groundwater model, MODFLOW. SWATMOD can be run in one of two modes. The first mode is where MODFLOW is treated as a subroutine of SWAT and is called at the end of each aquifer time step. The second mode involves SWAT and MODFLOW being performed successively and linked through a separate hydrologic balance data file.

ECOFLOW (Sokrut et al., 2001) links the distributed physically based hydrological model, ECOMAG (ECOlogical Model for Applied Geophysics) to MODFLOW in a

non-iterative manner. Since ECOMAG is a distributed catchment model rather than a specific open channel flow model, it makes it relatively easier to link to a catchment wide groundwater, simply by introducing a special sink term into the governing equations. The sink term is generated by the surface water model and implemented into the groundwater and solute equations. The ECOMAG model also had a bottom layer called the 'groundwater zone' which has been replaced by MODFLOW in the coupled model.

Morita and Yen (2002) also use a 2-D overland flow to couple a 3-D saturated groundwater flow in an iterative manner.

Monninkhoff (2002) coupled the WASY groundwater software FEFLOW with the DHI surface water software MIKE11. The coupling is not iterative. After each time step, discharges calculated by FEFLOW to the coupled boundary points are exported to MIKE11 as an additional boundary condition. MIKE 11 calculates its time step as often as needed to reach the actual time level of FEFLOW. The actual water levels in MIKE11 are then exported to the FEFLOW coupling boundary nodes and the time stepping continues.

FTSTREAM (Hussein and Schwartz, 2003) extended an existing 3-D groundwater flow and contaminant model, FTWORK to incorporate the fate of chemicals and transport in streams. The stream transport is based on a one-dimensional advection-dispersion equation and incorporates volatilisation, settling and decay as well. The equations for the stream and groundwater are solved simultaneously in order to

provide the head in the aquifer and the depth of flow in the stream so as to estimate the flow velocities.

Lin and Medina Jr, (2003) incorporated the transient storage concept in a conjunctive stream aquifer model. Three USGS models were coupled together: (1) MODFLOW handles groundwater flow in the aquifer; (2) DAFLOW computes unsteady stream flow by means of the diffusive wave routing technique, as well as stream-aquifer exchange simulated as streambed leakage, and (3) MOC3D compute solute transport in the groundwater zone. The conjunctive stream aquifer model with transient storage can handle well the bank storage effect under a flooding event. The stream aquifer interaction is such a strong sink/source for solute transport in streams that it must not be ignored in simulation.

Streamflow Routine Module (Prudic et al., 2004) is a groundwater-surface water model which couples a 1-D streamflow model with MODFLOW. It is capable of modelling solute transport through interconnected lakes, streams and aquifers.

MODHMS (Panday and Huyakorn, 2004) integrate a 1-D for streamflow and a 2-D overland flow based on diffusion wave approximation to the Saint Venant equation (for the surface flow) and a 3-D saturated and unsaturated subsurface flow model. The model is a fully integrated groundwater–surface water and water quality modelling. MODHMS includes dynamic interactions between overland flow, channel flow, and groundwater to simulate water supply management scenarios, flood control and river flow analyses, and wetland restoration analyses.

Gunduz and Aral (2005) also solve a 1-D channel flow and a 2-D vertically saturated flow simultaneously using a global matrix technique in their coupling approach. It is considered in this method that the seepage from the river is linked directly to the underlying aquifer whereupon no unsaturated zone is considered.

GSFLOW (Niswonger et al., 2006) is a new USGS model for groundwater–surface water interactions. GSFLOW couples PRMS (Precipitation Runoff modelling System) to MODFLOW with a new family of modules for simulating processes in the unsaturated zone.

Kollet and Maxwell (2006) presented a coupled model that incorporates a two-dimensional overland flow simulator into the parallel three-dimensional variably saturated subsurface flow code ParFlow; the overland flow simulator takes the form of an upper boundary condition and is, thus, fully integrated without relying on the conductance concept. Applying the model shows the propagation of uncertainty due to subsurface heterogeneity to the overland flow predictions.

HydroGeoSphere (Therrien et al. 2007) couple a 2-D diffusive wave approximation to the Saint Venant equations and the 3-D unsaturated groundwater flow approximation to the Richards equation. This is a distributed model that also includes transport capabilities.

DIVAST-SG (Sparks, 2007) also couples an existing two dimensional Depth Integrated Velocity And Transport (DIVAST) surface water model with a two-dimensional depth integrated groundwater model. The model, DIVAST-Surface

water-Groundwater (DIVAST-SG) is able to simulate hydrodynamics and solute transport in the two systems continually. It was originally designed for a vertical boundary at the seepage face of the two systems.

Liang et al (2007) also integrate a 2-D shallow water equation with a 2-D depth integrated groundwater flow equation to make flood predictions. The equations are solved simultaneously.

GSFLOW (Markstrom et al., 2008). This model is an improved version on GSFLOW (2006) developed by the same authors.

2SWEM (Peyrard et al., 2008) also took the model by Liang et al (2007) further by the inclusion of solute transport equations in the existing model.

Rassam and Werner (2008) have reviewed various coupled models and put them at various levels. The level of complexity is generally determined by the dimensions of the model, as well as the inclusion of all possible physical phenomena in the mathematical interpretation of the coupled system (Gunduz and Aral, 2005).They concede that, the most advanced model would involve coupling a three-dimensional surface flow component based on the complete Navier-Stokes equations and a three-dimensional variably saturated subsurface flow component. Due to the large computational powers and high data requirements of such models, modellers choose to reduce model dimensions for large-scale applications (Gunduz and Aral 2005). For example, Kollet and Maxwell (2006) used a two-dimensional surface flow component model with a three-dimensional variably saturated subsurface flow component.

Various researchers have used one-dimensional surface flow component model with either a two-dimensional or three dimensional subsurface flow component that models variably saturated flow or saturated flow only e.g., (Kollet and Maxwell 2006), (Jobson and Harbaugh, 1999), (Swain and Wexler 1996).

Although as indicated there are a quite number of these coupled models, most of them are 1-D surface water flow model linked to either a 2-D or a 3-D groundwater model but there are a few integrated models that link a 2-D surface water model with a 2-D groundwater model. This area is the focus of the study.

2.2 Decay of faecal coliform, diffusion and dispersion in surface water and groundwater flows.

2.2.1 Decay of faecal coliform, Diffusion and Dispersion in Surface water flows

Faecal coliform is increasingly becoming important in water quality management since it has been and is still being used as parameter indicator for the quality of receiving waters (Kay et al., 2007b). Some rivers and coastal waters are not meeting the standards set by regulatory agencies which these water bodies need to purge themselves. To be able to salvage these polluted receiving waters so that they could be used for both domestic and recreational purposes, the faecal coliform discharge, transport and other processes must be well understood. Like any non-conservative solute, faecal coliforms are diffused, dispersed and modified by chemical and biological transformation as they are transported through the water pathway. The main chemical change is the decaying of the concentrations as they move from

upstream to downstream. The persistence of pathogens in the aquatic environment is a function of both survival and transport. Different pathogens persist for different amounts of time and the major mode of inactivation or mortality may vary significantly. Factors that control inactivation include temperature, salinity, pressure, solar radiation (visible and UV) and predation by organisms higher in the food chain. However, light and temperature are the major inactivation mechanisms, although predation may be significant for some organisms. (Brookes et al, 2004). The implication is that low water temperatures may prolong pathogen survival.

There is a greater opportunity for die-off of faecal indicator organisms (FIOs) during transport in river reaches through exposure to UV light and microbial predation (Anderson et al., 2005; Kashefipour et al., 2006; Kay et al., 2005a; Sinton et al., 2002;Smith et al., 2003; Steets and Holden, 2003). The decay of pathogens therefore shall depend on the temperature of the river water and the amount of radiation that the water and for that matter the bacteria shall be subjected to during its transport downstream. In their work, Xu et al (2002) found out that decay rate varied from $0.08day^{-1}$ in winter to $58day^{-1}$ in summer for a lagoon in France. They observed that decay rates were higher in April and May where the solar intensity was quite high than in June and July where the solar intensity was fairly low. In their conclusion, Xu et al (2002) noted that temperature can explain only 31% of the variation of calculated decay rate values, while solar radiation can explain 78% of the variation. They intimate that the predictive accuracy increases to 87% when the two parameters are taken into account together whereas other parameters contribute very little to decay rate prediction. Evison (1989) found out that 90% die-off of E-coli in fresh water samples exposed to bright light (787Wh.m-2) took around 4 hours. In the dark

however, die-off may take a number of days. In this sense bacteria die off in surface water will be higher than in groundwaters if the two systems are polluted with faecal coliforms.

It has been substantiated that faecal indicator bacteria (FIB) die off rates are higher in water with higher conductivity levels (Boehm, 2003; Easton et al., 2004; Oliver et al., 2006), which in turn are affected by channel flow rates regulated by rainfall and time lapse from last rain event.

Chemical parameters that influence pathogen decay in reservoirs are probably limited to pH, which would be relevant in only a few reservoirs. Biological parameters that may be important are predation by protozoa and/or invertebrates (Simek et al., 2001; cited in Brookes et al., 2004; Xu et al., 2002).

Diffusion can be described as the spreading of a compound through the effects of molecular motion. It tends to mix areas of high concentration with areas of lower concentration. This implies that the rapidity of diffusive spreading is due to molecular velocities and path lengths between collisions. In natural rivers however, there are a good number of processes that occur so that mixing can occur much faster than by molecular diffusion. Owing to the turbulent nature of river flows, turbulent diffusion is more significant than molecular diffusion. The role of molecular diffusion is negligible as compared to that of turbulent diffusion in constituent transport (McCutcheon 1989; Deng et al., 2002). Typically, molecular diffusion coefficient in estuarine and coastal waters is in the region of 10^{-9} m^2/s and turbulent diffusion coefficient is in the neighbourhood of 1-100 m^2/s (Falconer, 2007).

Turbulent diffusion can be thought of as transport of a solute due to turbulence and time averaging of the product of the velocity and concentration fluctuations. Turbulence enhances momentum and mass transport. It should be noted that in a three-dimensional turbulence the largest eddies are usually limited by the smallest spatial dimension. In this case for a river whose width (W) is relatively bigger than the depth (h), the eddies created as a consequence of turbulence will be limited by the depth. This means that turbulent properties in a relatively wide river should be independent of the width but dependent on the depth. Turbulence is also thought of as being generated in zones of high shear and in the case of a river it would be the bed.

Thus if D_t is the turbulent diffusion coefficient then:

$$D_t \alpha U_* H$$

where, U_* is the bed shear velocity and H is the depth

Since the velocity profile is much different in the vertical direction in relation to the transverse direction, the coefficient D_t is not expected to be isotropic.

Dispersion is mixing which occurs due to differences in velocities of neighbouring parcels of fluid. The combined process of advection and lateral diffusion is called dispersion. In effect dispersion is transport of solutes due to velocity deviations in space due to the non-uniform velocity, or shear-flow profiles.

Turbulent diffusion and dispersion (due to the presence of horizontal or vertical velocity shear) are important in determining the distribution of particles, not only the changes in concentration of an initial distribution or cloud but also the differential

advection of particles within an initial cloud leading to some particles travelling significantly further than the centre of the initial cloud (Brookes et al., 2004).

Advection, dispersion and decay can control the transport of solutes (Thorbjarnarson et al, 2002). In all water bodies, diffusion of solutes will occur in the presence of concentration gradients. During advection and dispersion mass is conserved. Dispersion therefore is an important process in diluting plume concentrations but due to conservation of mass, this is at the cost of increased plume length (Thorbjarnarson et al., 2002).

In their work, Singh et al (2009) observed that the study of solute transport in open channels is crucial for an effective management of water quality. In discussing further the contribution of dispersion to the solute transport phenomenon, Singh et al (2009) acknowledged that polluting solutes of a watercourse are mixed vertically, transversely and longitudinally by the action of velocity shear, advection and diffusion (molecular and turbulent) process as they traverse downstream. Near the point of injection the mixing is three dimensional in nature; downstream from the site, the pollutants get mixed uniformly along the depth and the concentration varies only in the transverse directions. Further downstream, the pollutants are completely mixed across the cross-section of the stream and the variation of pollutant is only in the longitudinal direction. As can be seen from Figs (2.2 and 2.3); at t_0 the solute is injected uniformly and then stretched by the shear profile at t_1 until it becomes one-dimensional after the vertical gradients have been homogenised at t_2. This process is peculiar to both surface water and groundwater systems only that they occur at different spatial and temporal scales. River pollution has received much attention in recent years. The longitudinal dispersion coefficient is a fundamental parameter in

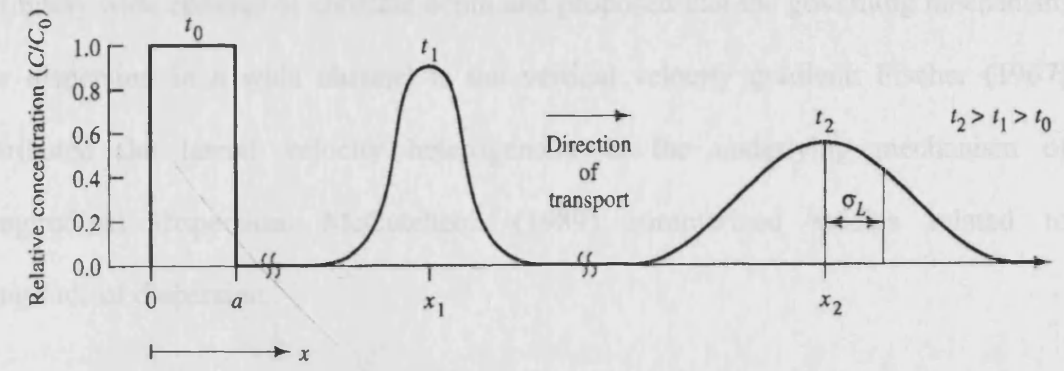

Figure 2.2: A schematic diagram showing the longitudinal dispersion process.

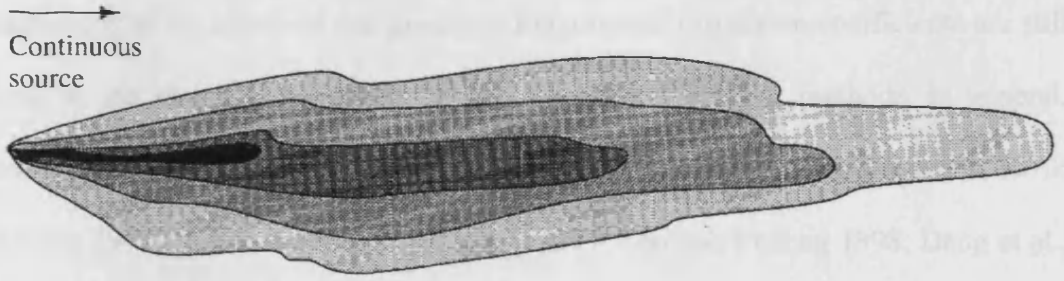

Figure 2.3: An aerial view of the dispersion process

hydraulic modelling of river pollution, for it is a measure of the intensity of the mixing of pollutants in natural streams and is, therefore, of great interest to river managers, environmental engineers, institutional researchers, among others, who are involved in river water pollution control (Deng et al., 2002).

Several researchers have made contributions to the understanding of the mechanisms of longitudinal dispersion in rivers. Taylor (1953) began with the simplest dispersion

of dissolved contaminants in laminar pipe and built on it to turbulent pipe flow (Taylor 1954). Elder (1959) extended the dispersion in pipe to the mixing in an infinitely wide channel of constant depth and proposed that the governing mechanism for dispersion in a wide channel is the vertical velocity gradient. Fischer (1967) attributed the lateral velocity heterogeneity to the underlying mechanism of longitudinal dispersion. McCutcheon (1989) summarized studies related to longitudinal dispersion.

Despite the pioneering work of Taylor and the landmark contribution of Fischer, and seminal studies of Elder (1959); Sooky (1969); Chatwin (1971); Czernuszenko (1990); and Rutherford (1994) among others, the discrepancies between the magnitudes of the observed and predicted longitudinal dispersion coefficients are still found in the range of 1–3 orders of magnitude and existing methods, in general, underestimate the dispersion coefficient (Sooky 1969; Godfrey and Frederick 1970; Chatwin 1971; Nordin and Sabol 1974; Liu 1977; Seo and Cheong 1998; Deng et al., 2002). Such substantial discrepancies are often attributed to the irregularity, spiral flow, and the storage in dead zones in natural streams (Deng et al., 2002). In their paper, Deng et al (2002) have concluded that the effective dispersion coefficient for a river channel with irregular variations in width and bed elevation could be ten or more times higher than the coefficient of a corresponding straight channel. They attribute this to two phenomena: Firstly, the concentration of high velocities on the outside of river bends results in increased dispersion. Second, river bends induce secondary currents and therefore increased transverse mixing, which means that the concentration of a pollutant tends to be more uniform in a cross section, and thus reduces the longitudinal dispersion.

The eddy turbulence at small scales is the predominant mechanism in the turbulent diffusion process, and the velocity variation in the cross section is the predominant mechanism in the longitudinal dispersion process (Deng et al., 2002).They claim that such an understanding of the dispersion mechanism is essential for the determination of an accurate expression defining the dispersion coefficient.

It has been suggested by (Piasecki and Katopodes, 1999; Deng et al., 2002) that a high-resolution numerical method can satisfactorily predict the longitudinal and lateral dispersion in natural streams with arbitrary geometry and bathymetry, provided the detailed field concentration measurements are made at strategically placed monitoring stations.

2.2.2 Decay of faecal coliform, Diffusion and Dispersion in Groundwater flows

Transport of contaminants in the groundwater system is affected by different processes. They include advection, dispersion, diffusion, adsorption and decay. These processes can work together or separate in groundwater flow.

Advection is the movement of the contaminant with the groundwater flow. The rate of flow is determined by Darcy's law, where the hydraulic conductivity of the soil is divided by its porosity to find the average linear velocity: As the groundwater moves it will carry the pollutant with it in the direction and distance it is travelling.

Adsorption is the ability of a compound to "attach" itself to the soil. It's determined highly on the properties of the soil and the compound.

Decay does not affect how fast or how far the pollutant will travel. Biological or chemical processes will reduce the amount of compound travelling thorough the system so that the effects of the advection will stay the same but with a lesser amount present. Soil and rock are good but imperfect traps for microbial pathogens released in sewage to the shallow subsurface via leaky sewers, septic tanks or pit latrines, as applied on the surface as part of fertiliser. This is evident from both widespread detection of microbial pathogens in groundwater (Powell et al., 2003 in Taylor et al., 2004) and the outbreaks of waterborne borne disease that derive from the consumption of sewage –contaminated groundwater (Howard, 2001; Taylor et al., 2004).

Groundwater systems globally provide 25-40% of the worlds drinking water (Morris et al., 2003; Lutterodt et al., 2009) and the importance of groundwater can often be attributed to the assumption that in general, the resource is free from pathogenic microorganisms (Bhaltcharjee et al., 2002; Lutterodt et al., 2009). Yet in many cases, water borne disease outbreaks are caused by the consumption of groundwater contaminated by pathogen microorganisms (Macler and Merkle, 2000; Powell et al., 2003; cited in Lutterodt et al., 2009).

Molecular diffusion is due to concentration gradients and the random motion of molecules. Diffusion does not need advective velocity to occur. It is a process due to the contaminant alone. The larger the amount of pollutant the greater and farther the effects of diffusion can be. It is also not a large factor in systems with large velocities because its effects can be small and slow in coming.

Advective groundwater flow is small compared to diffusive transport processes (Pfingsten, 2008) and especially in low permeability media, diffusion is dominant

(Huysmans and Dassargos, 2006). The time of travel of water (and / or contaminant) through groundwater system depends on the spatial and temporal gradients of hydraulic head, hydraulic conductivity and the porosity of the system (Alley et al., 2002). They observed that fractured rock systems in bedrock usually have smaller effective porosities than unconsolidated porous media systems such as sands and gravels, and flow velocities through fractured rocks can be relatively fast. The implication here is that different properties of pores especially pore size will directly affect contaminant transport.

Tortuosity which is a measure of the effect of the shape of the flow path can also have a significant effect on migration of contaminants. The flow path which also depends on the arrangement of soil particles can cause some fluid particles to travel longer than others. This may cause velocity variations and hence hydrodynamic dispersion which is a mix of diffusion and dispersion. For example clays may have smaller pores but they will also more likely have more pathways. As there are more paths for the flow to follow, there will be a corresponding increase in the path length. In the process some contaminant molecules will randomly have a longer path than others, thereby encouraging dispersion

2.3 Influence of decay relative to diffusion/ dispersion for river basin reaches.

In general, two main factors influence the bacterial concentrations: transport and mixing processes induced by the hydrodynamics; and the bacterial decay dynamics

expressed by the mortality (Schnauder et al., 2007). Transport and mixing processes are related to advection, diffusion and dispersion.

Decay can influence the transport of certain solutes. Many of the decay processes are characterised by an exponential function and a first-order decay rate constant .Viability of pathogens is primarily affected by temperature and ultraviolet light, and if inactivation leads to decomposition, distribution will also be limited.

Through advection and diffusion mechanisms, the water is transported to the open sea where it is mixed with the sea water. The processes of dispersion, dilution, horizontal and vertical transport determines the distribution of pathogens in water bodies (Brookes et al., 2004). The implication here is that the decay process does not in a way affect the transportation mechanism.

For an infinitely long reach, the steady state one –dimensional water quality model is based on the solution of the well known mass balance equation given by (Thomann and Mueller, 1987; Lowe and Groninger, 2005):

$$U\frac{dC}{dx} = E\frac{d^2}{dx^2}C - KC \qquad (2a)$$

where U=average velocity, E=dispersion coefficient, C=concentration and K= decay rate.

Lowe and Groninger (2005) in their analysis found that for a relatively long reach the advection term is dominant than the reactive term than the dispersive term in that order. They claim that the kinetic terms in water quality models may be small and hence the concentration gradients are small. This makes the second derivative

negligible and hence the advective term becoming dominant. For the longitudinal dispersion coefficient to approach the importance of the advective term, its value would have to be at least three orders of magnitude larger than the average velocity (Lowe and Groninger, 2005). In a simple analysis performed by the authors using calculations and applying equation (2a), the dispersive term was four-and-a-half orders of magnitude lower than the advective and reactive terms. In non tidal rivers, the dispersion coefficient is unlikely to be three or more orders of magnitude larger than the average velocity.

It has even been found out that, for steady state water quality models the dispersion coefficient is among the least sensitive of parameters (Himesh et al., 2000 cited in Lowe and Groninger, 2005). Lowe and Groninger (2005) have found out that unless a model is of a well-known, well-studied river, the chances that a measured value of a dispersion coefficient can be found are slim. They go on to say that even for a river where measurements have been made, it is common that large variations in dispersion occur for varying flowrates and for antecedent conditions at the same flowrate (Mitchell et al., 1998 in Lowe and Groninger, 2005). For example, (Gurdack et al., 2002 cited in Lowe and Groninger, 2005) reported a variation of $1.6m^2/s$ to $60.4m^2/s$ for Gore Creek in Colorado, over a flow range from $0.1m^3/s$ to $4.1m^3/s$. Even for groundwater system, for a longitudinal dispersivity of 0.5m, Elfeki et al (2007) found different dispersion coefficients for differing head differences. The results were 0.04, 0.125 and $0.83m^2/day$ for head differences of 1, 3, and 20m respectively.

2.4 Diffuse Source Inputs from Catchments

The pollution arising from land-use activities that are dispersed across a catchment namely diffuse source pollution; can have significant implications on the water quality of the receiving waters (Schnauder et al., 2007).

Diffuse sources largely comprise faeces voided directly in fields and animal wastes (e.g. slurry from dairy units) that have been spread to land. Direct voiding of faeces to watercourses also occurs where livestock have access to streams for drinking or at stock crossing points (Kay et al, 2008).

Diffuse source pollution has been identified in the United States as the biggest challenge in maintaining water quality (US EPA 2004) and is rapidly becoming a major problem in many areas of the UK. Agriculture is considered to be the industry generating the largest amount of diffuse source pollution (DEFRA 2004).

The best estimate of total amount of agricultural animal manure produced in the world is anywhere between 10^{10} and 10^{11} tons annually (Fayer and Trout, 2005; Pachespsky et al., 2006). If managed improperly it can cause substantial pollution of water. Pathogenic microorganisms that are found in manure can cause serious illness and death in humans (Cotruvo et al., 2004; Pachepsky et al., 2006). The manifestations of these microbial pollution are: deaths caused by rainfall-induced pathogen movement to a drinking water supply in Canada (Danon-Schaffer, 2001; Holme, 2003; Auld et al., 2004; Kay et al., 2007b); life-threatening , illnesses acquired from swimming in US lake water (Bruce et al., 2003; Kay et al., 2007b) and camping on Scottish pasture grazed by sheep (Ogden et al., 2002; Kay et al., 2007b); paediatric illnesses in USA acquired from disinfected swimming-pool water (Castor and Beach, 2004; Lim et al.,

2004; Kay et al., 2007b) and viral infections from a recreational water fountain in the Netherlands (Hoebe et al., 2004; Kay et al., 2007b). By the frequency of being the cause of water quality impairment, pathogens rank first and second among five leading pollutants in estuaries and rivers, respectively, in the United States (EPA, 2004; Pachepsky et al., 2006).

Riverine eutrophication due to diffuse pollution has been identified as a major problem in Ireland (Earle, 2003). About 87% of rivers; 50% of lakes; 35% of estuaries; 20% of coastal waters and 68% of groundwater are at risk of not achieving the objectives set in the Water Framework Directive because of diffuse pollution in UK (Environment Agency, 2007).

It is now becoming increasingly clear that runoff water generated by rainstorm carries a variety of contaminants including faecal indicator bacteria (FIB) from residential, agricultural, or industrial land-use areas, which contribute to elevated contaminant levels in receiving waters. According to USEPA, (2002), measurements of indicator bacterial densities are the basis for regulatory decisions regarding recreational and commercial uses of water bodies; however, this contamination is often linked to rain events and resulting storm water runoff from urban and agricultural regions (He and He, 2008). Rainfall events can increase turbidity, water depth and velocity and therefore reduce the chances of faecal bacteria die-off and sedimentation along watercourses (Kay et al, 2008). Faecal indicator organism fluxes are typically around two orders of magnitude greater at high flow than base flow, thereby impacting

massively upon microbial pollution concentrations in receiving waters—i.e. lakes and coastal waters (Kay et al, 2008).

Tide or wave height exerts impacts on the movement of near-shoreline sediment, which may be the place that harbours a significant amount of FIB (Boehm et al., 2007 He et al., 2007; Yamahara et al., 2007 all cited in He and He (2008)).Faecal coliform pollution in coastal waters is high priority problem worldwide that has not been completely ameliorated by secondary wastewater treatment (Steets and Holden, 2002). They continue to highlight other non-point sources that affect coastal water quality like stormwater runoff, septic systems, sanitary sewers and wildlife.

It has been estimated that between 627,800 and 1,479,200 excess gastrointestinal illnesses occur at beaches in Los Angeles and Orange Counties each year due to coastal pollution, corresponding to an annual economic loss of $21 or $51 million (Given et al., 2006; cited in He and He, 2008) due to the illnesses.

Numerous studies have found that inadequate soil properties, inappropriate site location of onsite wastewater treatment systems like septic tanks and poor management and maintenance techniques can lead to numerous scenarios of failing systems. This can lead to contamination of ground and surface water resources due to percolation of inadequately treated sewage effluent from soil based effluent disposal areas (Paul et al., 2000; Lipp et al., 2001; Pang et al., 2003;all cited in Carroll et al., 2009).

Microbial contamination of water resources is of critical concern due to public health risks (Hagedorn et al., 1999; cited in Carrol et al., 2009). To address the issue of microbial contamination from diffuse inputs especially from agricultural sources the use of water quality models come into the fore. Mathematical, process-based system models may be an important tool for hypothesis-building in the search for significant yet diffuse sources of faecal pollution (Steets and Holden, 2003). Sinclair et al. (2009) state that water quality models are becoming more widely used for developing watershed source water protection plans. Yet they concede that the dynamics of microbial pollutant generation and transport within terrestrial and aquatic ecosystems are extremely complicated.

Models that can predict pathogen discharges from catchments are rare (Ferguson et al., 2003; Haydon and Deletic, 2009). They go on to say that when pathogen modelling is attempted it is mainly done by an adaptation of more general models that have not been developed specifically for this application. It has been speculated that microbial catchment models are the least reliable of all catchment models (Novotny, 2003;in Haydon and Deletic, 2009).Operationally useful i.e. deterministic and process based, faecal indicator models that are able to predict the effects of individual remedial programmes of measures or best management practices on catchment scale faecal indicator organisms do not exist at the present (Kay et al., 2007b). Catchment microbial modelling is much less well-developed (Crowther et al., 2002, 2003; Kay et al., 2005b, 2007b).

To put it mildly, Yuan et al. (2007) say the current modelling capability in predicting the impact of diffuse pollution (on coastal receiving waters) is limited. Whilst it is not

difficult to assess and determine point source pollution, diffuse source pollution is daunting because of its widespread distribution over large areas. Although physically based models have been developed yet they remain difficult to use for watershed planning purposes (Jamieson et al., 2004; Sinclair et al., 2009). The importance of pollution arising out of land-use activities that are dispersed across catchments, has only been recognised recently and the current capability of predicting the impact of diffuse pollution on the aquatic environment is limited (Ebrahimi, 2004).

It is possible to mitigate non-point faecal coliform pollution through source delineation, field study, system analysis and field management (Steets and Holden, 2003)

Diffuse source pollution can be minimised by reducing the connectivity between sources and adjacent watercourses and by improving soil drainage, thereby reducing the volume of surface runoff, which tends to have greater faecal indicator organism (FIO) loadings than drain flow (Kay et al., 2007a). Recent work in Brighouse Bay, Scotland, has shown that significant reductions in FIO concentrations can be achieved where 30% or more of stream banks within a catchment are fenced (Kay et al., 2007a).

Controlling the production and use of certain hazardous chemicals to stop the pollution at source is a key part of the approach (Environment Agency, 2003; 2007). Soil protection is also central to reducing water pollution because soils are the route by which many pollutants reach water (Environment Agency, 2004; 2007).

2.5 Summary

In this part of the study, the works of previous researchers have been reviewed. The processes, i.e. advection, diffusion and dispersion that govern the transport of solute in surface and sub-surface flows have been discussed. These have been linked with the die-off rate of faecal coliforms in rivers, estuaries and groundwaters. It is worthy of note that in most situations, advection, dispersion and bacteria decay rate are significant in surface water bodies whereas diffusion is the significant mode of solute transport in sub-surface medium.

CHAPTER 3 GOVERNING EQUATIONS OF MOTION

3.1 Free Surface Flow Equations

Two sets of partial differential equations describe the motion of fluids. These are the continuity (or conservation of mass) and the momentum equations. Thus numerical models used by water and environmental engineers and managers to predict the flow, water quality and contaminant and sediment transport processes in water bodies are based on solving these equations.

3.1.1 3D Equations

For a Cartesian co-ordinate system, with the main body of flow in the horizontal plane, the corresponding 3-D Reynolds averaged equations for mass and momentum can be written in a general conservative form (Falconer, 1993 and Falconer et al, 2001b) for conservation of mass as:

$$\frac{\partial u}{\partial x}+\frac{\partial v}{\partial y}+\frac{\partial w}{\partial z}=0 \tag{3.1}$$

and for momentum conservation in the x-direction as:

$$\underbrace{\frac{\partial u}{\partial t}}_{1}+\underbrace{\frac{\partial u^2}{\partial x}+\frac{\partial uv}{\partial y}+\frac{\partial uw}{\partial z}}_{2}=\underbrace{X}_{3}-\underbrace{\frac{1}{\rho}\frac{\partial P}{\partial x}}_{4}+\underbrace{\frac{1}{\rho}\left\{\frac{\partial}{\partial x}\left[\mu\frac{\partial u}{\partial x}-\rho\overline{u'u'}\right]+\frac{\partial}{\partial y}\left[\mu\frac{\partial u}{\partial y}-\rho\overline{u'v'}\right]+\frac{\partial}{\partial z}\left[\mu\frac{\partial u}{\partial z}-\rho\overline{u'w'}\right]\right\}}_{5} \tag{3.2}$$

where, u, v, w =velocity in x, y, w directions; t= time; X= body force in x direction; ρ =fluid density; P= fluid pressure; μ = absolute fluid viscosity; and u', v' and w' = fluctuating velocity components in x, y and z directions respectively. In Equation (3.2), the terms 1 to 5 refer to: (1) local acceleration, (2) advective or convective acceleration, (3) body force, (4) pressure gradient, and (5) laminar and turbulent shear stresses respectively. The expressions $\rho\overline{u'u'}, \rho\overline{u'v'}$ and $\rho\overline{u'w'}$ are known as the Reynolds or apparent stresses in the x-direction on the x, y and z planes respectively. Similar equations can be written in the y and z directions as given by Falconer et al (2001b).

In modelling estuarine flows in two and three dimensions the effects of the earth's rotation will need to be included giving, for the body force components as Dronkers (1964):

$$\left.\begin{aligned} X &= 2v\omega\sin\varphi \\ Y &= -2u\omega\sin\varphi \\ Z &= -g \end{aligned}\right\} \qquad (3.3)$$

where ω = speed of earth's rotation, φ = latitude of site of interest and g = gravitational acceleration. The main effects of the earth's rotation, giving rise to the Coriolis acceleration, are to set up transverse water surface slopes across an estuary coastal basin and to enhance the effect of secondary currents. For three-dimensional flow predictions, either the full three-dimensional governing equations are solved, which leads to a complex numerical formulation to evaluate the pressure P, or, more usually, a hydrostatic pressure distribution is assumed to occur in the vertical (z) direction, which leads to an expression for P of the following form:

$$P(z) = \rho g(\zeta - z) + P_a \tag{3.4}$$

where ζ = water surface elevation above (positive) datum and P_a = atmospheric pressure. The corresponding derivative of Equation (3.4), for inclusion in Equation (3.2) is given as:

$$\frac{\partial P}{\partial x} = \rho g \frac{\partial \zeta}{\partial x} + \frac{\partial P_a}{\partial x} \tag{3.5}$$

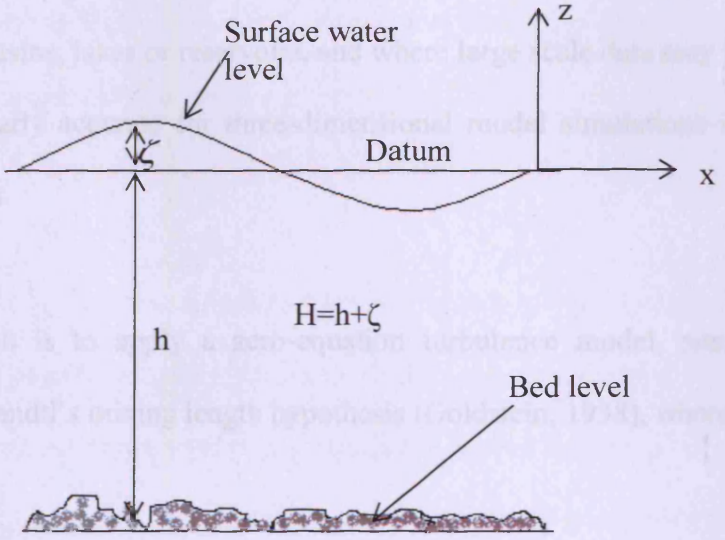

Figure 3.1: Surface water elevation in relation to the bed level

In solving for the Reynolds stresses, it was proposed they could be represented in a diffusive manner as Goldstein (1938):

$$\left.\begin{aligned} -\rho\overline{u'u'} &= \eta\left[\frac{\partial u}{\partial x} + \frac{\partial u}{\partial x}\right] \\ -\rho\overline{u'v'} &= \eta\left[\frac{\partial u}{\partial y} + \frac{\partial v}{\partial x}\right] \\ -\rho\overline{u'w'} &= \eta\left[\frac{\partial u}{\partial z} + \frac{\partial w}{\partial z}\right] \end{aligned}\right\} \tag{3.6}$$

where η =absolute eddy viscosity, or, as for laminar flow, ν_t = kinematic eddy viscosity = η/ρ

3.1.1.1 Determination of eddy viscosity (ν_t)

The determination of this parameter can be obtained in several ways (Rodi, 1987). The simplest method is to assume a constant value based on field data. Whilst this approach may be adequate for predicting velocity distributions in large water bodies, such as coastal basins, lakes or reservoirs, and where large scale data may be available, it is not particularly accurate for three-dimensional model simulations in river and estuarine systems.

Another approach is to apply a zero-equation turbulence model, similar to that obtained from Prandtl's mixing length hypothesis (Goldstein, 1938), wherein:

$$\nu_t = \ell^2 J \tag{3.7}$$

where ℓ = a characteristic mixing length and J = magnitude of local velocity gradients in x, y, z directions.

$$J = \left[\begin{array}{l} 2\left(\frac{\partial u}{\partial x}\right)^2 + 2\left(\frac{\partial v}{\partial y}\right)^2 + 2\left(\frac{\partial w}{\partial z}\right)^2 + \left(\frac{\partial w}{\partial y} + \frac{\partial v}{\partial z}\right)^2 \\ \left(\frac{\partial u}{\partial z} + \frac{\partial w}{\partial x}\right)^2 + \left(\frac{\partial v}{\partial x} + \frac{\partial u}{\partial y}\right)^2 \end{array} \right]^{1/2} \tag{3.8}$$

With this approach, the mixing length leads to a typical logarithmic type velocity profile, but for the complex flow fields where three-dimensional (3-D) models are appropriate, then the velocity distribution is unlikely to be primarily logarithmic in

form and secondary currents and stratification may require a more complex representation of the mixing length.

In the determination of ℓ, Prandtl (see Rodi, 2000) suggested that the mixing length was proportional to z near the wall giving:

$$\ell = \kappa z \tag{3.9}$$

where κ = von Karman's constant and z is the distance perpendicular to the bed or wall with z = 0 at the bed. A more refined version for ℓ was given by von Karman where for the x-direction, we have:

$$\ell = \kappa \left(\frac{\partial u}{\partial z} \Big/ \frac{\partial^2 u}{\partial z^2} \right) \tag{3.10}$$

For more complex hydrodynamic practical problems where 3-D models are desirable for estuarine and coastal systems, then the turbulent stresses given above need to be solved using more comprehensive two-equation turbulence models of the k-ε type, or a three-equation turbulence model of the algebraic stress type, wherein the Reynolds stress terms are solved directly. For the more usual approach, using either the linear or non-linear k-ε model, the eddy viscosity is defined as:

$$\nu_t = \frac{C_\mu k^2}{\varepsilon} \tag{3.11}$$

where C_μ = turbulent model coefficient (=1.68 from experimental data), k - turbulent kinetic energy and ε =dissipation rate of turbulent kinetic energy.

Transport equations derived for k and ε (Rodi, 1984), which include terms for the transport by kinetic energy and dissipation. At the walls and bed, the wall function is adopted adjacent to the bed, which expresses the velocity in terms of the local friction

velocity at the first grid point of the computational domain, adjacent to the wall. Similarly, at the free surface the velocity components and the turbulent fluctuations normal to the surface, and the normal derivatives of all other variables, are set to zero, except for the rate of turbulent energy dissipation ε. The expression for ε at the first grid point below the free surface is given by Noat and Rodi, (1982) as:

$$\varepsilon = \frac{C_D^{3/4} k^{3/2}}{\kappa}\left(\frac{1}{\gamma} + \frac{1}{0.07H}\right) \tag{3.12}$$

where γ = distance from surface and κ = von Karman's constant (=0.41), H =total depth of flow.

In this study, the mixing length model was applied instead of the k-ε model. For this work, the turbulence is assumed to be dominated by bed friction acting on the horizontal axes (x, y) where the bed height is the main factor influencing turbulence. The effect of this approach to the flow is to smoothen velocity gradients and can effectively stabilise the numerical solution. Thus in the numerical solution, a mixing length which is the bed height (which can be the height of a sand dune etc.) is specified.

3.1.2 Depth integrated equations

For many practical hydraulic studies there may be significant variations across the streamwise flow direction, such as in calculating tide induced circulation in estuaries and coastal waters. For such flow problems the vertical velocity component w is often relatively small compared to the horizontal velocity components u and v. In the studies considered herein, such flows are considered and the equations are integrated

over the depth and solved numerically to give the depth averaged velocity field U, V for the x, y depth averaged velocity. The two-dimensional depth integrated equations therefore become (Falconer et al, 2001a)

For continuity,

$$\frac{\partial \zeta}{\partial t} + \frac{\partial p}{\partial x} + \frac{\partial q}{\partial y} = 0 \tag{3.13}$$

and for momentum in x-direction

$$\frac{\partial p}{\partial t} + \beta\left[\frac{\partial Up}{\partial x} + \frac{\partial Vp}{\partial y}\right] = fq - gH\frac{\partial \zeta}{\partial x} + \frac{\partial}{\partial x}\left[\bar{\varepsilon}\left(\frac{\partial p}{\partial x} + \frac{\partial p}{\partial x}\right)\right] + \frac{\partial}{\partial y}\left[\bar{\varepsilon}\left(\frac{\partial p}{\partial y} + \frac{\partial q}{\partial x}\right)\right] + \frac{\tau_{sx} - \tau_{bx}}{\rho} \tag{3.14a}$$

and momentum in the y-direction

$$\frac{\partial q}{\partial t} + \beta\left[\frac{\partial Uq}{\partial x} + \frac{\partial Vq}{\partial y}\right] = -fp - gH\frac{\partial \zeta}{\partial y} + \frac{\partial}{\partial x}\left[\bar{\varepsilon}\left(\frac{\partial q}{\partial x} + \frac{\partial p}{\partial y}\right)\right] + \frac{\partial}{\partial y}\left[\bar{\varepsilon}\left(\frac{\partial q}{\partial y} + \frac{\partial q}{\partial y}\right)\right] + \frac{\tau_{sy} - \tau_{by}}{\rho} \tag{3.14b}$$

where p and q are discharges per unit width in the x and y directions respectively; β, is the momentum correction factor; f is the Coriolis parameter due to the earth's rotation; H is the total water depth $= \zeta + h$, (see Figure 3.1) ζ is water elevation above datum; $\bar{\varepsilon}$ is the depth averaged kinematic eddy viscosity; τ_{sx} and τ_{sy} are the surface wind stress components in the x and y directions respectively; τ_{bx} and τ_{by} are the bed friction components in the x and y directions respectively.

For the various terms of the depth integrated momentum equations, these are discussed in more detail below:

3.1.2.1 The momentum correction factor β

The parameter,β, known as the momentum correction coefficient or the Boussinesq coefficient, is usually greater than unity. It is generally found that the value of β for fairly straight prismatic channels varies approximately from 1.01 to1.12 and for natural stream and torrents it may be up to 1.17. The momentum correction factor,β can be calculated from the relation below (Falconer et al., 2001a):-

$$\beta = 1 + \frac{g}{C^2 \kappa^2} \tag{3.15}$$

For an assumed seventh power law velocity profile the value of β is 1.016 and 1.20 for an assumed quadratic velocity profile (Falconer and Chen, 1991; Falconer et al., 2001a).

3.1.2.2 Coriolis term, f

This term describes the effect that the earth's rotation has on the flow in a water body. It depends on the latitude and the flow velocity and acts perpendicular to the flow. Full details are given in Dronkers (1964). Along the coast this term affects tidal currents and tidal amplitude, causing the flow to rotate around points of zero amplitude. In estuaries, the Coriolis influence is usually very small compared with other effects, unless the modelling domain is very large.

3.1.2.3 Surface slope term

The term in the x-direction equation given as ($gH\frac{\partial \zeta}{\partial x}$) reflects the pressure gradient in the form of the effect of gravity and the water elevation interacting with the

topography of the water bodies. This term includes the bed and surface slopes and is non-linear. This term represents the governing driving force for a tidal flow.

3.1.2.4 Wind stress

The wind exerts a drag force as it flows over the water surface, with the effect being to dissipate or increase the momentum, depending on the wind direction relative to the fluid direction. For the surface wind stress components a quadratic friction law is assumed, based on a balance of the horizontal forces for steady uniform flow, giving (Dronkers, 1964):-

$$\left.\begin{aligned} \tau_{sx} &= C_S \rho_a W_x W_S \\ \tau_{sy} &= C_S \rho_a W_y W_S \end{aligned}\right\} \qquad (3.16)$$

where C_S= air-water resistance coefficient; ρ_a= air density (typically=1.292 kg/m^3), W_x, W_y= wind velocity components in x, y directions respectively and W_S= wind speed measured at 10m above the surface of the water body. Various empirical constants or formulae have been proposed for the air-water resistance coefficient, with one of the most widely used formulations being a piecewise representation as given by Wu (1969), giving:-

$$\left.\begin{aligned} C_S &= 1.25\times10^{-3} W_S^{-0.2} \quad \text{for} \quad W_S \le 1 m/s \\ C_S &= 0.50\times10^{-3} W_S^{0.5} \quad \text{for} \quad 1 < W_S < 15 m/s \\ C_S &= 2.60\times10^{-3} \quad \text{for} \quad W_S \ge 15 m/s \end{aligned}\right\} \qquad (3.17)$$

This formulation has been included in the model outlined herein and where a wind stress is appropriate.

3.1.2.5 Bed resistance

The bed friction has a non-linear effect in retarding the flow and dissipating momentum. For a two-dimensional flow then the bed shear stress can also be represented in the form of a quadratic friction law, as given by (Falconer and Chen, 1996):-

$$\left.\begin{aligned}\tau_{bx} &= \rho g U \frac{V_S}{C^2} \\ \tau_{by} &= \rho g V \frac{V_S}{C^2}\end{aligned}\right\} \qquad (3.18)$$

where C = de Chezy bed resistance coefficient. The more comprehensive friction formulation, given by Colebrook-White (Henderson, 1966) has been used in the current model, as given by:-

$$C = -17.715 \log_{10}\left(\frac{k_S}{12R} + \frac{0.282C}{R_e}\right) \qquad (3.19)$$

where: f = Darcy resistance coefficient, R = hydraulic radius and R_e = flow Reynolds number $\left(= \frac{4RU}{\nu}\right)$ and ν = kinematic laminar viscosity. For a wide-open channel flow, where the width is greater than 10 times the depth of the channel, then the hydraulic radius (R) can be equated to the total depth of water (H).

The main advantages of using this approach are two-fold:

(i) The assumption of a rough turbulent in all flows as prevailing in the Manning's formulation thereby ignoring Reynolds number effects will not apply for low velocity

flows whereas this approach takes into consideration where Reynolds effects may be significant.

(ii) The physical roughness parameter k_S can be directly related to the height of bed features, such as ripple or dunes, rather than based upon a descriptive representation of the bed characteristics, as for the Manning formulation.

3.1.2.6 Turbulence stresses

The Reynold's stresses in Equations (3.2) and (3.6) arising as a result of turbulent velocity fluctuations can be related to the velocity field through an eddy viscosity term as outlined previously. Hence, the Reynold's stresses are expressed in terms of the kinematic eddy viscosity ε and derivatives of the time averaged velocity components in horizontal co-ordinate directions (Streeter *et al*, 1998). There are a number of equations in the literature for defining the kinematic eddy viscosity, varying from simple relationships expressed in terms of the local hydraulic conditions, to complex differential equations governing the transport and decay of the turbulent kenetic energy etc. as outlined previously.

The depth averaged eddy viscosity $\bar{\varepsilon}$ can preferably be estimated from field data obtained from the vertical velocity profile, or by assuming that bed-generated turbulence dominates over free shear layer turbulence, and assuming a logarithmic velocity profile; for these assumptions then the depth averaged eddy viscosity is given by Elder (1959) as:-

$$\bar{\varepsilon} = 0.167\kappa U_* H \qquad (3.20)$$

where κ=0.4 and U_* = depth mean shear velocity given as:

$$U_* = \sqrt{gHS} \tag{3.21}$$

where S= bed slope.

Field data by Fischer (1973) for turbulent diffusion in rivers has shown that the value of $\bar{\varepsilon}$ is generally much higher than that given by Equation (3.20) and is more typically represented by:-

$$\bar{\varepsilon} = 0.15 U_* H \tag{3.22}$$

For most practical, river and estuarine modelling studies, even this value is still regarded as low compared to measured data subsequently recorded in well-mixed estuaries (Fischer *et al*, 1979), with values for $\frac{\bar{\varepsilon}}{U_* H}$ typically ranging from 0.42 to 1.62. In the current studies reported herein, the typical value of the constant for $\frac{\bar{\varepsilon}}{U_* H}$ has been assumed to be of the order of one.

3.2 Groundwater Flow Equations

One of the main objectives of the current study has been to refine a free surface flow and groundwater model and to verify this model against laboratory studies. Groundwater flow and transport models are based on governing equations for mass conservation and Darcy's and Fick's laws with appropriate initial and boundary conditions (Anderson and Woessner, 2002; Giudici et al., 2008) The resulting partial differential equations describe the state of the groundwater system in the form of piezometric head, or solute concentration, with physical parameters such as hydraulic conductivity, porosity, storativity, dispersivity, being included and with forcing terms such water withdrawal, recharge, etc.

3.2.1 3D Groundwater Flows

The three dimensional equations of motion for a groundwater as presented by Freeze and Cherry (1979) and Spanoudaki et al. (2005) are given as:

Mass Conservation (Continuity) equation

$$\frac{\partial u_p}{\partial x}+\frac{\partial v_p}{\partial y}+\frac{\partial w_p}{\partial z}+S_S\frac{\partial \zeta}{\partial t}+Q=0 \tag{3.23}$$

where, u_p, v_p, w_p are flows per unit area in the x, y and z-directions; S_S=storage, or for unconfined aquifer, the storage term is given by the porosity.

ζ = water elevation in the porous medium; and Q is a source term.

For the conservation of Momentum-Darcy's law

$$\left.\begin{aligned} u_p+K_x\frac{\partial \zeta}{\partial x}&=0\\ v_p+K_y\frac{\partial \zeta}{\partial y}&=0\\ w_p+K_z\frac{\partial \zeta}{\partial z}&=0 \end{aligned}\right\} \tag{3.24}$$

where, K_x, K_y, K_Z are hydraulic conductivities in x, y, z-directions respectively.

3.2.2 2-D Groundwater Flow Equations

For nearly horizontal aquifer flows with only a slightly inclined water table, then the Dupuit-Forchheimer assumption allows the three-dimensional equations to be reduced to the well-known two dimensional Boussinesq equations (Liang et al., 2007). For isotropic, homogeneous flows in an unconfined aquifer, the two-dimensional

continuity equation can be obtained from the 3-D equation (3.24) to give (Spanoudaki et al., 2005):

$$\frac{\partial p}{\partial x} + \frac{\partial q}{\partial y} + n_e \frac{\partial \zeta}{\partial t} = 0 \tag{3.25}$$

where p , q are flows per unit area in the x, y-directions; and n_e is the effective porosity of the porous medium.

Likewise, the momentum equation given by Darcy's law for 2-D flows can be written for the x- and y-directions as:

$$\left.\begin{aligned} p + KH\frac{\partial \zeta}{\partial x} = 0 \\ q + KH\frac{\partial \zeta}{\partial y} = 0 \end{aligned}\right\} \tag{3.26}$$

where K is the hydraulic conductivity or coefficient of permeability for the porous medium.

These are the governing equations used in the studies reported herein and are linked to the governing 2-D free surface flow equations with details of the linking being given later.

3.3 Solute Transport Equations

Solute transport in surface water and groundwater systems is governed by a suite of hydrologic and geochemical processes (Runkel, 2000). Knowledge of these processes is needed when assessing the fate of contaminants released into these systems. The

study of solute fate and transport is often aided by models that mathematically describe the underlying processes.

3.3.1 Free surface solute transport equations

In modelling numerically the flux of water quality constituents, contaminants or sediments within a river or estuarine system, the conservation of solute mass equation can be written in general terms for a three dimensional flow field as given by (Falconer et al., 2000)

$$\underbrace{\frac{\partial \varphi}{\partial t}}_{1} + \left[\underbrace{\frac{\partial u\varphi}{\partial x} + \frac{\partial v\varphi}{\partial y} + \frac{\partial w\varphi}{\partial z}}_{2}\right] + \left[\underbrace{\frac{\partial}{\partial x}\overline{u'\varphi'} + \frac{\partial}{\partial y}\overline{v'\varphi'} + \frac{\partial}{\partial z}\overline{w'\varphi'}}_{3}\right] = \left[\underbrace{\varphi_s + \varphi_d + \varphi_k}_{4}\right] \quad (3.27)$$

where φ =time averaged solute concentration, φ_s =source or sink solute input (e.g an outfall), φ_d = solute decay or growth term, and φ_k = total kinetic transformation rate for solute.

The individual terms in the advective-diffusion equation (3.27) are generally referred to as: local effects (term1), transport by advection (2), turbulence effects (3), and source (or sink), decay (or growth) and kinetic transformation effects (4). The cross-produced terms $\overline{u'\varphi'}$ etc. represent the mass flux of the solute due to the turbulent fluctuations and, by Fick's law of diffusion, it can be assumed that this flux is proportional to the mean concentration gradient and is in the direction of decreasing concentration (Fischer et al., 1979). Hence they can be written as:

$$\left.\begin{aligned}\overline{u'\varphi'} &= -D_{tx}\frac{\partial\varphi}{\partial x}\\ \overline{v'\varphi'} &= -D_{ty}\frac{\partial\varphi}{\partial y}\\ \overline{w'\varphi'} &= -D_{tz}\frac{\partial\varphi}{\partial z}\end{aligned}\right\} \qquad (3.28)$$

where D_{tx}, D_{ty}, D_{tz} = turbulent diffusion coefficients in x, y, z directions. Typical values for these terms are given in Fischer et al, (1979) and in their dimensionless form are in the range of 0.1 to 0.2

For river and estuarine systems, the vertical variation in concentration may be small due to the negligible vertical velocity, w and the 3-D solute transport equation (3.27) can be integrated over the depth to give the depth integrated solute transport equation of the form:

$$\frac{\partial H\phi}{\partial t}+\frac{\partial HU\phi}{\partial x}+\frac{\partial HV\phi}{\partial y}-\frac{\partial}{\partial x}\left[D_{xx}H\frac{\partial\phi}{\partial x}+D_{xy}H\frac{\partial\phi}{\partial y}\right]-\frac{\partial}{\partial y}\left[D_{yx}H\frac{\partial\phi}{\partial x}+D_{yy}H\frac{\partial\phi}{\partial y}\right]$$
$$=H[\phi_s+\phi_d+\phi_k] \qquad (3.29)$$

where ϕ = depth average solute concentration, D_{xx}, D_{xy}, D_{yx}, D_{yy} = depth average longitudinal dispersion and turbulent diffusion coefficients in x, y directions, and ϕ_s, ϕ_d and ϕ_k = depth averaged source (or sink), decay (or growth) and kinetic decay solute concentrations.

For the depth averaged dispersion-diffusion terms, these coefficients can be shown to be of the following form (Preston, 1985):

$$\left.\begin{aligned} D_{xx} &= \frac{(D_l U^2 + D_t V^2)H\sqrt{g}}{C\sqrt{U^2+V^2}} + D_w \\ D_{yy} &= \frac{(D_l V^2 + D_t U^2)H\sqrt{g}}{C\sqrt{U^2+V^2}} + D_w \\ D_{xy} = D_{yx} &= \frac{(D_l - D_t)UVH\sqrt{g}}{C\sqrt{U^2+V^2}} + D_w \end{aligned}\right\} \quad (3.30)$$

Where D_l = depth average longitudinal dispersion constant, D_t = depth average turbulent diffusion constant, and D_w = wind-induced dispersion coefficient

3.3.2 Groundwater solute transport equation

The effectiveness of the classical advection-dispersion equation to describe solute transport in heterogeneous aquifers has been challenged in many studies such as Bianchi et al. (2008). They showed that the model was not able to reproduce solute transport in porous media containing decimetre-scale preferential flow paths. Demissie et al. (2008) observed that the natural hydrogeological complexity and the inability to extensively monitor the subsurface flow and solute leads to uncertain and possibly inaccurate numerical simulations of groundwater flow and solute transport. The result of these assessments is an insufficient characterisation of the subsurface system by a single deterministic prediction of the state variable. However, one of the main purposes of the current study was to investigate this hypothesis for groundwater flow and solute transport through a homogeneous porous media.

Thus the transport equation governing solute flows in the current study were assumed to be similar to that of free surface flows. The significant dissimilarity is the

timescales of the two systems. Whereas it can take seconds or minutes or hours for a solute to travel from one point to another in surface waters, it can take hours, days or even years for the same solute to travel in the groundwater system for a relatively similar distance.

3.4 Equations for Diffusion/Dispersion terms

3.4.1 Diffusion

For free surface and groundwater flows with isotropic media, it is common to assume isotropic turbulence and to set the horizontal turbulent diffusion terms to equate to the depth mean diffusion coefficient as given by Fischer et al (1979) and Falconer et al (2001b) as:

$$D_h = CU_* H \tag{3.31}$$

where C = constant, typically ≈ 0.15.

Similarly, for the vertical diffusion coefficient, in the absence of stratification with an assumed linear shear stress distribution and a logarithmic velocity distribution respectively as given by Viera (1993) as:

$$D_v = U_* \kappa z(1 - z/H) \tag{3.32}$$

where z=elevation above the bed and κ=von Karman constant.

If (3.32) is integrated over the depth yields (3.31).

3.4.2 Dispersion

Modelling pollutant dispersion and transport is of great importance to evaluating risks from accidental releases of hazardous contaminants in watercourses (Fischer et al.,

1979; Grayman et al., 2001) and to understanding biogeochemical transport and fate within river ecosystems.

In open channel flow, Elder (1959) presented the first published analysis of the depth mean longitudinal dispersion coefficient based on Taylor's method (1954) by assuming a logarithmic vertical velocity distribution to give the well known equation given as:-

$$D_l = \left(\frac{0.4041}{\kappa^3} + \frac{\kappa}{6}\right) HU_* \quad \text{or} \quad D_l = 5.93 HU_* \tag{3.33}$$

It has been found that Elder's equation does not accurately describe longitudinal dispersion in natural streams and channels, and can significantly underestimate the dispersion coefficients (Kashefipour, 2001). This is thought to be due mainly to the exclusion of the transverse variation in the velocity profile across the stream in the derivation of Elder's equation. Studies undertaken using many measured data sets for natural rivers have shown that the value of D_l / HU_* may vary from 8.6 to 7500, with values being generally much greater than Elder's equation constant of 5.93 (Fischer *et al.*, 1979).

Seo and Cheong (1998) and Koussis and Rodriguez-Mirasol (1998) have published new equations for predicting the longitudinal dispersion coefficient. Seo and Cheong (1998) derived their equation using dimensional analysis and a regression analysis for the one-step Huber method, using 59 data sets measured in 26 streams in the USA. They used 35 of these measured data sets to establish their equation and then verified it against other data sets. Their equation can be written as:-

$$\frac{D_l}{HU_*} = 5.915\left(\frac{W}{H}\right)^{0.620}\left(\frac{U}{U_*}\right)^{1.428} \tag{3.34}$$

Koussis and Rodriguez-Mirasol (1998), using the original theory and equation proposed by Fischer (1967, 1968, and 1975), and applying von Karman's defect law derived a revised equation for D_l of the form:-

$$D_l = \Phi\frac{U_*W^2}{H} \tag{3.35}$$

They proposed a value of 0.6 for Φ and obtained this value by applying a regression analysis to 16 field data sets.

Deng et al. (2001) derived the following equation for estimation of the longitudinal dispersion coefficient in streams:

$$\frac{D_l}{HU_*} = \frac{0.01\Psi}{8\varepsilon_{to}}\left(\frac{B}{H}\right)^{5/3}\left(\frac{U}{U_*}\right)^2 \tag{3.36}$$

where, Ψ =transverse mixing coefficient, B= surface width of flow and H= cross-sectionally averaged flow depth. Ψ=1 was theoretically derived but Ψ = 15 was actually recommended to take account of the influence of transient storage zones in natural streams on the longitudinal dispersion.

3.5 Linked surface and sub-surface flows

3.5.1 Introduction

As it has been discussed in the previous chapter, surface water and groundwater are linked components of watersheds, and finding effective solutions to water quality problems often requires an understanding of both, as well as the interactions between them. Thus, this has informed the study herein.

3.5.2 Numerical Method

The current integrated modelling effort is related to the work of Liang et al. (2007) and Sparks (2007) but with the extension of the model to include solute fluxes.

In this study it has been assumed that the vertical flow in both the surface and sub-surface systems is negligible, so there is no movement of water or solute to and from the base of the river to the groundwater and vice-versa, i.e. the base of the surface water cell has been assumed to be impermeable. Thus the surface water and groundwater models have only be connected effectively side by side when using the two sets of governing equations outlined previously.

Figure 3.2 is schematic of the representation of the linkage between the two models. The ground is composed of the top porous layer and an impermeable base (rock). The linked model assumes no seepage face between the two separate models and ignores unsaturated zones. Therefore, there can be only one of the following three states at any position across the domain: free surface flow, groundwater flow or no-flow. The free surface flow model has a higher priority over the groundwater flow model. That is to say, the free surface flow model is switched on whenever the water surface level is found to be higher than the ground level. For the free surface flow, the water depth is calculated as:

$$H = \zeta - z_{bed} \tag{3.37}$$

If the water surface (or water table) position is found to be between the impermeable base level and the bed level, then the groundwater flow model is turned on, and the water depth is calculated from the following equation:

$$H = \zeta - z_{base} \tag{3.38}$$

Where z_{base} should be no larger than z_{bed}. If the water surface position is found to be lower than the impermeable base level, then this location is regarded to be dry. The velocity (and unit width discharge) components over the dry area are forced to zero, while the water surface position is unchanged to ensure mass balance. From the above description, it is seen that if z_{base} is equal to z_{bed} across the domain, then there will be no porous medium between the free surface water and the impermeable base and the combined model will reduce to the free surface model only.

3.5.3 The Moving Boundary

In this study a sloping groundwater –surface water situation was created in the laboratory flume for analysis as shown in Fig 3.2. The situation replicated in the laboratory was similar to a beach and coastal water flow where the boundary was subjected to alternating wetting and drying due to oscillations from the tides. Numerical modelling of such moving boundaries can present serious problems (Falconer et al, 2001a) as a result of the discretised representation of this hydrodynamic process, which generally varies physically in a smooth manner. However, in DIVAST, a refined flooding and drying routine has been developed and used in the model based upon extensive numerical tests in idealised channels and natural estuaries (Falconer et al., 2001a). The refined method pays particular attention subjected to alternating wetting and drying due to oscillations from the tides. Numerical modelling of such moving boundaries can present serious problems (Falconer et al, 2001a) as a result of the discretised representation of this hydrodynamic process, which generally varies physically in a smooth manner.

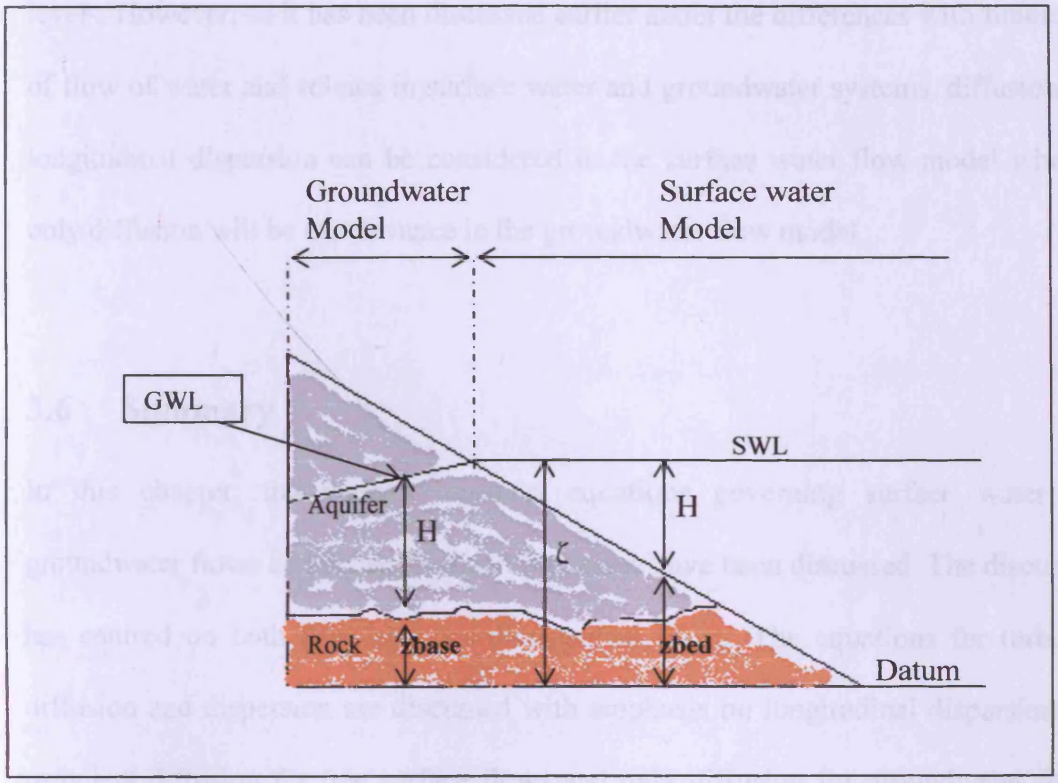

Figure 3.2: Schematic of surface water –groundwater linkage

For example, the water depths surrounding a wet cell are compared with bed roughness height, k_s. If any calculated side depths becomes less than k_s, then the corresponding depth velocity component is equated to zero. See Falconer et al (2001a) for details. Moreso, wetting and drying is borne out naturally without special treatment and guarantees mass conservation (Casulli and Cheng, 1992; Spanoudaki et al., 2009). The surface water and groundwater equations are solved continuously and simultaneously at every timestep within a common structure (the ADI scheme). Thus mass and momentum transfers between the two flow components are fully considered so there is no need for additional numerical effort to treat this boundary explicitly at every time step.

In this study solutes are added via outfalls following the flow patterns of the water levels. However, as it has been discussed earlier about the differences with timescales of flow of water and solutes in surface water and groundwater systems, diffusion and longitudinal dispersion can be considered in the surface water flow model whereas only diffusion will be of relevance in the groundwater flow model.

3.6 Summary

In this chapter, the various transport equations governing surface water and groundwater flows and solute transport processes have been discussed. The discussion has centred on both three-and two-dimensional flows. The equations for turbulent diffusion and dispersion are discussed with emphasis on longitudinal dispersion and turbulent diffusion for free surface flows and only diffusion for groundwater flows. Determination of longitudinal dispersion coefficients obtained by various researchers has been well noted. Lastly the linkage procedure between surface water and groundwater models for this study has been highlighted.

An extensive laboratory studies were conducted for the solute transport processes in idealised surface water-groundwater system whereupon the results are verified with the numerical model results. Thus, whereas previous researchers have looked at piezometric heads (or water levels) in the surface water-groundwater system, solute transport processes and predictions have been the new addition to such a linked model system.

CHAPTER 4 NUMERICAL MODEL DETAILS

4.1 Introduction

Models can be thought of as conceptual descriptions or approximations that can describe physical systems using mathematical equations. Although they may not be exact descriptions of the physical systems or processes, a measure of reasonable scenarios can be tested, predicted and compared for a relatively simplified hydrological situation if properly represented mathematically. Models can therefore be useful for water managers and other hydrological/hydrogeological professionals that are confronted with complex hydro-environmental challenges.

4.2` Numerical Scheme in DIVAST

The Depth Integrated Velocity And Solute Transport (DIVAST) is a model originally developed by Falconer (1977), which has since and is still been refined and used by a number of environmental managers and academics. This model solves the two-dimensional depth integrated Navier –Stokes equations using the Alternating Direction Implicit (ADI) scheme developed by Peaceman and Rachford (Peaceman and Rachford-Jr. 1955). The ADI method uses the finite difference method with square grids. Basically, the simultaneous equations are solved in a more efficient manner with a double sweep algorithm structure. The time-step is divided into two halves; one half for the x-sweep and another half for the y-sweep. As shown in Figure 4.1, the unknown water elevation ζ^{n+1} and the flow per unit width in the x-direction

p^{n+1} are solved during the first half time-step using the known values for the flow per unit width in the y-direction $q^{n+1/2}$. Similarly, in the second half time-step, the water elevation $\zeta^{n+3/2}$ and the flow per unit width in the y-direction $q^{n+3/2}$ are solved for using the already calculated value for the flow per unit width in the x-direction p^{n+1}.

Figure 4.2 shows how the area to be modelled is divided into the square cells which indicate the hydrodynamic and solute parameters that are to be simulated.

There are no stability constraints for this scheme, since the ADI method is implicit and time-centred. However, it has been recognised by earlier researchers that, to achieve reasonable computational accuracy, the time steps need to be restricted in relation to the grid-size. Stelling et al (1986) suggested a maximum Courant number for the ADI which is given as:

$$C_r = 2\Delta t\sqrt{gH\left(\frac{1}{\Delta x^2}+\frac{1}{\Delta y^2}\right)} \le 4\sqrt{2}$$

where H is the average depth of flow, $\Delta x, \Delta y, \Delta t$ are grid sizes and the time-step respectively, g is gravity. In a situation where the grid sizes are the same i.e. $\Delta x = \Delta y$, then the equation reduces to:

$$\frac{\Delta t}{\Delta x}\sqrt{gH} \le 4$$

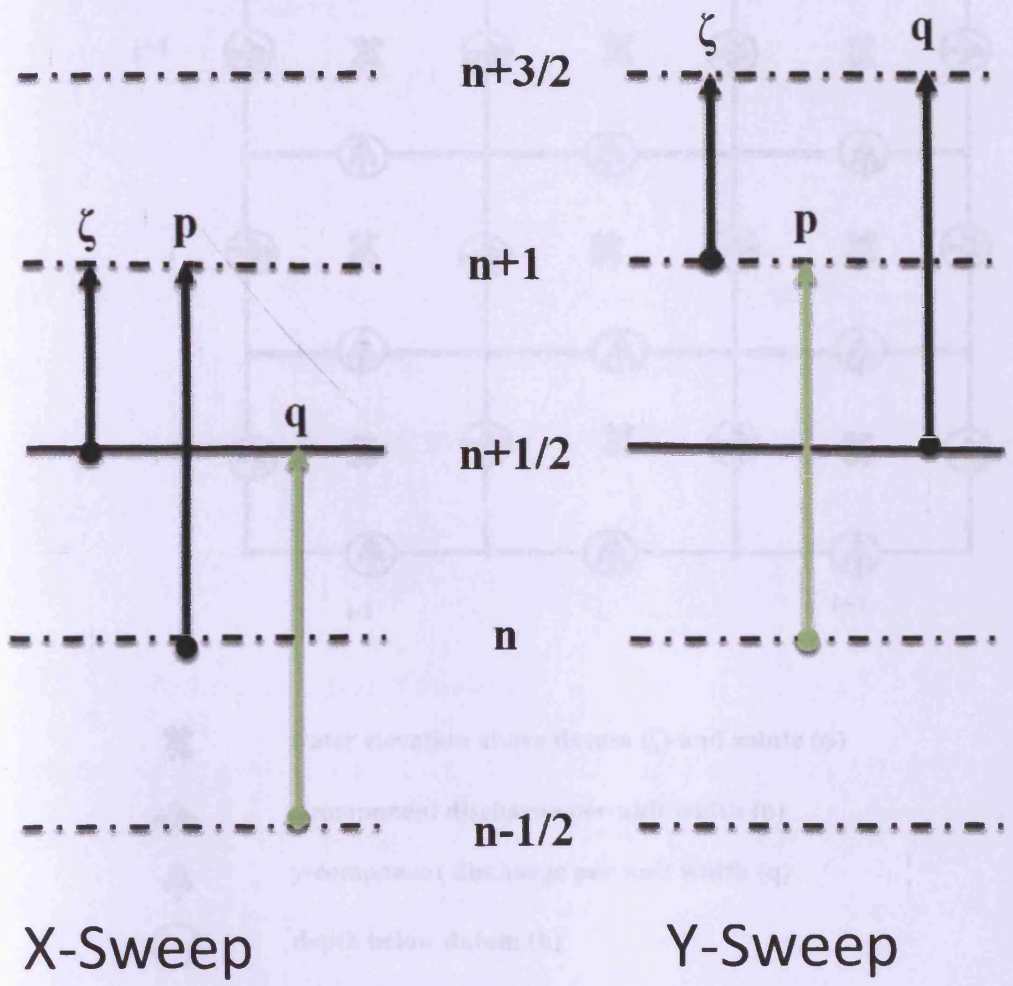

Figure 4.1: The ADI method where the green variable is known from previous time-step. (Adapted from Sparks, 2007).

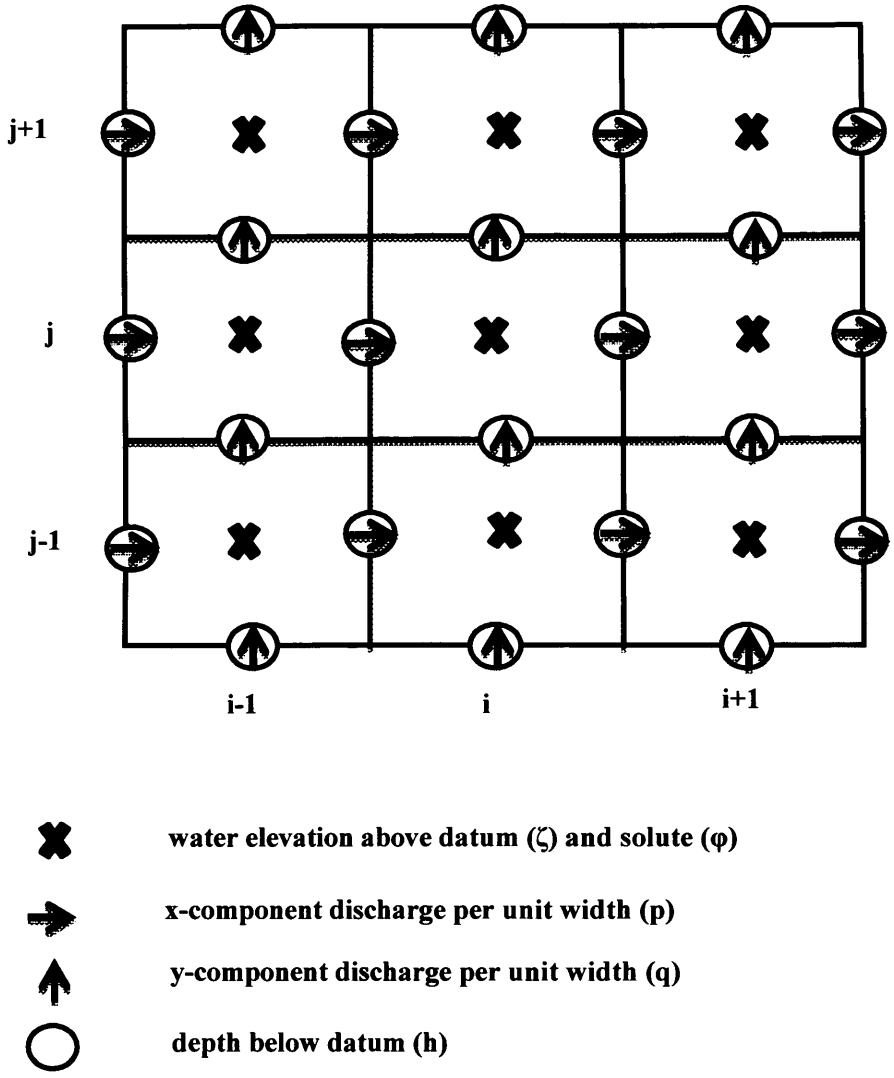

Figure 4.2: Computational space staggered grid (source: Falconer et al (2001a))

4.3 DIVAST-Groundwater Link

Freeze and Cherry (1979) and Sparks (2007) identify the various steps that need to be carried out in addressing hydrologic or hydrogeologic problems with the use of models. One needs to know:

a) the size and shape of the region of flow

b) the equation of flow within the region

c) the boundary conditions around the boundaries of the region

d) the initial conditions in the region

e) the spatial distribution of the hydrologic or hydrogeologic parameters that control the flow and

f) a numerical method of solution.

All the points except the numerical method for the solution have been dealt with in the text. The equations have to be adapted for computer simulations and part of this chapter is set to do that. The equations derived are to be discretised by the numerical method described.

4.3.1 Mass Conservation Equations

The governing equations for the DIVAST model have been deployed in sections 3.1.2 and 3.2.2. for both surface and sub-surface flows respectively. These equations are to be discretised for use in the refined DIVAST-SG model. The equations are repeated herein for ease and understanding of the discretisation procedure.

4.3.1.1 Surface Water

The surface water mass conservation equation can be discretised as following:

x-sweep mass conservation equation

$$\frac{\partial \zeta}{\partial t} + \frac{\partial p}{\partial x} + \frac{\partial q}{\partial y} = 0 \tag{4.1}$$

$$\left(\frac{\zeta_{i,j}^{n+1} - \zeta_{i,j}^{n+1/2}}{0.5\Delta t}\right) + \left(\frac{p_{i+1/2,j}^{n+1} - p_{i-1/2,j}^{n+1}}{\Delta x}\right) + \left(\frac{q_{i,j+1/2}^{n+1/2} - q_{i,j-1/2}^{n+1/2}}{\Delta y}\right) = 0$$

$$\zeta_{i,j}^{n+1} + \frac{1}{2}\frac{\Delta t}{\Delta x} p_{i+1/2,j}^{n+1} - \frac{1}{2}\frac{\Delta t}{\Delta x} p_{i-1/2,j}^{n+1} = \zeta_{i,j}^{n+1/2} - \frac{\Delta t}{2}\left(\frac{q_{i,j+1/2}^{n+1/2} - q_{i,j-1/2}^{n+1/2}}{\Delta y}\right) \tag{4.2a}$$

$$-\frac{1}{2}\frac{\Delta t}{\Delta x}p_{i-1/2,j}^{n+1}+\zeta_{i,j}^{n+1}+\frac{1}{2}\frac{\Delta t}{\Delta x}p_{i+1/2,j}^{n+1}=\zeta_{i,j}^{n+1/2}-\frac{\Delta t}{2}\left(\frac{q_{i,j+1/2}^{n+1/2}-q_{i,j-1/2}^{n+1/2}}{\Delta y}\right) \tag{4.2b}$$

Similarly for y-sweep mass conservation

$$\left(\frac{\zeta_{i,j}^{n+3/2}-\zeta_{i,j}^{n+1}}{0.5\Delta t}\right)+\left(\frac{p_{i+1/2,j}^{n+1}-p_{i-1/2,j}^{n+1}}{\Delta x}\right)+\left(\frac{q_{i,j+1/2}^{n+3/2}-q_{i,j-1/2}^{n+3/2}}{\Delta y}\right)=0$$

$$\zeta_{i,j}^{n+3/2}+\frac{1}{2}\frac{\Delta t}{\Delta y}q_{i,j+1/2}^{n+3/2}-\frac{1}{2}\frac{\Delta t}{\Delta y}q_{i,j-1/2}^{n+3/2}=\zeta_{i,j}^{n+1}-\frac{\Delta t}{2}\left(\frac{p_{i+1/2,j}^{n+1}-p_{i-1/2,j}^{n+1}}{\Delta x}\right) \tag{4.3a}$$

$$-\frac{1}{2}\frac{\Delta t}{\Delta y}q_{i,j-1/2}^{n+3/2}+\zeta_{i,j}^{n+3/2}+\frac{1}{2}\frac{\Delta t}{\Delta y}q_{i,j+1/2}^{n+3/2}=\zeta_{i,j}^{n+1}-\frac{\Delta t}{2}\left(\frac{p_{i+1/2,j}^{n+1}-p_{i-1/2}^{n+1}}{\Delta x}\right) \tag{4.3b}$$

The equations (4.2b) and (4.3b) can be written in a matrix form as:

$$Ap_{i-1/2}^{n+1}+B\zeta_i^{n+1}+Cp_{i+1/2}^{n+1}=D_x \tag{4.4a}$$

$$Aq_{j-1/2}^{n+3/2}+B\zeta_j^{n+3/2}+Cq_{j+1/2}^{n+3/2}=D_y \tag{4.4b}$$

where

$$A=-C=-\frac{1}{2}\frac{\Delta t}{\Delta x}\quad for\quad \Delta x=\Delta y$$

$$B=1$$

$$D_x=\zeta_{i,j}^{n+1/2}-\frac{\Delta t}{2}\left(\frac{q_{i,j+1/2}^{n+1/2}-q_{i,j-1/2}^{n+1/2}}{\Delta x}\right)$$

$$D_y=\zeta_{i,j}^{n+1}-\frac{\Delta t}{2}\left(\frac{p_{i+1/2,j}^{n+1}-p_{i-1/2,j}^{n+1}}{\Delta x}\right)$$

4.3.1.2 Groundwater

The x-sweep of groundwater mass conservation equation can be written as :

$$n_e.\frac{\partial \zeta}{\partial t}+\frac{\partial p}{\partial x}+\frac{\partial q}{\partial y}=0$$

$$n_e.\left(\frac{\zeta_{i,j}^{n+1}-\zeta_{i,j}^{n+1/2}}{0.5\Delta t}\right)+\left(\frac{p_{i+1/2,j}^{n+1}-p_{i-1/2,j}^{n+1}}{\Delta x}\right)+\left(\frac{q_{i,j+1/2}^{n+1/2}-q_{i,j-1/2}^{n+1/2}}{\Delta y}\right)=0 \qquad (4.5a)$$

$$n_e.\zeta_{i,j}^{n+1}+\frac{1}{2}\frac{\Delta t}{\Delta x}p_{i+1/2,j}^{n+1}-\frac{1}{2}\frac{\Delta t}{\Delta x}p_{i-1/2,j}^{n+1}=n_e.\zeta_{i,j}^{n+1/2}-\frac{\Delta t}{2}\left(\frac{q_{i,j+1/2}^{n+1/2}-q_{i,j-1/2}^{n+1/2}}{\Delta y}\right)$$

$$-\frac{1}{2}\frac{\Delta t}{\Delta x}p_{i-1/2,j}^{n+1}+n_e.\zeta_{i,j}^{n+1}+\frac{1}{2}\frac{\Delta t}{\Delta x}p_{i+1/2}^{n+1}=n_e.\zeta_{i,j}^{n+1/2}-\frac{\Delta t}{2}\left(\frac{q_{i,j+1/2}^{n+1/2}-q_{i,j-1/2}^{n+1/2}}{\Delta y}\right) \qquad (4.5b)$$

Likewise, the y-sweep mass conservation equation for groundwater becomes:

$$n_e.\frac{\partial \zeta}{\partial t}+\frac{\partial p}{\partial x}+\frac{\partial q}{\partial y}=0$$

$$n_e.\left(\frac{\zeta_{i,j}^{n+3/2}-\zeta_{i,j}^{n+1}}{0.5\Delta t}\right)+\left(\frac{p_{i+1/2,j}^{n+1}-p_{i-1/2,j}^{n+1}}{\Delta x}\right)+\left(\frac{q_{i,j+1/2}^{n+3/2}-q_{i,j-1/2}^{n+3/2}}{\Delta y}\right)=0 \qquad (4.6a)$$

$$n_e.\zeta_{i,j}^{n+3/2}+\frac{1}{2}\frac{\Delta t}{\Delta y}q_{i,j+1/2}^{n+3/2}-\frac{1}{2}\frac{\Delta t}{\Delta y}q_{i,j-1/2}^{n+3/2}=n_e.\zeta_{i,j}^{n+1}-\frac{\Delta t}{2}\left(\frac{p_{i+1/2,j}^{n+1}-p_{i-1/2,j}^{n+1}}{\Delta x}\right)$$

$$-\frac{1}{2}\frac{\Delta t}{\Delta y}q_{i,j-1/2}^{n+3/2}+n_e.\zeta_{i,j}^{n+3/2}+\frac{1}{2}\frac{\Delta t}{\Delta y}q_{i,j+1/2}^{n+3/2}=n_e.\zeta_{i,j}^{n+1}-\frac{\Delta t}{2}\left(\frac{p_{i+1/2,j}^{n+1}-p_{i-1/2,j}^{n+1}}{}\right) \qquad (4.6b)$$

where n_e = effective porosity for unconfined aquifers.

Equations (4.5b) and (4.6b) can therefore be written in matrix form as:

$$A^* p_{i-1/2}^{n+1}+B^*\zeta_i^{n+1}+C^* p_{i+1/2}^{n+1}=D_x^* \qquad (4.7a)$$

$$A^* q_{j-1/2}^{n+3/2}+B^*\zeta_j^{3/2}+C^* q_{j+1/2}^{n+3/2}=D_y^* \qquad (4.7b)$$

where

$$A^* = -C^* = -\frac{1}{2}\frac{\Delta t}{\Delta x}$$

$$B^* = n_e$$

$$D_x^* = n_e \zeta_{i,j}^n - \frac{\Delta t}{2}\left(\frac{q_{i,j+1/2}^{n+1/2} - q_{i,j-1/2}^{n+1/2}}{\Delta x}\right)$$

$$D_y^* = n_e . \zeta_{i,j}^{n+1/2} - \frac{\Delta t}{2}\left(\frac{p_{i+1/2,j}^{n+1} - p_{i-1/2,j}^{n+1}}{\Delta x}\right)$$

4.3.2 Momentum Conservation

4.3.2.1 Surface Water

Combining equations (3.14), (3.16), (3.17) and (3.18) the momentum equation in the x-direction can be simplified as:

$$\frac{\partial p}{\partial t} + \frac{\partial \beta p U}{\partial x} + \frac{\partial \beta p V}{\partial y} + gH\frac{\partial \zeta}{\partial x} + \frac{gp\sqrt{p^2+q^2}}{C^2H^2} - \bar{\varepsilon}\left[2\frac{\partial^2 p}{\partial x^2} + \frac{\partial^2 p}{\partial y^2} + \frac{\partial^2 q}{\partial x \partial y}\right] = 0 \tag{4.8}$$

and for y-direction,

$$\frac{\partial q}{\partial t} + \frac{\partial \beta q U}{\partial x} + \frac{\partial \beta q V}{\partial y} + gH\frac{\partial \zeta}{\partial y} + \frac{gq\sqrt{p^2+q^2}}{C^2H^2} - \bar{\varepsilon}\left[\frac{\partial^2 q}{\partial x^2} + 2\frac{\partial^2 q}{\partial y^2} + \frac{\partial^2 p}{\partial x \partial y}\right] = 0 \tag{4.9}$$

where wind stresses and Coriolis factor in x and y directions are insignificant since the model is to be used for idealised laboratory situation

Based on the equations above, the momentum equations in the x and y directions are discretised with the following concepts: (i) the equations are discretised in time and space, and (ii) the x-direction discretisations are centred around i+1/2,j and n+1/2

whereas y-discretisations are centred around i,j+1/2 and n+1. Taking the first three terms and the sixth term individually for the equations, the discretisations can be written as follows:

$$\frac{\partial p}{\partial t} = \left(\frac{p^{n+1}_{i+1/2,j} - p^{n}_{i+1/2,j}}{\Delta t} \right) \tag{4.10}$$

$$\begin{aligned}
\frac{\partial \beta pU}{\partial x} &= \beta \left[\frac{\partial pU}{\partial x} \right] = \left[\frac{(pU)^{n}_{i+1,j} - (pU)^{n}_{i,j}}{\Delta x} \right] \\
&= \frac{\beta}{\Delta x} \left[\frac{\left(p^{n}_{i+3/2} + p^{n}_{i+1/2}\right)}{2} \cdot \frac{\left(U^{n}_{i+3/2} + U^{n}_{i+1/2}\right)}{2} - \frac{\left(p^{n}_{i+1/2} + p^{n}_{i-1/2}\right)}{2} \cdot \frac{\left(U^{n}_{i+1/2} + U^{n}_{i-1/2}\right)}{2} \right] \\
&= \frac{\beta}{4\Delta x} \left[\left(p^{n}_{i+3/2} + p^{n}_{i+1/2}\right)\left(U^{n}_{i+3/2} + U^{n}_{i+1/2}\right) - \left(p^{n}_{i+1/2} + p^{n}_{i-1/2}\right)\left(U^{n}_{i+1/2} + U^{n}_{i-1/2}\right) \right]
\end{aligned} \tag{4.11}$$

$$\begin{aligned}
\frac{\partial \beta pV}{\partial y} &= \frac{\partial \beta UHV}{\partial y} = \frac{\partial \beta qU}{\partial y} \\
&= \beta \left[\frac{\partial qU}{\partial y} \right] = \beta \left[\frac{(qU)^{n}_{i+1/2,j+1/2} - (qU)^{n}_{i+1/2,j-1/2}}{\Delta y} \right] \\
&= \frac{\beta}{\Delta y} \left[\frac{\left(q^{n+1/2}_{i+1,j+1/2} + q^{n+1/2}_{i,j+1/2}\right)}{2} . U^{n}_{i+1/2,j} - \frac{\left(q^{n+1/2}_{i+1,j-1/2} + q^{n+1/2}_{i,j-1/2}\right)}{2} . U^{n}_{i+1/2,j} \right] \\
&= \frac{\beta}{2\Delta y} \left[\left(q^{n+1/2}_{i+1,j+1/2} + q^{n+1/2}_{i,j+1/2}\right) U^{n}_{i+1/2,j} - \left(q^{n+1/2}_{i+1,j-1/2} + q^{n+1/2}_{i,j-1/2}\right) U^{n}_{i+1/2,j} \right]
\end{aligned} \tag{4.12}$$

$$\bar{\varepsilon}\left[2\frac{\partial^2 p}{\partial x^2}+\frac{\partial^2 p}{\partial y^2}+\frac{\partial^2 q}{\partial x\partial y}\right]=\bar{\varepsilon}\left[2\frac{\partial^2 HU}{\partial x^2}+\frac{\partial^2 HU}{\partial y^2}+\frac{\partial^2 HV}{\partial x\partial y}\right]$$

$$=\bar{\varepsilon}\left[\begin{array}{l}2\dfrac{H_{i+1/2,j}\left(\dfrac{U_{i+3/2}-U_{i+1/2}}{\Delta x}-\dfrac{U_{i+1/2}-U_{i-1/2}}{\Delta x}\right)}{\Delta x}+\\ \dfrac{H_{i+1/2,j}\left(\dfrac{U_{i+1/2,j+1}-U_{i+1/2,j}}{\Delta y}-\dfrac{U_{i+1/2,j}-U_{i+1/2,j-1}}{\Delta y}\right)}{\Delta y}+\\ \dfrac{H_{i+1/2,j}\left(\dfrac{V_{i+1,j+1/2}-V_{i+1,j-1/2}}{\Delta y}-\dfrac{V_{i,j+1/2}-V_{i,j-1/2}}{\Delta y}\right)}{\Delta x}\end{array}\right]$$

$$=\frac{\bar{\varepsilon}.H_{i+1/2,j}}{\Delta x^2}\left[2\left(U_{i+3/2,j}+U_{i-1/2,j}\right)-6U_{i+1/2,j}+U_{i+1/2,j+1}+U_{i+1/2,j-1}+V_{i+1,j+1/2}-V_{i+1,j-1/2}-V_{i,j+1/2}+V_{i,j-1/}\right.$$

(4.13)

Putting all together and discretising the other terms for the x-direction gives:

$$\left(\frac{p_{i+1/2,j}^{n+1}-p_{i+1/2,j}^{n}}{\Delta t}\right)+\frac{\beta}{4\Delta x}\left[\left(p_{i+3/2}^{n}+p_{i+1/2}^{n}\right)\left(U_{i+3/2}^{n}+U_{i+1/2}^{n}\right)-\left(p_{i+1/2}^{n}+p_{i-1/2}^{n}\right)\left(U_{i+1/2}^{n}+U_{i-1/2}^{n}\right)\right]$$

$$+\frac{\beta}{2\Delta y}\left[\left(q_{i+1,j+1/2}^{n+1/2}+q_{i,j+1/2}^{n+1/2}\right)U_{i+1/2,j}^{n}-\left(q_{i+1,j-1/2}^{n+1/2}+q_{i,j-1/2}^{n+1/2}\right)U_{i+1/2,j}^{n}\right]$$

$$+\frac{g}{2\Delta x}.\left(H_{i+1/2,j}^{n}\right)\left(\zeta_{i+1}^{n+1}-\zeta_{i}^{n+1}+\zeta_{i+1}^{n+1/2}-\zeta_{i}^{n+1/2}\right)$$

$$+\frac{g.\left(p_{i+1/2,j}^{n+1}+p_{i+1/2,j}^{n}\right)}{2}.\frac{\sqrt{\left(p_{i+1/2,j}^{n+1/2}\right)^2+\left(q_{i+1/2,j}^{n+1/2}\right)^2}}{\left(C_{i+1/2,j}^{n}\right)^2\left(H_{i+1/2,j}^{n}\right)^2}$$

$$-\frac{\bar{\varepsilon}H_{i+1/2,j}^{n}}{\Delta x^2}\left[2\left(\hat{U}_{i+3/2,j}^{n}+\hat{U}_{i-1/2,j}^{n}\right)+\hat{U}_{i+1/2,j+1}^{n}+\hat{U}_{i+1/2,j-1}^{n}-6\hat{U}_{i+1/2,j}^{n}+V_{i,j-1/2}^{n}-V_{i,j+1/2}^{n}-V_{i+1,j-1/2}^{n}+V_{i+1,j+1/2}^{n}\right.$$

$$=0$$

(4.14)

Rearranging to give in terms of the unknown values gives:

$$-\zeta_i^{n+1}\frac{g.\Delta t.H^n_{i+1/2,j}}{2\Delta x}+p^{n+1}_{i+1/2,j}\left(1+\frac{g\Delta t}{2}.\frac{\sqrt{\left(p^{n+1/2}_{i+1/2,j}\right)^2+\left(q^{n+1/2}_{i+1/2,j}\right)^2}}{\left(C^n_{i+1/2,j}\right)^2\left(H^n_{i+1/2,j}\right)^2}\right)+\zeta^{n+1}_{i+1}\frac{g.\Delta t.H^n_{i+1/2,j}}{2\Delta x}$$

$$=p^n_{i+1/2,j}-\frac{\beta\Delta t}{4\Delta x}\left[\left(p^n_{i+3/2}+p^n_{i+1/2}\right)\left(U^n_{i+3/2}+U^n_{i+1/2}\right)-\left(p^n_{i+1/2}+p^n_{i-1/2}\right)\left(U^n_{i+1/2}+U^n_{i-1/2}\right)\right]-$$

$$\frac{\beta\Delta t}{2\Delta y}\left[\left(q^{n+1/2}_{i+1,j+1/2}+q^{n+1/2}_{i,j+1/2}\right)U^n_{i+1/2,j}-\left(q^{n+1/2}_{i+1,j-1/2}+q^{n+1/2}_{i,j-1/2}\right)U^n_{i+1/2,j}\right]-$$

$$\frac{g\Delta t}{2\Delta x}.\left(H^n_{i+1/2,j}\right)\left(\zeta^{n+1/2}_{i+1}-\zeta^{n+1/2}_i\right)+\frac{\bar{\varepsilon}\Delta t H^n_{i+1/2,j}}{\Delta x^2}\left[2\left(\hat{U}^n_{i+3/2,j}+\hat{U}^n_{i-1/2,j}\right)+\hat{U}^n_{i+1/2,j+1}+\hat{U}^n_{i+1/2,j-1}\right.$$

$$\left.-6\hat{U}^n_{i+1/2,j}+V^n_{i,j-1/2}-V^n_{i,j+1/2}-V^n_{i+1,j-1/2}+V^n_{i+1,j+1/2}\right]-\frac{g\Delta t\left(p^n_{i+1/2,j}\right)}{2}.\frac{\sqrt{\left(p^{n+1/2}_{i+1/2,j}\right)^2+\left(q^{n+1/2}_{i+1/2,j}\right)}}{\left(C^n_{i+1/2,j}\right)^2\left(H^n_{i+1/2,j}\right)^2}$$

$$=0 \qquad (4.15)$$

where $\hat{U}$ denotes a value corrected by iteration by setting:

$$\hat{U}^n=\begin{cases}U^{n-1/2} & \textit{for the first iteration,}\\ \frac{1}{2}\left(U^{n-1/2}+U^{n+1/2}\right) & \textit{for the second and remaining iterations}\end{cases} \qquad (4.16)$$

The corrections of the velocities (U and V) were necessary due to the fact that non-linear terms in the momentum equations can give rise to instabilities even though an implicit scheme has been used (Weare, 1976; Falconer et al., 2001a). Different researchers have identified different approaches to overcome this problem. Some of them include time centring differences using three time levels or a velocity smoothing algorithm or time centred iteration for the non-linear advective acceleration and the eddy viscosity terms. The latter approach had been used for this study. For further details see Falconer et al (2001a).

and for the second sweep in the y-direction and using similar analysis

$$\frac{\partial q}{\partial t}=\left(\frac{q^{n+3/2}_{i,j+1/2}-q^{n+1/2}_{i,j+1/2}}{\Delta t}\right) \qquad (4.17)$$

$$\begin{aligned}\frac{\partial \beta qU}{\partial x} &= \frac{\partial \beta UHV}{\partial x} = \frac{\partial \beta pV}{\partial x} \\ &= \beta\left[\frac{\partial pV}{\partial x}\right] = \beta\left[\frac{(pV)^{n+1}_{i+1/2,j+1/2} - (pV)^{n+1}_{i-1/2,j+1/2}}{\Delta x}\right] \\ &= \frac{\beta}{\Delta x}\left[\frac{\left(p^{n+1}_{i+1/2,j+1} + p^{n+1}_{i+1/2,j}\right)}{2} V^{n+1/2}_{i,j+1/2} - \frac{\left(p^{n+1}_{i-1/2,j+1} + p^{n+1}_{i-1/2,j}\right)}{2}\right] \\ &= \frac{\beta}{2\Delta x}\left[\left(p^{n+1}_{i+1/2,j+1} + p^{n+1}_{i+1/2,j}\right)V^{n+1/2}_{i,j+1/2} - \left(p^{n+1}_{i-1/2,j+1} + p^{n+1}_{i-1/2,j}\right)V^{n+1/2}_{i,j+1/2}\right]\end{aligned} \tag{4.18}$$

$$\begin{aligned}\frac{\partial \beta qV}{\partial y} &= \beta\left[\frac{\partial qV}{\partial y}\right] = \left[\frac{(qV)^{n+1}_{i,j+1} - (qV)^{n+1}_{i,j}}{\Delta y}\right] \\ &= \frac{\beta}{\Delta y}\left[\frac{\left(q^{n+1}_{j+3/2} + q^{n+1}_{j+1/2}\right)}{2} \cdot \frac{\left(V^{n+1}_{j+3/2} + V^{n+1}_{j+1/2}\right)}{2} - \frac{\left(q^{n+1}_{j+1/2} + q^{n+1}_{j-1/2}\right)}{2} \cdot \frac{\left(V^{n+1}_{j+1/2} + V^{n+1}_{j-1/2}\right)}{2}\right] \\ &= \frac{\beta}{4\Delta y}\left[\left(q^{n+1}_{j+3/2} + p^{n+1}_{j+1/2}\right)\left(V^{n+1}_{j+3/2} + V^{n+1}_{j+1/2}\right) - \left(q^{n+1}_{j+1/2} + q^{n+1}_{j-1/2}\right)\left(V^{n+1}_{j+1/2} + V^{n+1}_{j-1/2}\right)\right]\end{aligned} \tag{4.19}$$

Combining all the discretisations and arranging gives:

$$\left(\frac{q_{i,j+1/2}^{n+3/2}-q_{i,j+1/2}^{n+1/2}}{\Delta t}\right)+\frac{\beta}{2\Delta x}\left[\left(p_{i+1/2,j+1}^{n+1}+p_{i+1/2,j}^{n+1}\right)V_{i,j+1/2}^{n+1/2}-\left(p_{i-1/2,j+1}^{n+1}+p_{i-1/2,j}^{n+1}\right)V_{i,j+1/2}^{n+1/2}\right]$$

$$+\frac{\beta}{4\Delta y}\left[\left(q_{j+3/2}^{n+1}+q_{j+1/2}^{n+1}\right)\left(V_{j+3/2}^{n+1}+V_{j+1/2}^{n+1}\right)-\left(q_{j+1/2}^{n+1}+q_{j-1/2}^{n+1}\right)\left(V_{j+1/2}^{n+1}+V_{j-1/2}^{n+1}\right)\right]$$

$$+\frac{g}{4\Delta y}.\left(H_{i,j+1/2}^{n+1}\right)\left(\zeta_{j+1}^{n+3/2}-\zeta_{j}^{n+3/2}+\zeta_{j+1}^{n+1}-\zeta_{j}^{n+1}\right)$$

$$+\frac{g\left(q_{i,j+1/2}^{n+3/2}+q_{i,j+1/2}^{n+1/2}\right)}{2}.\frac{\sqrt{\left(p_{i,j+1/2}^{n+1}\right)^2+\left(q_{i,j+1/2}^{n+1}\right)^2}}{\left(C_{i,j+1/2}^{n+1}\right)^2\left(H_{i,j+1/2}\right)^2}$$

$$-\frac{\bar{\varepsilon}H_{i,j+1/2}^{n+1}}{\Delta y^2}\left[2\left(\hat{V}_{i+3/2,j}^{n+1}+\hat{V}_{i,j-1/2}^{n+1}\right)+\hat{V}_{i+1,j+1/2}^{n+1}+\hat{V}_{i-1,j+1/2}^{n+1}\right.$$

$$\left.-6\hat{V}_{i,j+1/2}^{n+1}+U_{i-1/2,j}^{n+1}-U_{i+1/2,j}^{n+1}-U_{i-1/2,j+1}^{n+1}+U_{i+1/2,j+1}^{n+1}\right]=0$$

(4.20)

Isolating the terms gives:

$$-\zeta_{j}^{n+3/2}\frac{g.\Delta t.H_{i,j+1/2}^{n+1}}{2\Delta x}+q_{i,j+1/2}^{n+3/2}\left(1+\frac{g\Delta t}{2}.\frac{\sqrt{\left(p_{i,j+1/2}^{n+1}\right)^2+\left(q_{i,j+1/2}^{n+1}\right)^2}}{\left(C_{i,j+1/2}^{n+1}\right)^2\left(H_{i,j+1/2}^{n+1}\right)^2}\right)+\zeta_{j+1}^{n+3/2}\frac{g.\Delta t.H_{i,j+1/2}^{n+1}}{2\Delta x}$$

$$=q_{i,j+1/2}^{n+1/2}-\frac{\beta}{2\Delta x}\left[\left(p_{i+1/2,j+1}^{n+1}+p_{i+1/2,j}^{n+1}\right)V_{i,j+1/2}^{n+1/2}-\left(p_{i-1/2,j+1}^{n+1}+p_{i-1/2,j}^{n+1}\right)V_{i,j+1/2}^{n+1/2}\right]-$$

$$\frac{\beta}{4\Delta y}\left[\left(q_{j+3/2}^{n+1}+q_{j+1/2}^{n+1}\right)\left(V_{j+3/2}^{n+1}+V_{j+1/2}^{n+1}\right)-\left(q_{j+1/2}^{n+1}+q_{j-1/2}^{n+1}\right)\left(V_{j+1/2}^{n+1}+V_{j-1/2}^{n+1}\right)\right]-$$

$$\frac{g\Delta t}{2\Delta x}.\left(H_{i,j+1/2}^{n+1}\right)\left(\zeta_{j+1}^{n+1}-\zeta_{j}^{n+1}\right)+\frac{\bar{\varepsilon}\Delta t H_{i,j+1/2}^{n+1}}{\Delta x^2}\left[2\left(\hat{V}_{i+3/2,j}^{n+1}+\hat{V}_{i,j-1/2}^{n+1}\right)+\hat{V}_{i+1,j+1/2}^{n+1}+\hat{V}_{i-1,j+1/2}^{n+1}\right.$$

$$\left.-6\hat{V}_{i,j+1/2}^{n+1}+U_{i-1/2,j}^{n+1}-U_{i+1/2,j}^{n+1}-U_{i-1/2,j+1}^{n+1}+U_{i+1/2,j+1}^{n+1}\right]-\frac{g\Delta t\left(q_{i,j+1/2}^{n+1}\right)}{2}.\frac{\sqrt{\left(p_{i,j+1/2}^{n+1}\right)^2+\left(q_{i,j+1/2}^{n+1}\right)^2}}{\left(C_{i,j+1/2}^{n+1}\right)^2\left(H_{i,j+1/2}^{n+1}\right)}$$

(4.21)

$$\hat{V}^{n+1}=\begin{cases}V^{n+1/2} & \textit{for the first iteration}\\ \frac{1}{2}\left(V^{n+1/2}+V^{n+3/2}\right) & \textit{for the second iteration and remaining ones}\end{cases}$$

In summary, the surface water coefficients for momentum discretisation can be written in matrix form as:

$$E\zeta_i^{n+1} + Fp_{i+1/2}^{n+1} + G\zeta_{i+1}^{n+1} = L_x \qquad (4.22a)$$

$$E\zeta_j^{n+3/2} + Fq_{j+1/2}^{n+3/2} + G\zeta_{j+1}^{n+3/2} = L_y \qquad (4.22b)$$

where

$$E = -\frac{g.\Delta tH}{2\Delta x} = -G$$

$$F = \left(1 + \frac{g\Delta t}{2}.\frac{\sqrt{p^2+q^2}}{C^2H^2}\right)$$

$$L_x = p_{i+1/2,j}^n - \frac{\beta\Delta t}{4\Delta x}\left[\left(p_{i+3/2}^n + p_{i+1/2}^n\right)\left(U_{i+3/2}^n + U_{i+1/2}^n\right) - \left(p_{i+1/2}^n + p_{i-1/2}^n\right)\left(U_{i+1/2}^n + U_{i-1/2}^n\right)\right] -$$

$$\frac{\beta\Delta t}{2\Delta y}\left[\left(q_{i+1,j+1/2}^{n+1/2} + q_{i,j+1/2}^{n+1/2}\right)U_{i+1/2,j}^n - \left(q_{i+1,j-1/2}^{n+1/2} + q_{i,j-1/2}^{n+1/2}\right)U_{i+1/2,j}^n\right] -$$

$$\frac{g\Delta t}{2\Delta x}.\left(H_{i+1/2,j}^n\right)\left(\zeta_{i+1}^{n+1/2} - \zeta_i^{n+1/2}\right) + \frac{\bar{\varepsilon}\Delta tH_{i+1/2,j}^{n+1/2}}{\Delta x^2}\left[2\left(\hat{U}_{i+3/2,j}^n + \hat{U}_{i-1/2,j}^n\right) + \hat{U}_{i+1/2,j+1}^n + U_{i+1/2,j-1}^n\right.$$

$$\left. - 6\hat{U}_{i+1/2,j}^n + V_{i,j-1/2}^n - V_{i,j+1/2}^n - V_{i+1,j-1/2}^n + V_{i+1,j+1/2}^n\right] - \frac{g\Delta t\left(p_{i+1/2,j}^n\right)}{2}.\frac{\sqrt{\left(p_{i+1/2,j}^{n+1/2}\right)^2 + \left(q_{i+1/2,j}^{n+1/2}\right)^2}}{\left(C_{i+1/2,j}^n\right)^2\left(H_{i+1/2,j}^n\right)^2}$$

$$L_y = q_{i,j+1/2}^{n+1/2} - \frac{\beta}{2\Delta x}\left[\left(p_{i+1/2,j+1}^{n+1} + p_{i+1/2,j}^{n+1}\right)V_{i,j+1/2}^{n+1/2} - \left(p_{i-1/2,j+1}^{n+1} + p_{i-1/2,j}^{n+1}\right)V_{i,j+1/2}^{n+1/2}\right] -$$

$$\frac{\beta}{4\Delta y}\left[\left(q_{j+3/2}^{n+1} + q_{j+1/2}^{n+1}\right)\left(V_{j+3/2}^{n+1} + V_{j+1/2}^{n+1}\right) - \left(q_{j+1/2}^{n+1} + q_{j-1/2}^{n+1}\right)\left(V_{j+1/2}^{n+1} + V_{j-1/2}^{n+1}\right)\right] -$$

$$\frac{g\Delta t}{2\Delta x}.\left(H_{i,j+1/2}^{n+1}\right)\left(\zeta_{j+1}^{n+1} - \zeta_j^{n+1}\right) + \frac{\bar{\varepsilon}\Delta tH_{i,j+1/2}^{n+1}}{\Delta x^2}\left[2\left(\hat{V}_{i+3/2}^{n+1} + \hat{V}_{i,j-1/2}^{n+1}\right) + \hat{V}_{i+1,j+1/2}^{n+1} + \hat{V}_{i-1,j+1/2}^{n+1}\right.$$

$$\left. - 6\hat{V}_{i,j+1/2}^{n+1} + U_{i-1/2,j}^{n+1} - U_{i+1/2,j}^{n+1} - U_{i-1/2,j+1}^{n+1} + \hat{U}_{i+1/2,j+1}^{n+1}\right] - \frac{g\Delta t\left(q_{i,j+1/2}^{n+1}\right)}{2}.\frac{\sqrt{\left(p_{i,j+1/2}^{n+1}\right)^2 + \left(q_{i,j+1/2}^{n+1}\right)^2}}{\left(C_{i,j+1/2}^{n+1}\right)^2\left(H_{i,j+1/2}^{n+1}\right)^2}$$

4.3.2.2 Groundwater

From the Darcy's law as given by equation (3.27),

$$\left.\begin{aligned} p + KH\frac{\partial \zeta}{\partial x} = 0 \\ q + KH\frac{\partial \zeta}{\partial y} = 0 \end{aligned}\right\} \tag{4.23}$$

where the symbols have their usual meanings.

Discretising the equation in the x-direction gives:

$$p_{i+1/2}^{n+1} + K_{i+1/2}H_{i+1/2}^{n+1/2}\left(\frac{1}{2}\frac{\zeta_{i+1}^{n+1} - \zeta_i^{n+1}}{\Delta x} + \frac{1}{2}\frac{\zeta_{i+1}^{n+1/2} - \zeta_i^{n+1/2}}{\Delta x}\right) = 0$$

$$-\frac{K_{i+1/2}H_{i+1/2}^{n+1/2}}{2\Delta x}.\zeta_i^{n+1} + p_{i+1/2}^{n+1} + \frac{K_{i+1/2}H_{i+1/2}^{n+1/2}}{2\Delta x}.\zeta_{i+1}^{n+1} = -\frac{K_{i+1/2}H_{i+1/2}^{n+1/2}}{2\Delta x}.\left(\zeta_{i+1}^{n+1/2} - \zeta_i^{n+1/2}\right) \tag{4.24}$$

For the y-direction, the discretisation is given by:

$$q_{j+1/2}^{n+3/2} + K_{j+1/2}H_{j+1/2}^{n+1}\left(\frac{1}{2}\frac{\zeta_{j+1}^{n+3/2} - \zeta_j^{n+3/2}}{\Delta y} + \frac{1}{2}\frac{\zeta_{j+1}^{n+1} - \zeta_j^{n+1}}{\Delta y}\right) = 0$$

$$-\frac{K_{j+1/2}H_{j+1/2}^{n+1}}{2\Delta y}.\zeta_j^{n+3/2} + q_{j+1/2}^{n+3/2} + \frac{K_{j+1/2}H_{j+1/2}^{n+1}}{2\Delta y}.\zeta_{j+1}^{n+3/2} = -\frac{K_{j+1/2}H_{j+1/2}^{n+1}}{2\Delta y}.\left(\zeta_{j+1}^{n+1} - \zeta_j^{n+1}\right) \tag{4.25}$$

In summary, the groundwater coefficients for the momentum discretisation can be written in matrix forms as:

$$E^*\zeta_i^{n+1} + F^* p_{i+1/2}^{n+1} + G^*\zeta_{i+1}^{n+1} = L_x^* \tag{4.26a}$$

$$E^*\zeta_j^{n+3/2} + F^* q_{j+1/2}^{n+3/2} + G^*\zeta_{j+1}^{n+3/2} = L_y^* \tag{4.26b}$$

where

$$E^* = -\frac{KH}{2\Delta x} = -G^*$$

$$F^* = 1$$

$$L_x^* = -\frac{K_{i+1/2}H_{i+1/2}^{n+1/2}}{2\Delta x}\left(\zeta_{i+1}^{n+1/2} - \zeta_i^{n+1/2}\right)$$

$$L_y^* = -\frac{K_{j+1/2}H_{j+1/2}^{n+1}}{2\Delta y}\left(\zeta_{j+1}^{n+1} - \zeta_j^{n+1}\right)$$

4.3.3 Solution procedure of discretised equations

The equations are solved by re-arranging the terms in such a way that recurrence relationships are defined for their solution. These equations can be written for the respective directions as follows:

X-direction

$$Ap_{i-1/2}^{n+1} + B\zeta_i^{n+1} + Cp_{i+1/2}^{n+1} = D_x$$
$$E\zeta_i^{n+1} + Fp_{i+1/2}^{n+1} + G\zeta_{i+1}^{n+1} = L_x$$

Y-direction

$$Aq_{j-1/2}^{n+3/2} + B\zeta_j^{n+3/2} + Cq_{j+1}^{n+3/2} = D_y$$
$$E\zeta_j^{n+3/2} + Fq_{j+1/2}^{n+3/2} + G\zeta_{j+1}^{n+3/2} = L_y$$
$$E\zeta_j^{n+3/2} + Fq_{j+1/2}^{n+3/2} + G\zeta_{j+1}^{n+3/2} = L_y$$

Separating the unknown variables ζ_i^{n+1} and $p_{i+1/2}^{n+1}$ gives:

$$\zeta_i^{n+1} = \frac{D_x - Cp_{i+1/2}^{n+1} - Ap_{i-1/2}^{n+1}}{B} = \frac{-C}{B} p_{i+1/2}^{n+1} + \frac{D_x - Ap_{i-1/2}^{n+1}}{B}$$

and

$$p_{i+1/2}^{n+1} = \frac{L_x - G\zeta_{i+1}^{n+1} - E\zeta_i^{n+1}}{F} = \frac{-G}{F}\zeta_{i+1}^{n+1} + \frac{L_x - E\zeta_i^{n+1}}{F}$$

These equations can now be re-written as:

(a) $\zeta_i^{n+1} = -P_i p_{i+1/2}^{n+1} + Q_i$ and (b) $p_{i+1/2}^{n+1} = -R_i\zeta_{i+1}^{n+1} + S_i$

where

$$P_i = \frac{C}{B} \quad \text{and} \quad Q_i = \frac{D_x - Ap_{i-1/2}^{n+1}}{B}$$

$$R_i = \frac{G}{F} \quad \text{and} \quad S_i = \frac{L_x - E\zeta_i^{n+1}}{F}$$

In writing equation (b) in an i-1/2 format gives:

$$p_{i+1/2}^{n+1} = -R_i\zeta_{i+1}^{n+1} + S_i$$
$$p_{i-1/2}^{n+1} = -R_{i-1}\zeta_i^{n+1} + S_{i-1}$$

where

$$R_{i-1} = \frac{G}{F}, \quad S_{i-1} = \frac{L_x - E\zeta_{i-1}^{n+1}}{F}$$

By now applying re-cursive techniques and back substitution, we can re-write the original equation for ζ_i^{n+1} as:

$$\zeta_i^{n+1} = \frac{-C}{B} p_{i+1/2}^{n+1} + \frac{D_x - Ap_{i-1/2}^{n+1}}{B}$$

$$= -\frac{C}{B} p_{i+1/2}^{n+1} + \frac{D_x - A\left(-R_{i-1}\zeta_i^{n+1} + S_{i-1}\right)}{B}$$

$$B\zeta_i^{n+1} = -Cp_{i+1/2}^{n+1} + D_x + AR_{i-1}\zeta_i^{n+1} - AS_{i-1}$$

$$\zeta_i^{n+1}\left(B - AR_{i-1}\right) = -Cp_{i+1/2}^{n+1} + D_x - AS_{i-1}$$

$$\zeta_i^{n+1} = \frac{-C}{B - AR_{i-1}} p_{i+1/2}^{n+1} + \frac{D_x - AS_{i-1}}{B - AR_{i-1}}$$

The same formulation can be used for the equation for $p_{i+1/2}^{n+1}$ whereupon, giving:

$$p_{i+1/2}^{n+1} = -\frac{G}{F}\zeta_{i+1}^{n+1} + \frac{L_x - E\left(-P_i p_{i+1/2}^{n+1} + Q_i\right)}{F}$$

$$p_{i+1/2}^{n+1} = \frac{-G}{F - EP_i}\zeta_{i+1}^{n+1} + \frac{L_x - EQ_i}{F - EP_i}$$

Hence the recurrence relationships become:

$$P_i = \frac{C}{B - AR_{i-1}}, \quad R_i = \frac{G}{F - EP_i}$$
$$Q_i = \frac{D_x - AS_{i-1}}{B - AR_{i-1}}, \quad S_i = \frac{L_x - EQ_i}{F - EP_i}$$

From the above equation, $A = -C$ and $E = -G$, giving for the relationships:

$$P_i = \frac{C_i}{B_i + C_i R_{i-1}}, \quad R_i = \frac{G_i}{F_i - G_i P_i}$$
$$Q_i = \frac{D_{xi} + C_i S_{i-1}}{B_i + C_i R_{i-1}}, \quad S_i = \frac{L_{xi} + G_i Q_i}{F_i + G_i P_i}$$

The same procedure can be used for the y-direction equations starting from:

$$\zeta_j^{n+3/2} = -P_j q_{j+1/2}^{n+3/2} + Q_j$$
$$q_{j+1/2}^{n+3/2} = -R_j \zeta_{j+1}^{n+1} + S_j$$

4.3.4 Equations of solute transport

The governing solute transport equation for x and y directions can be found in section 3.2.1 and re-written for purposes of the discretisation procedure.

$$\frac{\partial H\phi}{\partial t} + \frac{\partial HU\phi}{\partial x} + \frac{\partial HV\phi}{\partial y} - \frac{\partial}{\partial x}\left[D_{xx} H \frac{\partial \phi}{\partial x} + D_{xy} H \frac{\partial \phi}{\partial y}\right] - \frac{\partial}{\partial y}\left[D_{yx} H \frac{\partial \phi}{\partial x} + D_{yy} H \frac{\partial \phi}{\partial y}\right]$$
$$= H[\phi_s + \phi_d + \phi_k] \qquad (4.27)$$

The discretisation procedure was based on Figures 4.1 and 4.2 with the solute ϕ having the same level as the water elevation ζ. In solving the solute transport equation for each time step, it should be noted that the choice of the time step should take into consideration the stability conditions of the solute transport equation.

Thus the two-dimensional solute transport equation can be written for the first half time step as Falconer et al (2001a):

$$
\begin{aligned}
&(\phi H)_{i,j}^{n+1}+\frac{\Delta t}{4\Delta x}\left[p_{i+1/2,j}^{n+1}\left(\phi_{i+1,j}^{n+1}+\phi_{i,j}^{n+1}\right)-p_{i-1/2,j}^{n+1}\left(\phi_{i,j}^{n+1}-\phi_{i-1,j}^{n+1}\right)\right]\\
&-\frac{\Delta t}{2\Delta x^{2}}\left[\left(HD_{xx}\right)_{i+1/2,j}^{n+1}\left(\phi_{i+1,j}^{n+1}+\phi_{i,j}^{n+1}\right)-\left(HD_{xx}\right)_{i-1/2,j}^{n+1}\left(\phi_{i,j}^{n+1}-\phi_{i-1,j}^{n+1}\right)\right]\\
&=(\phi H)_{i,j}^{n+1/2}-\frac{\Delta t}{4\Delta y}\left[q_{i,j+1/2}^{n+1/2}\left(\phi_{i,j+1}^{n+1/2}+\phi_{i,j}^{n+1/2}\right)-q_{i,j-1/2}^{n+1/2}\left(\phi_{i,j}^{n+1/2}+\phi_{i,j-1}^{n+1/2}\right)\right]\\
&+\frac{\Delta t}{2\Delta y^{2}}\left[\left(HD_{yy}\right)_{i,j+1/2}^{n+1/2}\left(\phi_{i,j+1}^{n+1/2}+\phi_{i,j}^{n+1/2}\right)-\left(HD_{yy}\right)_{i,j-1/2}^{n+1/2}\left(\phi_{i,j}^{n+1/2}-\phi_{i,j-1}^{n+1/2}\right)\right]\\
&+\frac{\Delta t}{2\Delta x\Delta y}\left[\left(HD_{xy}\right)_{i+1/2,j}^{n+1/2}\left(\phi_{i+1/2,j+1/2}^{n+1/2}-\phi_{i+1/2,j-1/2}^{n+1/2}\right)\right]-\left[\left(HD_{xy}\right)_{i-1/2,j}^{n+1/2}\left(\phi_{i-1/2,j+1/2}^{n+1/2}-\phi_{i-1/2,j-1/2}^{n+1/2}\right)\right]\\
&+\frac{\Delta t}{2\Delta x\Delta y}\left[\left(HD_{yx}\right)_{i,j+1/2}^{n+1/2}\left(\phi_{i+1/2,j+1/2}^{n+1/2}-\phi_{i+1/2,j+1/2}^{n+1/2}\right)\right]-\left[\left(HD_{yx}\right)_{i,j-1/2}^{n+1/2}\left(\phi_{i-1/2,j-1/2}^{n+1/2}-\phi_{i-1/2,j-1/2}^{n+1/2}\right)\right]\\
&+\frac{\beta^{s}\Delta t}{2\Delta x}\left[p_{i+1/2,j}^{n+1}\nabla_{xx}^{2}\phi_{i+1/2,j}^{n+1/2}-p_{i-1/2,j}^{n+1}\nabla_{xx}^{2}\phi_{i-1/2,j}^{n+1/2}\right]\\
&+\frac{\beta^{s}\Delta t}{2\Delta y}\left[q_{i,j+1/2}^{n+1/2}\nabla_{yy}^{2}\phi_{i,j+1/2}^{n+1/2}-q_{i,j-1/2}^{n}\Delta_{yy}^{2}\phi_{i,j-1/2}^{n+1/2}\right]+\frac{\Delta t}{2}\theta_{s}\delta(x_{s},y_{s})
\end{aligned}
\tag{4.28}
$$

where

$$
\nabla_{yy}^{2}\phi_{i,j+1/2}^{n+1/2}=\begin{cases}\phi_{i,j+1}^{n+1/2}-2\phi_{i,j}^{n+1/2}+\phi_{i,j-1}^{n+1/2} & \text{if} \quad V_{i,j+1/2}^{n+1/2}\geq 0\\ \phi_{i,j+2}^{n+1/2}-2\phi_{i,j+1}^{n+1/2}+\phi_{i,j}^{n+1/2} & \text{if} \quad V_{i+1/2,j}^{n+1/2}\leq 0\end{cases}
\tag{4.29}
$$

$$
\nabla_{xx}^{2}\phi_{i+1/2,j}^{n+1/2}=\begin{cases}\phi_{i+1,j}^{n+1/2}-2\phi_{i,j}^{n+1/2}+\phi_{i-1,j}^{n+1/2} & \text{if} \quad U_{i+1/2,j}^{n+1/2}\geq 0\\ \phi_{i+2,j}^{n+1/2}-2\phi_{i+1,j}^{n+1/2}+\phi_{i,j}^{n+1/2} & \text{if} \quad U_{i+1/2,j}^{n+1/2}\leq 0\end{cases}
\tag{4.30}
$$

$$
\phi_{i+1/2,j+1/2}^{n+1/2}=\frac{1}{4}\left(\phi_{i+1,j+1}^{n+1/2}+\phi_{i+j}^{n+1/2}+\phi_{i,j+1}^{n+1/2}+\phi_{i,j}^{n+1/2}\right)
\tag{4.31}
$$

where $\delta(x_s,y_s)$ is a point unit pulse function used to introduce source or sink at the given point (x_s,y_s). The function takes the value:

$$
\delta(x_s,y_s)=\begin{cases}1 & \text{if } x=x_s \quad \text{and } y=y_s\\ 0 & \text{otherwise}\end{cases}
\tag{4.32}
$$

The value for β^s of 1/6, 1/8 and 0 corresponds to ADI-TOASOD, ADI-QUICK and second order central difference schemes respectively, where TOASOD stands for Third Order Advection and Second Order Diffusion, and QUICK stands for Quadratic Upwind Interpolation for Convective Kinematics.

For the second half time step the scheme is as follows:

$$
\begin{aligned}
&(\phi H)_{i,j}^{n+3/2} + \frac{\Delta t}{4\Delta y}\left[q_{i,j+1/2}^{n+3/2}\left(\phi_{i,j+1}^{n+3/2} + \phi_{i,j}^{n+3/2}\right) - q_{i,j-1/2}^{n+3/2}\left(\phi_{i,j}^{n+3/2} - \phi_{i,j-1}^{n+3/2}\right)\right] \\
&- \frac{\Delta t}{2\Delta y^2}\left[\left(HD_{yy}\right)_{i,j+1/2}^{n+3/2}\left(\phi_{i,j+1}^{n+3/2} + \phi_{i,j}^{n+3/2}\right) - \left(HD_{yy}\right)_{i,j-1/2}^{n+3/2}\left(\phi_{i,j}^{n+3/2} - \phi_{i,j-1}^{n+3/2}\right)\right] \\
&= (\phi H)_{i,j}^{n+1} - \frac{\Delta t}{4\Delta x}\left[p_{i+1/2,j}^{n+1}\left(\phi_{i+1,j}^{n+1} + \phi_{i,j}^{n+1}\right) - p_{i-1/2,j}^{n+1}\left(\phi_{i,j}^{n+1} + \phi_{i-1,j}^{n+1}\right)\right] \\
&+ \frac{\Delta t}{2\Delta x^2}\left[\left(HD_{xx}\right)_{i,j+1/2}^{n+1}\left(\phi_{i+1,j}^{n+1} + \phi_{i,j}^{n+1}\right) - \left(HD_{xx}\right)_{i-1/2,j}^{n+1}\left(\phi_{i,j}^{n+1} - \phi_{i-1,j}^{n+1}\right)\right] \\
&+ \frac{\Delta t}{2\Delta x\Delta y}\left[\left(HD_{xy}\right)_{i+1/2,j}^{n+1}\left(\phi_{i+1/2,j+1/2}^{n+1} - \phi_{i+1/2,j-1/2}^{n+1}\right)\right] - \left[\left(HD_{xy}\right)_{i-1/2,j}^{n+1}\left(\phi_{i-1/2,j+1/2}^{n+1} - \phi_{i-1/2,j-1/2}^{n+1}\right)\right] \\
&+ \frac{\Delta t}{2\Delta x\Delta y}\left[\left(HD_{yx}\right)_{i,j+1/2}^{n+1}\left(\phi_{i+1/2,j+1/2}^{n+1} - \phi_{i+1/2,j+1/2}^{n+1}\right)\right] - \left[\left(HD_{yx}\right)_{i,j-1/2}^{n+1}\left(\phi_{i+1/2,j-1/2}^{n+1} - \phi_{i-1/2,j-1/2}^{n+1}\right)\right] \\
&+ \frac{\beta^s \Delta t}{2\Delta x}\left[p_{i+1/2,j}^{n+1}\nabla_{xx}^2\phi_{i+1/2,j}^{n+1} - p_{i-1/2,j}^{n+1}\nabla_{xx}^2\phi_{i-1/2,j}^{n+1}\right] \\
&+ \frac{\beta^s \Delta t}{2\Delta y}\left[q_{i,j+1/2}^{n+1/2}\nabla_{yy}^2\phi_{i,j+1/2}^{n+1} - q_{i,j-1/2}^{n+1/2}\Delta_{yy}^2\phi_{i,j-1/2}^{n+1}\right] + \frac{\Delta t}{2}\theta_s\delta(x_s, y_s)
\end{aligned}
\tag{4.33}
$$

The expressions for $\nabla_{xx}^2\phi_{i+1/2,j}^{n+1}$, $\nabla_{yy}^2\phi_{i,j+1/2}^{n+1}$, $\phi_{i+1/2,j+1/2}^{n+1}$ are similar to those given in equations (4.29) to (4.31), only the time level index n+1/2 being replaced by n+1. The resulting discretised equations for both the first-half and second-half time steps are arranged into a tri-diagonal system and solved by the method of Gauss elimination and back substitution.

Falconer et al (2001a) discuss the solution criteria in applying these sets of equations and argue that although the second order central difference scheme (where β =0) is unconditionally stable, the scheme gives rise to severe oscillations especially when the transport processes are advection dominated. The ADI-TOASOD and ADI-QUICK schemes have the same stability constraint for the case of pure advection, given as:

$$\frac{U\Delta t}{\Delta x}+\frac{V\Delta t}{\Delta y}\leq 2$$

It has less restrictive requirements for combined advection and diffusion.

Although the ADI-TOASOD and ADI-QUICK schemes are similar in formulation, the former has a third order accuracy in space whereas the latter only has a second accuracy. Therefore in this study, the ADI-TOASOD is the scheme of choice.

4.4 Boundary Conditions (and Initial Conditions for the Severn Estuary Studies)

Falconer et al. (2001b) discuss initial and boundary conditions for both hydrodynamic and solute transport processes in rivers and estuaries and which are highlighted below. The model refined for this study was a linked 1D-2D so briefly boundary conditions for both rivers (1D) and estuaries (2D) are discussed herein.

4.4.3 Initial conditions (Hydrodynamics)

Initial values for the dependent variables need to be specified in any numerical model. In the case of lateral inflows or outflows, initial values need to be specified for river models. For a cold start the initial discharges or velocities are usually set to zero

across the domain for each river reach, and the water surface elevations are set horizontally, and usually equal to high water for tidal simulations with this corresponding to slack water and minimal currents.

4.4.4 Boundary Conditions (Hydrodynamics)

1D Flows

Several authors have discussed one dimensional channel flows for instance Cunge et al. (1980). The authors have highlighted that one dimensional unsteady flows in channels can be described by two dependent variables, e.g. water stage Z and discharge Q at any river cross section with the basic assumption that the density is constant. Since the fluid motion along the water course is defined by these two dependent variables as a function of two independent variables, space and time, they must be specified at the downstream and upstream ends of the river when solving the hydrodynamic equations. Falconer et al (2001b) give the possible combinations as shown in Table 4.1.

Table 4.1 Types of boundary combinations

Type of Reach	Type of	Boundary
	Upstream	Downstream
1	Water Elevation	Water Elevation
2	Flow	Water Elevation
3	Flow	Flow
4	Water Elevation	Flow

There are four possible combinations along each reach as shown in Table 4.1 above. Time histories of the relevant boundary variables are specified as solution progresses. Depending on the nature of the problem, other pairs of dependent variables e.g. velocity and depth could be defined (Cunge et al., 1980). The equation would be different for different pairs of variables, but the physical assumption would be the same.

2D Flows

Boundary conditions can either be closed or open which are explained below.

It must be understood that the existing model uses the ADI method (described earlier), and that the velocity components in the orthogonal directions are not specified at the same points for the square grid so the solution of the equations parallel to the boundary requires some of the variables to be specified outside the boundary. Thus the specification of boundary conditions for two-dimensional flows is different from one-dimensional flows.

4.4.2.1 Closed Boundary Conditions

A closed boundary can be regarded as a 'wall' boundary so that no flow is permitted to cross the close boundary. This type of boundary may be a land boundary which occurs along coastlines or rivers or adjacent to structures. Values outside the modelling domain, are obtained by assuming a 'no slip' condition (or zero flow velocity at a wall) parallel to the boundary and zero flow perpendicular to the boundary. In addition to this, Nguyen and Quahsine (1997) suggest that the water surface gradient normal to walls be taken as zero as a boundary condition.

Fig 4.3 describes the representation of the closed boundary in the existing model, DIVAST. With this format, values outside the modelling domain are assumed to have a 'no slip condition' parallel to the boundary and zero flow perpendicular to the boundary.

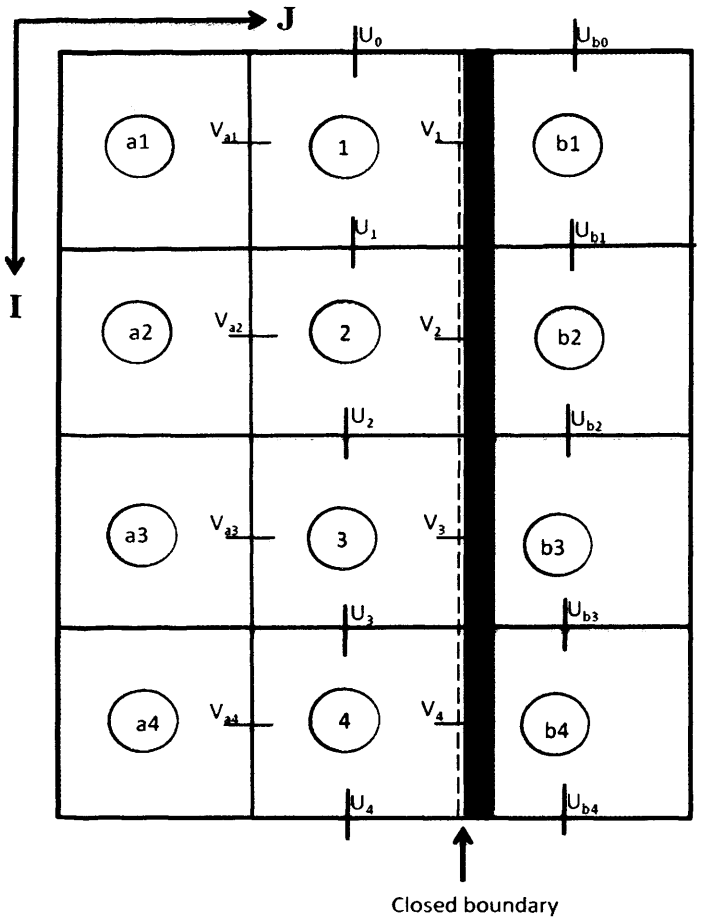

Figure 4.3: Closed boundary (adapted from Falconer et al, 2001a)

In this case, all velocities parallel to the wall are set to zero, whilst the velocities outside the boundary are assigned the same value as the corresponding velocity inside that domain, but negated.

Thus:

$V_1 = V_2 = V_3 = V_4 = 0$

$U_i = -U_{bi}$ $(i=0, 1, 2, 3.....)$

The implication of this condition is that there is no flow across the boundary.

4.4.2.2 Open Boundary Conditions

Unlike the close boundary, the flow and solute fluxes for open boundaries are allowed to cross a boundary. Appropriate hydrodynamic and solute conditions should be specified e.g. measured surface water elevations, velocities and solute values. A free slip boundary condition is used by assuming zero gradient of a variable perpendicular to the open boundary.

Figure 4.4 shows the representation of flow boundary condition as used in this study. The description is outlined below:

$$\begin{cases} V_i = V_{bi}; & (i = 1,2,3,4) \\ U_{bi} = U_i & (i = 0,1,...,4) \end{cases}$$

meaning that the V velocity at the wall is given by the boundary and the corresponding U velocity outside the domain is set equal to the boundary value.

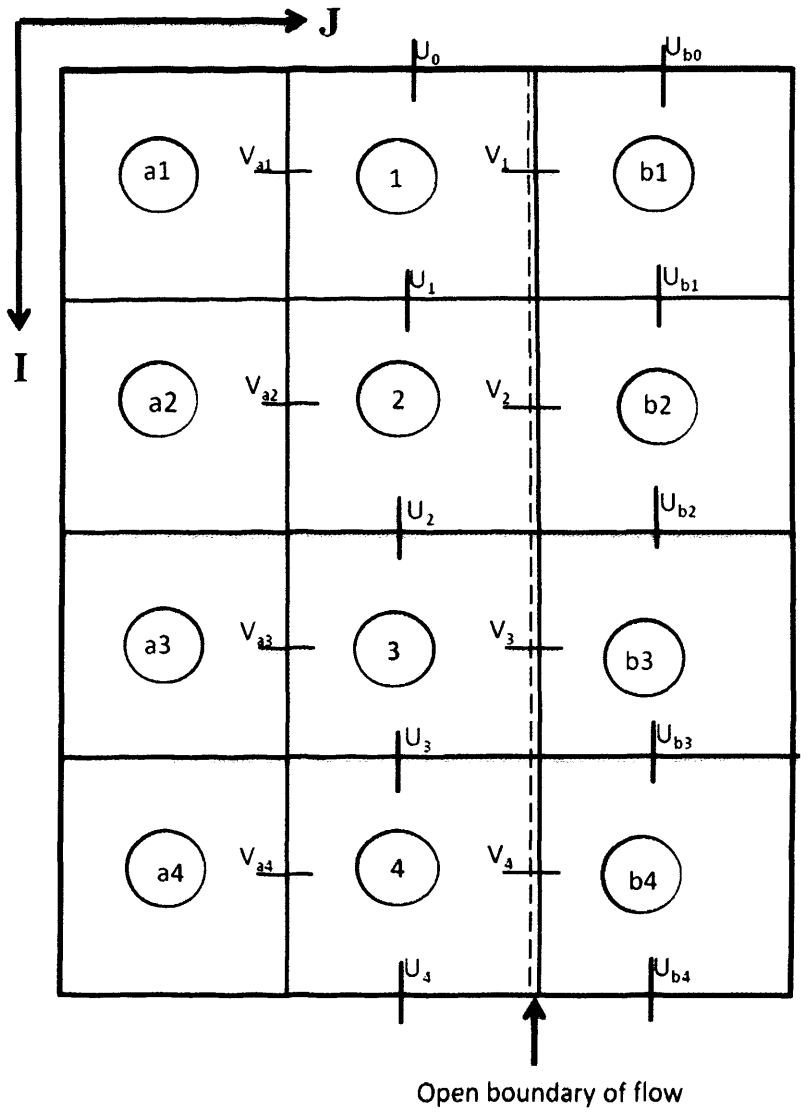

Figure 4.4: Flow open boundary

For a water elevation open boundary as shown in Figure 4.5, the description is as follows:

$$\begin{cases} U_i = U_{ai} & (i = 1,...4) \\ V_i = V_{ai} & (i = 1,...4) \\ \zeta_i = \zeta_{bi} & (i = 1,...4) \end{cases}$$

where ζ_{bi} is the known water elevation at the open boundary.

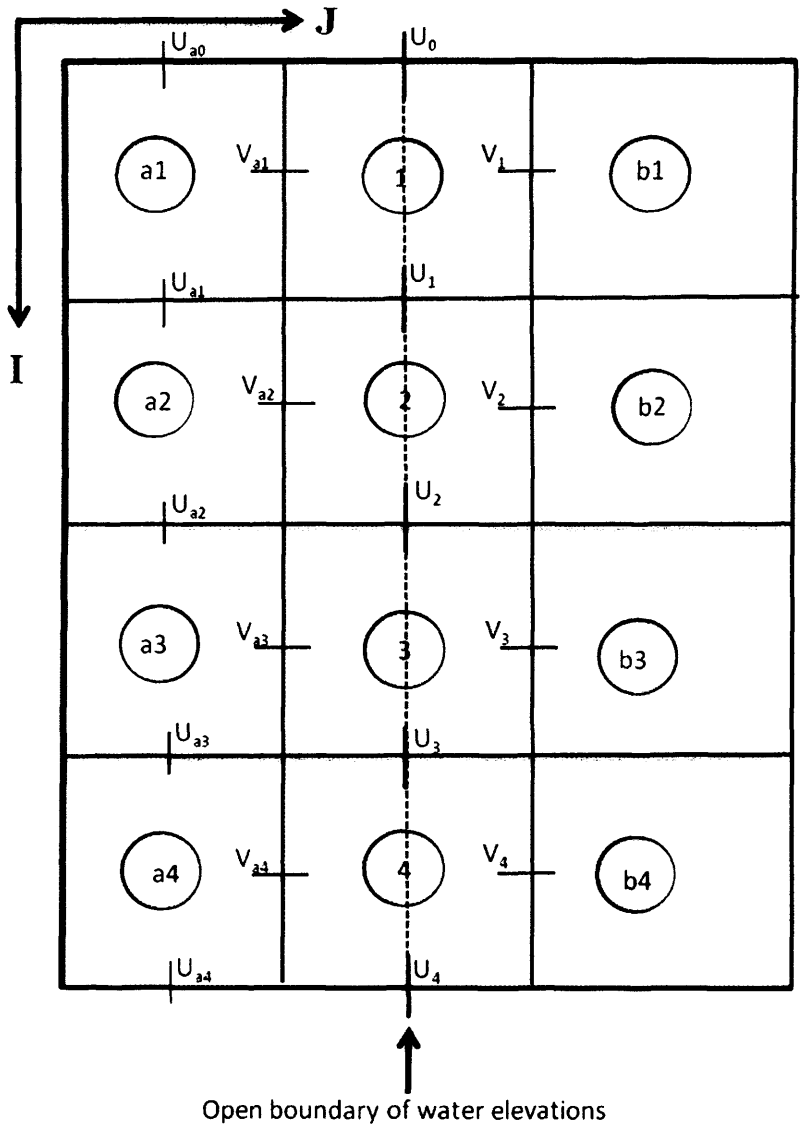

Figure 4.5: Water elevation open boundary

In discussing boundary conditions, Nguyen and Quahsine (1997) observed that one of the principal difficulties in modelling a coastal sea is the problem associated with accurately specifying the seaward open boundary conditions. They agree that in general, at the open boundaries, the tidal surface elevation is a priori prescribed as a Dirichlet condition at all times and also no boundary condition is necessary for the outflow in respect of the momentum equations. This is because the flux can be

calculated from the model. However, when the flow is into the domain, it is necessary to prescribe the advective flux only, with information often not being available at the open boundaries. Nguyen and Quahsine (1997) conclude that the imposition of boundary conditions which do not appropriately match the natural system response can lead to spurious results

4.4.5 Initial Conditions (Solute Transport)

The specification of initial concentration of a solute is not different from specification of hydrodynamic parameters. As discussed by Falconer et al (2001a), in general the concentration is set to zero across the domain at the start of the simulations, or some predetermined concentration when the base concentration is not zero. Reflecting on the initial conditions, Falconer et al (2001a) recommend that the solute concentration be set to a constant value if the solute distribution is initially uniform; and in the following runs during the simulation period the solute concentration is then set to the condition at the end of a previous run so that equilibrium is eventually reached.

4.4.4 Boundary Conditions (Solute Transport)

4.4.4.1 Closed Boundary Conditions

Like the hydrodynamic parameters, the concentration of a solute does not change parallel to a closed boundary and that there is no solute flux across a solid boundary.

For the situation described in Figure 4.3, the solute boundary condition (i.e. at the wall boundary) is given as:

$$\frac{\partial \phi}{\partial y}\Big|_w = 0 \qquad \text{and} \qquad \frac{\partial^2 \phi}{\partial y^2}\Big|_w = 0$$

whereupon the concentration does not change parallel to the closed boundary and that there is no solute flux across the solid boundary.

4.4.4.2 Open Boundary Conditions

The solute concentration must be specified for both the upstream and downstream reaches of a river or an estuary. The solute fluxes are allowed to cross an open boundary. In the case of open boundaries, as shown in Figures 4.4 and 4.5, the solute can be specified as follows:

$$\phi_i = \phi_{bi}$$

For the input of solute concentration levels at the upstream end of a river reach, or through outfalls etc., the concentration has to be specified for known conditions, e.g. where the concentration is zero or at a base value, or preferably from field data (Falconer et al., 2000). In contrast, at the downstream boundary the concentration is extrapolated from within the domain for outgoing flows (Falconer, 1986). For inflow across a downstream boundary, e.g. where the model is applied to an estuary reach and the tide is incoming, then preferably the concentration level is available from field data (e.g. for salinity), or the net outgoing concentration is determined from the ebb tide simulations and a scaling factor is applied to estimate the return current concentration (Falconer, 1986). In their discussions, Falconer et al (2001a) imply that if the flows at the boundary are leaving the domain, specification of solute values outside the boundary is not needed; however if the flows across the open boundary are entering the domain, then solute values immediately outside the boundary are required.

4.4.5 The Severn Estuary

In this study, the Severn Estuary has been used as part of the integrated modelling regime and the open boundaries are stated here for completeness.

In the Severn Estuary model study, for the 1-D part the downstream boundary was specified as a tidal water elevation boundary at the Severn Bridge for the M4 whereas the upstream boundary was specified at the tidal limit of the river at Haw Bridge in the form of an open flow boundary. The latter was set to the average flow rate of the River Severn. The downstream water level was obtained from the Proudman Oceanographic Laboratory (POL) tidal harmonic model for the Bristol Channel. The bed elevation was referenced to ordinance datum at Avonmouth.

For the solute (bacteria) boundary condition, it was assumed that there was no input of bacteria from both the seaward and upstream boundaries.

Since the modelling regime of the estuary was dynamically linked one-and two-dimensional model, the one dimensional model provided the velocity or discharge data at the upstream boundary of the 2-D model, whereas the 2-D model provided the water elevation data at the downstream boundary of the 1-D model.

4.5 Numerical Tests

The refined model has been tested against extensive laboratory data that was collected in the Hyder Hydraulics Laboratory in Cardiff University. The results which are shown in Chapter 6 of this thesis have proven that the model is able to make

predictions correctly for both hydrodynamics and solute transport and for both the surface and sub-surface flows.

4.6 Summary

In this chapter, the numerical solution procedure for the governing equations for both the hydrodynamic and solute transport models are reviewed, and for both the surface and sub-surface flow models. The discretisation method (i.e. alternating direction implicit) for the mass and momentum conservation equations both for the surface and sub-surface equations are given. In addition, the boundary conditions used in the model schemes are also highlighted.

CHAPTER 5 LABORATORY STUDIES

5.1 Introduction

There have been a good number of mathematical models that have been developed and used to study the hydrodynamic and solute transport processes in groundwater and surface water systems in the past decades, but few physical models have integrated both. According to Hughes (1995), field studies provide the best data, but they are usually expensive and involve too many parameters. There can be difficulties in the interpretation of data measured from the field. Comparable to field data collection, physical models have proven to be most realistic relative to the disadvantages of field data collection, which have been enumerated. The major shortcomings of experimental approaches (with the use of physical models) are scaling, non-adaptability, operating costs, equipment needs and technical support (Tannehill et al., 1997; Falconer and Lin, 2003). They may have also over-riding disadvantages of providing erroneous predictions especially in solute transport studies since the processes of dispersion and diffusion are unlikely to be scaled properly, they do have some underlying advantages. In general, physical models enable data to be collected easily and provide controlled data. Falconer (1992) not only noted that physical models could be generally used as an additional engineering design tool, but added that for coastal studies the model domain often needed to be significantly scaled down both vertically and horizontally. In relation to modelling solute transport in porous media, Harris et al. (2000) pointed out that physical models also offer major time-scaling advantages. For example, pore fluid seepage at prototype scales, i.e. over

a period of years, can be simulated in the model in a matter of hours. However, current knowledge on the integrated process relating to tidal, groundwater and shallow surface water flow is rather limited (Ebrahimi K, 2004). In this study a physical model has been set up in the laboratory linking surface and groundwater, and used to provide flow and solute transport data.

The experiments were conducted in the Hyder Hydraulics Laboratory at Cardiff University which has a large tidal basin suitable for this purpose. The laboratory set up generated was not to mimic any prototype but to provide a stand alone approach to hydrodynamics and solute transport phenomenon, between groundwater and surface water systems.

5.2 Tidal Basin

Figure 5.1 shows the flume prior to the start of the study reported herein. A rectangular tank with a suspended base was used for the tidal basin. The overall dimensions of the laboratory flume were 5.3m x 4.1m. Water was supplied from pipes connected to the main re-circulation tank. Water enters the basin through a large perforated pipe as shown in Figure 5.1, and accumulates underneath the suspended base of the model. Holes in the suspended floor of the basin allowed the water level to rise to a predefined elevation within the flume. The water level in the main area of the flume was controlled by a movable weir on the right hand side of the figure. Water was pumped into the area between the baffle and the weir, to ensure that the water level is always the same as the weir elevation. The weir was then raised or lowered manually, or via a computer program and the water levels in the flume followed the movement of the weir (see Fig5.2 (a) and (b)). The first baffle after the weir reduced

the turbulence the pumped inlet from entering the flume area, thus ensuring that water levels in the flume area changed smoothly.

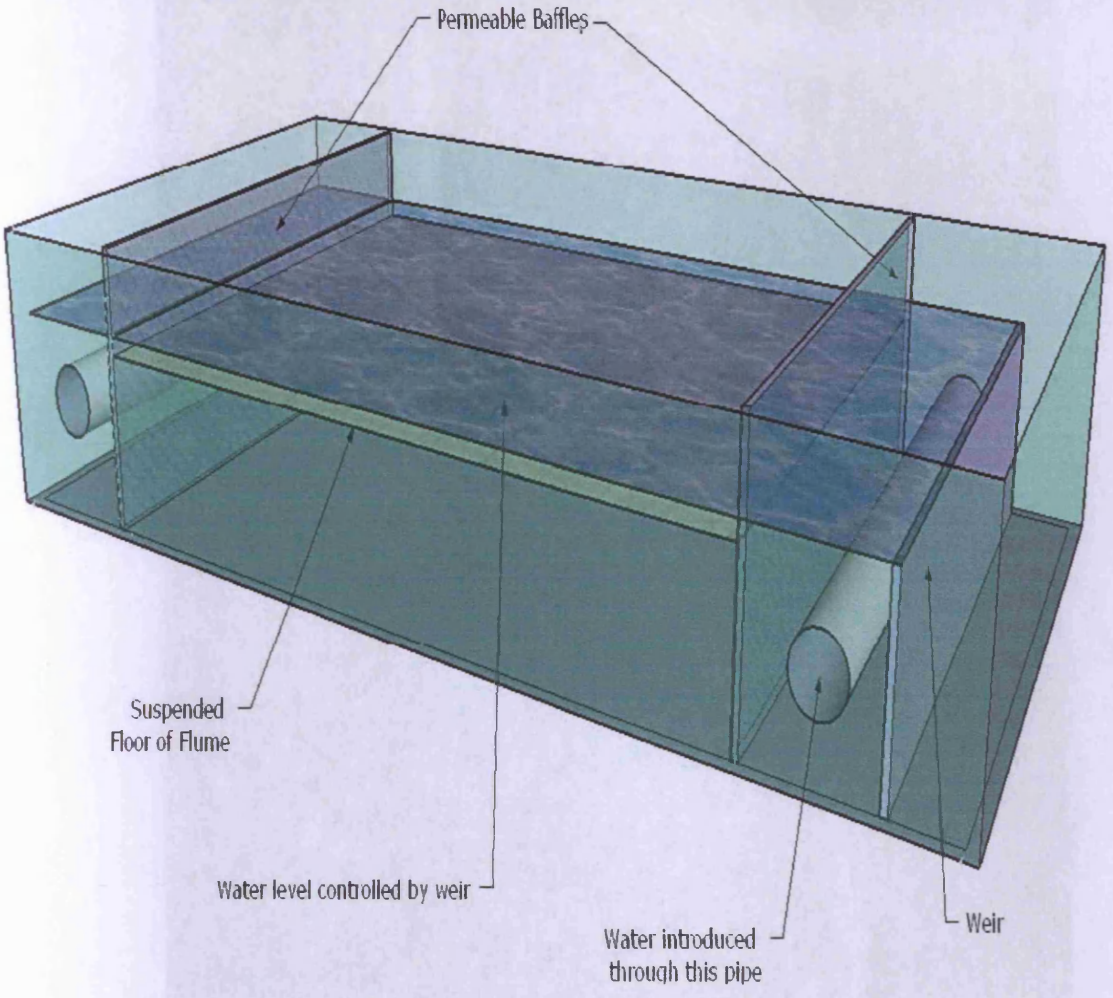

Figure 5.1: Arrangements in the tidal basin

5.3 Foam in the tidal basin

Figures 5.3 and 5.4 show the layout of foam blocks as the initial studies set up in the flume. Four holes were bored in each block of foam to measure the head and solute levels; in contrast the original studies had two holes bored across each transect. The number was increased after efforts were made to find a way to allow the dye to move into the holes. Thus most of the water level measurements were conducted with two holes in each transect as a section is shown in Figure 5.7.

(a)

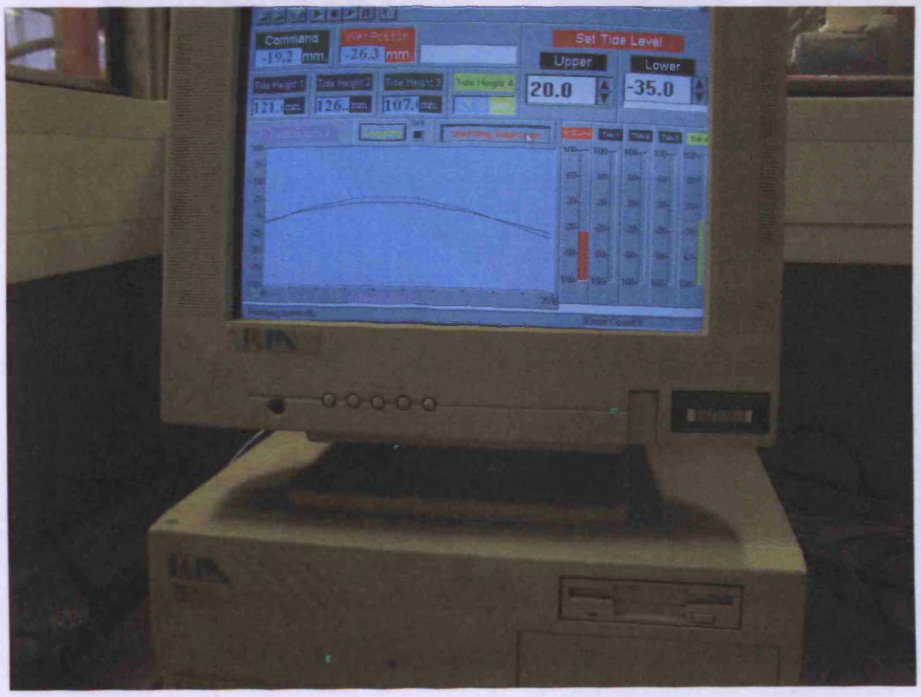

(b)

Figure 5.2: (a) Oscillating weir and foam as lay out in the flume (b) coupled computer to tidal basin showing tidal cycles

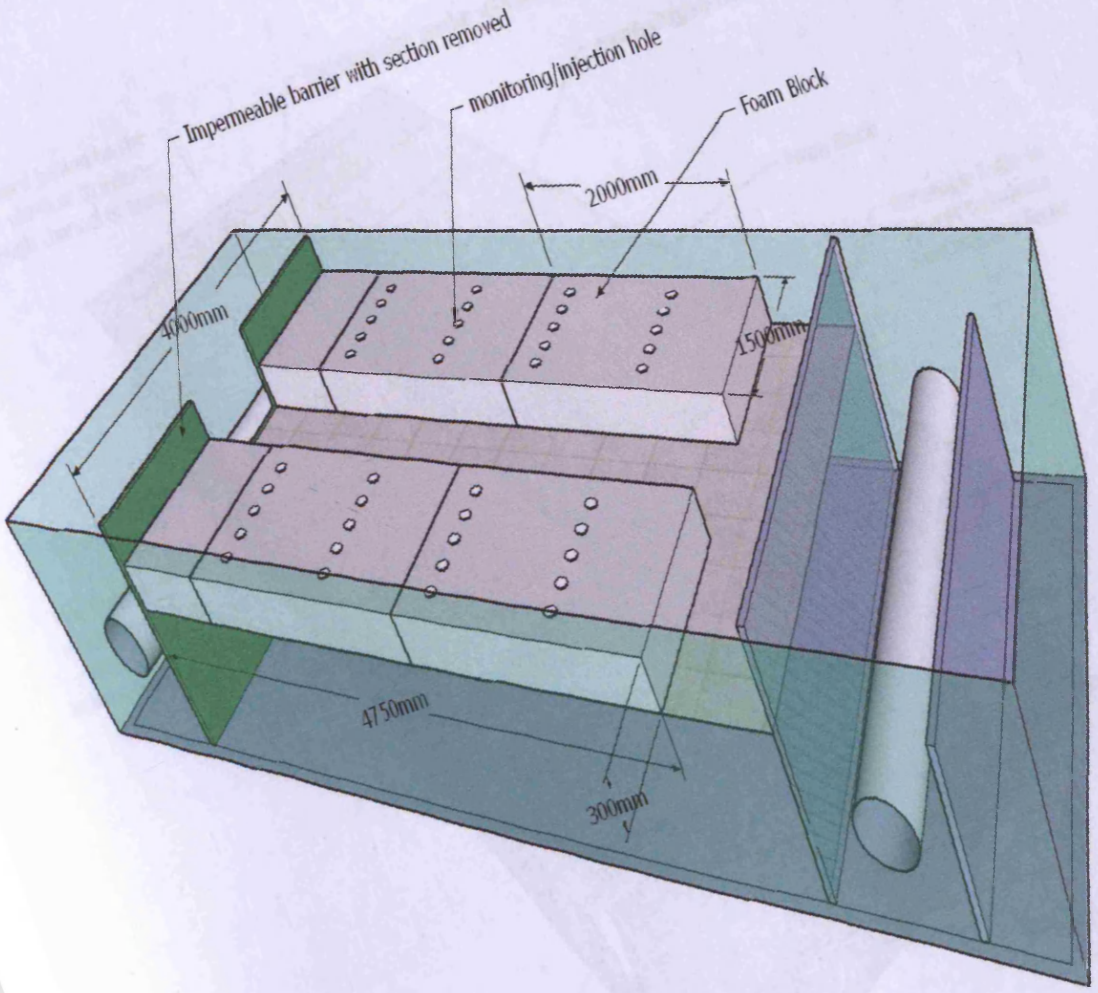

Figure 5.3: Side view of foam configuration in tidal basin

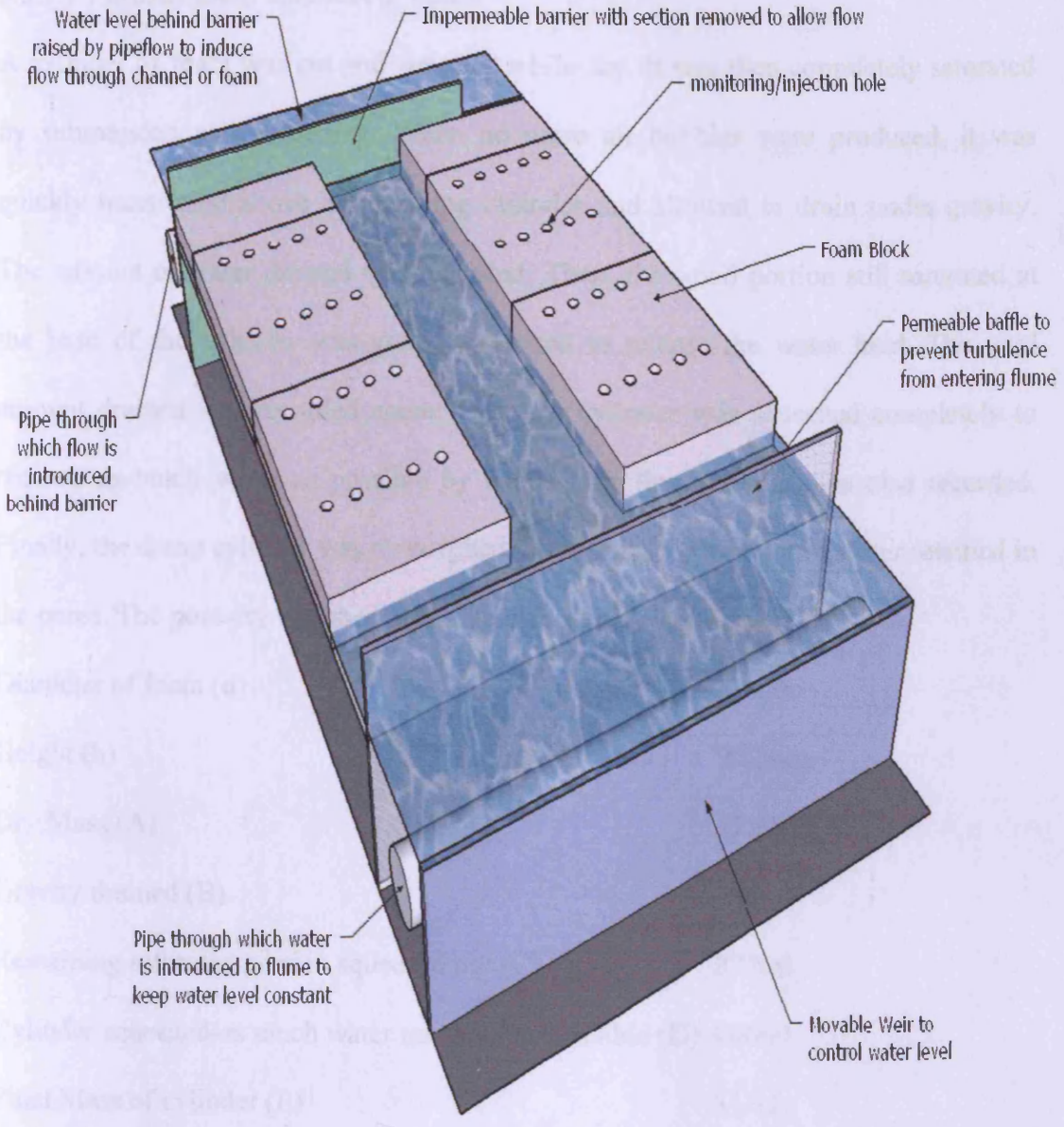

Figure 5.4: Aerial view of foam configuration in the tidal basin

5.3.1 Porosity and Permeability Determination of Foam

As shown in the governing equations the two most important parameters for any groundwater studies are the porosity and hydraulic conductivity i.e. coefficient of permeability. Porosity determination may be easily obtained either by a water absorption test or via mass and volume calculations (Innocentini et al, 1999).

5.3.1.1 Porosity Determination of Foam

A cylinder of foam was cut and weighed while dry. It was then completely saturated by submersion and squeezing. When no more air bubbles were produced, it was quickly transferred above a measuring cylinder and allowed to drain under gravity. The amount of water drained was recorded. Then, the small portion still saturated at the base of the cylinder was gently squeezed to release the water held. The total amount drained was recorded again. Then the cylinder was squeezed completely to remove as much water as possible by hand. This final amount was also recorded. Finally, the damp cylinder was re-weighed to measure the amount of water retained in the pores. The porosity was then calculated from these measurements.

Diameter of foam (d)	50mm
Height (h)	272mm
Dry Mass (A)	12.395g
Gravity drained (B)	260ml
Remaining saturated portion squeezed out (C)	375ml
Cylinder squeezed-as much water removed as possible (D)	400ml
Final Mass of cylinder (E)	31.41g
Water remaining in cylinder (E-A) = F	19.015g
Total water held in foam (D+F) = (G)	419.015ml
Volume of Cylinder (H) = PI x (d/2)2 x h	534.0708ml
Porosity = (G)/(H) = 419.01/534.0708	0.78457

5.3.1.2 Permeability Determination of Foam

British Standard BS 1377: Part 5: 1990 describes the procedure for testing the permeability of soils. Although foam does not take the shape of its container, with

some authors believing that it is generally much more porous and not quite so easy to use, see (Sparks, 2007), this method was applied in this study. The equipment, illustrated in Figure 5.5 and consisting of a constant head permeameter, was used to measure the hydraulic conductivity (co-efficient of permeability). Basically, water is pumped to the overhead reservoir through the inflow pipe, and the head was kept constant by continuous flow throughout the experiment. There was an overflow pipe in case of spill. There was a controlling pipe connected to the reservoir to a foam specimen of a certain height and diameter that controls the flow rate via a controlling

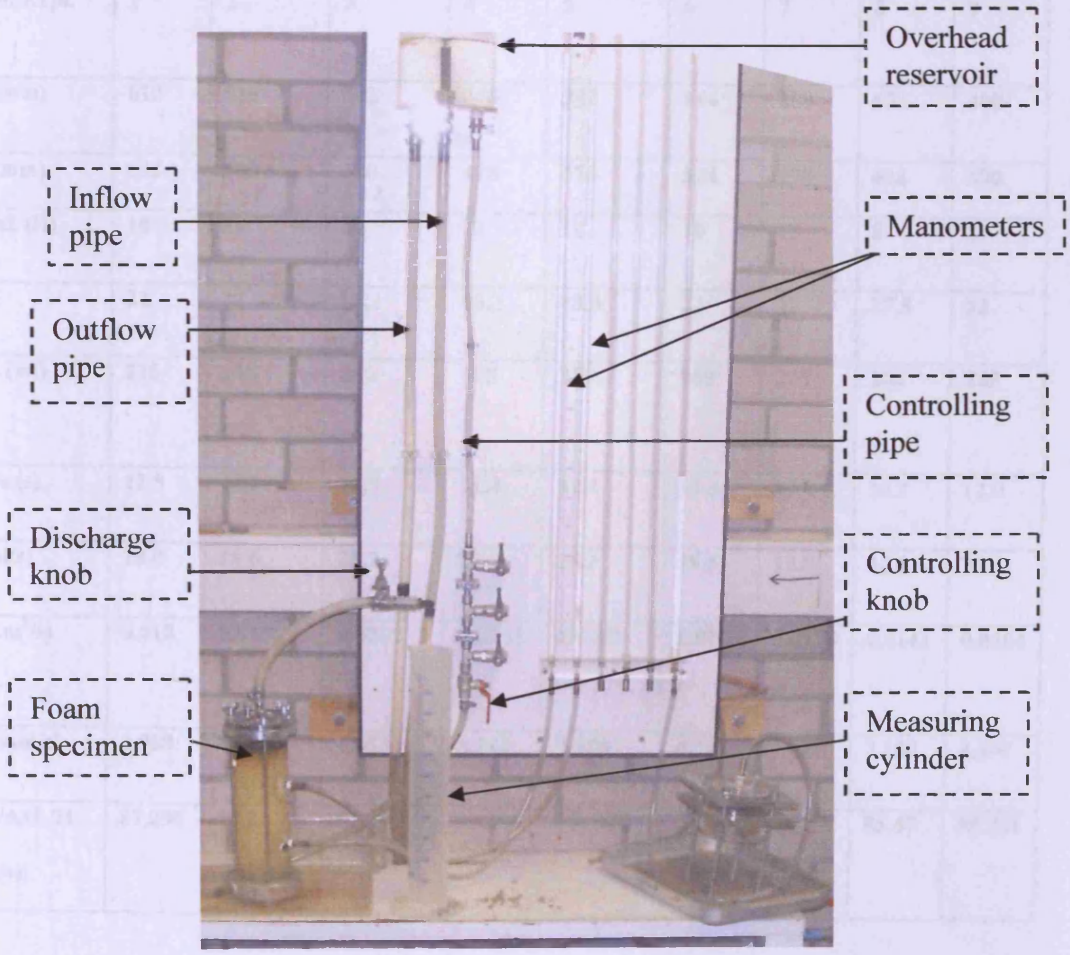

Figure 5.5: Laboratory set-up for the determination of hydraulic conductivity (coefficient of permeability) of foam.

knob. Two manometers were connected to the foam specimen at different positions. Whilst the flow rate was kept at a certain value by adjusting the controlling knob, water was discharged through the foam via the discharge knob into the measuring cylinder. The rate of flow was measured with the aid of a stop clock. The difference between the manometer readings gave the difference in head. The experiment was repeated for different flow rates and for different discharges. The results are as shown in Table 5.1

Table 5.1: Results from permeability determination experiments

No of Expt.	1	2	3	4	5	6	7	8	9
h1 (mm)	612	510	542	440	382	544	288	632	400
h2 (mm)	602	500	530	428	370	534	278	624	390
h1-h2 (H)	10	10	12	12	12	10	10	8	8
L/H	22	22	18.3	18.3	18.3	22	22	27.5	22
Vol. (ml)	225	245	260	265	280	250	220	200	245
Time (s)	12.5	13.2	12.9	11.4	11.1	12.8	12.4	14.2	12.0
q (ml/s)	18.0	18.6	20.2	23.2	25.2	19.5	17.8	14.1	20.4
q.(mm^3/s)	0.018	0.0186	0.0202	0.0232	0.0252	0.0195	0.0178	0.0141	0.0204
q/A(mm/s)	3.968	4.100	4.453	5.114	5.555	4.299	3.924	3.108	4.497
K=q/AxL/H (mm/s)	87.296	90.2	81.49	93.586	101.657	94.578	86.174	85.47	98.934

Initial readings of manometer: h1 = 990mm; h2 = 990mm

Diameter (d) of foam specimen = 760mm

10mins respectively. As shown, the time for low water for the 5mins tide was 150.8s and the time for high tide was 305s about double the time for low tide. The time for low water for 10mins tide was 305.6s and the corresponding time for high water was 612s almost double the time for low water. It was expected that the time for low water for 10mins tide should be double that of 5mins tide for low water. In this case, the times for low water for 10mins and 5mins tide were 305.6s and 150.8s respectively. Similarly, the time of high water for 5mins tide should be half of that for 10mins tide and again this had been demonstrated with values of 305s and 612s for 5mins and 10mins tides respectively.

This part of the experiments was significant because of the basic reason of minimising errors in the experiments.

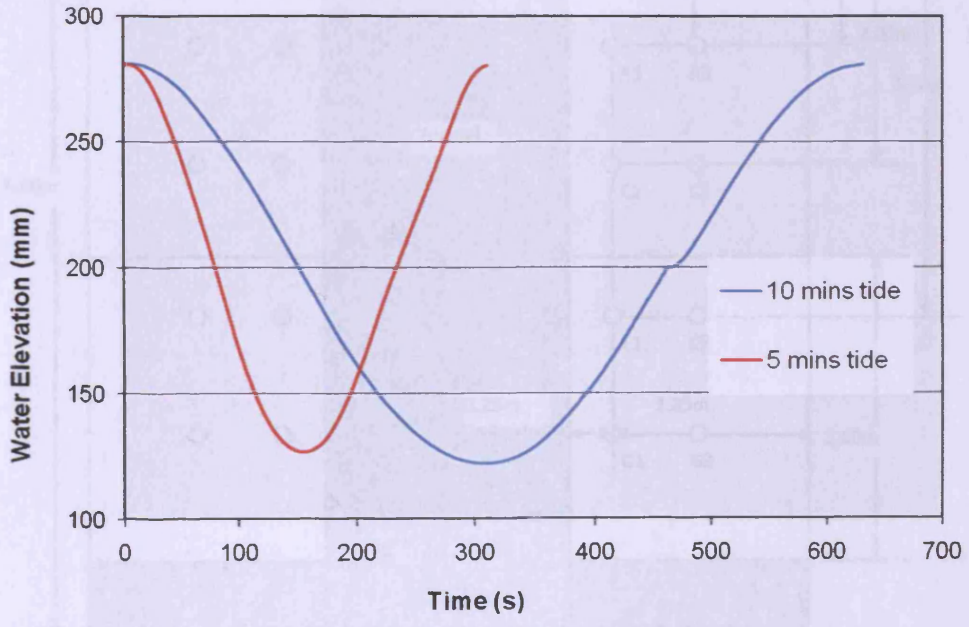

Figure 5.6: Comparison of tides for tidal period of 10mins and 5 mins respectively

Figure 5.7 is the section through the foam blocks before more holes were bored as shown in Figure 5.3. Thus tidal cycles for five, seven-and-half and 10 minutes were run for this configuration. Results for the channel and holes 1 and 3 are herein shown for each transect. Figures 5.8 (a and b) and 5.9(a and b) show five minute tidal cycles for transects A, C, E and G. As expected, the amplitude of the tide for the channel was higher and it reduces as it moved through the foam material. Thus the amplitude of the channel at A was higher than at hole A1 and higher than at hole A3. In addition as expected and due to increased permeability, there was a phase difference between channel at A and hole at A1 and hole at A3. For example, high tide arrives in channel

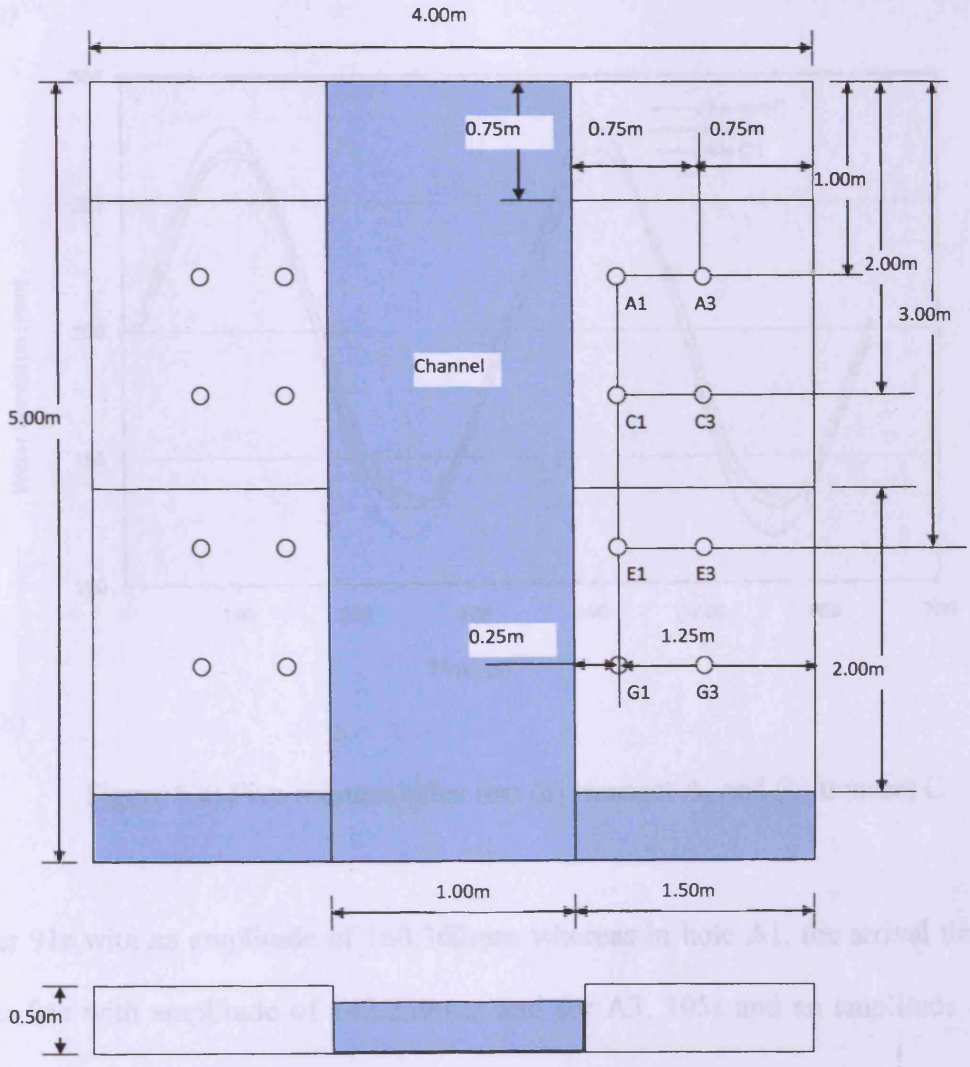

Figure 5.7: Section through the foam before additional holes were added

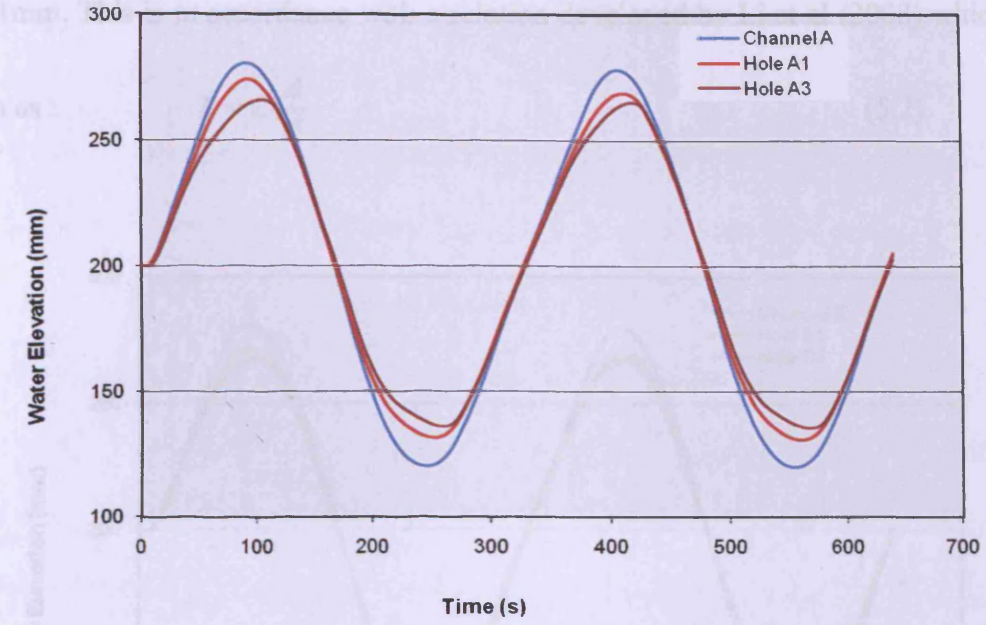

(a)

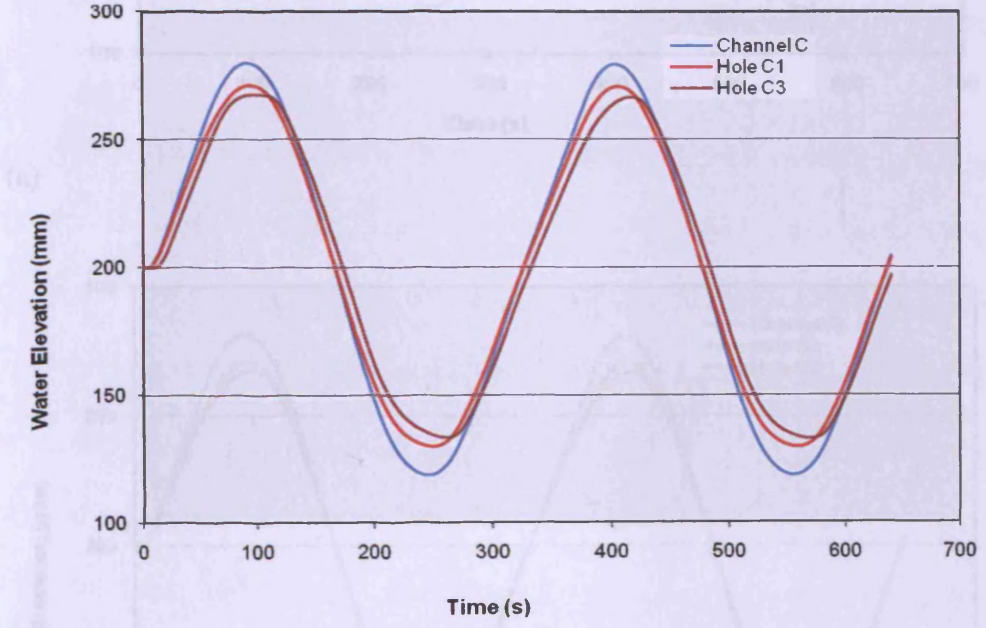

(b)

Figure 5.8: Five minutes tides for: (a) transect A, and (b) transect C

at A after 91s with an amplitude of 160.362mm whereas in hole A1, the arrival time was after 94s with amplitude of 142.239mm and for A3, 105s and an amplitude of

129.501mm. This is in accordance with a relation developed by Li et al (2008) which is given as : $$T = C\frac{A}{K} \quad (5.2)$$

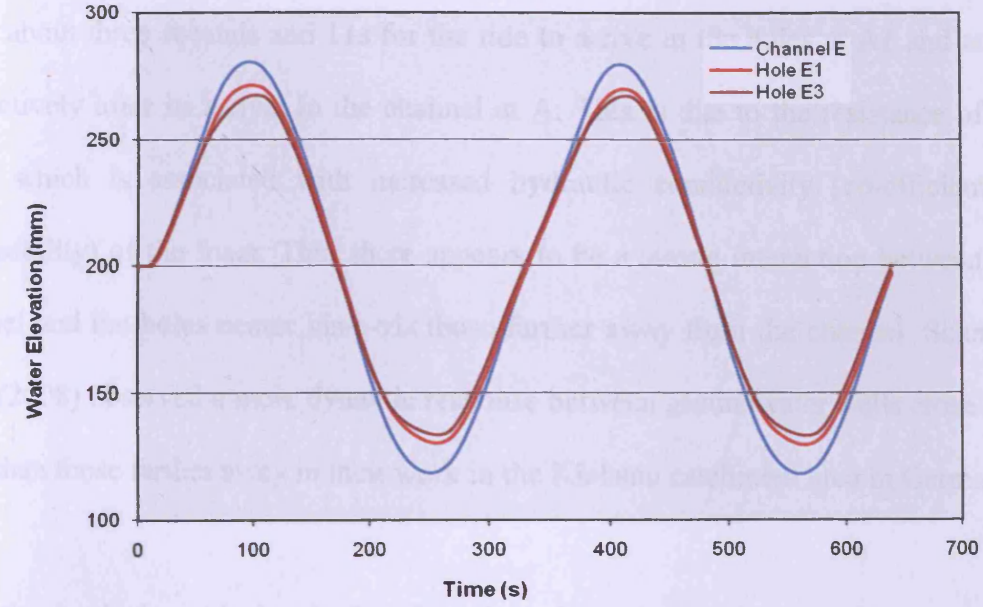

(a)

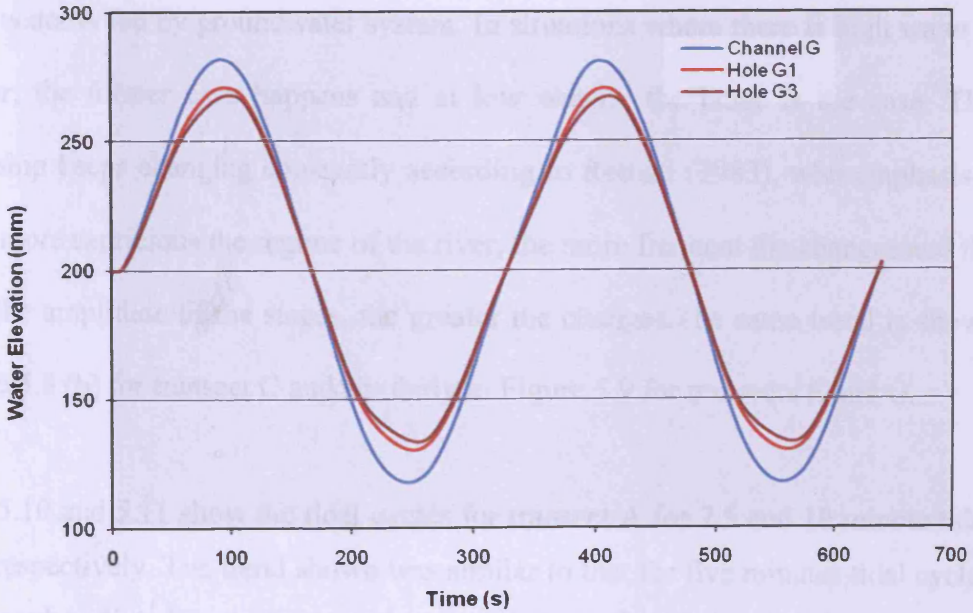

Figure 5.9: Five minutes tides for: (a) transect E, and (b) for transect G

where T (T) is the tidal period, A (L) is the tidal amplitude, K (LT^{-1}) is the hydraulic conductivity (coefficient of permeability), and C is a dimensionless constant. Thus for a constant tidal period, an increased permeability will lead to a corresponding decrease in tidal amplitude to satisfy Eq (5.2). It is therefore not surprising that it takes about three seconds and 11s for the tide to arrive in the holes at A1 and at A3 respectively after its arrival in the channel at A. This is due to the resistance of the foam which is associated with increased hydraulic conductivity (co-efficient of permeability) of the foam. Thus there appears to be a strong interaction between the channel and the holes nearer vis-a-vis those farther away from the channel. Schmalz et al. (2008) observed a more dynamic response between groundwater wells close to a river than those farther away in their work in the Kielstau catchment area in Germany.

Thus the implied conclusion is that there is a direct hydraulic connection between groundwater and surface water. A groundwater is either fed by a surface water or surface water is fed by groundwater system. In situations where there is high water in the river, the former case happens and at low waters, the latter is the case. This relationship keeps changing constantly according to Rethati (1983), who emphasised that the more capricious the regime of the river, the more frequent the changes and the greater the amplitude of the stages, the greater the changes.The same trend is shown in Figure 5.8 (b) for transect C and similarly in Figure 5.9 for transects E and G.

Figures 5.10 and 5.11 show the tidal cycles for transect A for 7.5 and 10 minute tidal periods respectively. The trend shown was similar to that for five minutes tidal cycles as discussed earlier. However it can be seen that, as the tidal period increases the phase difference between the channel and the adjacent holes becomes more pronounced. Thus the phase difference between channel at A and hole at A1 was higher for 10 minute tide than for five minute tide. This is expected as for same

permeability, the frequency of a five minute tide was higher than 7.5min than 10 minute tide. For example it took 10s and 30s for the tide to arrive in hole A1 and A3 respectively from the channel for 10 minute tidal cycle whereas 3s and 11s are observed for A1 and A3 for five tidal cycle. Similar trends were shown for all the

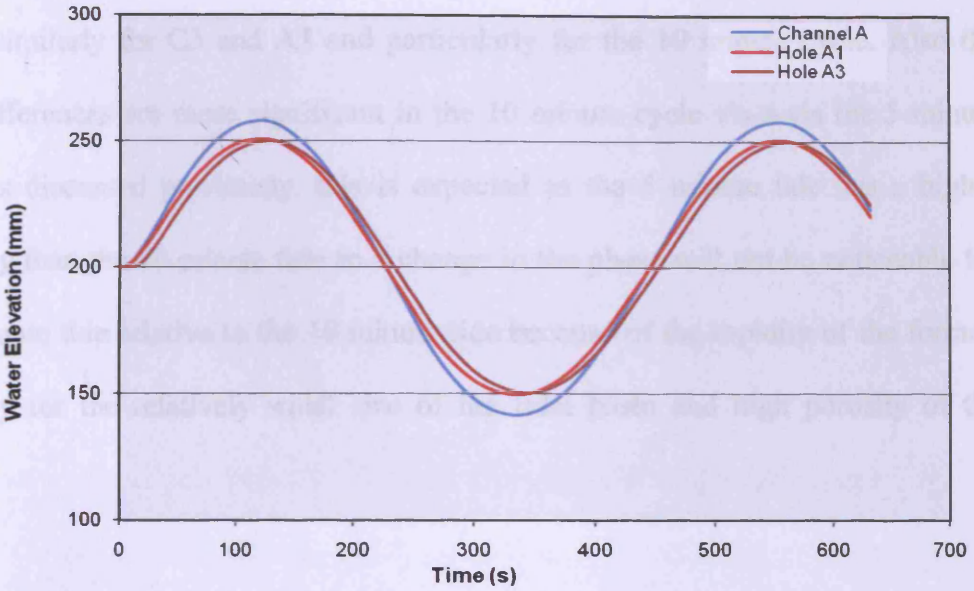

Figure 5.10: Seven- and-half minutes tidal cycles for transect A

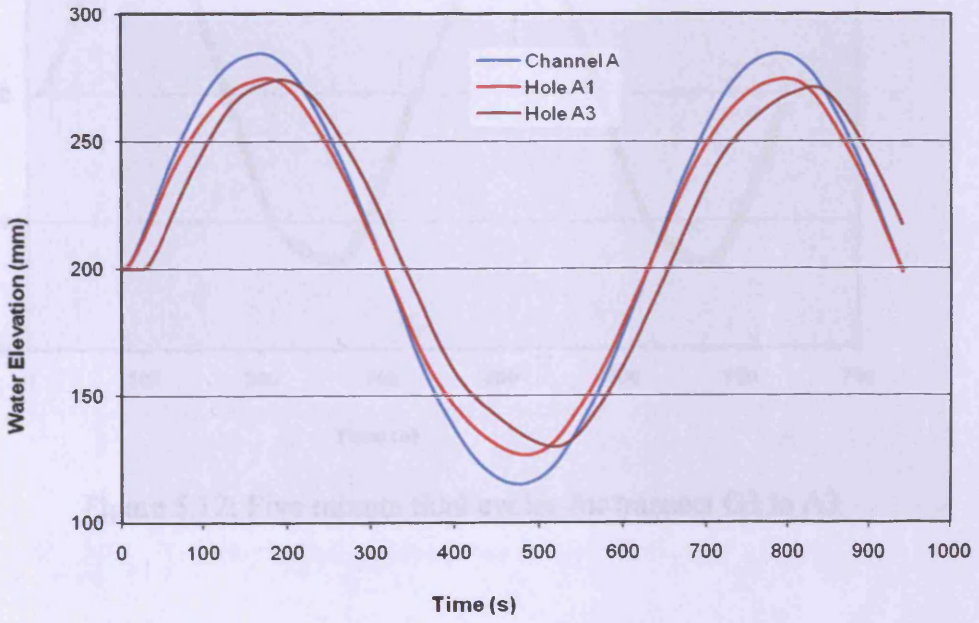

Figure 5.11: 10 minutes tidal cycles for transect A

other transects.

Figures 5.12 and 5.13 show the tidal cycles for transect G3 to A3 for 10 minute and 5 minute respectively. It can be observed that the amplitude of G3 is slightly higher than E3 and similarly for C3 and A3 and particularly for the 10 minute cycle. Also the phase differences are more significant in the 10 minute cycle vis-a-vis the 5 minute cycle. As discussed previously, this is expected as the 5 minute tide has a higher frequency than the 10 minute tide so a change in the phase will not be noticeable for the 5 minute tide relative to the 10 minute tide because of the rapidity of the former, especially for the relatively small size of the tidal basin and high porosity of the material.

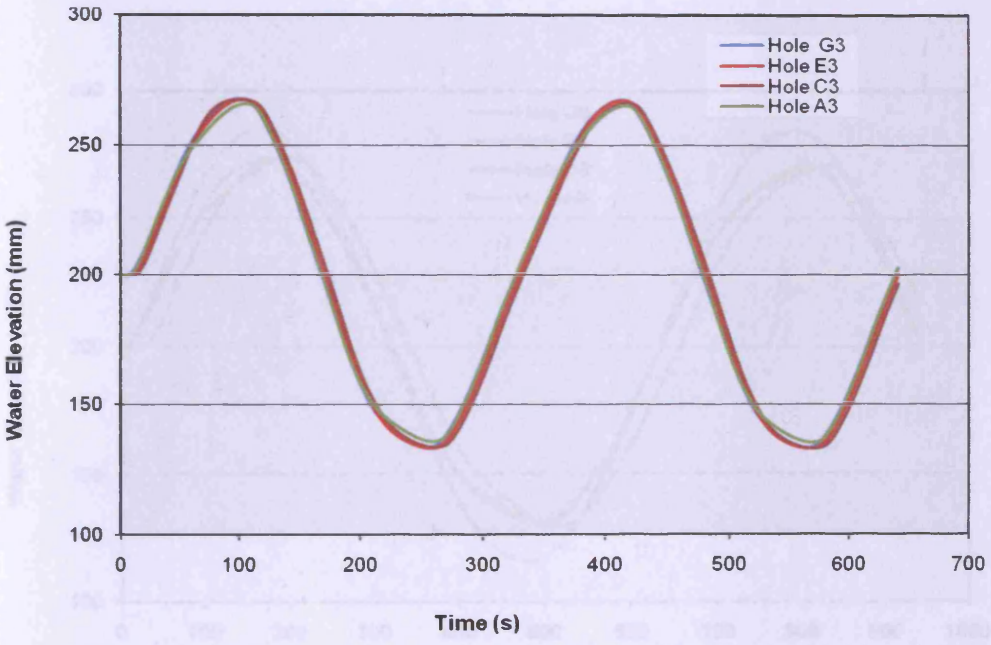

Figure 5.12: Five minute tidal cycles for transect G3 to A3

The other factor may also be errors associated with the use of water level probes and other equipments. For instance, it has been observed that for the 5 minute tide,(Fig.

5.12), the tide reached high water at around 98s and receded to low water at 255s for hole G3 with an amplitude of 134.145mm. Thus for that half-cycle, the period should be 150s to reflect a tidal period of 5 minutes, but in this case 157s were recorded. Moreso, the observed values for the other holes were significantly different. The tide peaked at holes E3, C3 and A3 around 100s, 100s and 105s respectively and was a minimum at 256.2s, 262s and 259s with amplitudes of 134.079, 133.747 and 129.700mm for the three holes respectively. The implied half-tidal cycle period for E3, C3 and A3 was therefore 156.2s, 162s and 154s respectively which was different from the median of 150s and showed no uniqueness for all the four holes.

For the 10 minute cycle (Fig. 5.13), the observed tidal amplitudes were 169.169, 142.902, 141.642 and 144.623mm for G3, E3, C3 and A3 respectively. The values

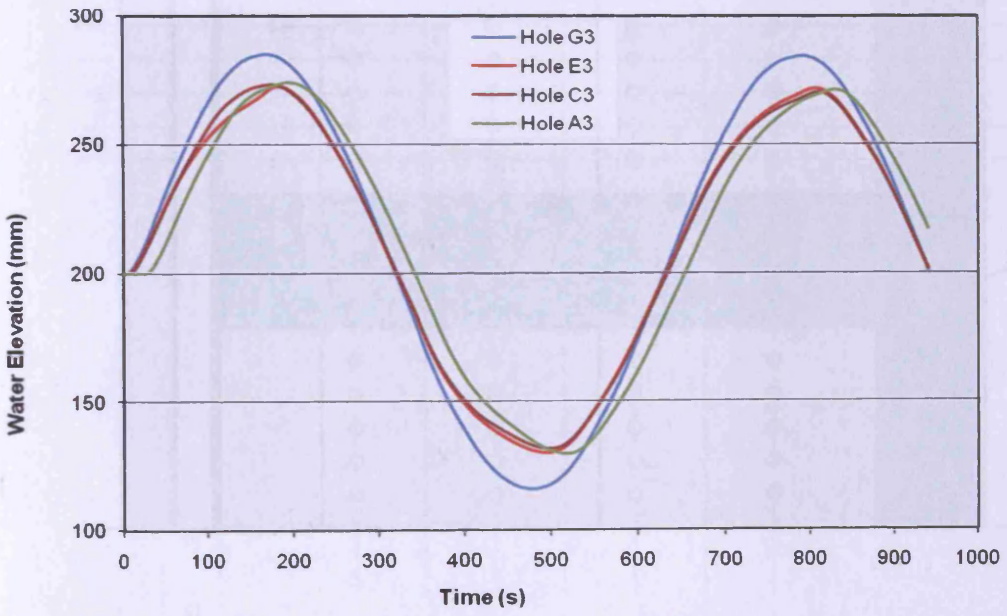

Figure 5.13: 10 minute tidal cycles for transect G3 to A3

follow the correct trend except for the value for A3 which differs in that the amplitude was decreasing for E3 and C3 but A3 increased suggesting that fluid ws held in the

foam which would go to butress the point that foam materials can hold polar fluids like water by surface tension forces. The implication is that foam materials may not behave like the traditional sand which is normally used for experiments of such nature. The other properties of foam materials are discussed later in the text. However, what was significant was that the amplitude at G3 was higher than A3. The arrival times for high water at G3, E3, C3 and A3 were 169, 184, 174 and 195s respectively

For the configuration shown in Figure 5.14 (i.e. after additional holes bored), 15 minute tidal cycles were run for that configuration, whereupon some results are shown for transects A, C and G; and for transect G3 to A3 and G5 to A5, as shown in

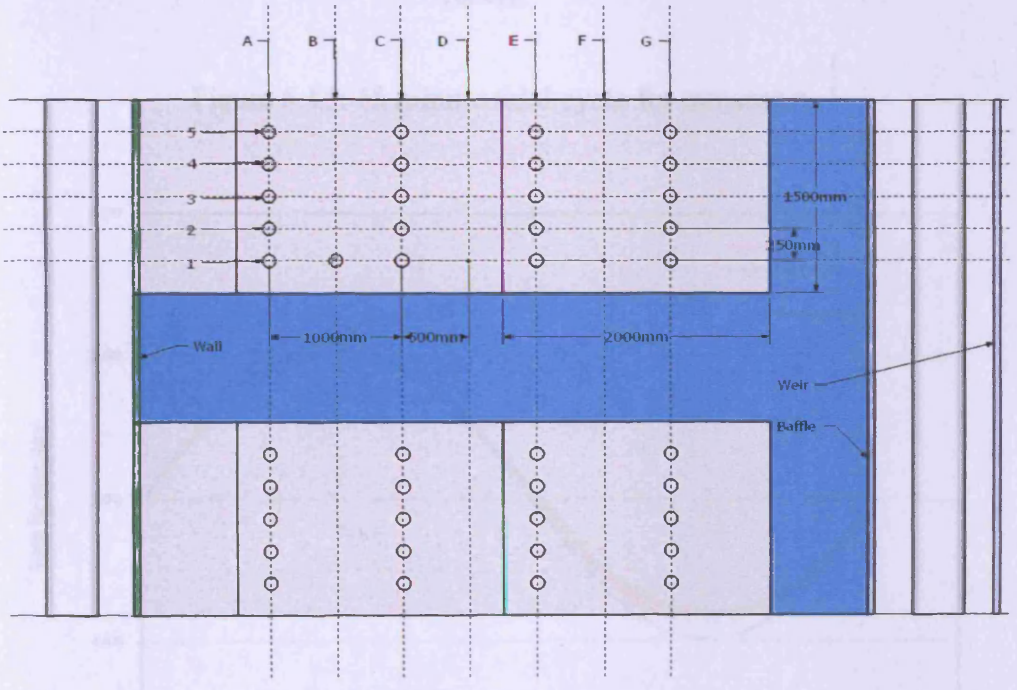

Figure 5.14: Section through the foam for final configuration

Figures 5.15, 5.16, and 5.17; and Figures 5.18 and 5.19 respectively. The trend shown in the previous section is replicated here. Thus for all cases and in all transects, the

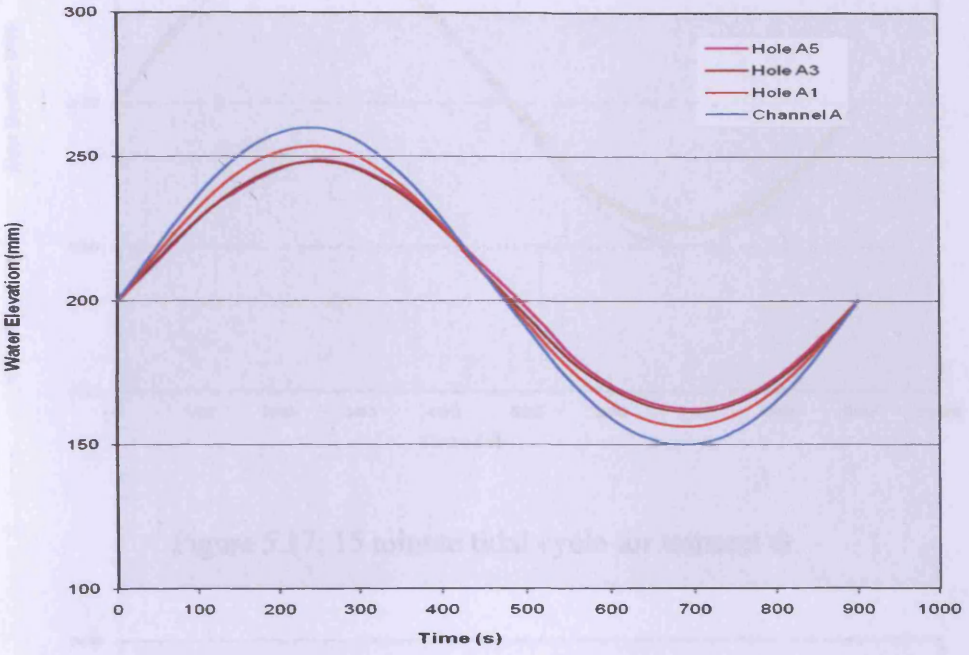

Figure 5.15: 15 minute tidal cycle for transect A

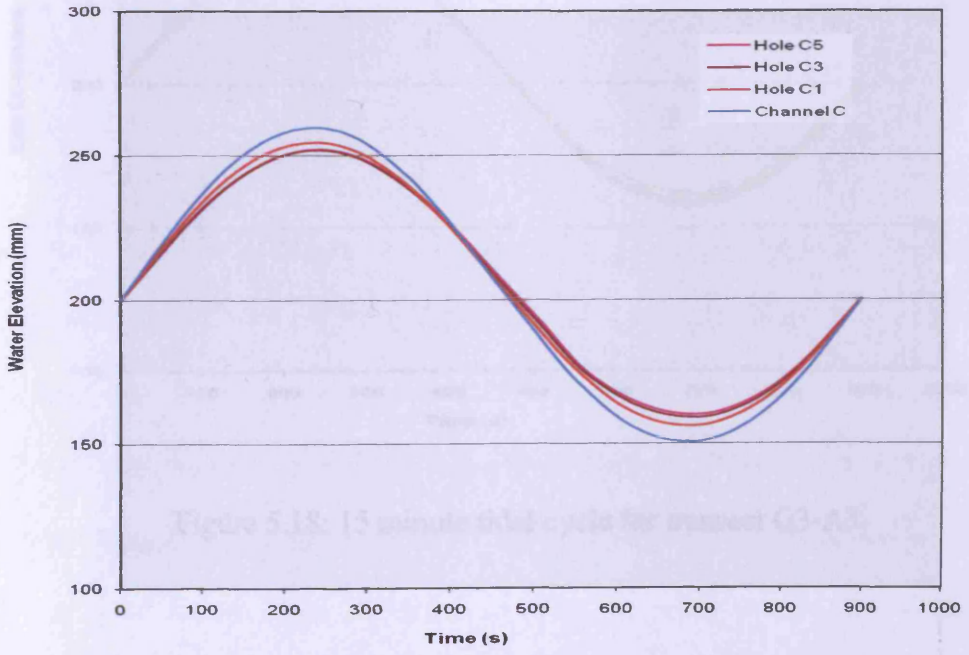

Figure 5.16: 15 minute tidal cycle for transect C

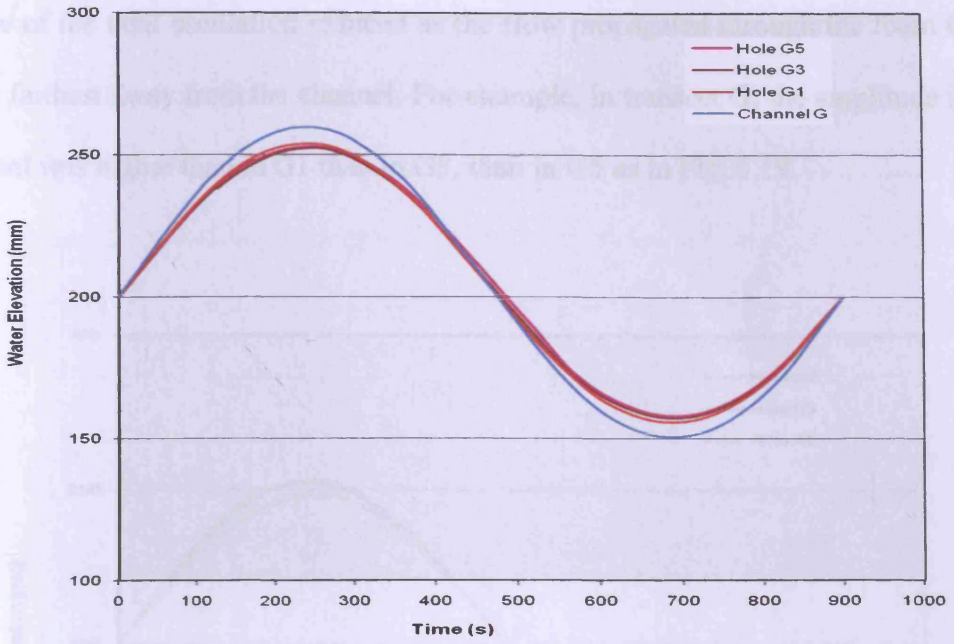

Figure 5.17: 15 minute tidal cycle for transect G

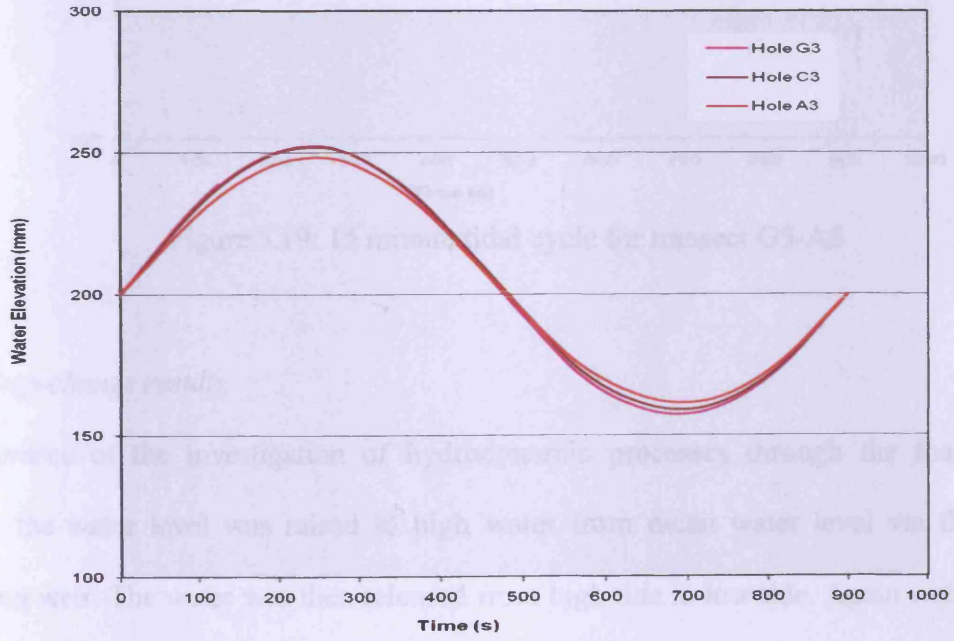

Figure 5.18: 15 minute tidal cycle for transect G3-A3

amplitude of the tidal oscillation reduced as the flow propagated through the foam to the holes farthest away from the channel. For example, in transect G; the amplitude in the channel was higher than in G1 than in G3, than in G5 as in Fig. 5.19.

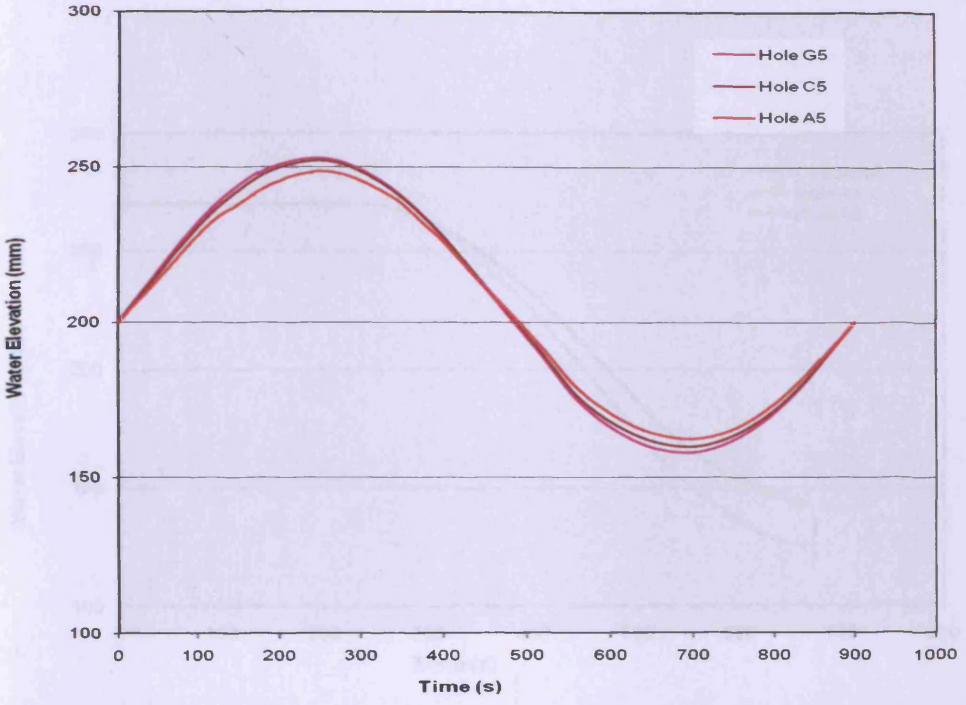

Figure 5.19: 15 minute tidal cycle for transect G5-A5

5.3.2.2 Step-change results

In furtherance of the investigation of hydrodynamic processes through the foam material, the water level was raised to high water from mean water level via the controlling weir. The water was then released from high tide to low tide. Again water levels in the channel were compared with the water levels in the adjacent boreholes. The results are as shown in Figures 5.20 to 5.21 for different transects for a tidal period of 15mins As shown in all the transects when the water was released at high water it took a shorter time to reach low water in the channel than in the immediate hole adjacent to the channel than the farthest due to increased hydraulic conductivity

as discussed in the previous section. Thus the drop in the water level in the channel at A was faster than in the holes at A1 and at A3. It was observed that it took 312s for the water level to drop from 270mm to 150mm in the channel at A whilst 369 and 381s were recorded for the holes at A1 and at A3 respectively. For all the other transects the results were similar. The values recorded for transect C were

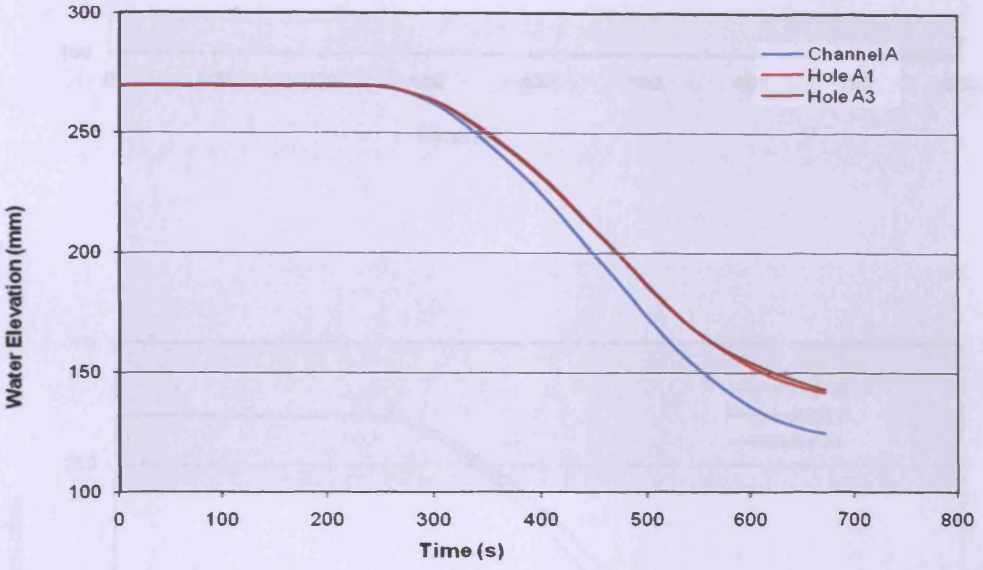

(a)

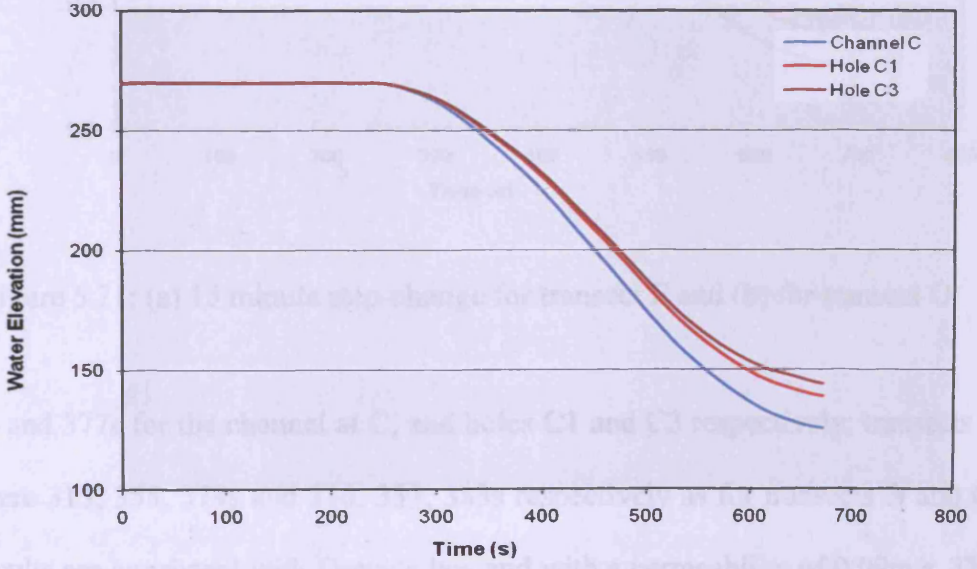

(b)

Figure 5.20: (a) 15 minute step-change for transect A and (b) for transect C

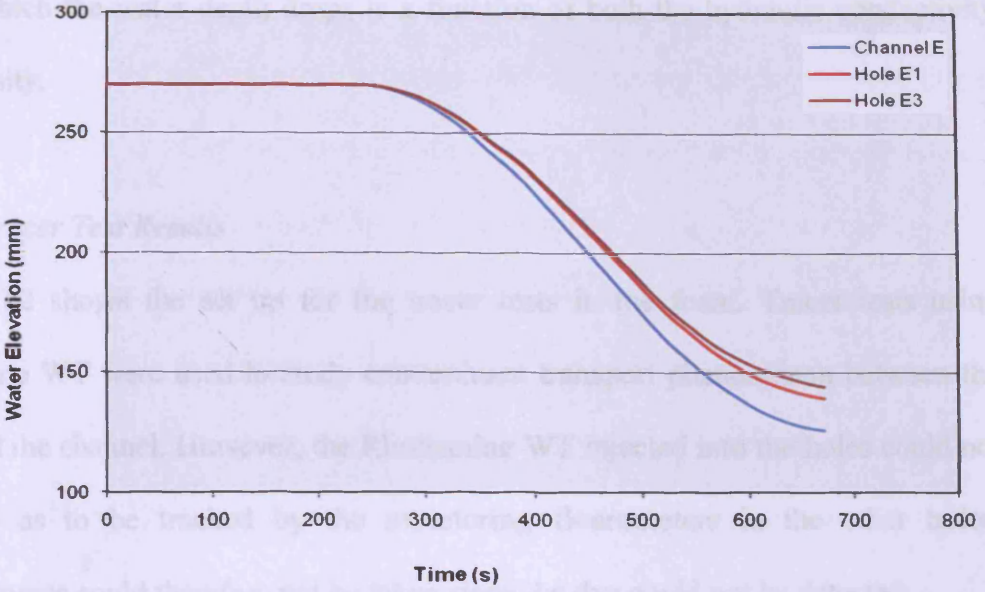

(a)

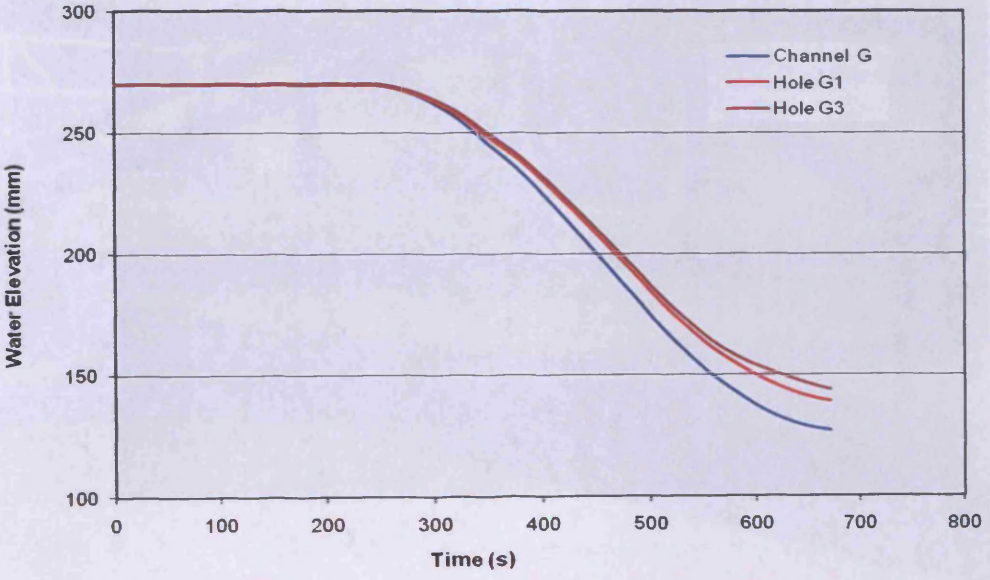

(b)

Figure 5.21: (a) 15 minute step-change for transect E and (b) for transect G

313, 353 and 377s for the channel at C, and holes C1 and C3 respectively; transects E and G were 315, 355, 379s and 316, 353, 383s respectively as for transects A and C. These results are consistent with Darcy's law and with a permeability of 0.09m/s. The

rate at which the water depth drops is a function of both the hydraulic conductivity and porosity.

5.3.2.3 Tracer Test Results

Figure 5.22 shows the set up for the tracer tests in the foam. Tracer tests using Rhodamine WT were used to study contaminant transport phenomenon between the foam and the channel. However, the Rhodamine WT injected into the holes could not move so as to be tracked by the monitoring flourometers in the other holes. Measurements could therefore not be taken since the dye could not be detected.

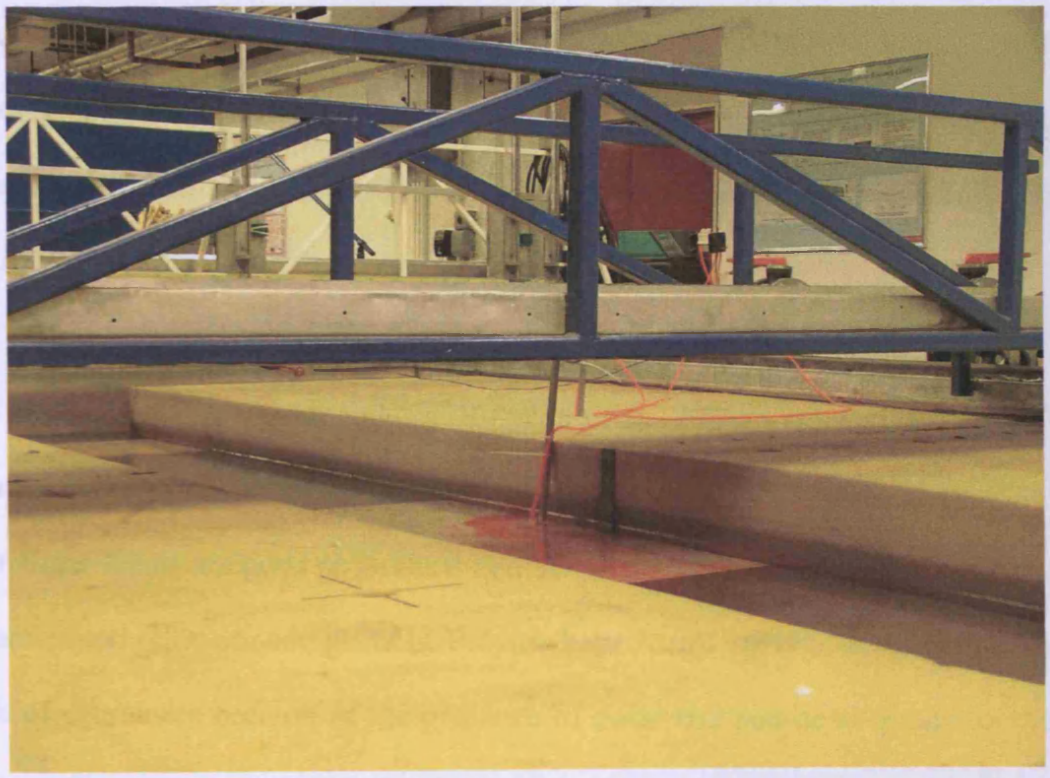

Figure 5.22: Tracer tests in the foam

The ease with which a fluid would be transported through any porous medium is an expression of the hydraulic conductivity or coefficient of permeability. In effect, the

process of the flow rate is related to the medium properties and the fluid properties. Grain-size distribution, shape of the grains and the porosity are the relevant intrinsic properties of the medium, whereas the density and viscosity are key properties of the fluid. Thus hydraulic conductivity depends on the intrinsic permeability of the medium and the properties of the fluid, i.e. the density and viscosity. This phenomenon could therefore be attributed to the intrinsic properties of the foam material. Unlike sand, foam materials have no grains or they are not well distributed and have no defined shape. Therefore the medium was subject to all sorts of interpretations. This can be due to the electrical or electrostatics properties of the foam in contact with water which is polarised. In determining the intrinsic permeabilities of different grades of foam, Dawson et al. (2007) found out that saturating polyurethane foam with a polar fluid (like water) reduces the strength and stiffness of the foam. This could create surface tension forces which would impede the movement of the solute from one point to the other.

It has been observed by some authors (Robaina et al., 2009; Baldex et al., 2008; El-Shahawi and Aldhaheri, 1996; El-Shahawi, 1994; Fong and Chow, 1992)) that polyurethane foams are good absorbents and adsorbents of dyes including families of Rhodamine and other organic phenols. Polyurethane foams are able to retain different classes of substances because of the presence of polar and non-polar groups in their structures (Baldex et al., 2008). In discussing the transport of sorbing solutes in homogeneous porous media, Abulaban et al. (1998), observed that as local dispersion tends to spread the plume and dilute the concentration, there is an increase in a retardation coefficient that tends to slow its progress. They argued that, this phenomenon can be construed as self-restraining process imposed by the plume itself

and thus the plume tends to resist hydrodynamic dispersion. In the process, according to Abulaban et al. (1998), the concentration approaches zero as the retardation coefficient tends to infinity and consequently the solute can hardly move at such low concentrations. This may be one of the plausible reasons why the dye could not move in the foam.

5.4 Sand Embankment

As discussed in the previous section, tracer tests were not successful using the foam material. Since the foam did not work well, the foam was therefore replaced with a traditional sand embankment which is normally used for experiments of this nature. Figures 5.24 to 5.26 show the laboratory set up of the sand embankment in the tidal basin. One of the main objectives of this study was to look at the solute transport processes in surface water-groundwater systems with the use of dye studies. Figure 5.23 shows the laboratory set up that was used to determine the permeability of the sand. The procedure was as shown for the foam material (see Section 5.3.12)

A cohesive sand of 1mm diameter with measured porosity of 0.41 and permeability of 0.01m/s was used to form a trapezoidal embankment of side slope 1:2 and top width of 0.2m and bottom width of 1.20m with height of 0.25m above the flume bed. The tidal basin was coupled to a tide generating weir which was computer controlled to generate varying water levels in the basin according to the weir movement. A pump was used to generate flow through the basin and measurements were taken for elevations in channel 1 (Ch1), hole 1 (H1), hole 2 (H2) and channel 2 (Ch2) as shown in Figure 5.24. Similar notations were used for the other transects.

Figure 5.23: Laboratory set up for determination of hydraulic conductivity of sand

Figure 5.24: Sand embankment in the tidal basin before pumping of water

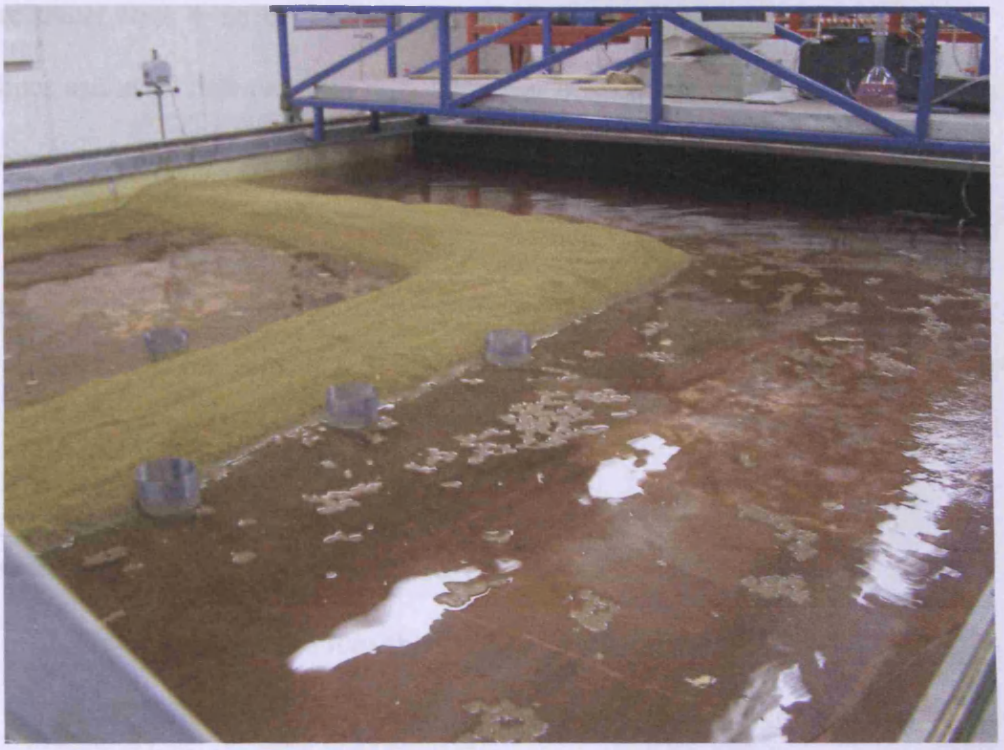

Figure 5.25: Tidal basin after pumping of water

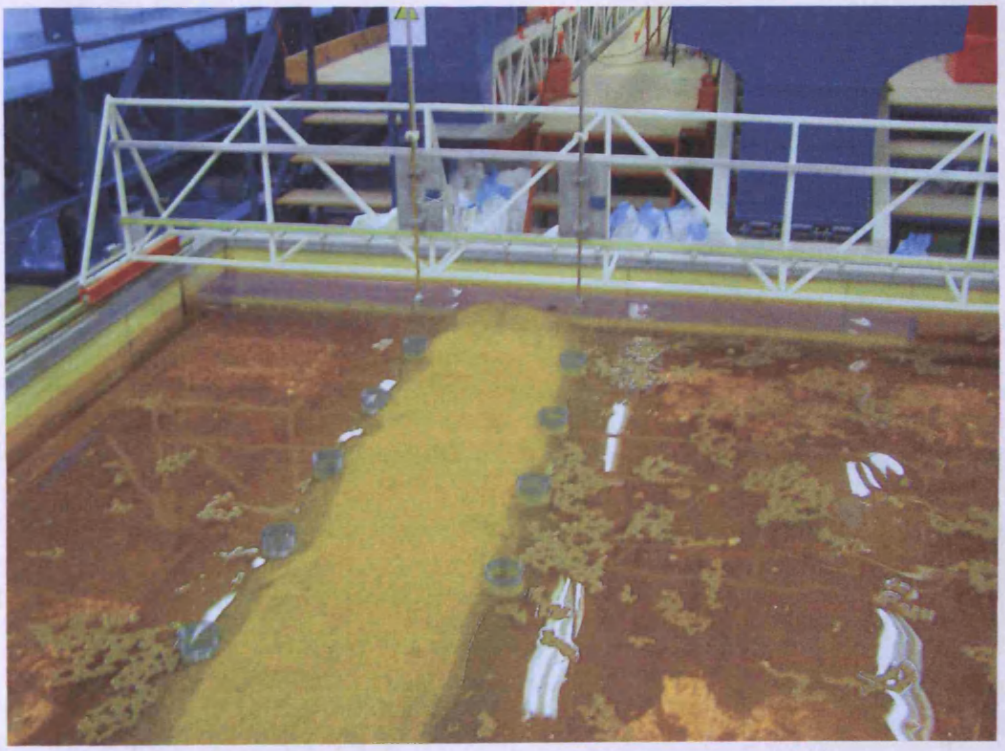

Figure 5.26: Tidal cycles about to start, showing water level probe meters

Before tracer tests were conducted water level measurements were taken across all grid lines and at all holes on that grid. This was done to determine the head difference between injection holes and monitoring holes. Figure 5.28 shows a section through the sand embankment. Nine 0.01m diameter holes were created through the sand embankment, serving as boreholes in a real situation.

5.4.1 Water level results

The tracer tests were conducted under two scenarios:

1. Water was pumped into the basin, and creating a situation where the water level behind the embankment (wetland side) was higher than water level in front of the embankment (seaside), so that the dye was injected after a head difference had been created; and
2. As for scenario 1 but with the tide generated switched on and an upstream flow interacting with a tide.

These two scenarios are depicted in Figure 5.27 where water was pumped to the basin at initial water level of 120mm at a rate of $0.0006m^3/s$ and sustained for one hour before a 10min tidal cycle was started. As can be seen for about an hour the water levels reached a quasi –steady state where continuous pumping at that rate did not alter the water levels. When this condition had been achieved the dye was then injected for the case in scenario 1. For the case in scenario 2, the dye would be injected after the tide had been generated as shown in Figure 5.27.

This case was similar for all transects.

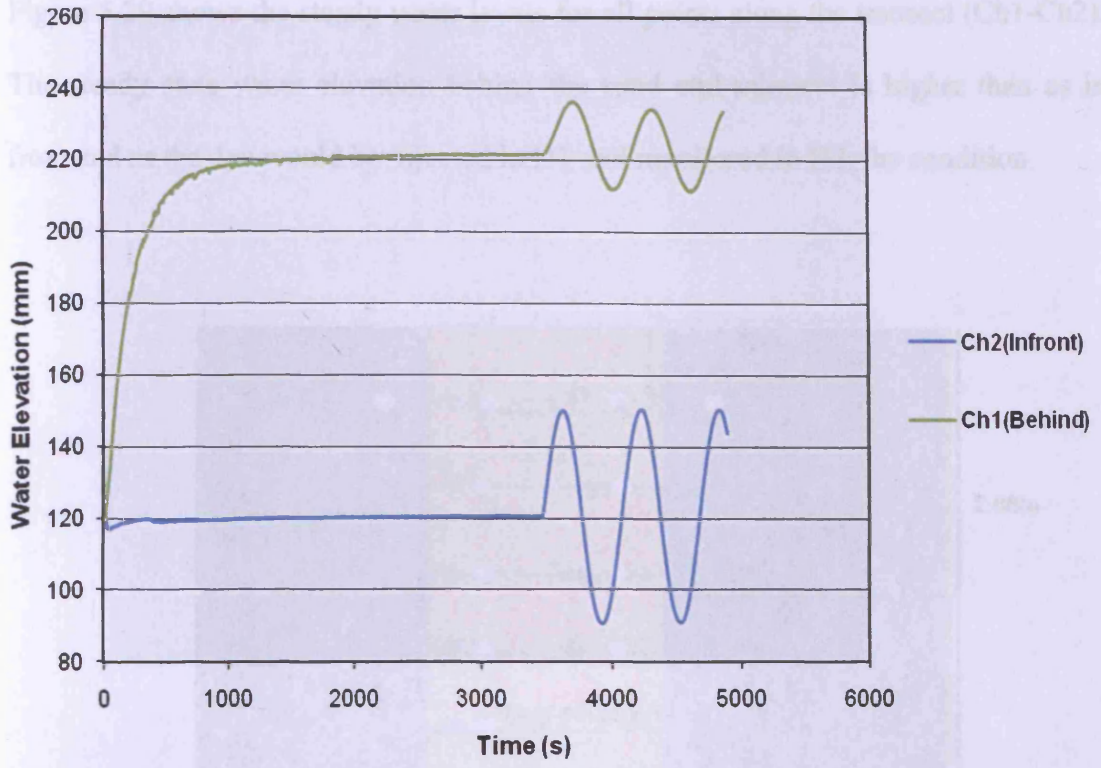

Figure 5.27: Water levels before pumping and after 0.0005m^3/s pumping for an hour and with 10mins tide.

With this background water level measurements were taken for these two situations to look at how the water levels varied along the transects: for example, from Ch1 through to Ch2 via H1, and H2 and similarly for the other transects where injection would take place. In scenario 1, water was pumped to the basin for two or three hours when it was assumed that the water level had reached a quasi-steady state. The water elevations were then measured at the four points along the transect and plotted against the distance from Ch1 which was the reference point for the transect (see Fig 5.28). Initially, tidal cycles were run for the channels in front and behind the embankment without pumping water to the basin to check whether the amplitude in front and behind the embankment would be different.

Figure 5.29 shows the steady water levels for all points along the transect (Ch1-Ch2). The steady state water elevation behind the sand embankment is higher than as in front and as the dye would be injected in H1 and monitored in H2, the condition

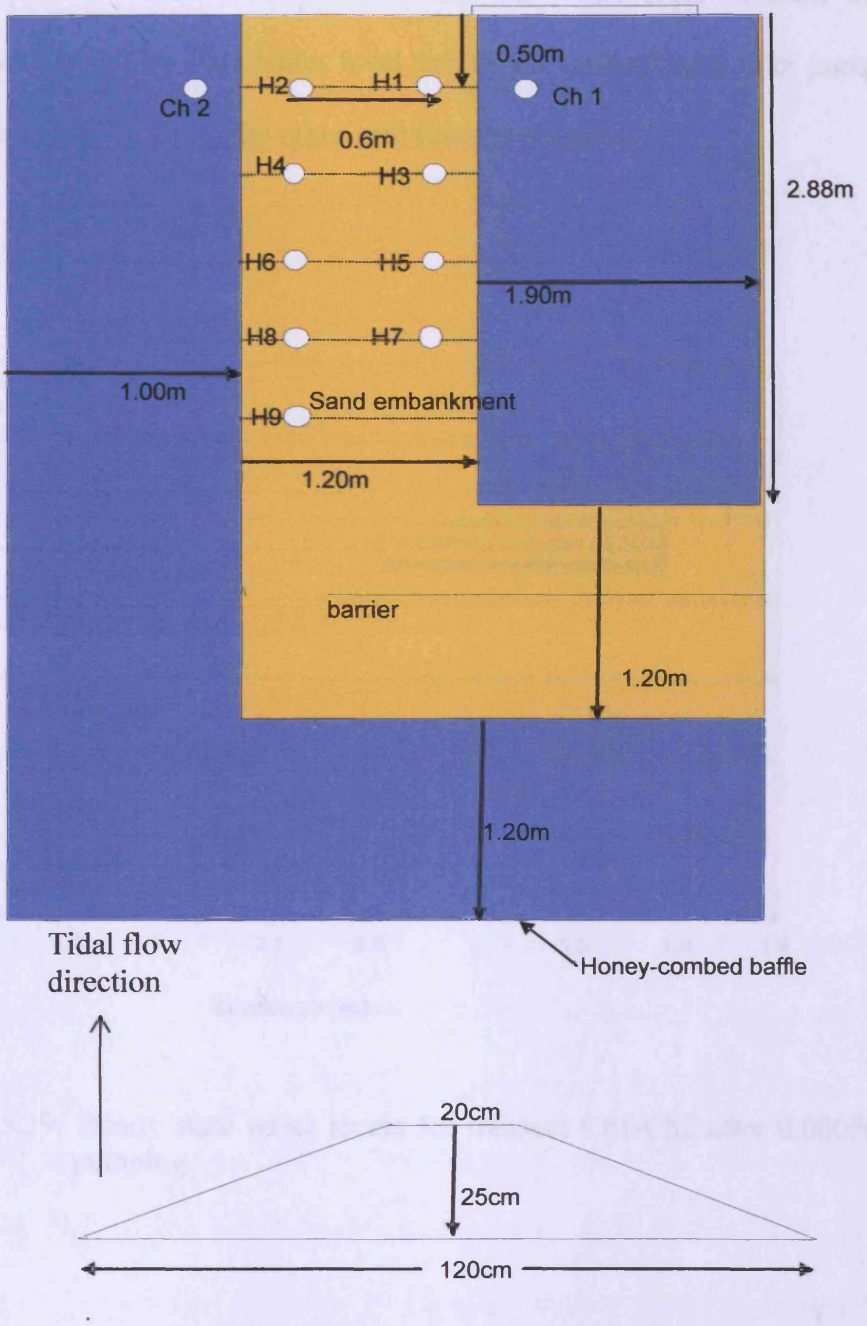

Figure 5.28: (a) Sand embankment as located in the tidal basin, and (b) a section through the embankment

would be good for the flow of water or solute after injection Similarly the situation was the same for Ch7 (behind the embankment) through to Ch 8 (in front of the embankment) as shown in Figure 5.30. These results showed that as the water flowed through the sand the amplitude reduced owing to high resistance due to increased permeability. Thus the head difference between the water level in front of the embankment was far higher than water level behind the embankment after pumping. The situation was similar for all the other grid lines or transects

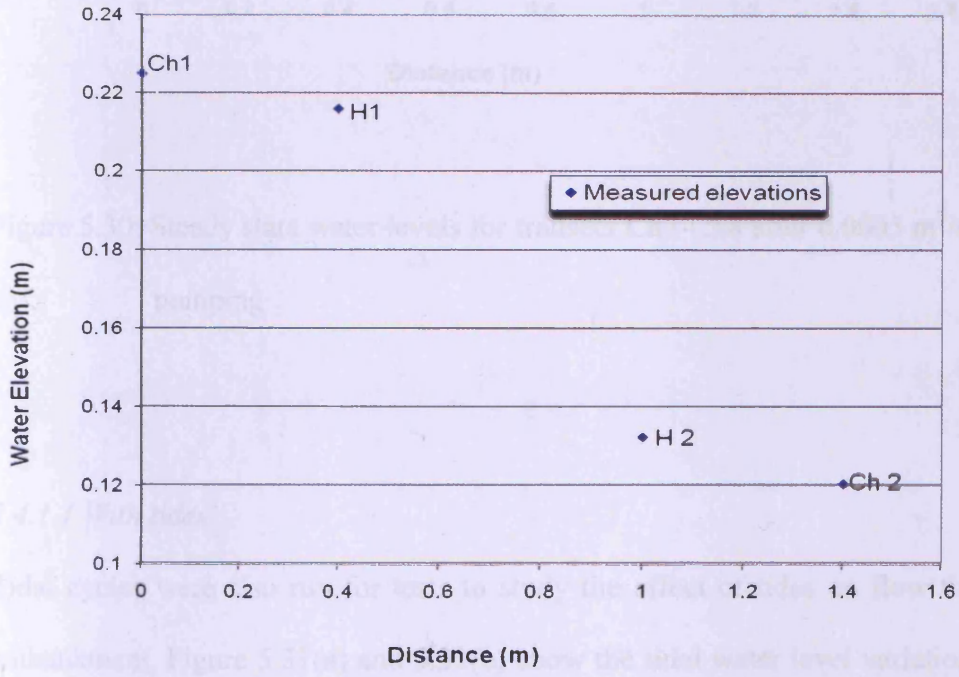

Figure 5.29: Steady state water levels for transect Ch1-Ch2 after 0.0005m^3/s pumping

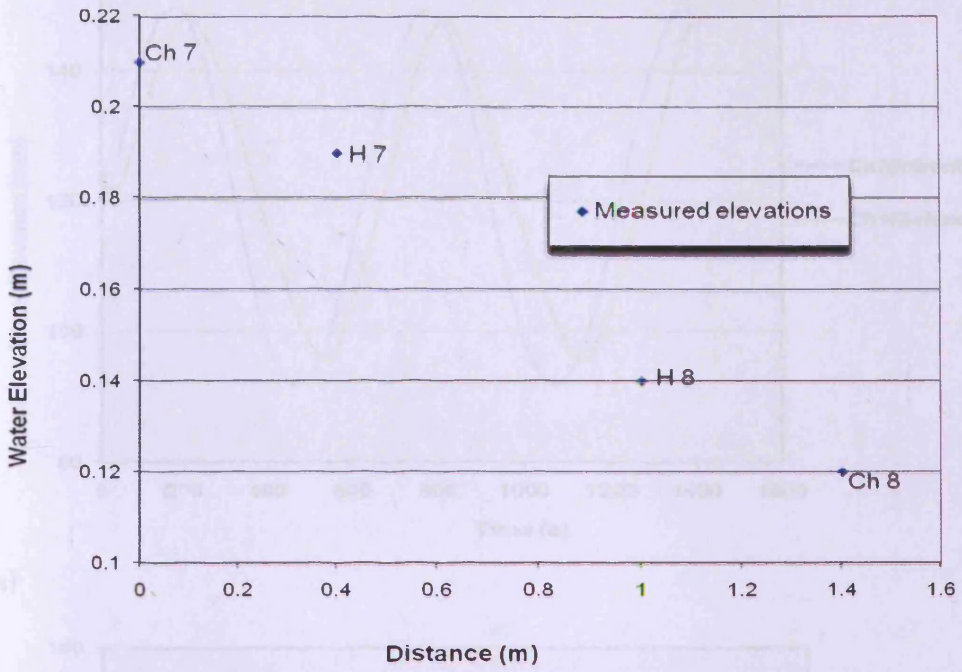

Figure 5.30: Steady state water levels for transect Ch7-Ch8 after 0.0005 m^3/s pumping

5.4.1.1 With tides

Tidal cycles were also run for tests to study the effect of tides on flow through the embankment. Figure 5.31(a) and 5.31(b) show the tidal water level variations for two transects (Ch1-Ch2) and (Ch7-Ch8) without any pumping into the basin. The tide was started at mean water level, and as can be seen the amplitude of the tide was reduced as it propagated through the embankment to the other side of the channel. This phenomenon runs up from Ch8 (in front of the embankment) through to H8 to Ch7 (behind the embankment) as shown in Fig 5.32. H8 is out of phase with Ch8 and H7 leads Ch7.

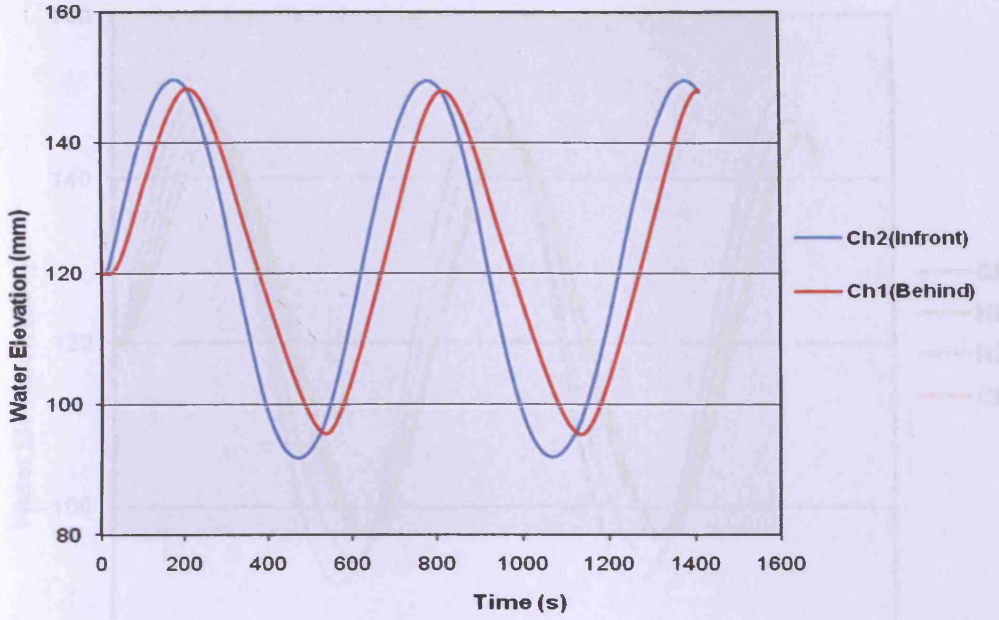

(a)

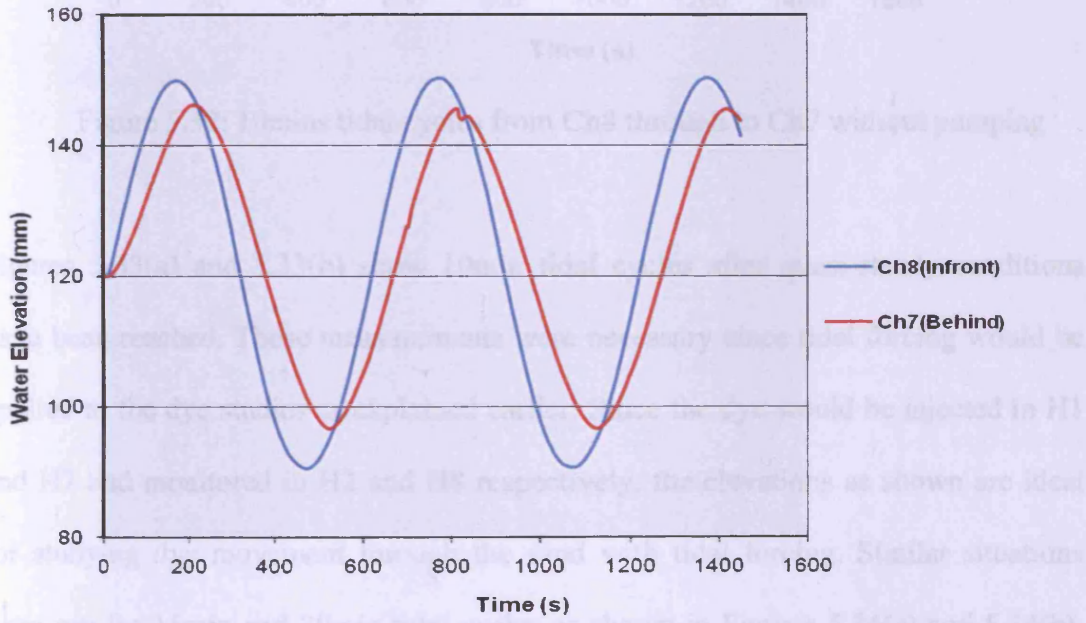

(b)

Figure 5.31(a): 10mins tidal cycles in front and behind the embankment for (Ch1 andCh2) and (b) for (Ch7 and Ch8) without pumping

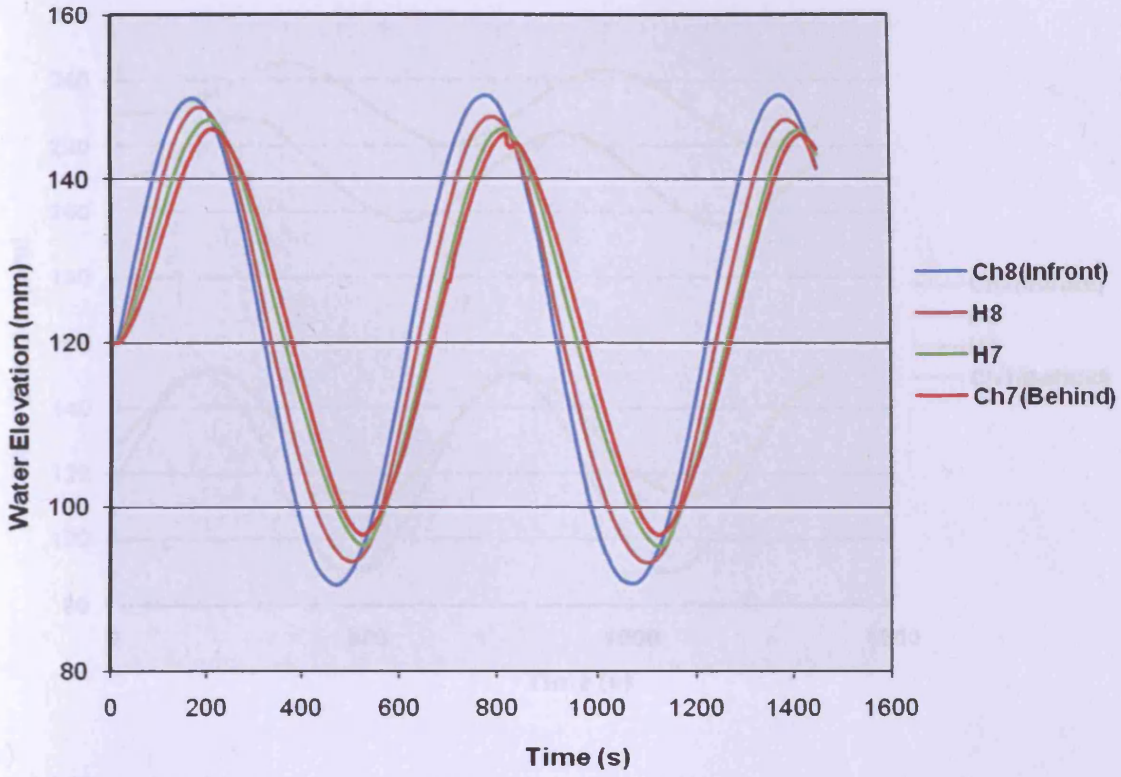

Figure 5.32: 10mins tidal cycles from Ch8 through to Ch7 without pumping

Figures 5.33(a) and 5.33(b) show 10min tidal cycles after quasi-steady conditions have been reached. These measurements were necessary since tidal forcing would be applied to the dye studies as explained earlier. Since the dye would be injected in H1 and H7 and monitored in H2 and H8 respectively, the elevations as shown are ideal for studying dye movement through the sand with tidal forcing. Similar situations were run for 15min and 20min tidal cycles as shown in Figures 5.34(a) and 5.34(b). The trends were not different from that of the 10min tidal cycle.

These results have demonstrated that increased permeability of the medium affected the flow of water. In this particular case increased permeability affected the amplitude and phase of the tide as it propagated through the sand.

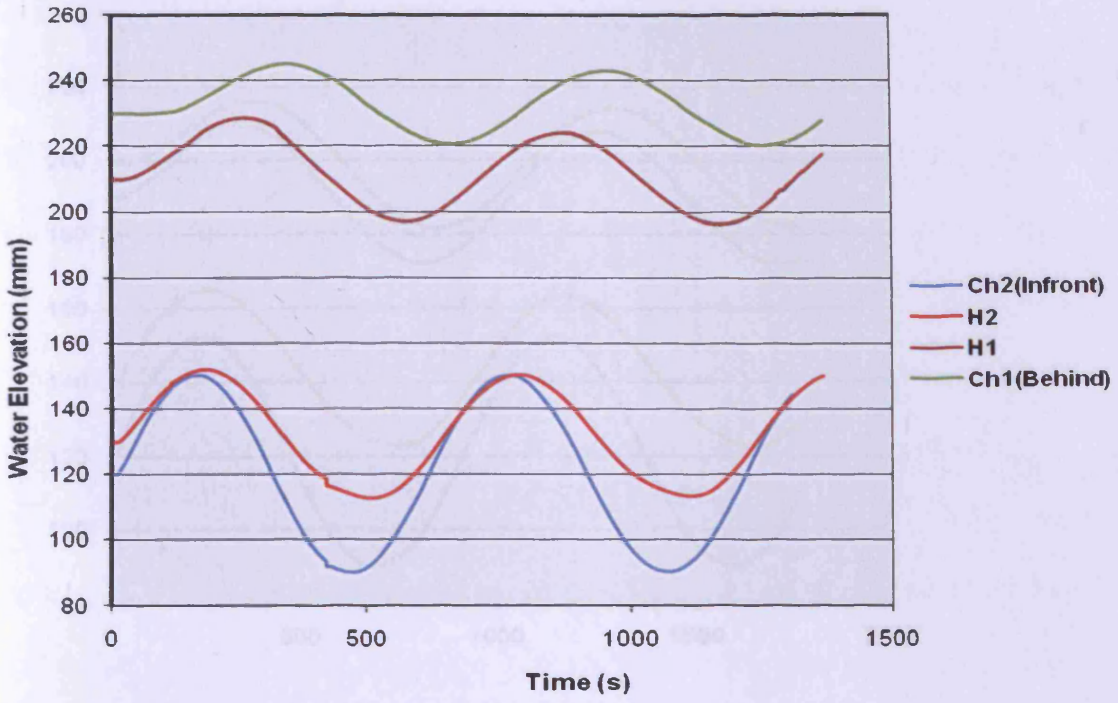

(a)

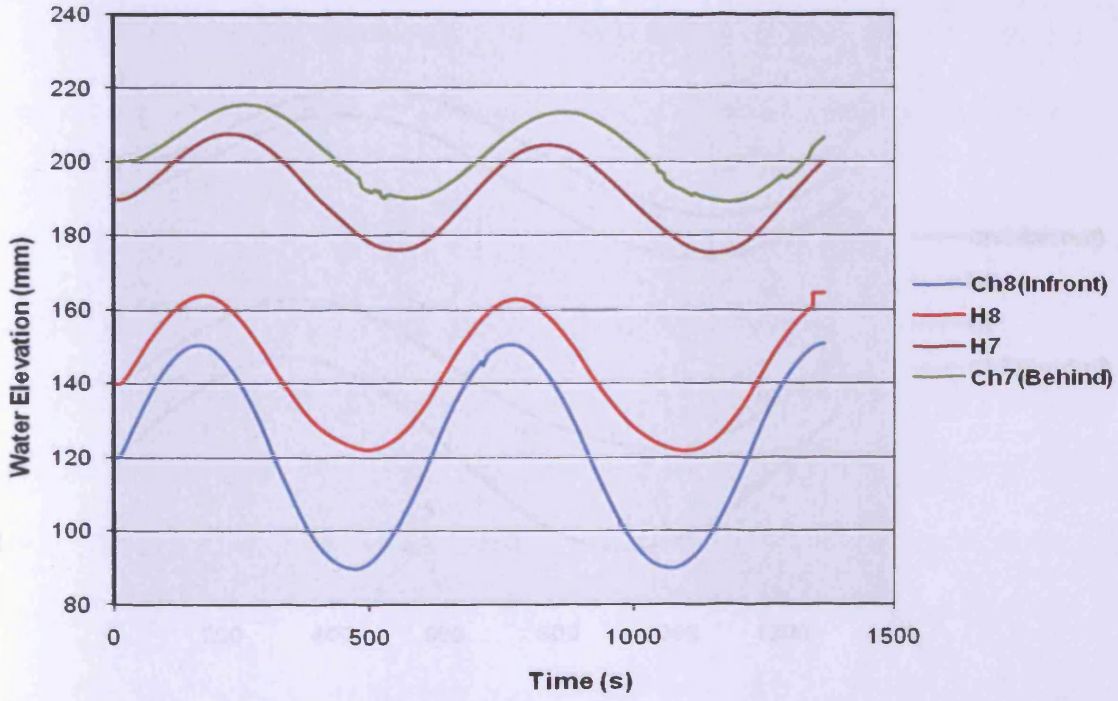

(b)

Figure 5.33: (a) 10mins tidal cycles for Ch1-Ch2 and (b) Ch7-Ch8 after steady state Pumping rate -0.0005m^3/s

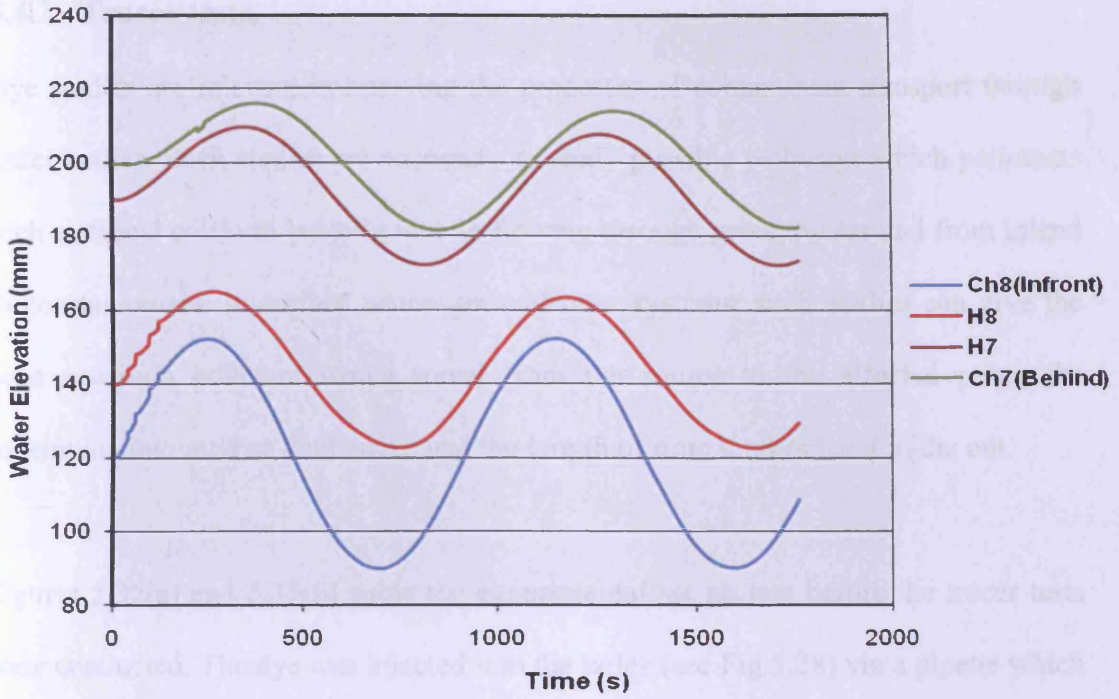

(a)

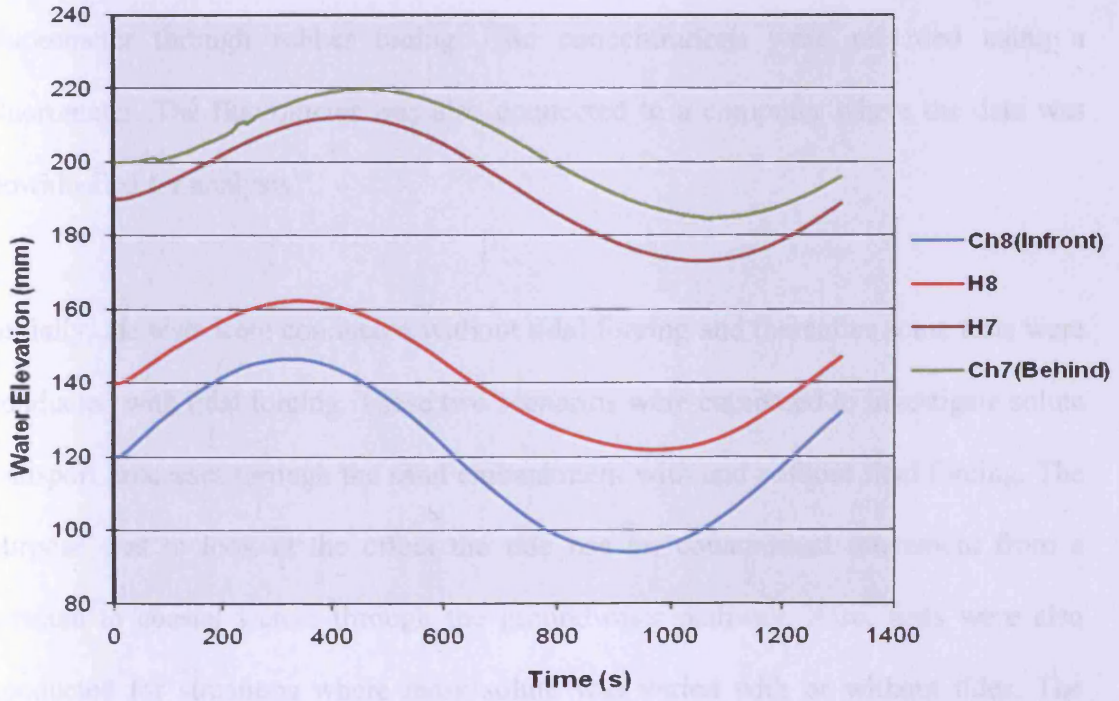

(b)

Figure5.34: (a) 15mins and (b) 20mins tidal cycles for Ch7-Ch8 after steady state

Pumping rate -0.0005m^3/s

5.4.2 Tracer tests.

Dye studies are relevant in knowing the processes of contaminant transport through water bodies. Such studies are necessary to study possible pathways which pollutants such as faecal coliform bacteria take in flowing through groundwater and from inland to coastal waters. In surface water- groundwater systems, such studies can give the time a certain pollutant would travel from the source to the affected point, the maximum amount that shall arrive and the length of time it takes for it to die out.

Figures 5.35(a) and 5.35(b) show the experimental set up just before the tracer tests were conducted. The dye was injected into the holes (see Fig 5.28) via a pipette which is mounted just above the injection hole. The monitoring hole was coupled to a fluorometer through rubber tubing. The concentrations were recorded using a fluorometer. The fluorometer was also connected to a computer where the data was downloaded for analysis.

Initially, the tests were conducted without tidal forcing and thereafter some tests were conducted with tidal forcing. These two scenarios were compared to investigate solute transport processes through the sand embankment with and without tidal forcing. The purpose was to look at the effect the tide has on contaminant movement from a wetland to coastal waters through the groundwater pathway. Also, tests were also conducted for situations where mass solute was varied with or without tides. The purpose was to look at the effect mass solute has on the concentration distribution in coastal waters when the adjacent wetland had been contaminated by a certain amount of solute.

(a)

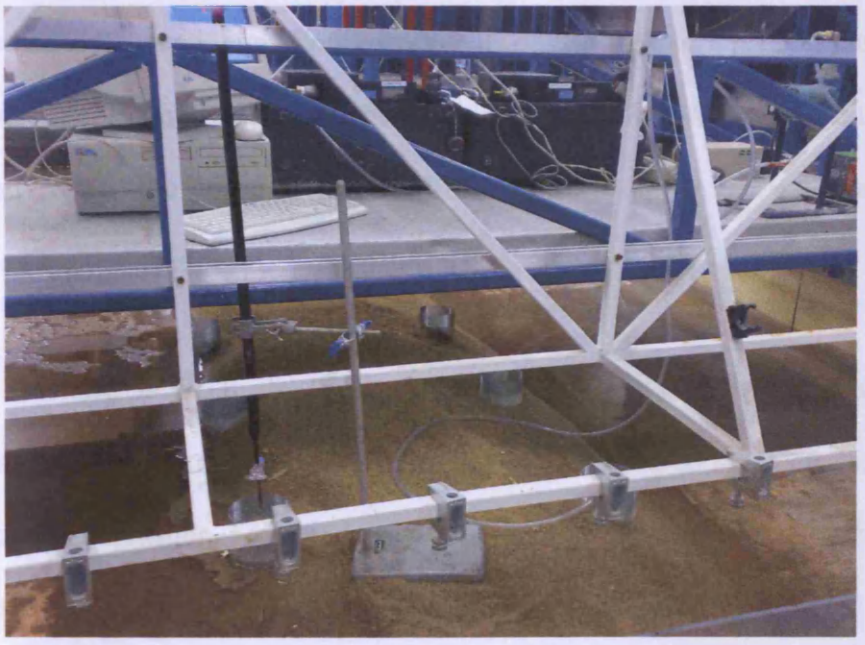

(b)

Figure 5.35: (a) and (b): Tracer tests set ups

5.4.2.1 Tracer tests results

Figure 5.36 shows the results of two tests where similar conditions were applied but

the injected volumes were different. In the two situations, the concentration injected in H1 (see Fig. 5.28) was 1ppt and but the volume of tracer was 50ml and 100ml respectively. Injection took place when steady state had been reached without any tidal forcing whilst observations were taken place at H2 (see Fig. 5.28).

In the first case where the volume was 50ml, the observed concentration rose from zero to a concentration of 266ppb within 116s then reduced to a minimum of 252ppb within 33s and then rose again to a maximum concentration of 269ppb within 36s after which it decayed to zero. In effect, two peaks were observed within about a minute which is normally not what had been expected. The reason for the double peak was thought to be due to some tracer being trapped within the sediments and being released after the continuous flow of water through the sand with that amount having given rise to the concentration as observed in Figure 5.36. However, the two peaks of 266 and 269ppb are not significantly different from each other and the trend is as observed in the literature.

In the second case where the volume of tracer was doubled whilst maintaining the same injected concentration as in the first case, the observed concentration rose from zero to 587ppb within 141s and then decayed to its lowest point which was an asymptote to the original.The observed concentration was almost doubled as shown in Figure 5.36, with this being a reflection of the mass of solutes for the two scenarios. It took 141s for the latter to reach its peak concentration, whereas it took 135s for the former to reach its first peak concentration and 186s to reach the second peak. In considering the first peak for the two hydrographs, the times of 135 and 141s are close to each other with a difference of 6s being small relative to.the time to peak typically

of 140s. In effect, it took almost the same time for a pollutant to reach its peak

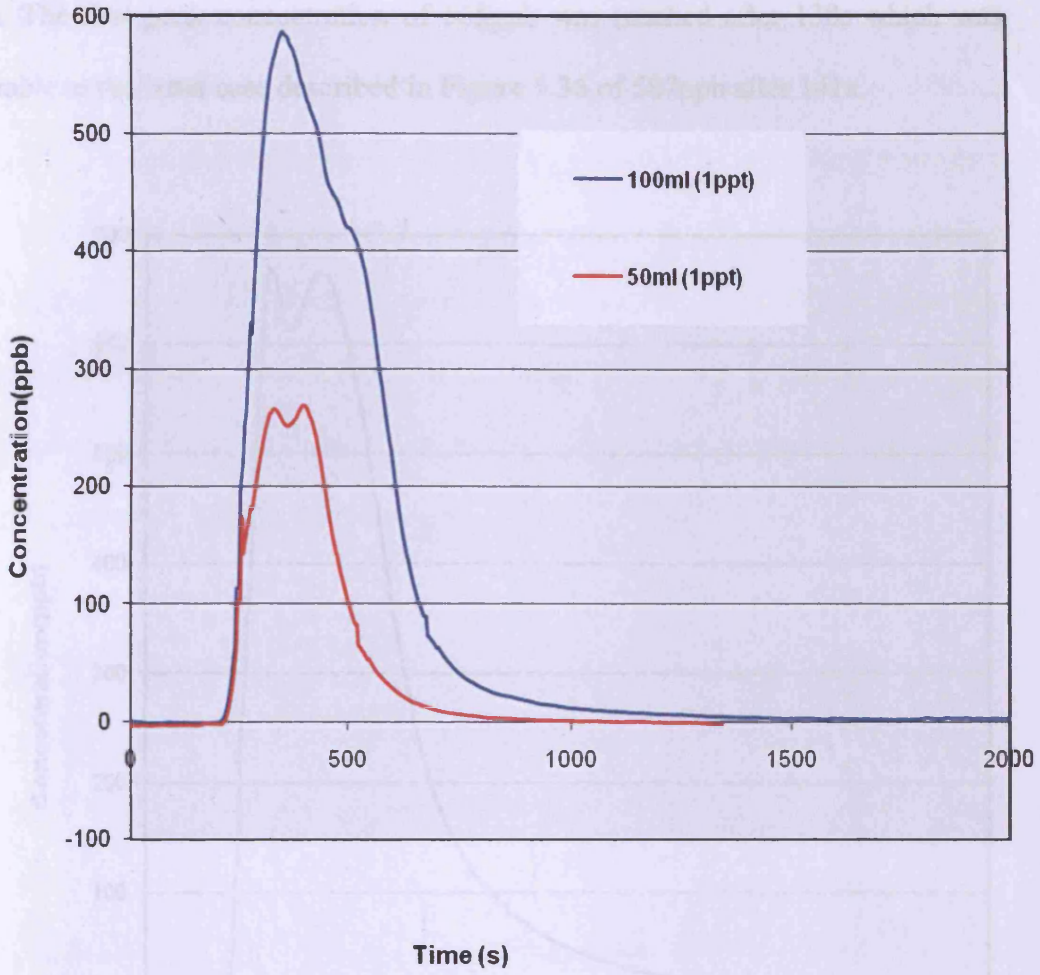

Figure 5.36: Concentration distribution for 50ml, 1ppt and 100ml, 1ppt injections at H1 and monitored at H2 respectively.

concentration after a spill through a medium with the same properties but differing in concentration levels. Hence the maximum concentration was found to be proportional to the volume of the spill. Figure 5.37 shows the concentration distribution at H4, with a similar injection regime as for the latter case described in Figure 5.36. The only different condition was that the injection of the tracer was at H3 and the observations were made at H4, as compared with the previous case where injection was at H1 and

observation at H2. Again two peaks were observed as described in the previous section. The first peak concentration of 668ppb was reached after 138s which was comparable to the latter case described in Figure 5.36 of 587ppb after 141s.

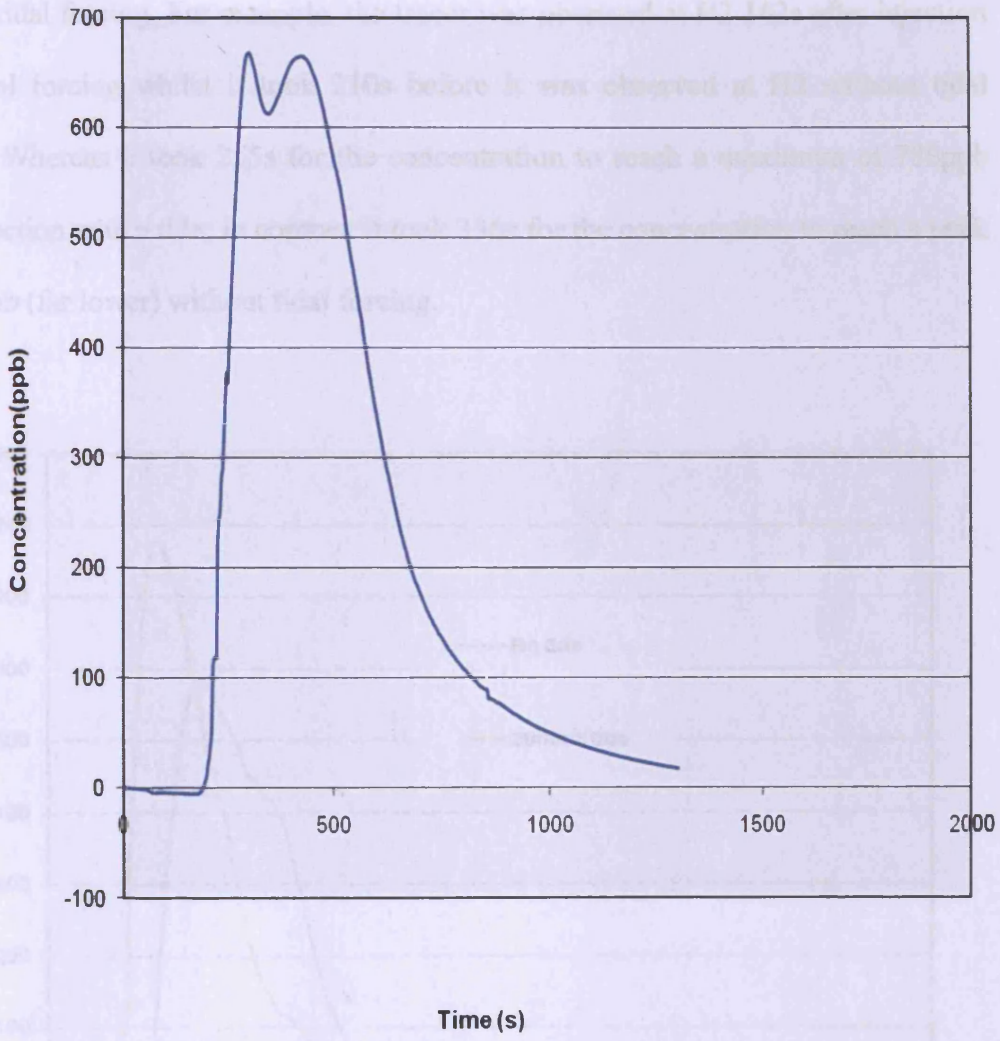

Figure 5.37: Concentration distribution at H4 for 100ml, 1ppt injection at H3

5.4.3 Tracer tests with tidal forcing

As indicated in the earlier section, tracer tests were also conducted with tidal forcing. Figure 5.38 shows the concentration distributions for tests with and without tidal

forcing with all other conditions remaining unchanged. The injected concentration was 1ppt at H1 with a volume of 100ml and monitored at H2. It was observed that, the monitored concentration peaked earlier with the tidal forcing than for the case without tidal forcing. The peak concentration was also higher with the tide than for the case without tidal forcing. For example, the tracer was observed at H2 162s after injection with tidal forcing whilst it took 210s before it was observed at H2 without tidal forcing. Whereas it took 255s for the concentration to reach a maximum of 780ppb after injection with a tide; in contrast it took 336s for the concentration to reach a peak of 587ppb (far lower) without tidal forcing.

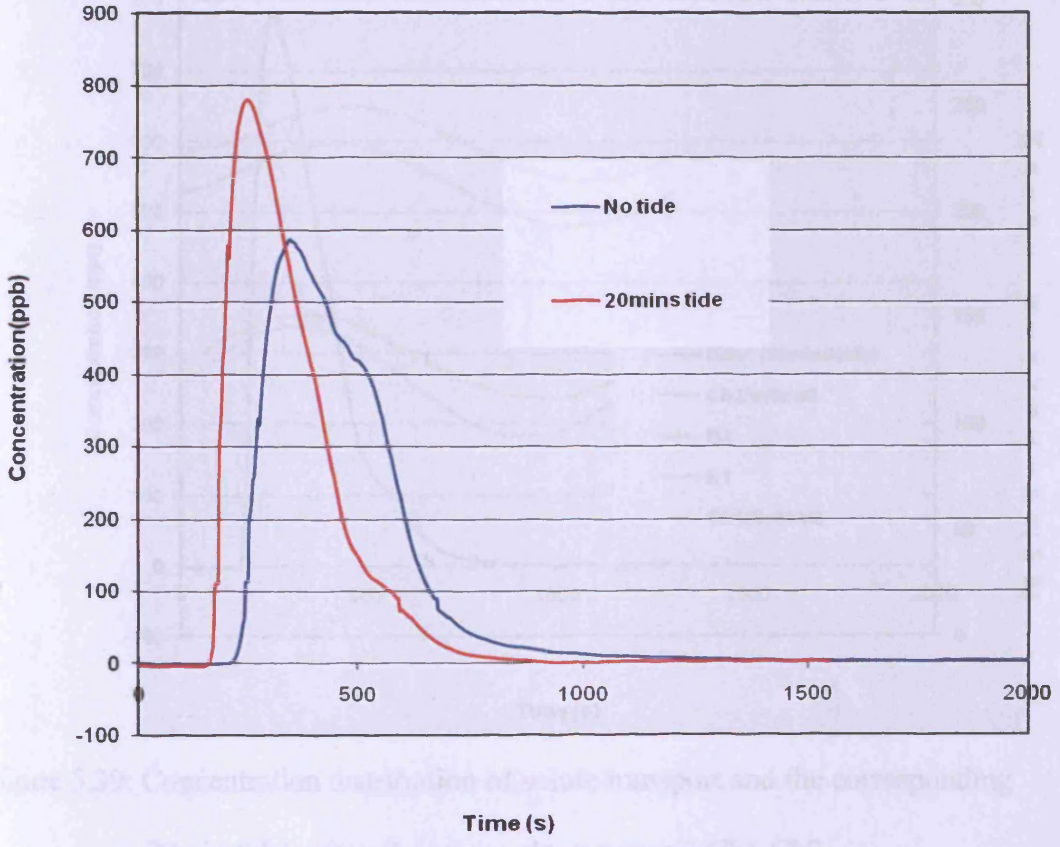

Figure 5.38: Comparison of concentration distribution at H2 with and without tidal forcing (same conditions) for tidal period of 20mins.

The main reason may be due to high flows and resultant increase in currents as a result of the tide as can be depicted from Figure 5.39 where the concentration distribution is compared with tidal water elevations. At the time of injection the tide would push the dye in the injection hole and thereby increase advection for the dye to reach the monitoring station quickly than the case without tidal influence. The tide would also remove all the solute which otherwise would have been attached to the sediments and travel quickly to the monitoring station hence the peak concentration would be higher for the situation where there was a tidal influence than the case without.

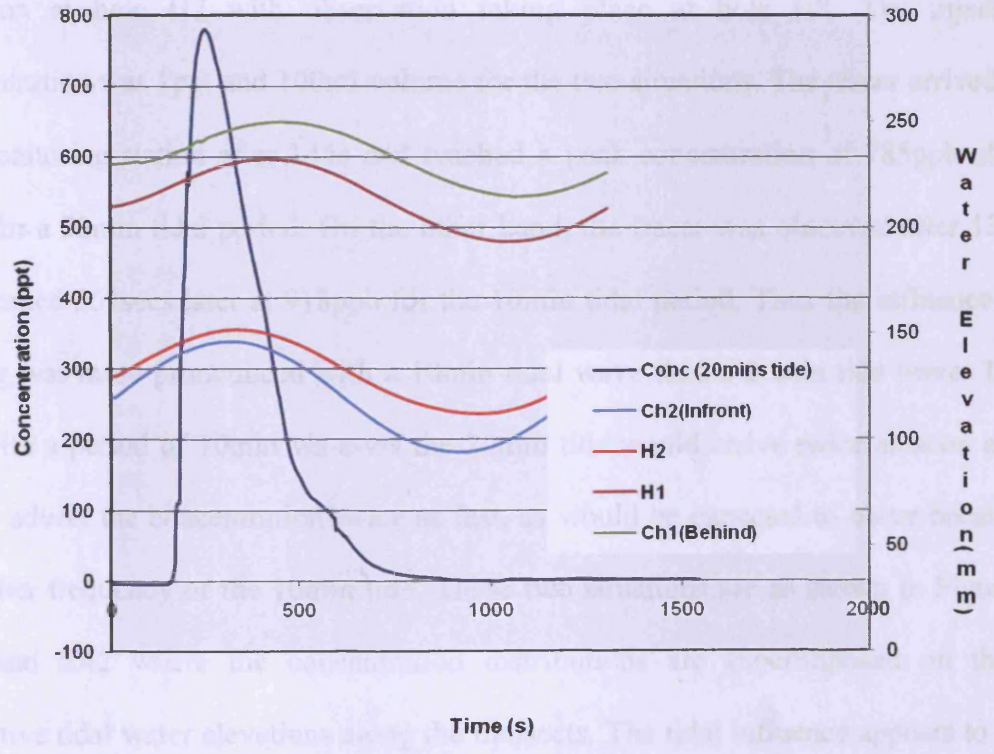

Figure 5.39: Concentration distribution of solute transport and the corresponding 20min tidal water elevations along transect Ch1-Ch2.

However, since the tidal period of 20mins was longer, all the solute would have moved to the monitoring hole by the time the tide was ebbing and thereby would not affect the concentration during the ebb tide as can be seen from Figure 5.39.

In their work Li et al (2004) found that residence time of contaminants reduced due to tidal oscillations in coastal aquifers and that resulted in rapid aquifer flushing and consequently led to contaminant transfer to the ocean. This is what has been observed in this study.

Figure 5.40 shows concentration distribution for 20min and 10min tidal forcing for injection at hole H7 with observation taking place at hole H8. The injected concentration was 1ppt and 100ml volume for the two situations. The tracer arrived at the monitoring station after 144s and reached a peak concentration of 785ppb after 300s for a 20min tidal period. On the other hand, the tracer was observed after 132s and peaked 261secs later at 918ppb for the 10min tidal period. Thus the influence of mixing was more pronounced with a 10min tidal wave than a 20min tide wave. The tide with a period of 10min vis-a-vis the 20min tide would arrive twice as soon and would advect the concentration twice as fast, as would be expected to occur because of higher frequency of the 10min tide. These two situations are as shown in Figures 5.41 and 5.42 where the concentration distributions are superimposed on their respective tidal water elevations along the transects. The tidal influence appears to be more pronounced with the 10mins tide (Fig. 5.41) than with the 20mins tide.

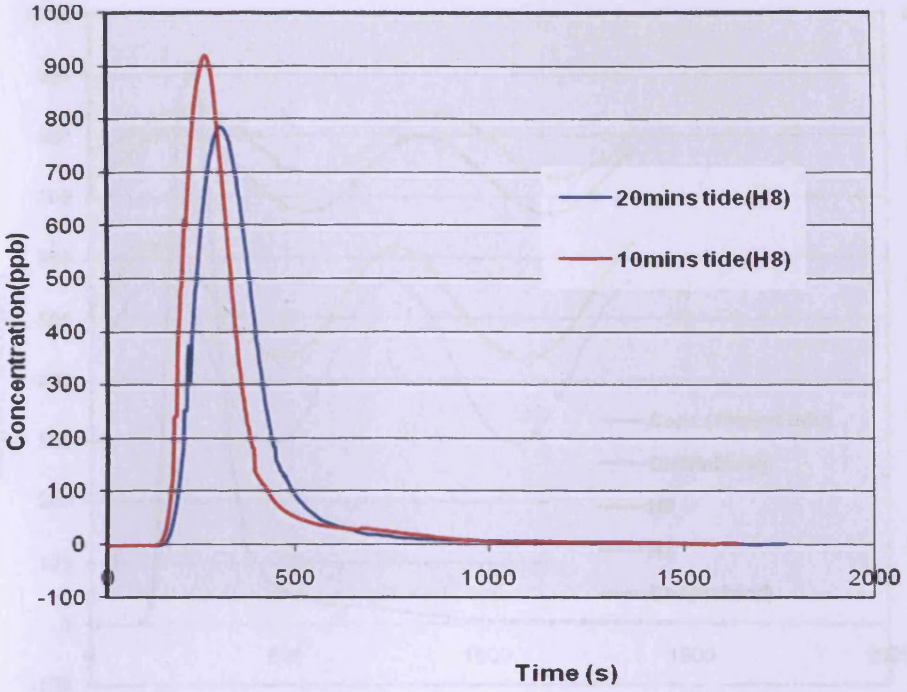

Figure 5.40: Comparison of 20mins and 10mins tidal forcing compared for H8

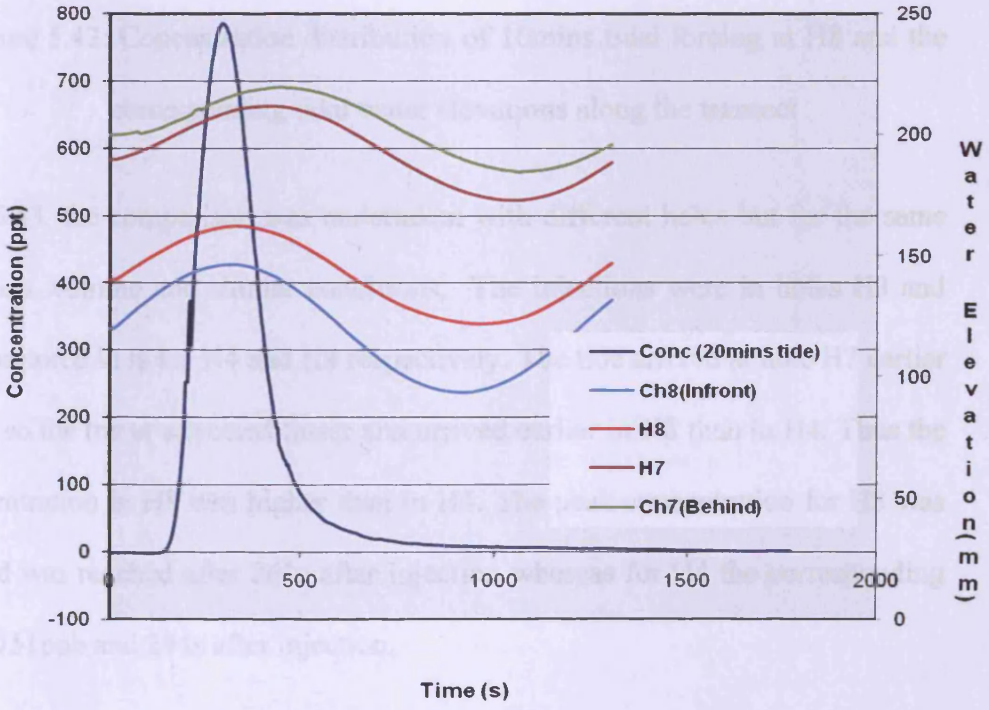

Figure 5.41: Concentration distribution of 20mins tidal forcing at H8 and the corresponding tidal water elevations along the transect

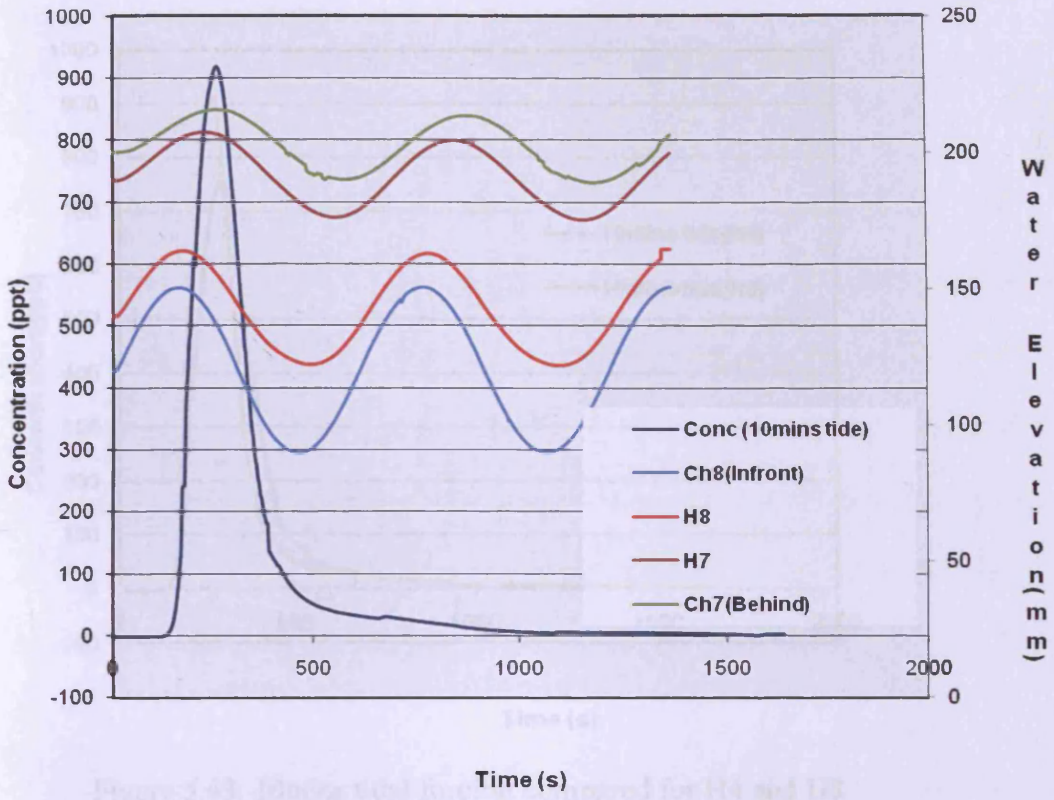

Figure 5.42: Concentration distribution of 10mins tidal forcing at H8 and the corresponding tidal water elevations along the transect

In Figure 5.43, the comparison was undertaken with different holes but for the same concentration, volume and similar conditions, The injections were in holes H3 and H7 and monitored in holes H4 and H8 respectively. The tide arrived at hole H7 earlier than at H3 so the tracer advected faster and arrived earlier in H8 than in H4. Thus the peak concentration in H8 was higher than in H4. The peak concentration for H8 was 918ppb and was reached after 261s after injection whereas for H4 the corresponding value was 751ppb and 294s after injection.

Figure 5.44 shows the concentration distribution at H4 for a10mins tide being superimposed by the water elevations as discussed earlier in Figure 5.42.

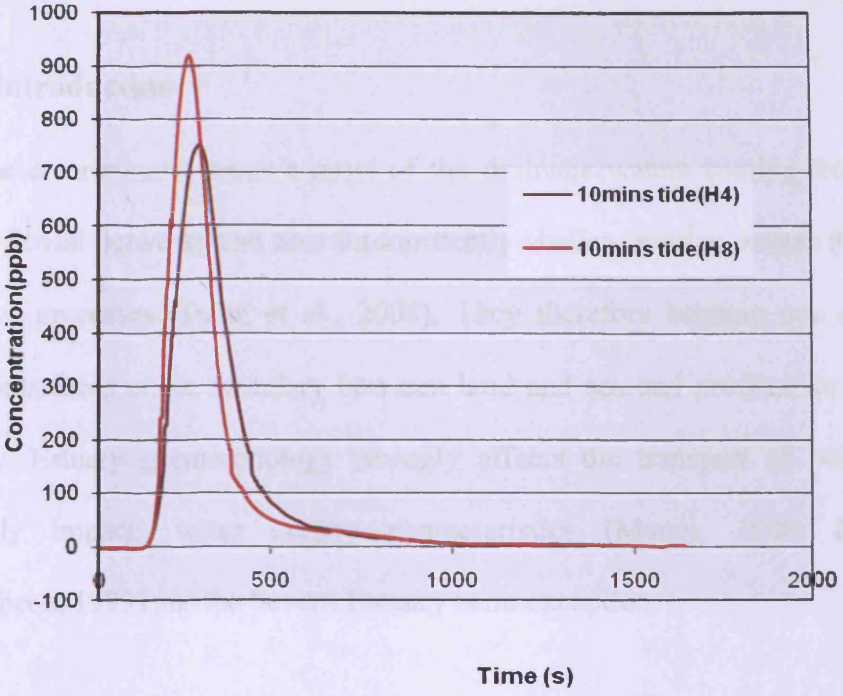

Figure 5.43: 10mins tidal forcing compared for H4 and H8

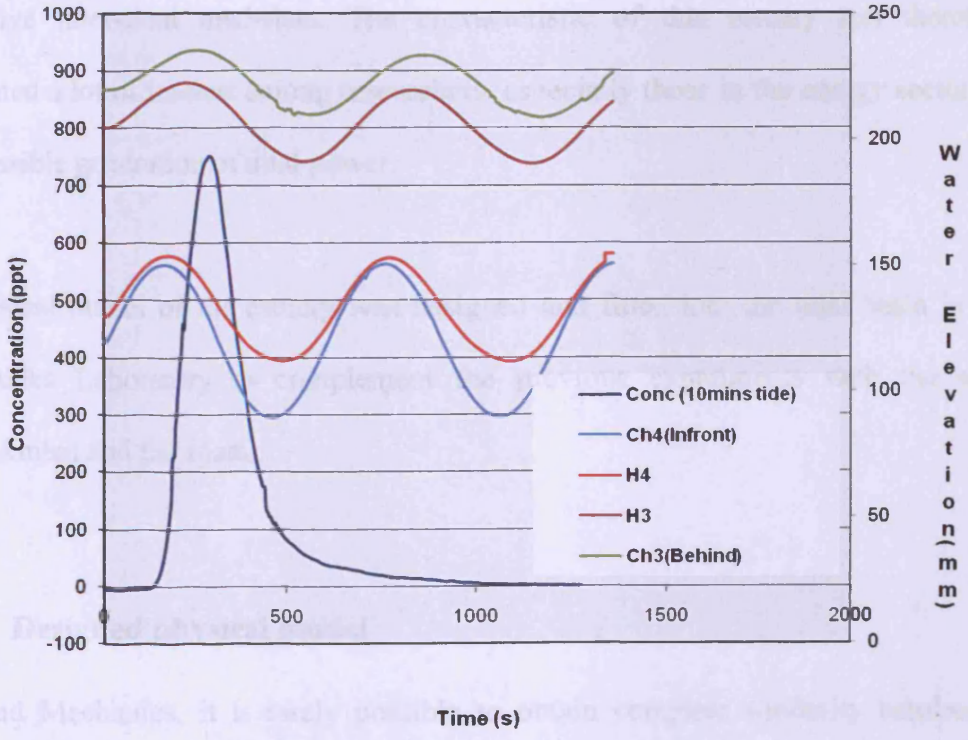

Figure 5.44: Concentration distribution of 10mins tidal forcing at H4 and the corresponding tidal water elevations along the transect.

5.5 Severn Estuary physical model

5.5.1 Introduction

Estuarine environments receive most of the drainage waters coming from the land through fluvial networks and also intermittently shallow marine waters through tidal and wave processes (Traini et al., 2008). They therefore become one of the main critical interfaces at the boundary between land and sea and produce an exceptional diversity. Estuary geomorphology strongly affects the transport of pollutants and ultimately impacts water quality characteristics (Manoj, 2008; Martin and McCutcheon, 1999) and the Severn Estuary is no exception.

It is well known that the Severn Estuary has an extremely large tidal range of over 14m at Avonmouth (Xia et al., 2010) and a mean spring tide of 12.2m and therefore extensive inter-tidal mud-flats. The characteristic of this estuary has therefore generated a lot of interest among researchers, especially those in the energy sector for the possible generation of tidal power.

A physical model of the estuary was designed and fitted into the tidal basin in the Hydraulics Laboratory to complement the previous experiments with the sand embankment and the foam.

5.5.2 Designed physical model

In Fluid Mechanics, it is rarely possible to obtain complete similarity between a model and its corresponding prototype (Falconer, 1974). The best dynamic similarity

would be obtained by maintaining the constancy of the Froude and Strouhal Numbers (Falconer, 1974) which are given as:

$$F_R = \frac{V^2}{gL} \quad \text{and} \quad S = \frac{L}{VT}$$

where F_R and S = Froude and Strouhal numbers respectively, L = length scale; V = velocity; g = acceleration due to gravity and T=period.

Consequently, the following holds true for the scaling parameters used for the design:
If L and H are the horizontal and vertical lengths and T is the period then,
Horizontal area, $A = L^2$; vertical area, a = LH; velocity, $v = H^{0.5}$ and time, $T = LH^{-0.5}$
In the main Severn Estuary the maximum tidal range is 14m at Avonmouth and the tidal period is about 12.4hours. Based on Falconer (1974), the distorted physical model was designed giving a tidal range of 12cm and a tidal period of 20s with a vertical scale of 1:150 and a horizontal scale of 1:25,000. However, this situation could not be achieved in its totality. The limitations of the model meant that a tidal range of 10cm and a tidal period of 40sec were the limiting conditions in the physical model. Figure 5.40 shows the Admiralty Chart 1179 which serves as the base map from which the physical model domain was designed based on a 1:25,000 horizontal scale

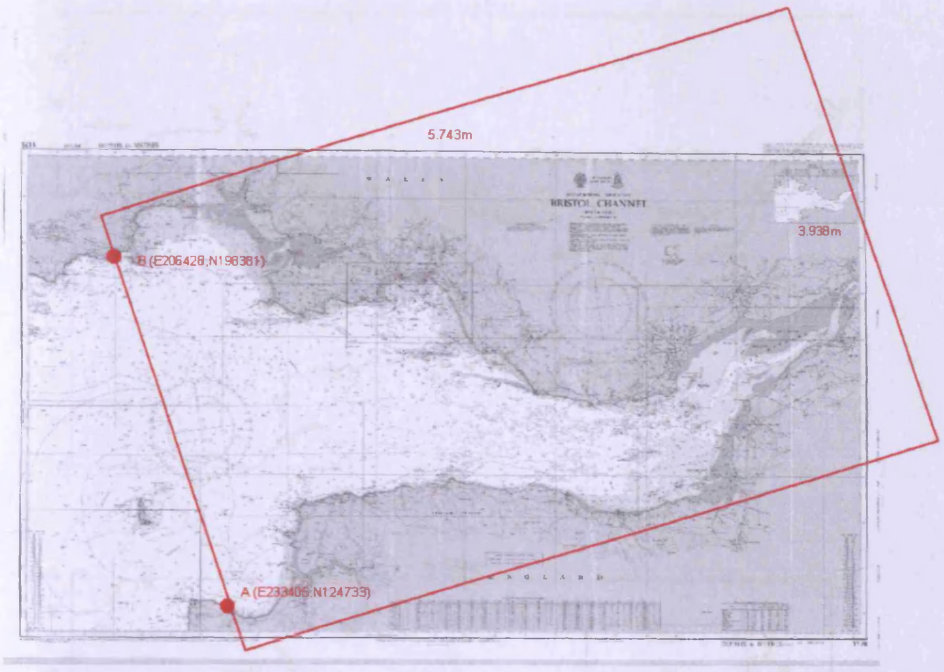

Figure 5.45: Severn estuary physical model domain

The shape of the prototype as shown in Figure.5.46 (a) could not fit into the tidal basin, so upstream of the river Severn from the Old Severn Bridge to the tidal limit at Haw Bridge, the model turned slightly in the basin domain as shown in Figure 5.46 (b). Included in this physical model was a 2.0m x 1.2m x 0.075m rectangular box designed to hold sand and connected to the river and estuary by four small channels as shown in Figure 5.46 (b). The sandbox was to provide the link with the previous studies, with discussions to follow. Also included in the physical model is a removable model barrage to simulate the effects of the proposed structure on the hydrodynamic and solute transport processes in the Severn Estuary. Figure 5.47 shows the proposed location of the barrage as in the main estuary and as it appears in the physical model as shown in Figure 5.46(b). However, the model barrage was not included in the study presented herein. It has been mentioned just for completion.

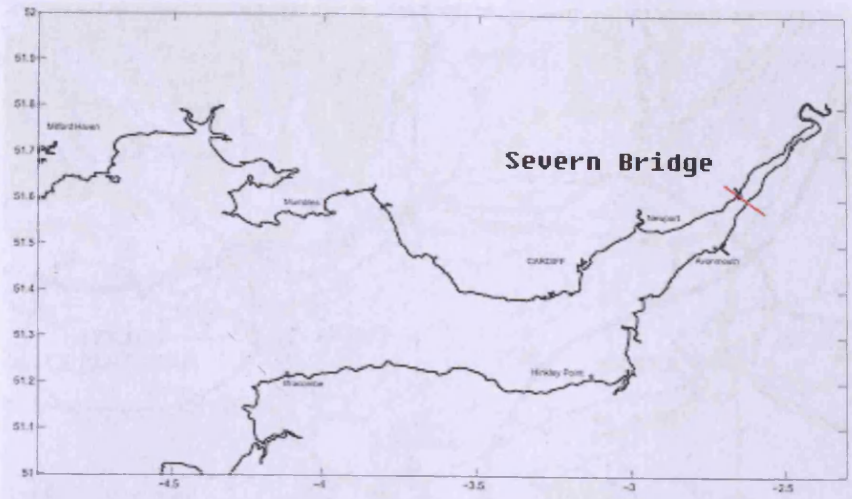

(a)

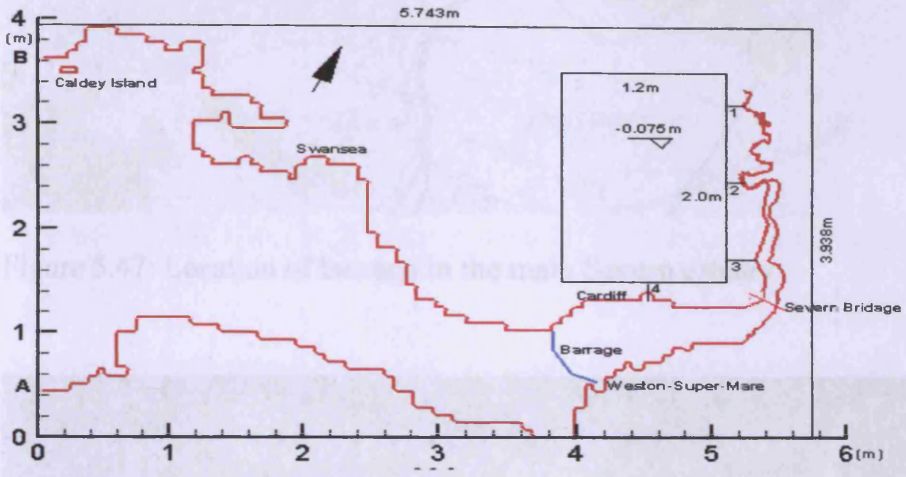

(b)

Figure 5.46 (a): Severn estuary (prototype) and (b) as sited in the tidal basin showing the location of the bend in the model.

Figures 5.48 and 5.49 show the aerial and side views of the designed physical model as laid out in the tidal basin for the studies to be undertaken herein. Figure 5.50 also shows the tidal basin with tide running.

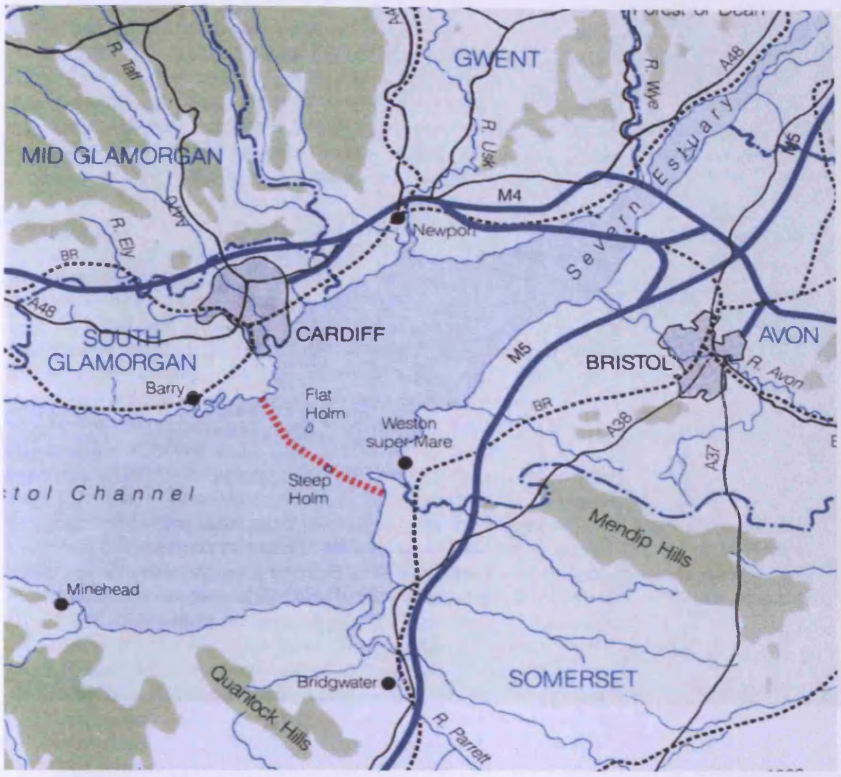

Figure 5.47: Location of barrage in the main Severn estuary

Figure 5.48: Aerial view of the physical model as laid out in the tidal basin

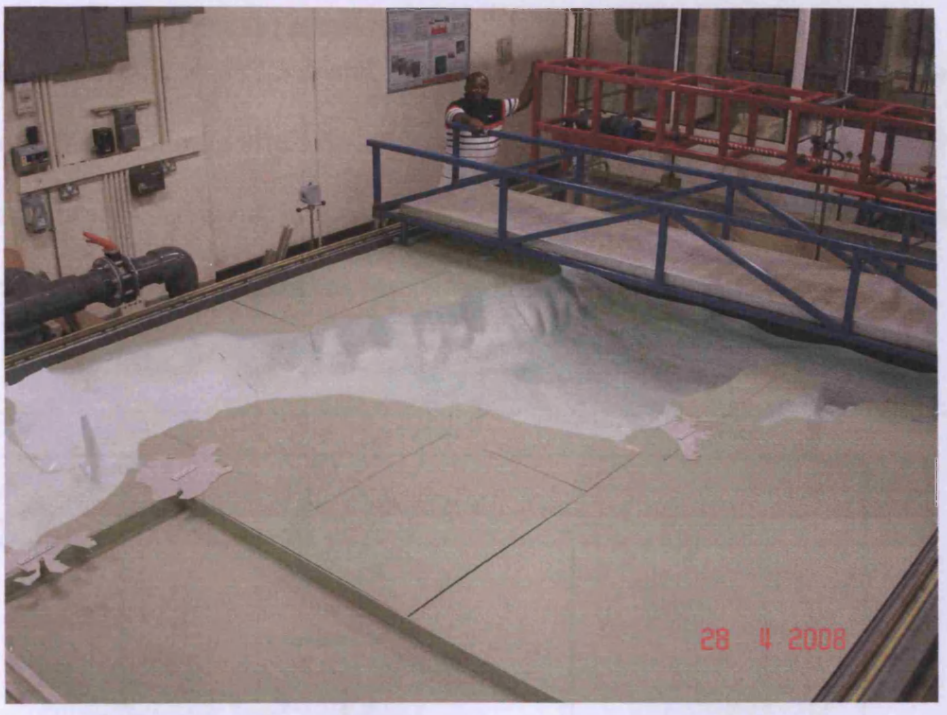

Figure 5.49: Side view of the physical model as laid out in the tidal basin

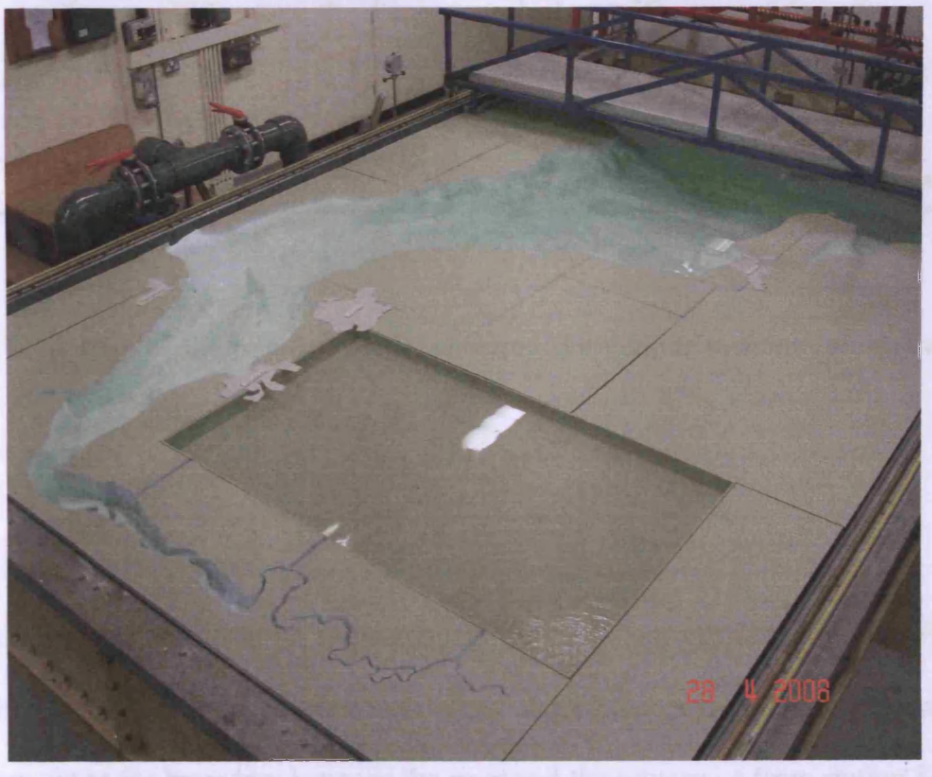

Figure 5.50: Tide running in the physical model

5.5.3 Water level measurements.

As part of this study, water level and velocity data were collected at selected locations or stations as shown in Figure 5.51. Figures 5.52(a) and (b) show the estuary with the water level probes and the ADV (Acoustic Doppler Velocimeter) for the start of water level and velocity measurements as discussed later.

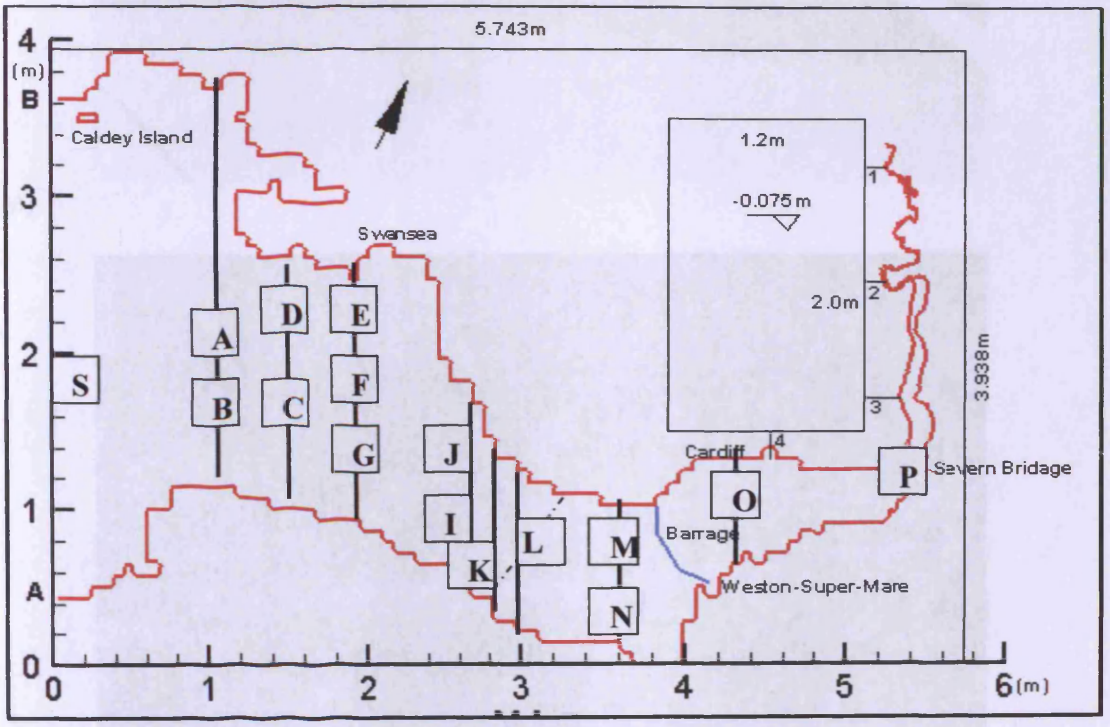

Figure 5.51: Map of the physical model showing the various stations (points) where data were colleted

5.5.3.1 Water Level results

The results of water elevation measurement variations are presented herein. Figure 5.53 shows the results of four stations along the whole estuary from the seaward boundary, up to the boundary between the river and the estuary i.e from station S to P. It was observed that the water elevation increased from station S up to station P. This

(a)

(b)

Figure 5.52: (a) Tidal basin showing water level and ADV probes and (b) water level probes for data collection

same trend was replicated as the tide moved from station A to station O as shown in Figure 5.54. This meant that as the estuary became narrower, water level rose and the amplitude magnified. Thus the contraction of the section of the estuary had an effect on the water elevation. Table 5.2 shows the water level elevations for the prototype as

presented by Xia et al.(2010) and the trend is similar to what has been observed in this study. The points G, L, O and P represent Swansea, Minehead, Cardiff and Beachley respectively as shown in the table. As the channel convergence increases, the distortion of the tidal wave is enhanced and both tidal wave speed and wavelength increase (Lanzoni and Seminara, 1998). Robinson (1980) in Hashemi et al. (2008), observed that energy density is concentrated by the funnelling effect of the wedge-shaped topography of the Bristol Channel and hence a large tidal range at the mouth of the estuary can be converted into a large tidal range at the head of the estuary.

Table 5.2: Water level elevation for the main Severn Estuary (source: Xia et al, 2010)

	Water levels(m)		
Sites within Estuary	Maximum	Minimum	Tidal range
Swansea	4.37	-3.95	8.32
Minehead	5.24	-4.74	9.98
Cardiff	5.95	-5.20	11.15
Avonmouth	6.59	-5.16	11.75
Beachley	6.88	-4.89	11.77

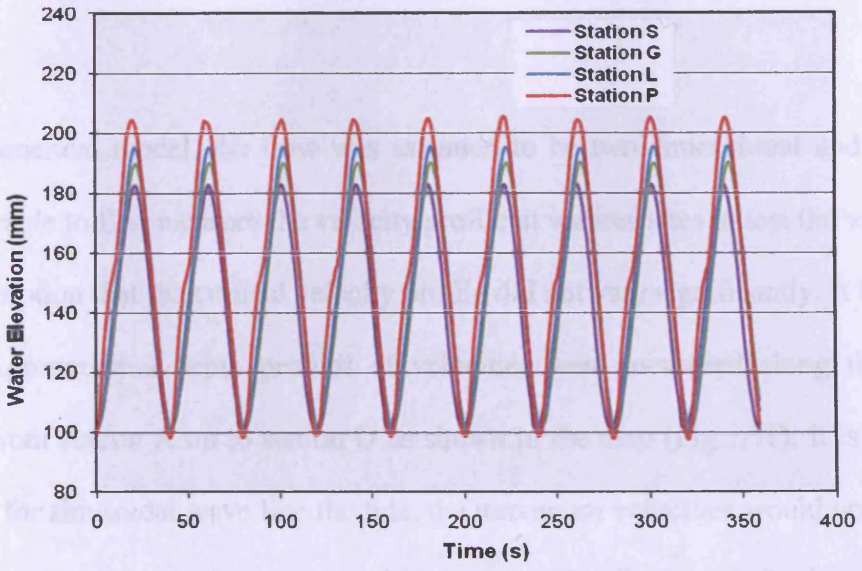

Figure 5.53: Water elevations for stations S, G, L, and P

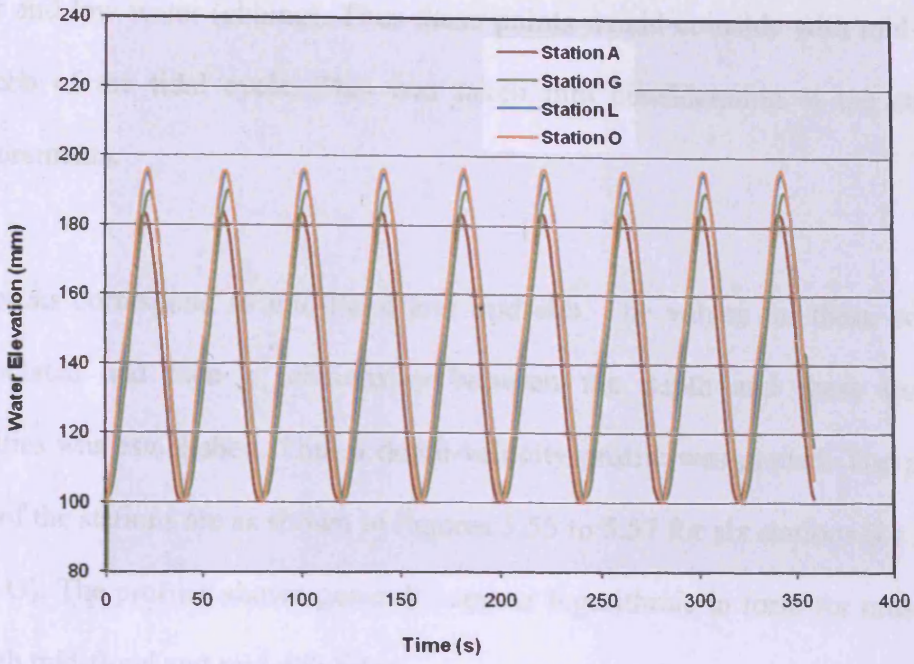

Figure 5.54: Water elevations for stations A, G, L, and O

5.5.5 Velocity Measurements

Extensive velocity measurements were then taken using the ADVs as shown in Figure 5.52 (a) .The ADV probes were connected to a computer whereupon the data were downloaded for analysis. The probes measure velocities in three dimensions, i.e. x, y, and z.

In the numerical model, the flow was assumed to be two-dimensional and hence it was desirable to first measure the velocity profile at various sites to test the validity of this assumption that the vertical velocity profile did not vary significantly. It is against this background that depth profiles of velocities were measured along the whole estuary from station A up to station O as shown in the map (Fig.5.51). It is assumed also that for sinusoidal wave like the tide, the maximum velocities would occur when the tide was between the low water and high water (flooding); and also between high

water and low water (ebbing). Thus these points would coincide with mid-flood and mid-ebb of the tidal cycle. This was taken into consideration at the start of the measurements.

The peaks correspond to mid-flood and mid-ebb. The values for these points were extrapolated and then a relationship between the depth and these extrapolated velocities was established. Thus a depth-velocity profile was plotted. The profiles of some of the stations are as shown in Figures 5.55 to 5.57 for six stations (i.e D, G, I, J, L and O). The profiles shown generally appear logarithmic in form for most stations, for both mid-flood and mid-ebb tides.

Figures (5.58-5.65) show the depth averaged current speeds for the various stations as indicated earlier. These correspond to the current speed measured at 0.4 depth from the bed at each particular position. In all the graphs there appears to be two or more peaks at the mid flood or mid ebb. This phenomenon can be attributed to circulation within the estuary. Frick et al(2007) report that tidal exchange produces large velocities at the mouth of the Yaquina estuary in the US during flood and ebb and that tidal circulation is influenced by tides. For example in this estuary, velocity magnitudes during ebb and flood, are generally of the order of 0.25m/s in the coastal region and 1.0m/s in the main channel of the estuary. Tidal eddies often exist in coastal and estuarine waters when coastlines are irregular (Frick et al.,2007). (Uchiyama, 1999) found that tidal oscillations mainly bring about the formation of local circulation. Another observation was that for almost all of the stations the velocities at mid-ebb were higher than for those at mid-flood. Thus there was an

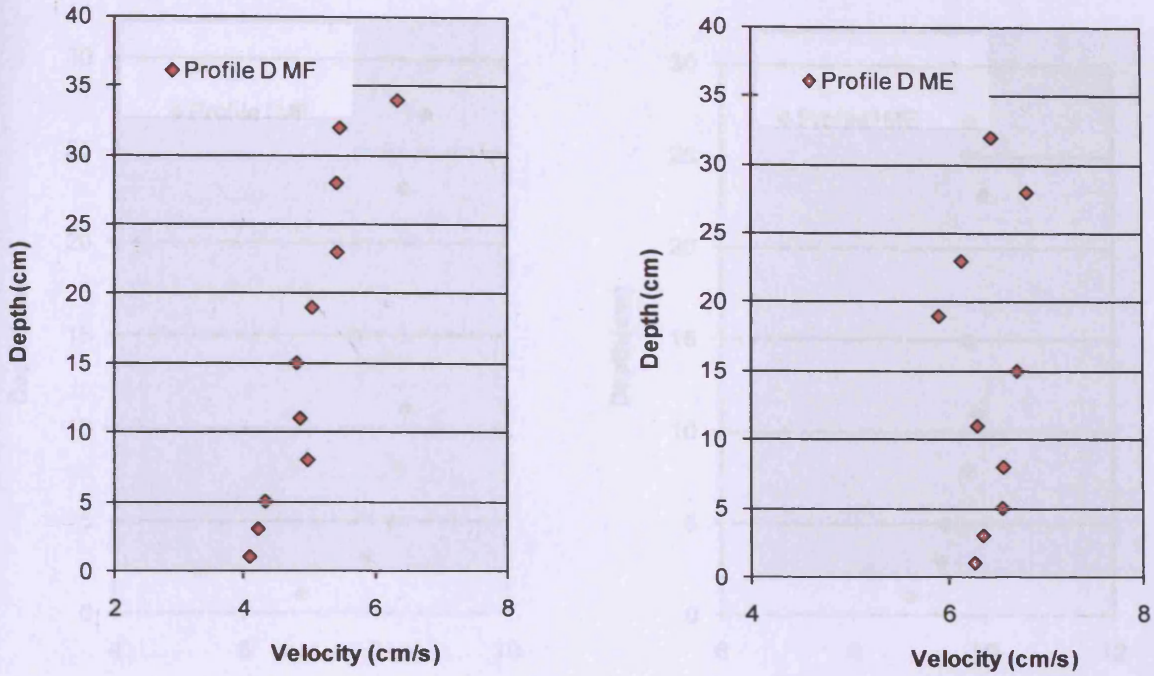

(a)

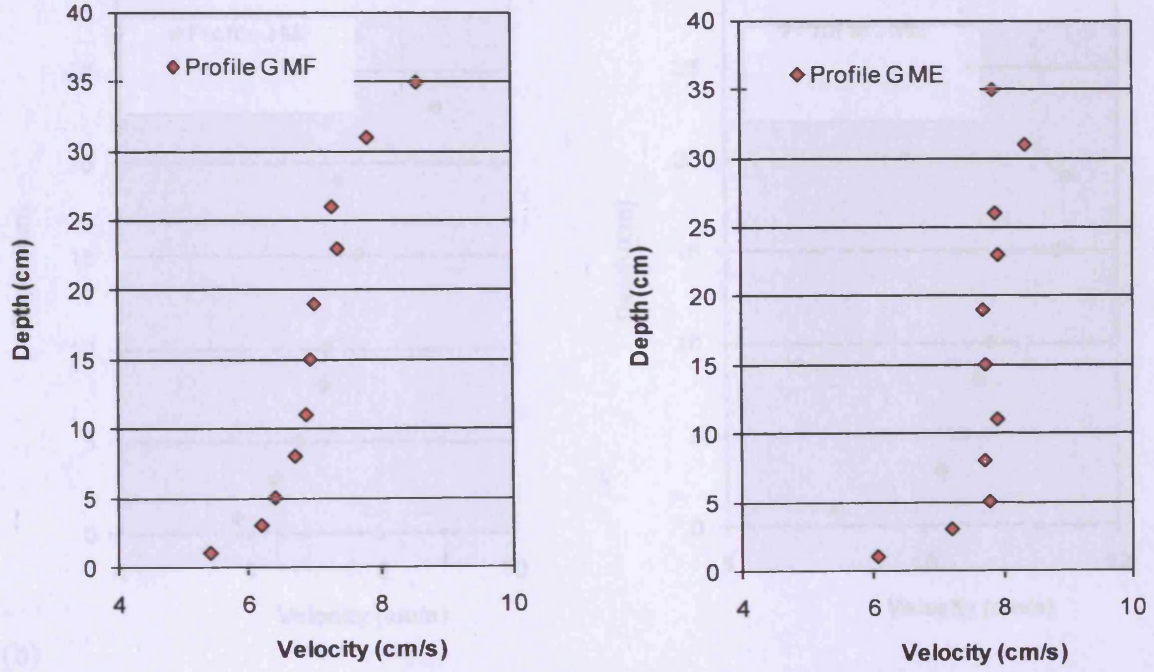

(b)

Figure 5.55: Velocity profiles for mid-flood (MF) and mid-ebb (ME) for station (a) D and (b) G

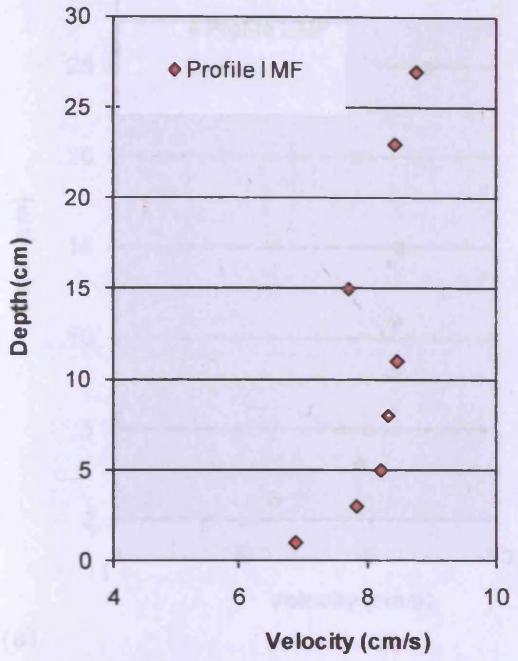

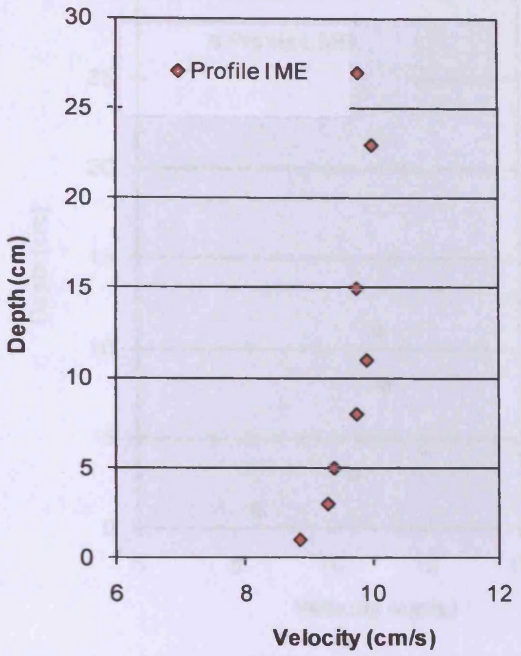

(a)

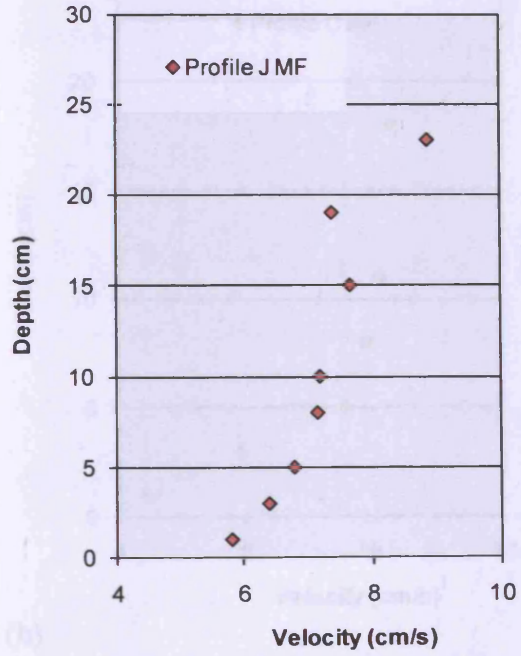

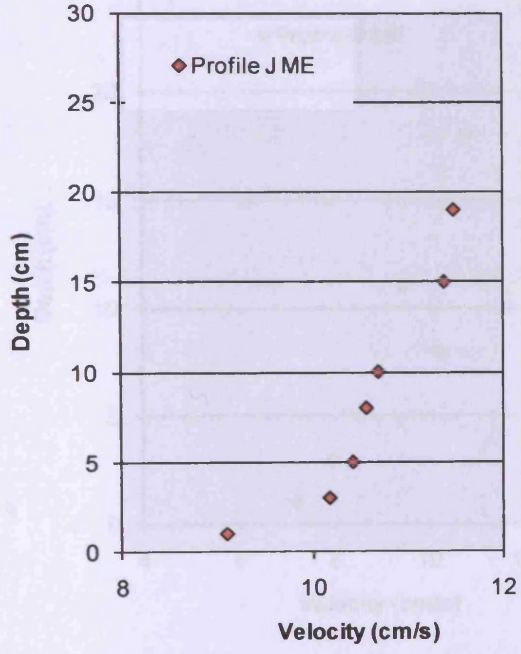

(b)

Figure 5.56: Velocity profiles for mid-flood (MF) and mid-ebb (ME) for station (a) I and (b) J

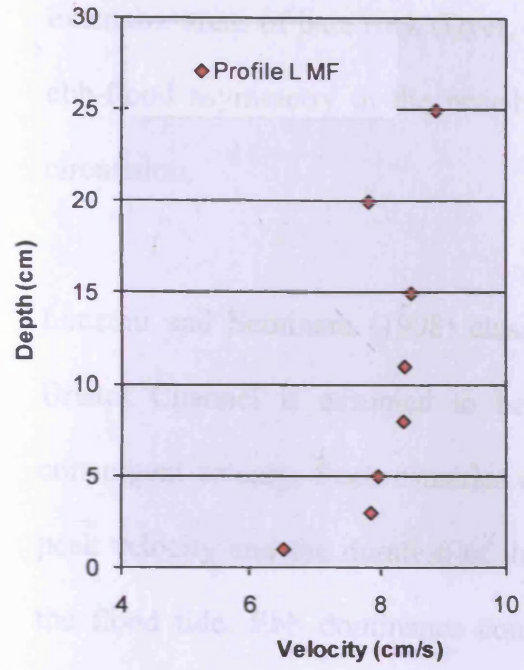

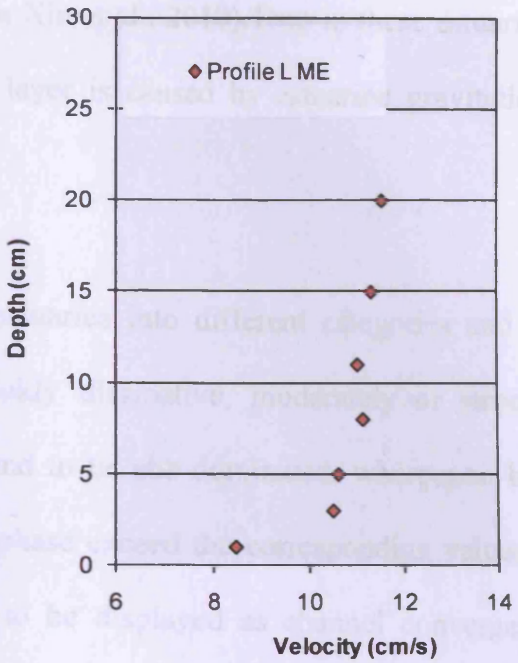

(a)

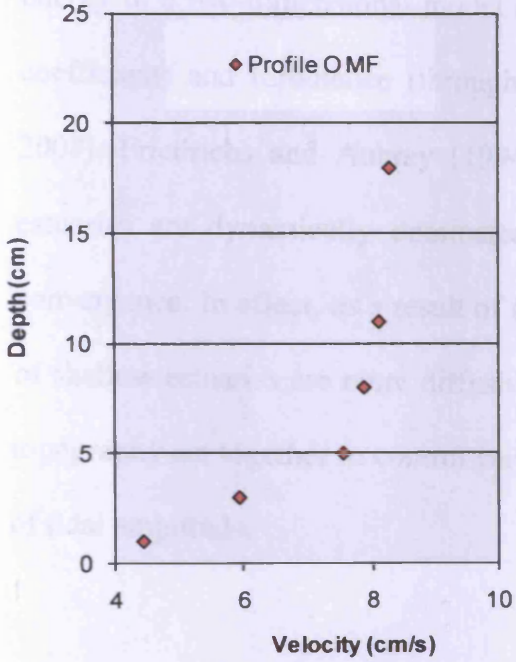

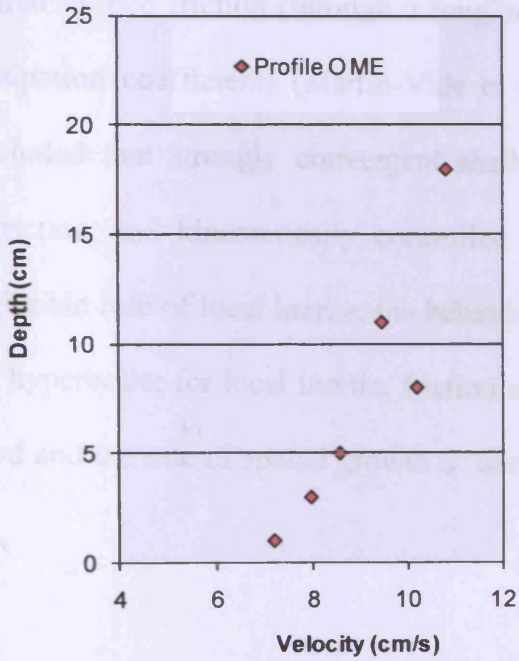

(b)

Figure 5.57: Velocity profiles for mid-flood (MF) and mid-ebb (ME) for station (a) L and (b) O

assymetry in the maximum values for flood and ebb tides. This trend as shown in the bed of the Bristol Channel and the Severn Estuary comprises a wide range of distinct

lithologies, and much of the seabed is stripped of unconsolidated sediments, leaving extensive areas of bare rock (Dyer, 1984 in Xia et al., 2010).Thus in these estuaries a ebb-flood asymmetry in the near-bottom layer is caused by estuarine gravitational circulation.

Lanzoni and Seminara (1998) classified estuaries into different categories and the Bristol Channel is assumed to be a weakly dissipative, moderately or strongly convergent estuary. Such estuaries are found to be ebb-dominated, whereupon both peak velocity and the duration of the ebb phase exceed the corresponding values of the flood tide. Ebb dominance continues to be displayed as channel convergence increases. Thus this phenomenon is due to energy changes in the estuary as losses of energy in a two-dimensional model are shared by bed friction (through a roughness coefficient) and turbulence (through a dissipation coefficient) (Martin-Vide et al., 2008). Friedrichs and Aubrey (1994) concluded that strongly convergent shallow estuaries are dynamically dominated by friction and kinematically controlled by convergence. In effect, as a result of the negligible role of local inertia, the behaviour of shallow estuaries are more diffusive than hyperbolic; for local inertia, friction and topography act together to control wave speed and the rate of spatial growth or decay of tidal amplitude.

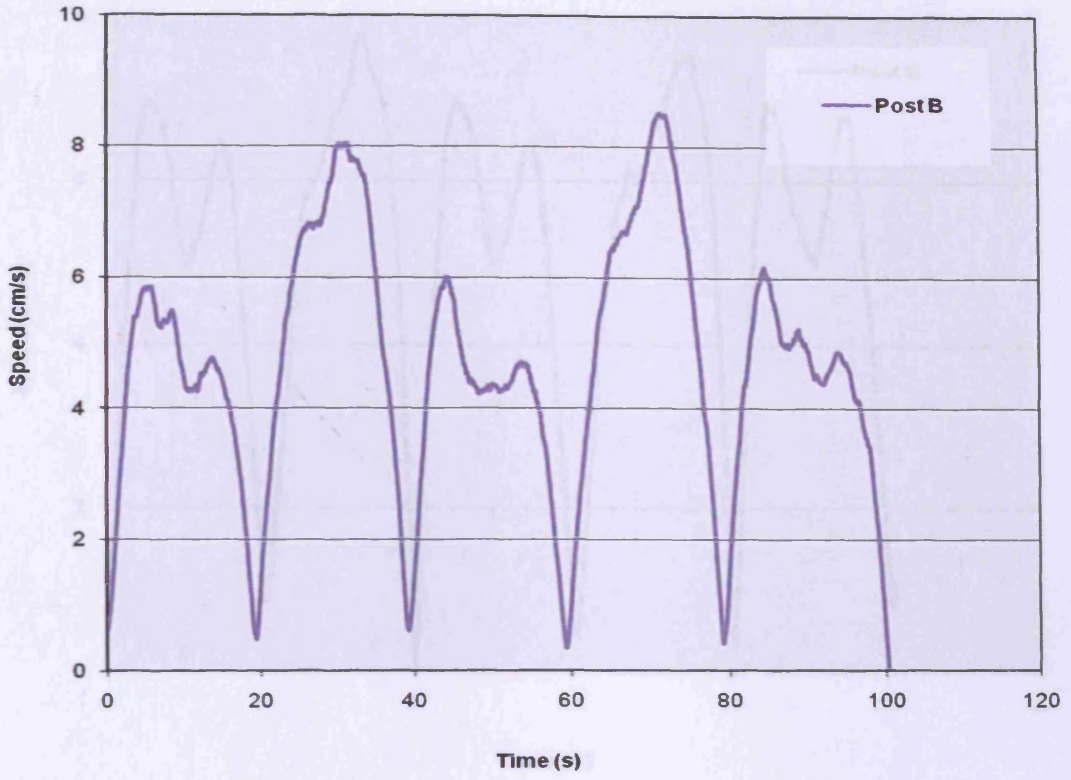

Figure 5.58: Current speed at station B

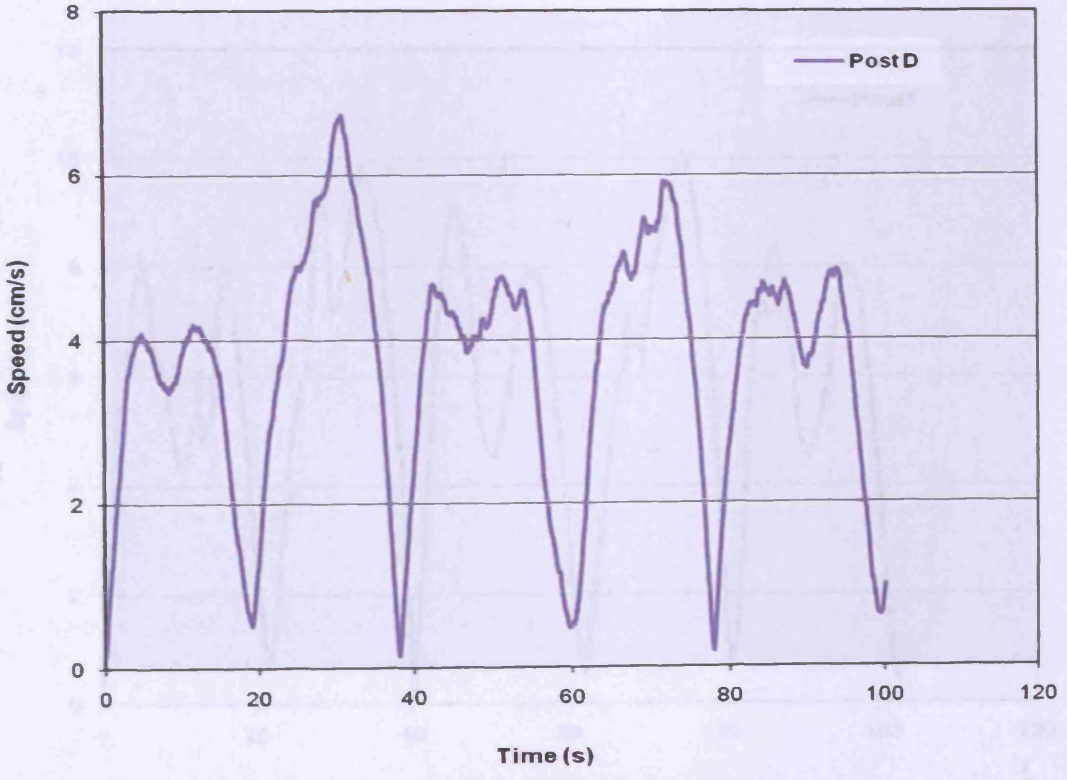

Figure 5.59: Current speed at station D

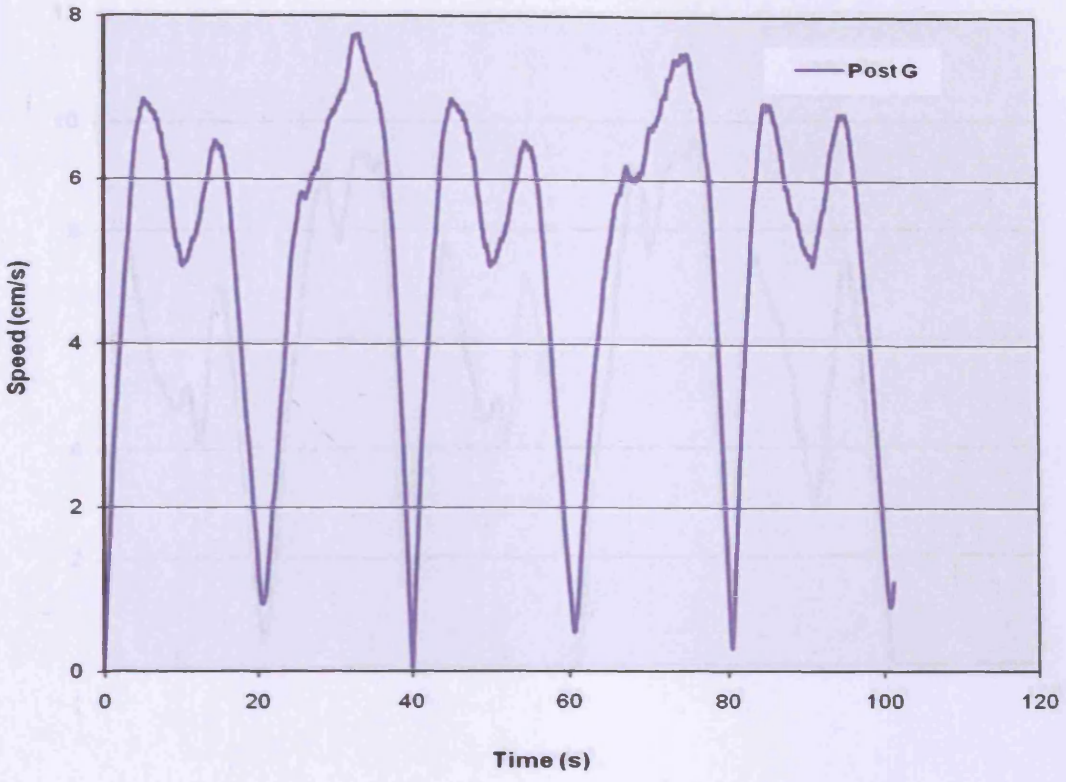

Figure 5.60: Current speed at station G

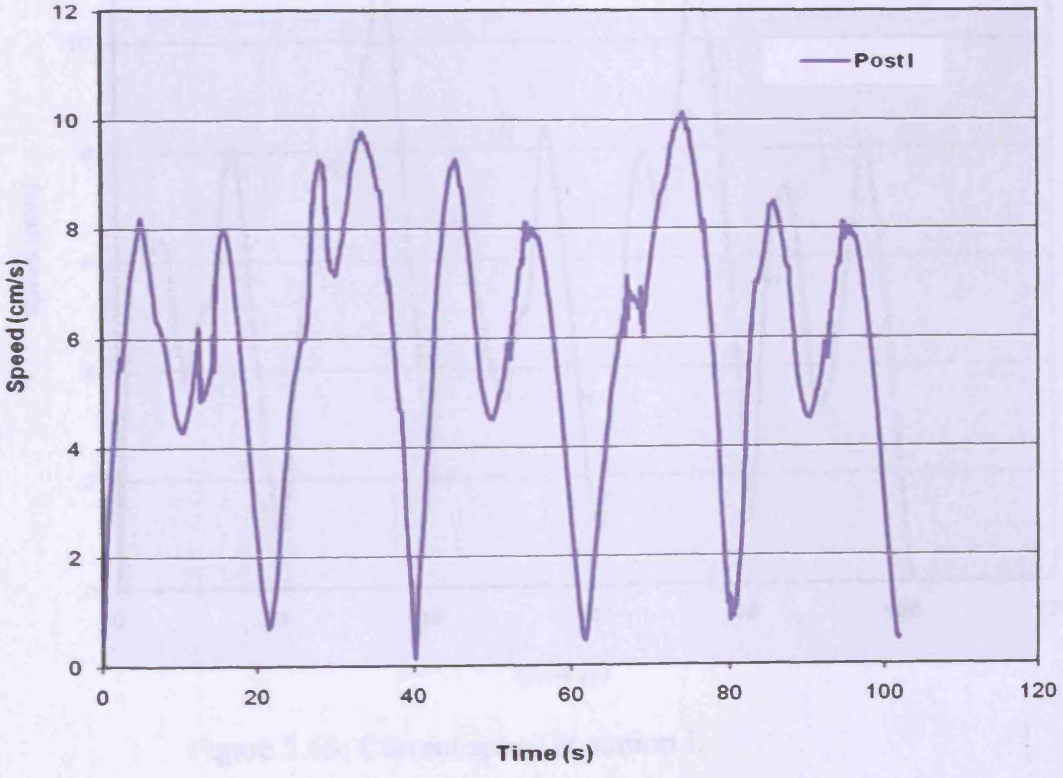

Figure 5.61: Current speed at station I

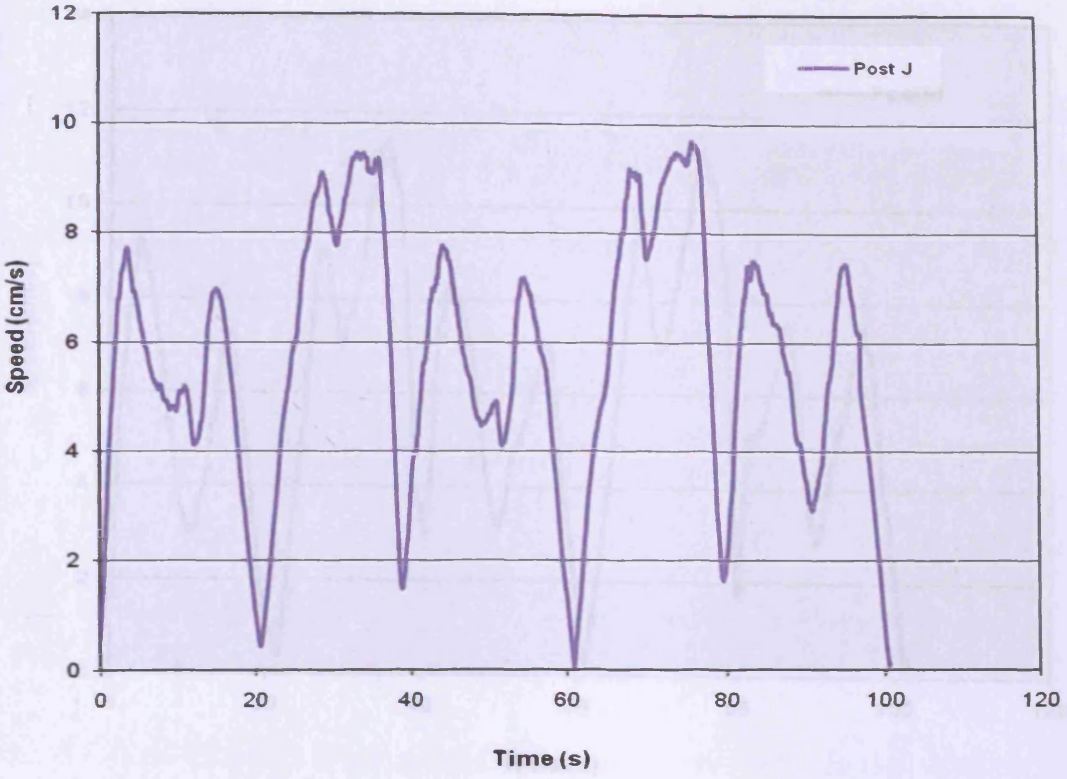

Figure 5.62: Current speed at station J

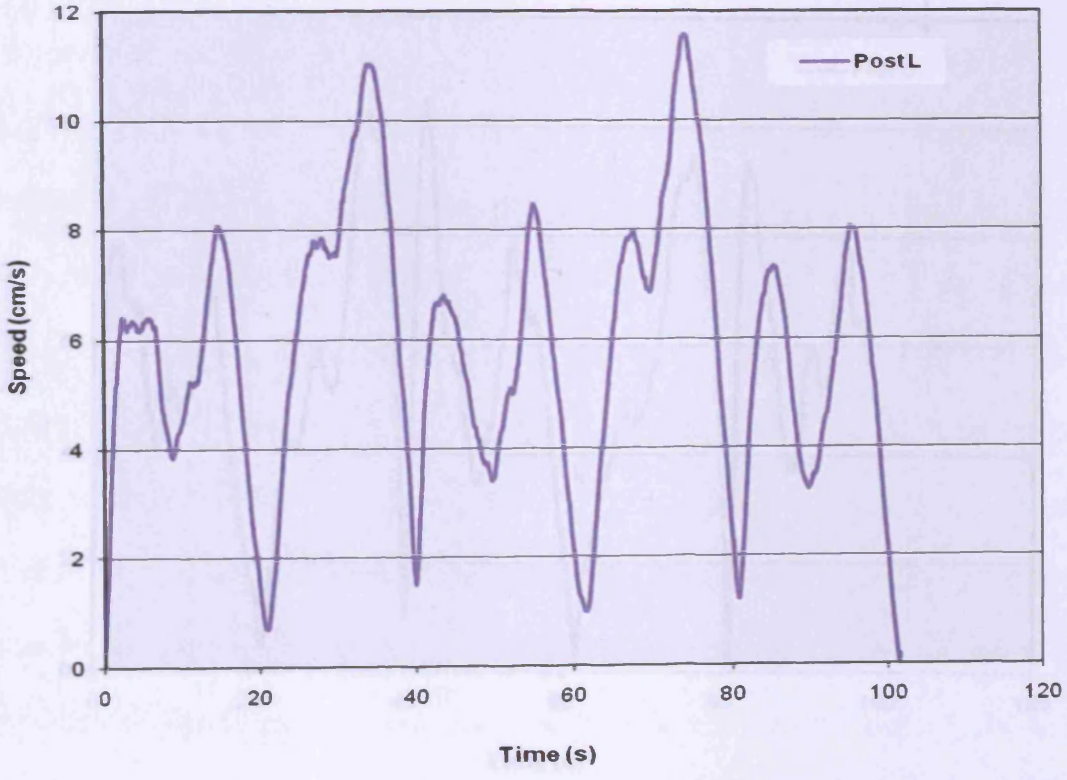

Figure 5.63: Current speed at station L

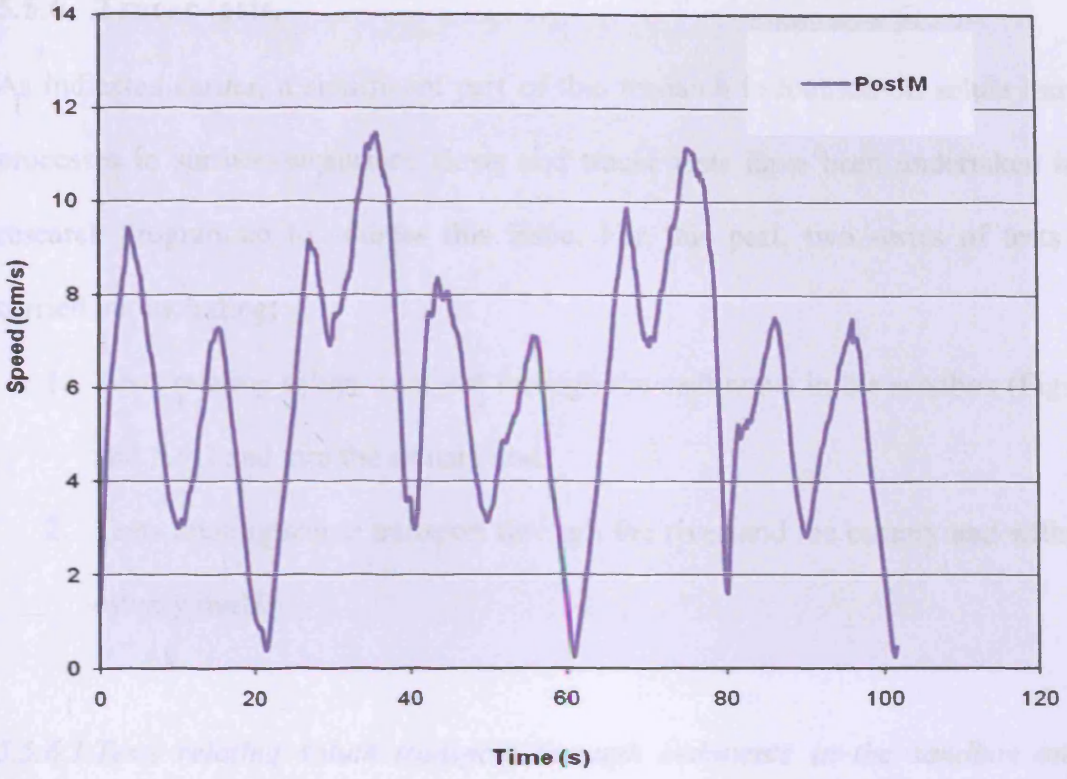

Figure 5.64: Current speed at station M

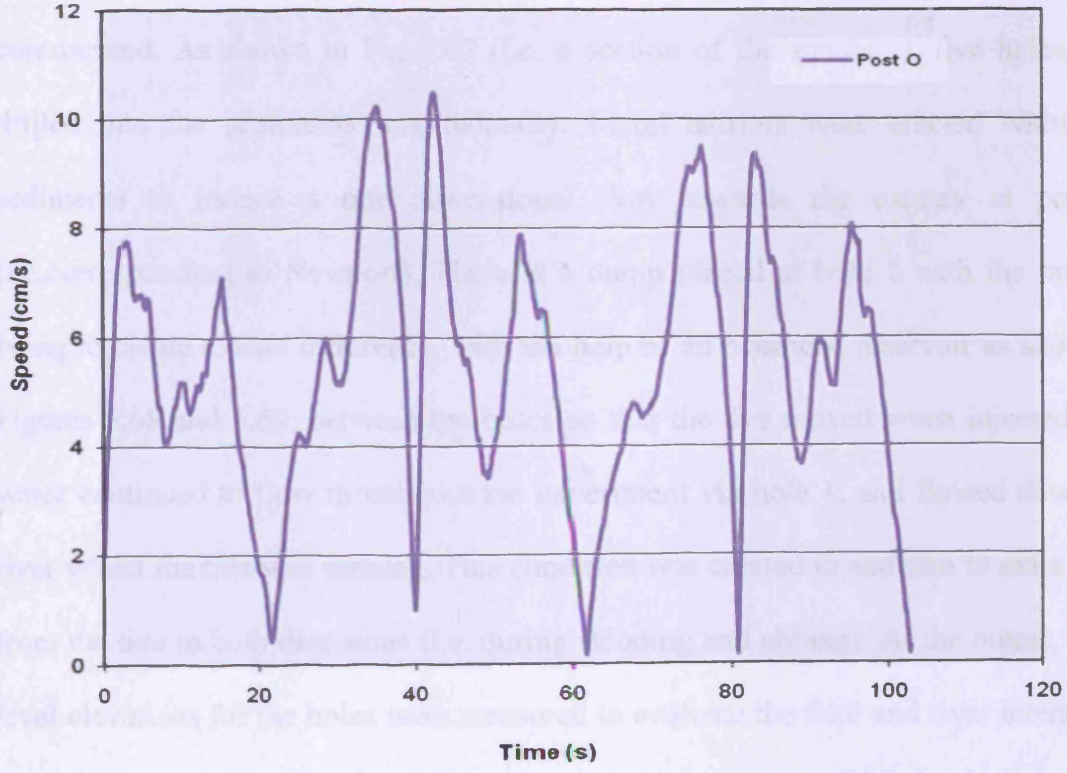

Figure 5.65: Current speed at station O

5.5.6 Tracer tests.

As indicated earlier, a significant part of this research is focused on solute transport processes in surface-subsurface flows and tracer tests have been undertaken in this research programme to address this issue. For this part, two series of tests were carried out including:

1. Tests relating solute transport through the sediments in the sandbox (Figs 5.48 and 5.51) and into the estuary and
2. Tests relating solute transport through the river and the estuary and within the estuary itself.

5.5.6.1 Tests relating solute transport through sediments in the sandbox and the estuary.

Figure 5.66 shows the aerial view of sediments in the sandbox before tidal cycles commenced. As shown in Fig 5.67 (i.e. a section of the sandbox), five holes were drilled into the sediments longitudinally. Metal barriers were erected within the sediments to induce a one dimensional flow towards the estuary at point 4 (i.e.corresponding to Newport). There is a pump placed at hole 1 with the purpose being to create a head difference, with the help of an overhead reservoir as shown in Figures 5.68 and 5.69, between the holes so that the dye moved when injected. The water continued to flow throuhgout the experiment via hole 1, and flowed down the river whilst the tide was running. This condition was created in addition to extra force from the tide in both directions (i.e. during flooding and ebbing). At the outset, water level elevations for the holes were measured to evaluate the tidal and river interaction along the basin and especially at the point of discharge, point 4 (Newport).

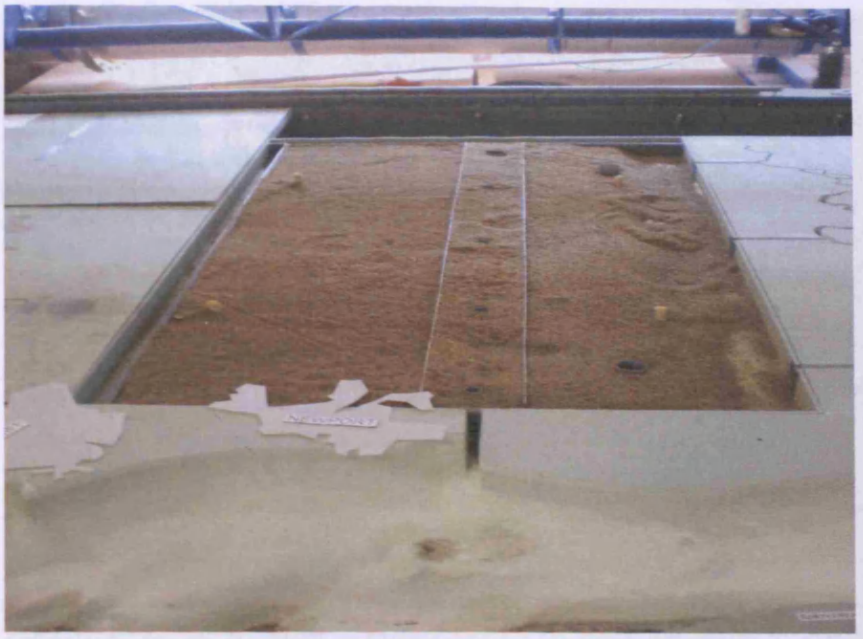

Figure 5.66: Aerial view of sandbox in the estuary showing holes 1-5 and Newport (point 4)

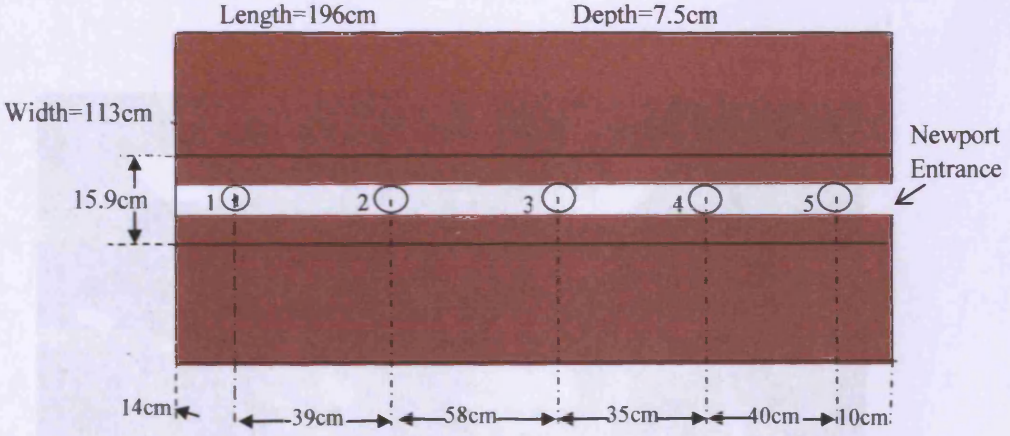

Figure 5.67: Section through the sandbox showing holes 1-5 and Newport entrance (not drawn to scale)

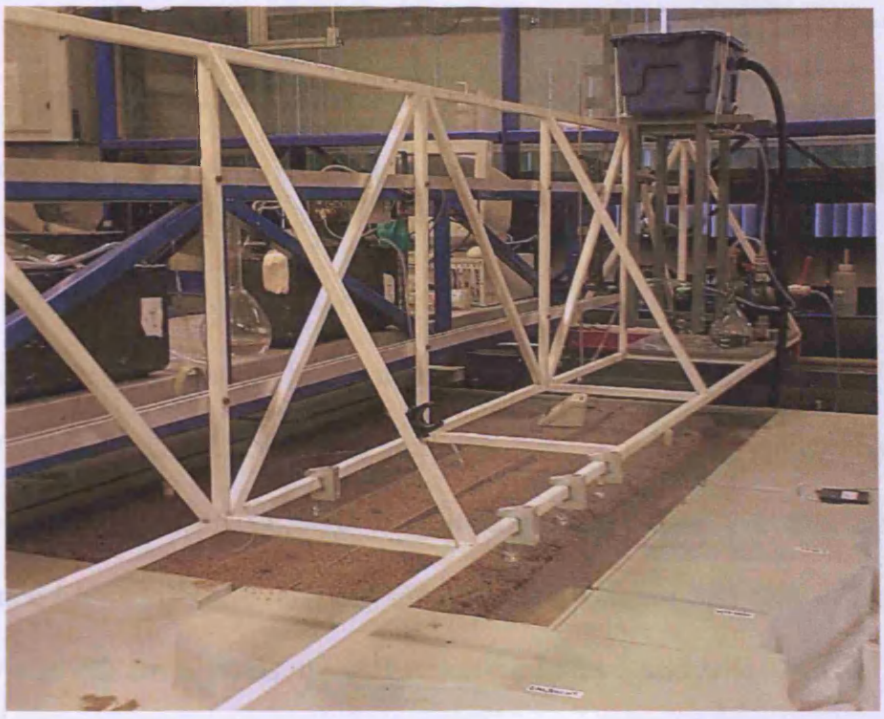

Figure 5.68: Sandbox in the estuary with the overhead reservoir and all tracer tests instrumentation ready for the tests

Figure 5.69: Overhead reservoir creating the head and pump for river flow

Figure 5.70 shows the experimental set-up for collection of data. The dye was injected in hole 2 and observed in holes 4, 5 and at the entrance of the estuary, i.e. at Newport (point 4). Thus water levels were taken simultaneously at these three locations.

Figure 5.71 shows the results for this part of the study. As per the pump, at low tide the head difference between hole 4 and the estuary was 43.1mm; for hole 4 and hole 5 the difference was 21.7mm; and between hole 5 and the estuary was 21.4mm. However, at high tide the trend was reversed after 20s. For this case, the head difference between hole 5 and the estuary was -4.6mm; and that of hole 4 and the estuary was -22.2mm, whilst the difference for holes 5 and hole 4 was 17.5mm. These results showed that for a tidal cycle of 40s, the flow of water from the sediments to the estuary was impeded after every 40s when the tide was in flood. The flow of water and solute from the sediments was reversed when the tide returned and then the cycle repeats itself. This meant that it took a considerable time for the solute to be transported from the sediments to the estuary.

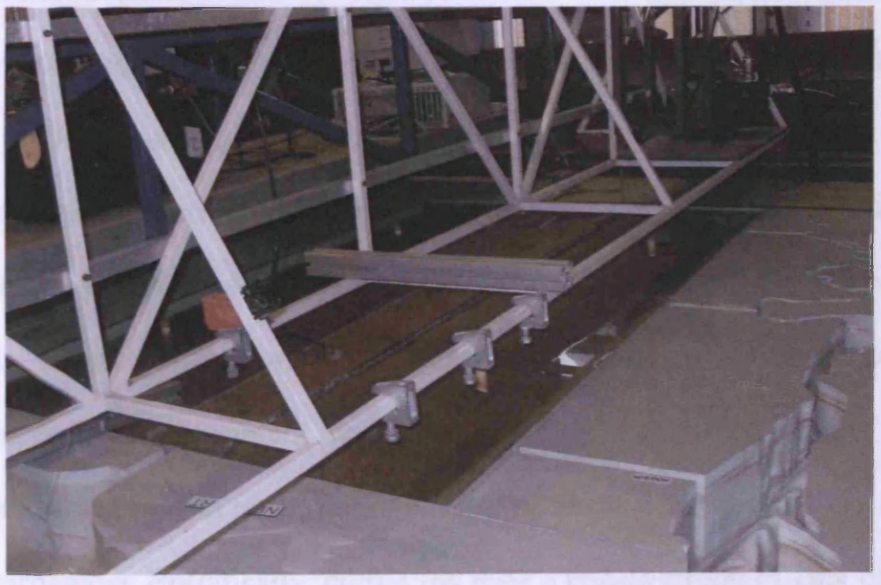

Figure 5.70: Experimental set up for water level measurement in the sediments

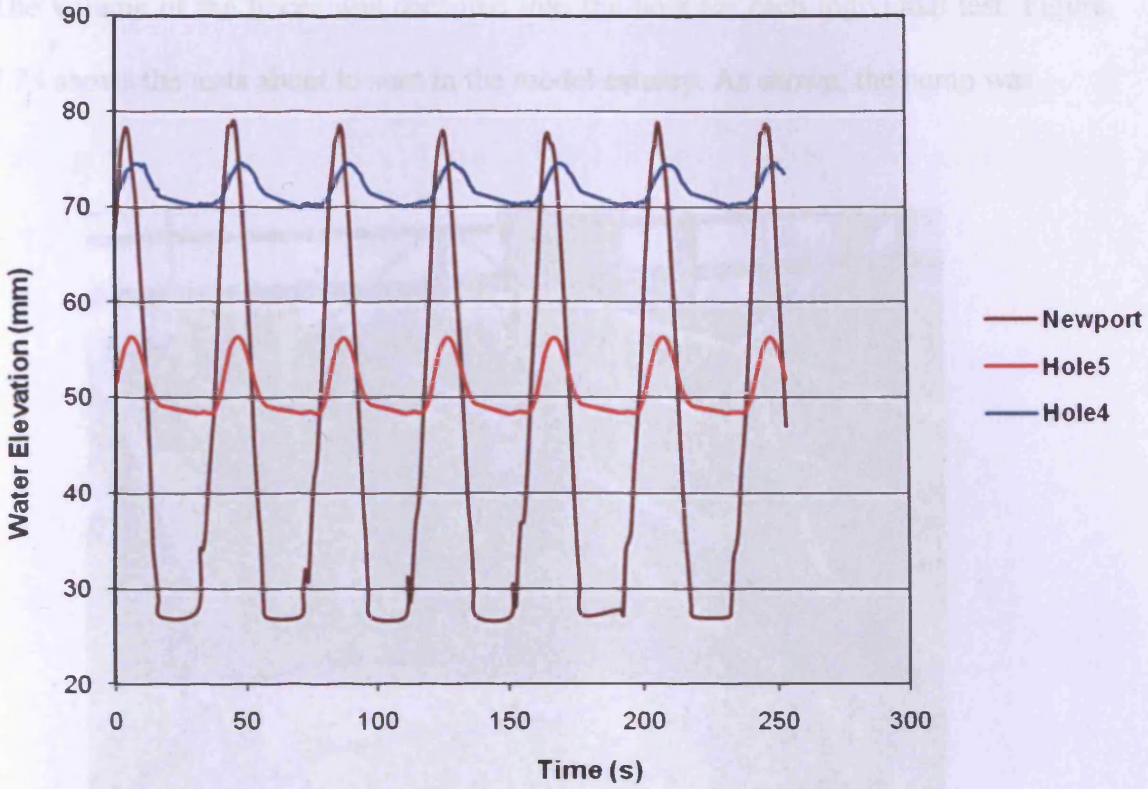

Figure 5.71: Relative water elevations at holes 4 and 5 and Newport

Tracer tests procedure

Basically a dye of a known mass was injected into hole 2 while there was a river flow through hole 1 (refer Fig 5.67). The dye was monitored in holes 4 and 5 and at the estuary entrance, using a fluorometer connected to a pump, with the tubing being placed at the monitoring locations at fixed times. Before the fluorometer was used for the tests, it was calibrated with a well prepared standard dye solution. After the tests, the data was downloaded from the fluorometer via a computer programme for analysis. Figure 5.72 shows the instrumentation used for the tests, including the fluorometer and the computer for the downloading of data. The pumps, the standard solution (for calibration of the fluorometer), the tracer itself were all key to these tests to be carried out. Specifically, during the tests a concentration of 1ppt of Rhodamine WT with volume varying between 0.5ml and 2ml was used for the injection in hole 1.

The volume of the tracer was decanted into the hole for each individual test. Figure 5.73 shows the tests about to start in the model estuary. As shown, the pump was

Figure 5.72: Tracer tests instrumentation: pumps, fluorometer,computer for downloading data and and standard solution ready for the tests.

Figure 5.73: Tracer test in hole 4 with the pump in hole 1.

connected to a rubber tube in hole 1 as water flowed and created a head difference likewise the fluorometer was connected to a pump via the rubber tubing for siphoning the tracer to be measured by the instrument. Figure 5.74 shows the movement of tracer along the estuary after injection.

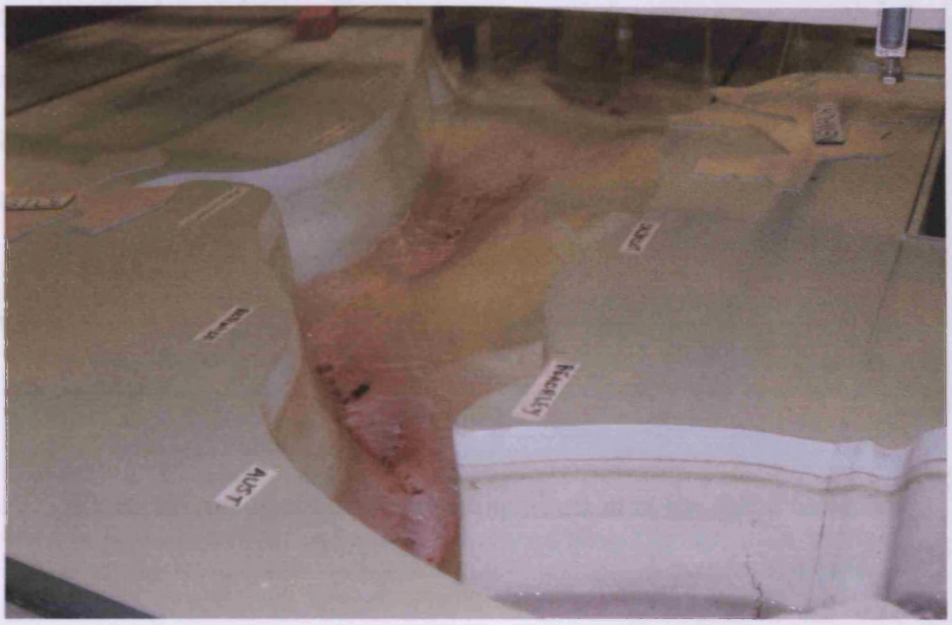

Figure 5.74: Tracer in the estuary

Tracer tests results

Figure 5.75 shows the concentration distributions for all three locations viz holes 4, 5 and Newport. The dye concentration injected in hole 1 was 1ppt with 0.5ml in volume. The distributions are normal for such tests and they are oscillatory due to the tide. Following the discussion earlier relating to the water elevations, this trend could be expected since at certain times the tracer would be pushed back by the tide and then flushed out in a cyclical manner, with the shape of the curve being periodic as it appears to follow the same path.

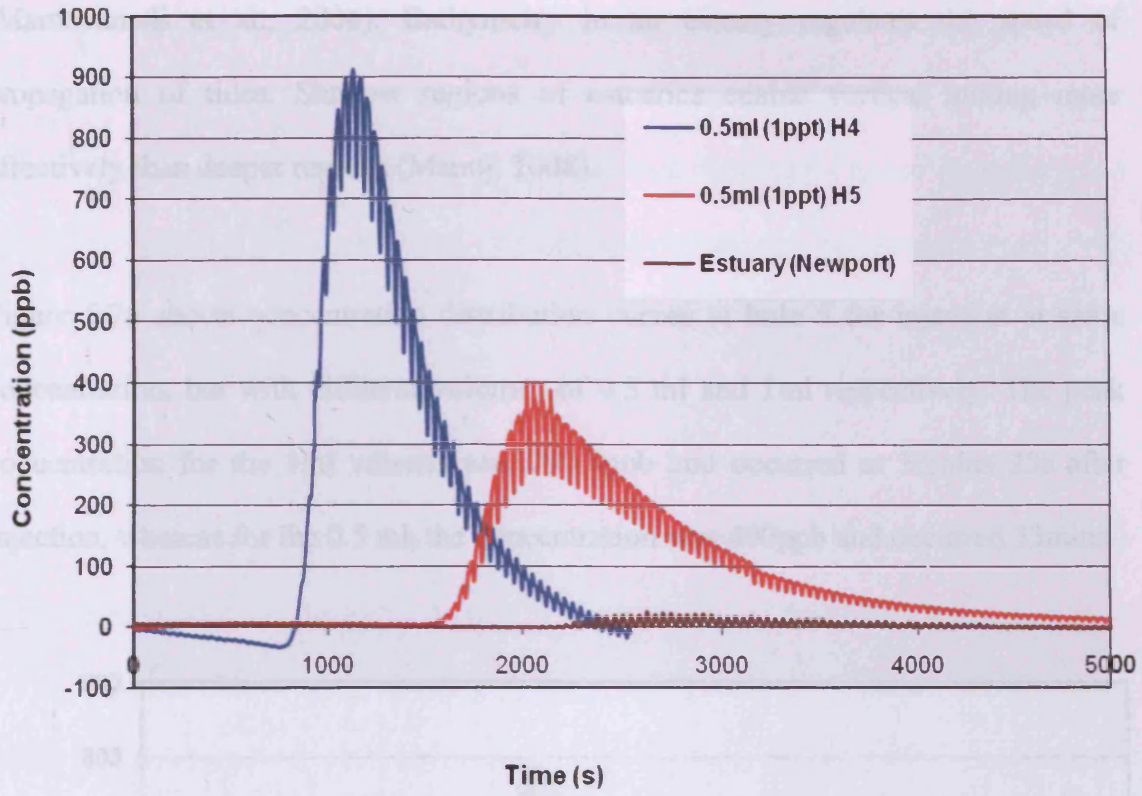

Figure 5.75: Comparison of concentration distribution at the three locations

The tracer was observed earlier in hole 4 than in hole 5 and also earlier in hole 5 than in the estuary. This was self explanatory since hole 4 is the first to occur after injection and it follows in that order. The peak concentration in hole 4 was highest amongst the three locations. This was to be expected since dilution of the tracer as a result of the tide flooding would be more pronounced at Newport than in hole 5 and even less so in hole 4. Hence, for the same mass of tracer, the concentration would be higher in hole 4 than in hole 5 and likewise than in Newport, as was observed.

Circulation and transport mechanisms in estuaries are complex and subject to a large spatial and temporal variability derived from the interaction of river discharge and tides. These forces drive the gravitational circulation and turbulent diffusion which are the main processes controlling the transport of properties in estuaries

(Mantovanelli et al., 2004). Bathymetry in an estuary regulates the speed of propagation of tides. Shallow regions of estuaries enable vertical mixing more effectively than deeper regions (Manoj, 2008).

Figure 5.76 shows concentration distribution curves at hole 5 for injection at same concentration, but with different volumes of 0.5 ml and 1ml respectively. The peak concentration for the 1ml volume was 790.8ppb and occurred at 33mins 25s after injection, whereas for the 0.5 ml, the concentration was 400ppb and occurred 33mins

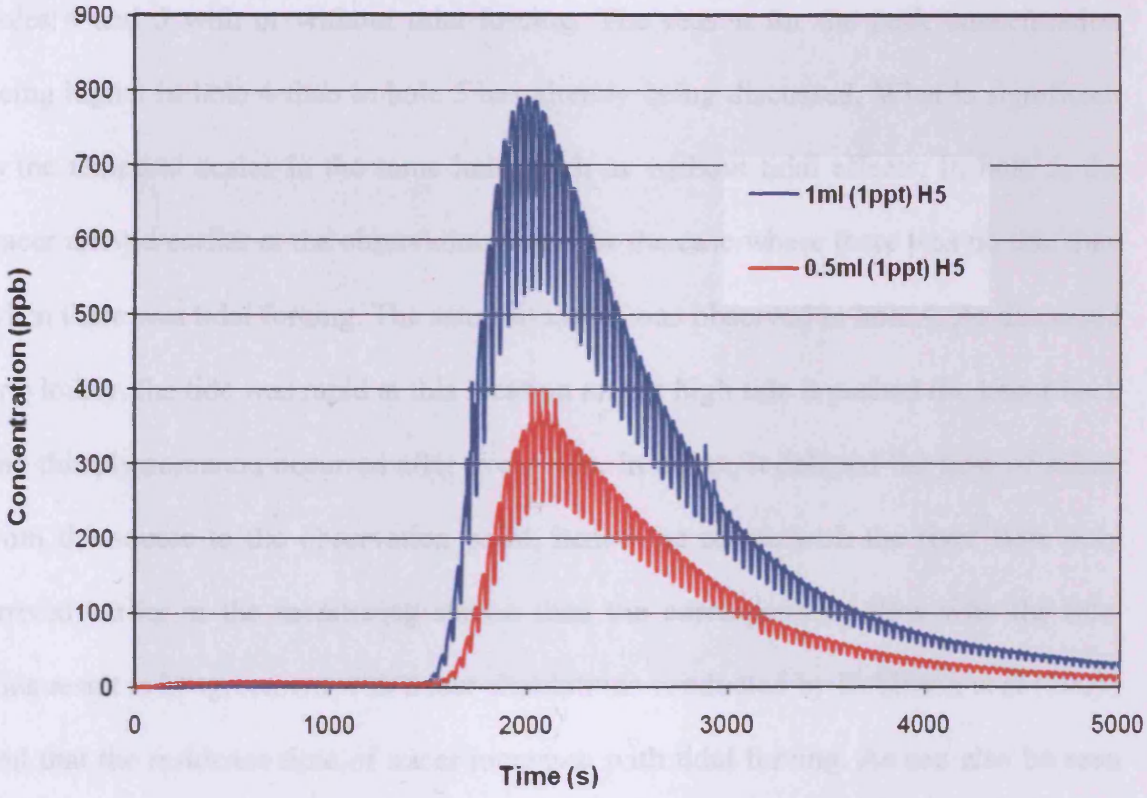

Figure 5.76: Comparison of concentration distribution at hole 5 for different conditions

44s after injection. The peak concentration of the latter was about half that of the former, which reflected the input concentration being the same multiplication factor.

The tracer seemed to appear in the hole a little bit earlier with the 1ml volume than the 0.5ml and this was reflected in the peak concentration being recorded earlier for the former than the latter. This was to be expected since the 0.5ml volume would be more diluted so it would have to accumulate a lot more of the dye before recordings could take place. Hence this would take a little more time than the 1ml volume concentration.

Finally, the study looked at the effect of the solute transport regime within the sediments without tidal forcing. Figure 5.77 shows the concentration distribution in holes 4 and 5 with or without tidal forcing. The reason for the peak concentration being higher in hole 4 than in hole 5 has already being discussed. What is significant is the temporal scales in the same hole, with or without tidal effects. In hole 5, the tracer arrived earlier at the observation point for the case where there was no tide than when there was tidal forcing. The same situation was observed in hole 4. As discussed previously, the tide was rapid at this location and at high tide it pushed the tracer back and this phenomenon occurred after every 40s. In effect, it delayed the flow of solute from the source to the observation point, hence the solute with the river flow only arrived earlier at the monitoring station than the corresponding flow with the tide. This result is in agreement with tracer simulations conducted by Robinson et al (2007) and that the residence time of tracer increases with tidal forcing. As can also be seen from Fig. 5.75, the longitudinal spread of the plume increases with the tide with a lower peak concentration which is similar to the results obtained by Robinson et al (2007) whereupon they concluded that tides may decrease the threat of groundwater-borne contaminants on the marine ecosystem, rather than having the potential to

worsen it since tidal effects may also enhance the overall transverse spread of contaminants.

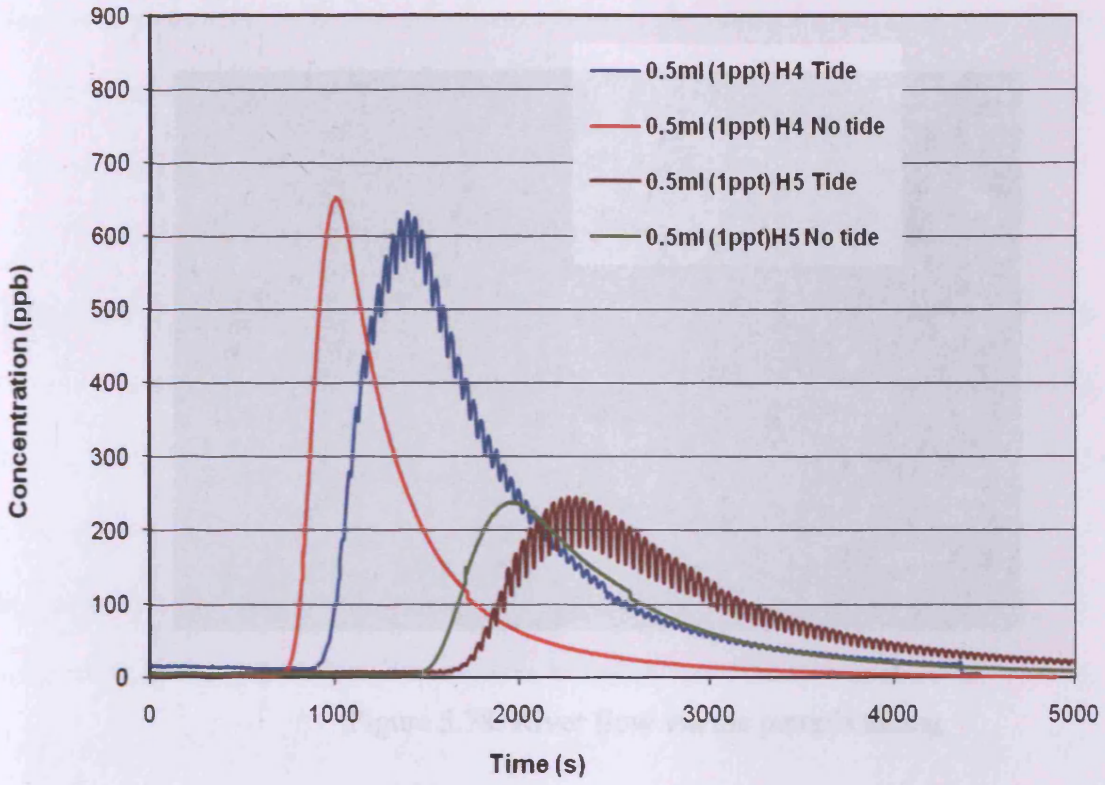

Figure 5.77: Comparison of concentration distribution for hole 4 and 5 with and without tidal forcing

5.5.6.2 Tests relating the river and the estuary and within the estuary itself.

Figure 5.78 shows the start of tracer tests from the river and monitored in the estuary. There was a river flow at the tidal limit which, in conjunction with the tide advected the injected tracer along the course of the river, down to the estuary, and where it was monitored. In this part of the dye studies, the tracer was injected at two different points along the river, whilst monitoring takes place at two stations (O and L) within the estuary. Also, the tracer was injected at point P and monitored at the two stations.

Figure 5.79 shows the dispersal of tracer within the river from the point of injection to the estuary. The energy available in the tide that drives steady circulation, otherwise known as tidal pumping can be an important part of tidal circulation producing

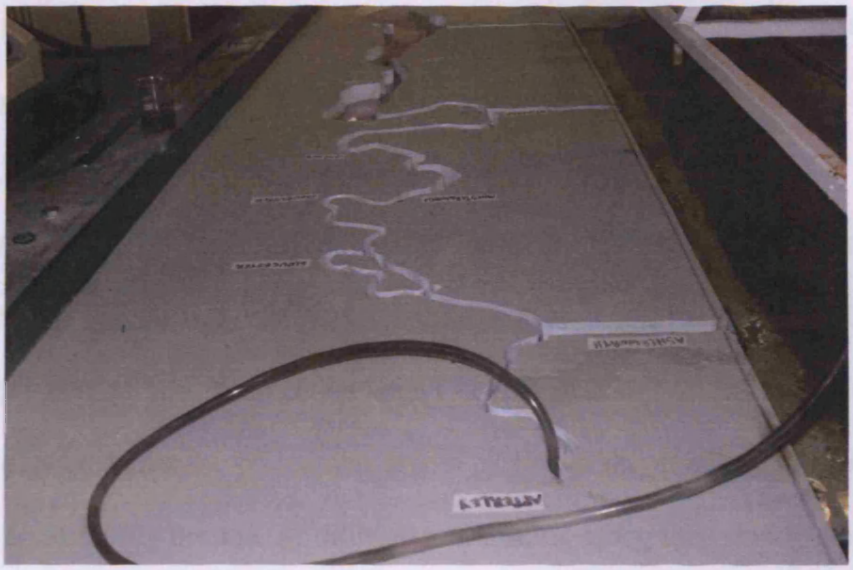

Figure 5.78: River flow via the pump's tubing

Figure 5.79: Tracer dispersed in the river as it moves towards the estuary

longitudinal dispersion. This phenomenon is caused by tidal residual horizontal circulation, which can either be as a consequence of the interaction of the tidal flow with a pronounced flood-ebb channel system or interaction of the tidal flow with an irregular bathymetry. Residual ebb-flood channel circulation is an important large-scale mixing mechanism for moving pollutants and transporting salinity upstream against a mean outflow of freshwater (Savenije, 2005)

Figure 5.80 shows the concentration distribution (breakthrough curves) at monitoring stations O and L as shown in Fig.5.51, after injection of 1ppt of tracer with 2ml in volume at P. The longitudinal distance between P and O is 1.1m and that of P and L is 2.4m, so it is expected that the tracer will arrive earlier at the monitoring station O than at station L. Similarly because of dilution and mixing along the estuary, the peak concentration would be higher at O than at L. These two phenomena are shown in the distribution as the maximum concentration at O is an order of magnitude greater than that at L and the fluorometer picked up the tracer earlier at the monitoring station O than at L.

It has been demonstrated by McCarthy (1993) that tide-driven mixing is dominant in the downstream part of estuaries, while density-driven mixing is dominant in the upstream part of estuaries. Density-driven mixing is a function of the salinity gradient, whereas tide-driven mixing is a function of the salinity and the width. The trend therefore was as observed by early researchers even though density driven processes are not directly relevant to the current studies. In Figure 5.81, the same concentration but different volumes of dye were used and the monitoring was carried out at the same station L, whereas injection was at P. It was observed that the tracer arrived at the monitoring station at the same time, since the distance was the same for the two

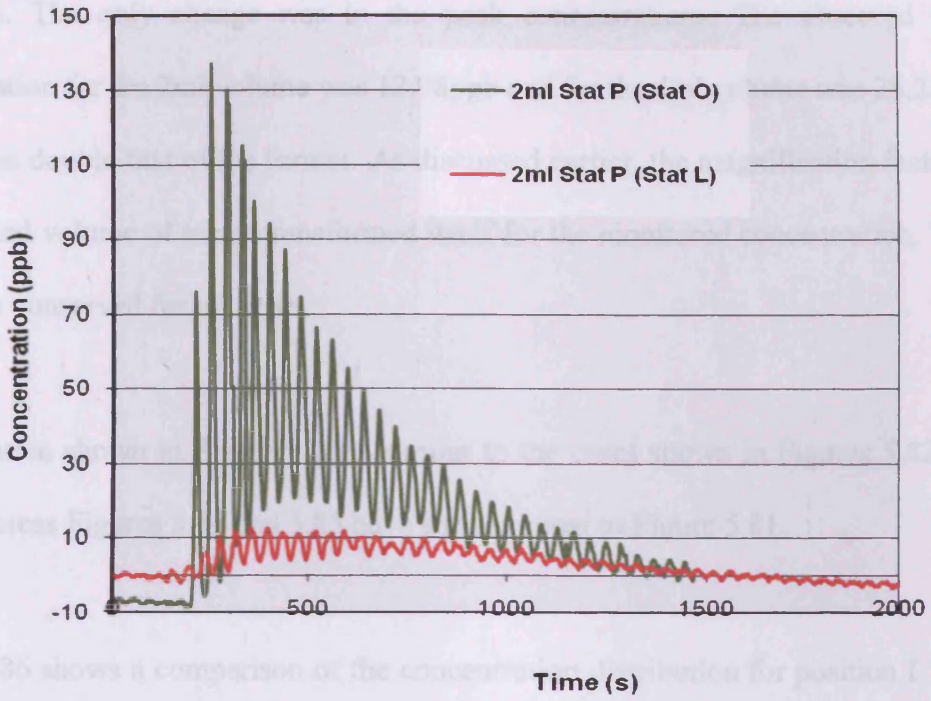

Figure 5.80: Comparison of concentration distribution for stations O (nearer) and L (farther) with 2ml dye injection at point P

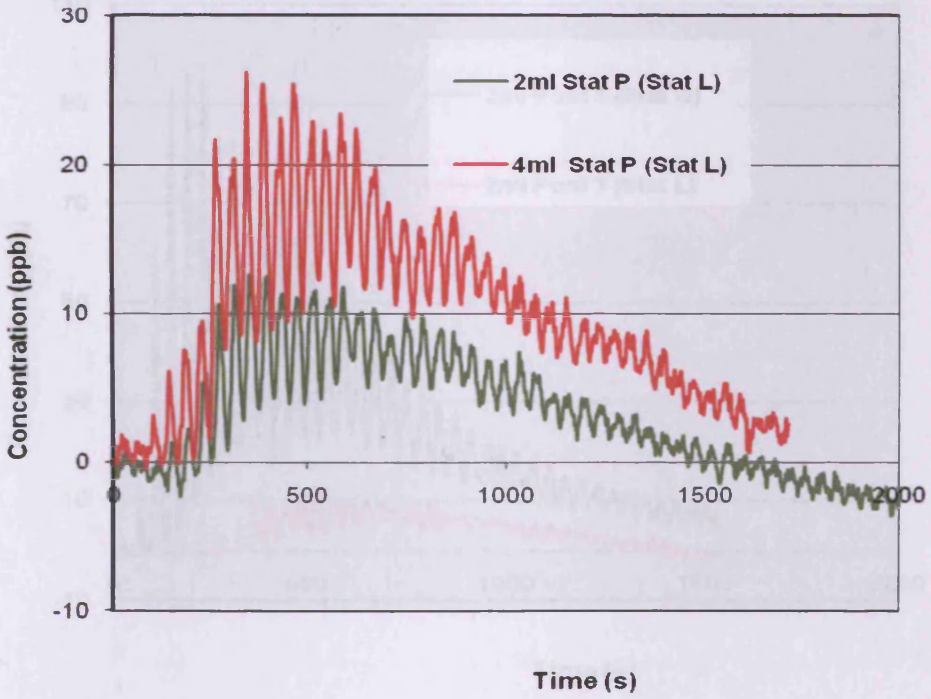

Figure 5.81: Comparison of concentration distribution for station L with 2ml and 4ml dye injection at point P respectively

situations. The only change was in the peak concentrations. The observed peak concentration for the 2ml volume was 12.98ppb and for the 4ml volume was 26.25ppb, which was double that of the former. As discussed earlier, the magnification factor of the injected volume of tracer transformed itself for the monitored concentration. Thus mass was conserved for all cases.

The situation shown in Figure 5.80 is similar to the cases shown in Figures 5.82 and 5.84, whereas Figures 5.83 and 5.85 have similar cases to Figure 5.81.

Figure 5.86 shows a comparison of the concentration distribution for position L with 4ml injection at positions 2 and 3 respectively. Position 2 is farther away from the

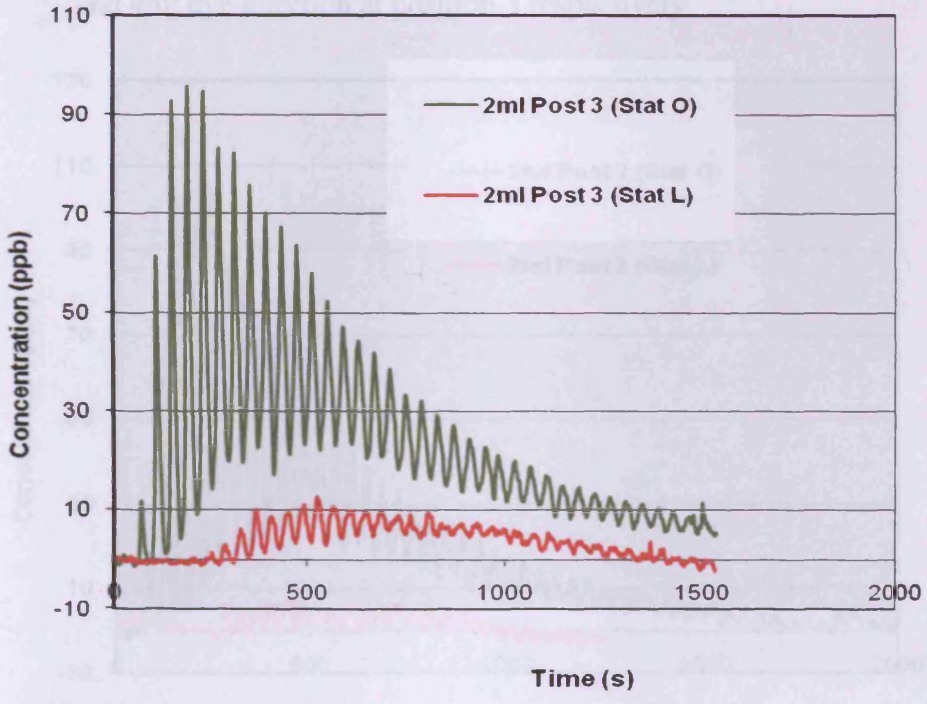

Figure 5.82: Comparison of concentration distribution for stations O and L with 2ml dye injection at position 3 in the river

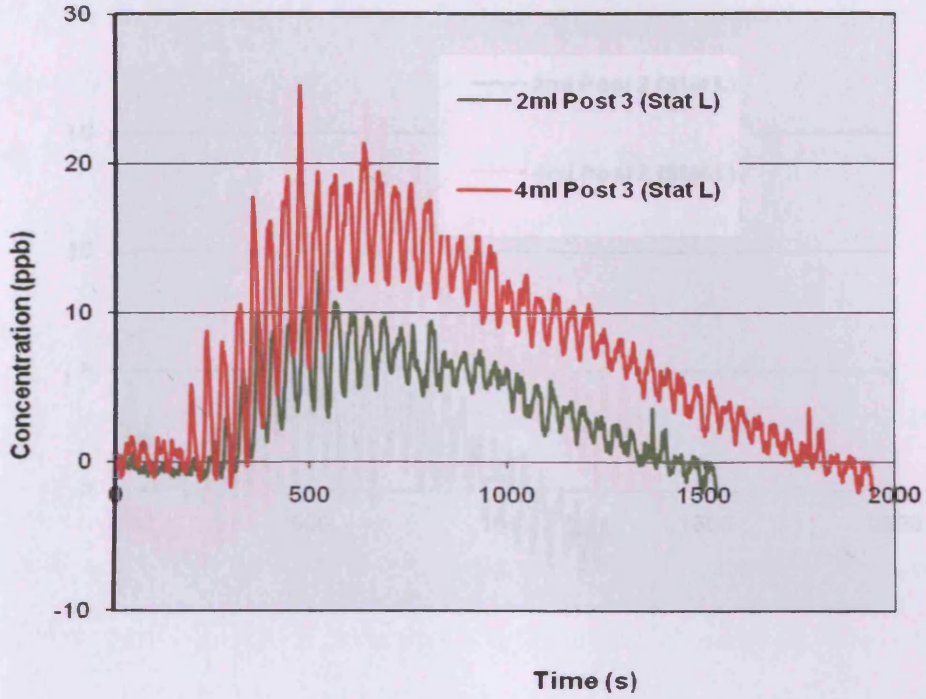

Figure 5.83: Comparison of concentration distribution for station L with 2ml and 4ml dye injection at position 3 respectively

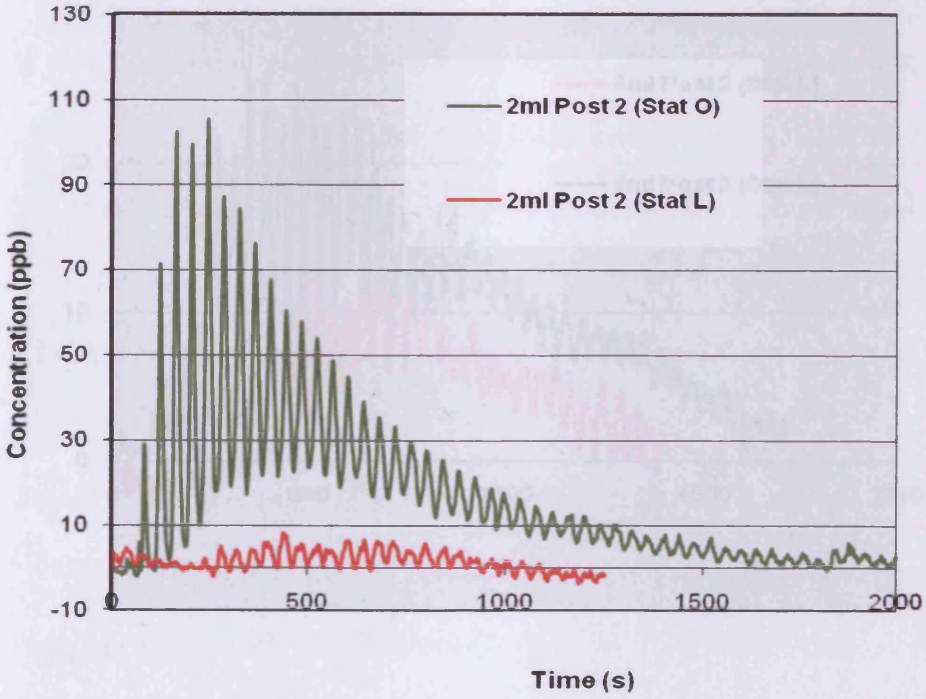

Figure 5.84: Comparison of concentration distribution for stations O and L respectively with 2ml dye injection at position 2 in the river

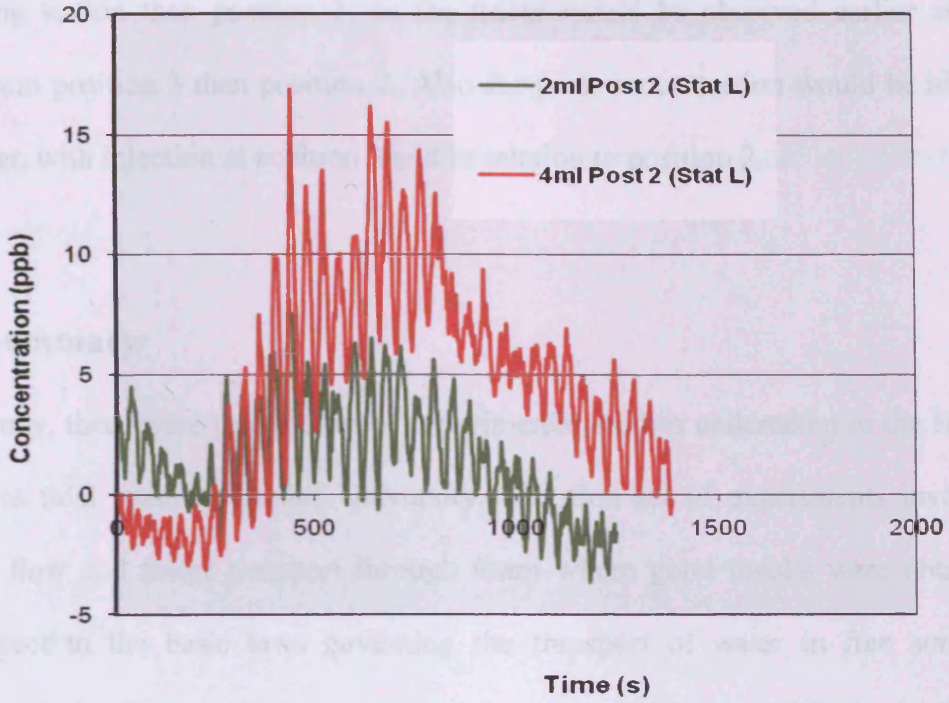

Figure 5.85: Comparison of concentration distribution for station L with 2ml and 4ml dye injection at position 2 respectively

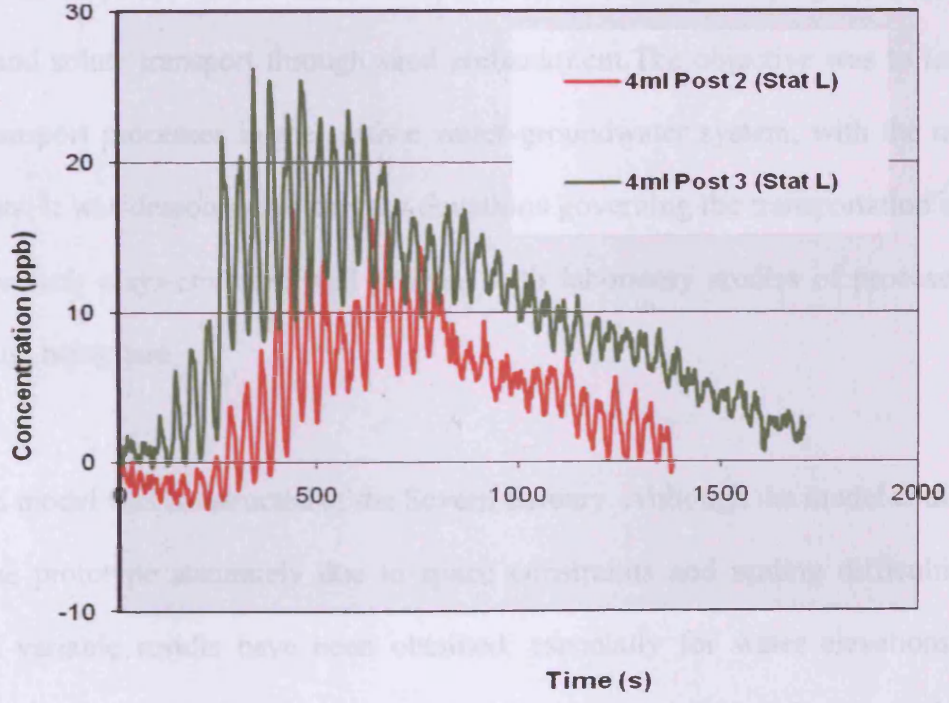

Figure 5.86: Comparison of concentration distribution for station L with 4ml dye injection at positions 2 and 3 respectively

monitoring station than position 3, so the tracer would be observed earlier at the station from position 3 than position 2. Also the peak concentration would be higher and earlier, with injection at position 3 and in relation to position 2.

5.6 Summary

In this study, there were three series of experimental studies undertaken in the Hyder Hydraulics tidal basin at Cardiff University. The first set of experiments involved studying flow and tracer transport through foam where good results were obtained with respect to the basic laws governing the transport of water in free surface-subsurface flows. Hoever, the movement of the dye in this system failed, which was attributed to surface tension forces and sorption properties of the foam.

The main thrust of the second series of experiments involving studying the behaviour of flow and solute transport through sand embankment.The objective was to look at solute transport processes in the surface water-groundwater system, with the use of tracer tests. It was demonstrated that the equations governing the transportation of the solute for such a system were well proven, with laboratory studies of processes in such nature being rare.

Finally, a model was constructed of the Severn Estuary. Although the model could not match the prototype accurately due to space constraints and scaling difficulties, a range of variable results have been obtained, especially for water elevations and current velocities. These results have compared favourably well with measured field data.

The purpose of these experiments was to investigate the manner in which flow and a conservative tracer interacted between surface and sub-surface flows for simulated riverine and tidal conditions. These experiments and the corresponding datasets are thought to be unique.

CHAPTER 6 COMPUTATIONAL MODEL STUDIES

6.1 Introduction

The governing partial differential equations and the associated bed friction were expressed in an alternating direction implicit finite difference form using a space staggered scheme. For the foam and sand embankment studies the grid spacing was 10 cm with a time step of 0.25 s. The maximum number of grid points was 61 and 42 in the x and y directions respectively. The solution procedure had been outlined in Chapter 4.

6.2 Foam studies

6.2.1 Water Levels

As discussed in the previous chapter, a series of water level measurements were first taken for the foam. Consequently, predictions were made under the same conditions using the numerical model. The model was set up for the foam configuration as shown in Figure 5.28. The grid spacing of 10cm required 59 grid cells in the X-direction and 40 cells in the Y-direction. Along the X=0 axis, the tide was inserted in a sinusoidal form, with a mean depth of 20cm and an amplitude of 8cm. As stated above, the time step was 0.25s. At the head of estuary (i.e. X=5m) then the normal current u was set to zero in the river and through the foam, and the flow through the foam at the boundary of the basin i.e at Y=0 and Y=4m was also set to zero for all time t. The permeability of the foam was assumed to be constant everywhere with a value of

0.09m/s, and the estuary bed roughness was assumed to be k_s = 1mm. The initial water elevation was set to high water everywhere across the domain, i.e. ζ = 8cm, and the initial velocity components u and v were set to zero everywhere. The eddy viscosity coefficient was set to 0.15, based model calibration and the Coriolis and wind stress terms were both excluded. The details of the results are given below.

6.2.1.1 Tidal cycle results

Figures 6.1 and 6.2 show the measured and predicted water elevations for 5min and 10 min tidal cycles for transect A respectively. The predictions are coincident with the measured water elevations. There is a small phase difference (about 2s) between the predicted and measured elevations at some phases of the cycle between the two situations and this difference could not be reduced by changing the friction. These

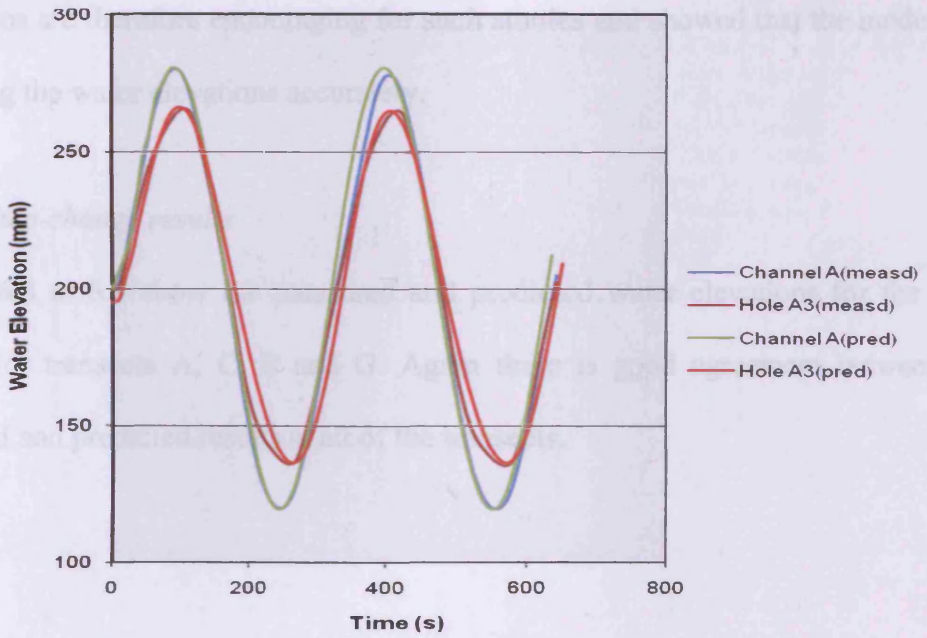

Figure 6.1: Measured and predicted water elevations for 5min tidal cycle at transect A

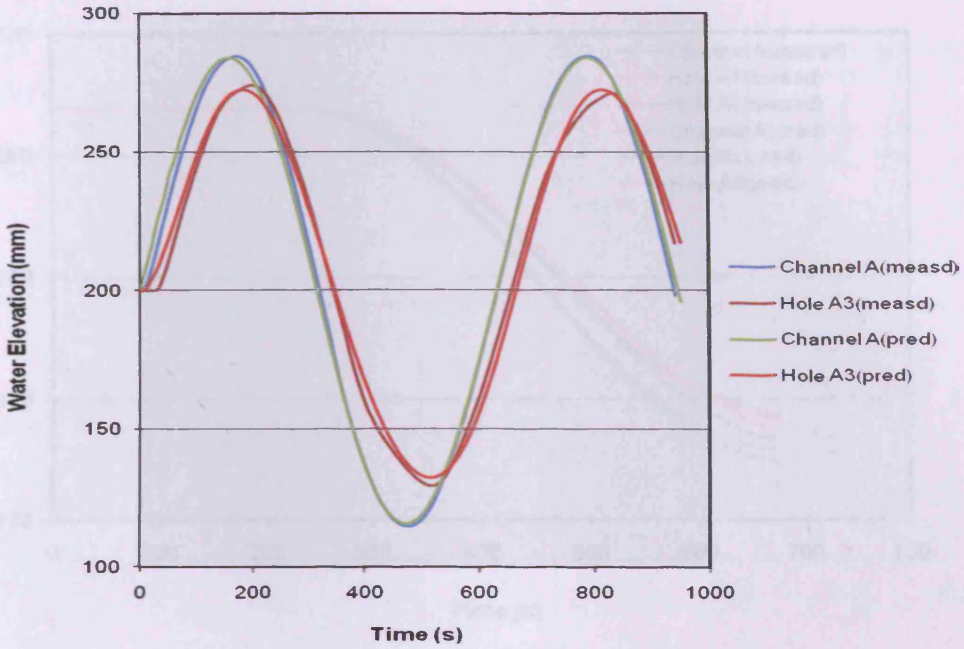

Figure 6.2: Measured and predicted water elevations for 10mins tidal cycles at transect A

predictions are therefore encouraging for such studies and showed that the model was predicting the water elevations accurately.

6.2.1.2 Step-change results

Figures 6.3 to 6.6 show the measured and predicted water elevations for the step-change for transects A, C, E and G. Again there is good agreement between the measured and predicted results at all of the transects.

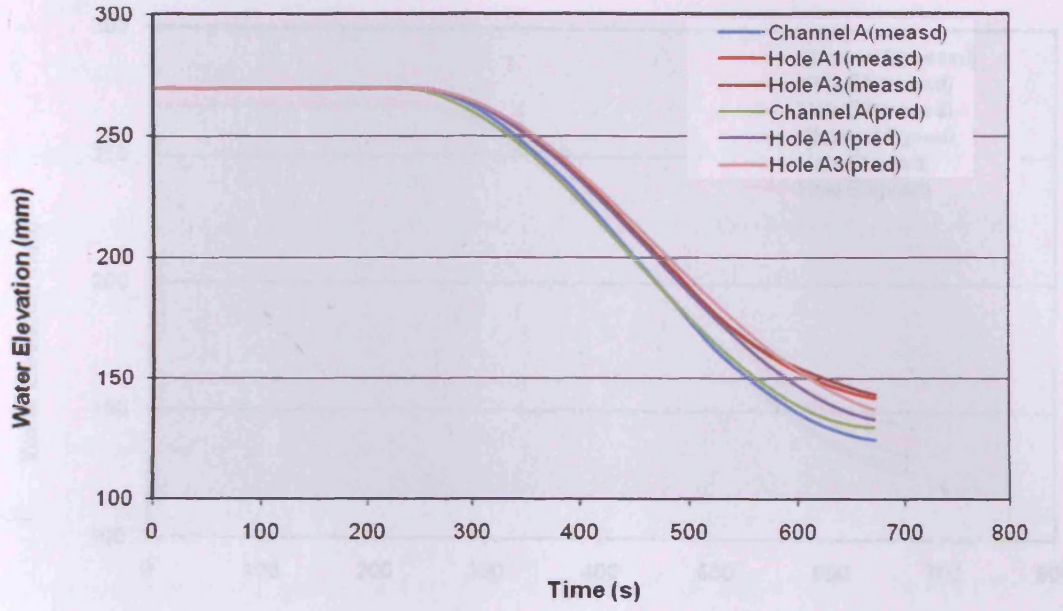

Figure 6.3: Comparison of measured and predicted elevations for 15min step-change at transect A

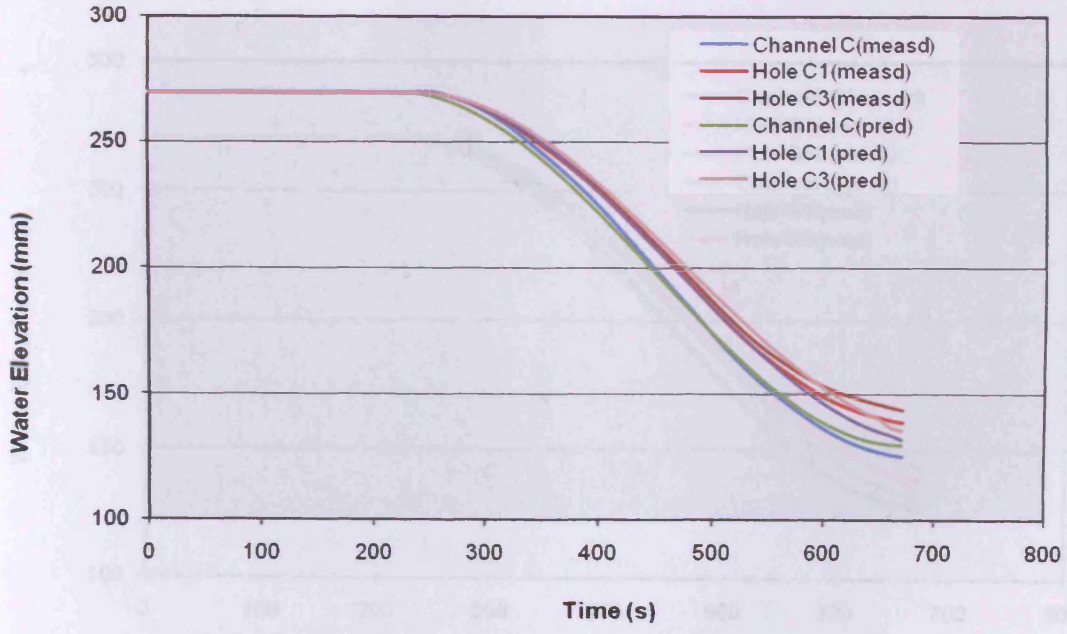

Figure 6.4: Comparison of measured and predicted elevations for 15min step-change at transect C

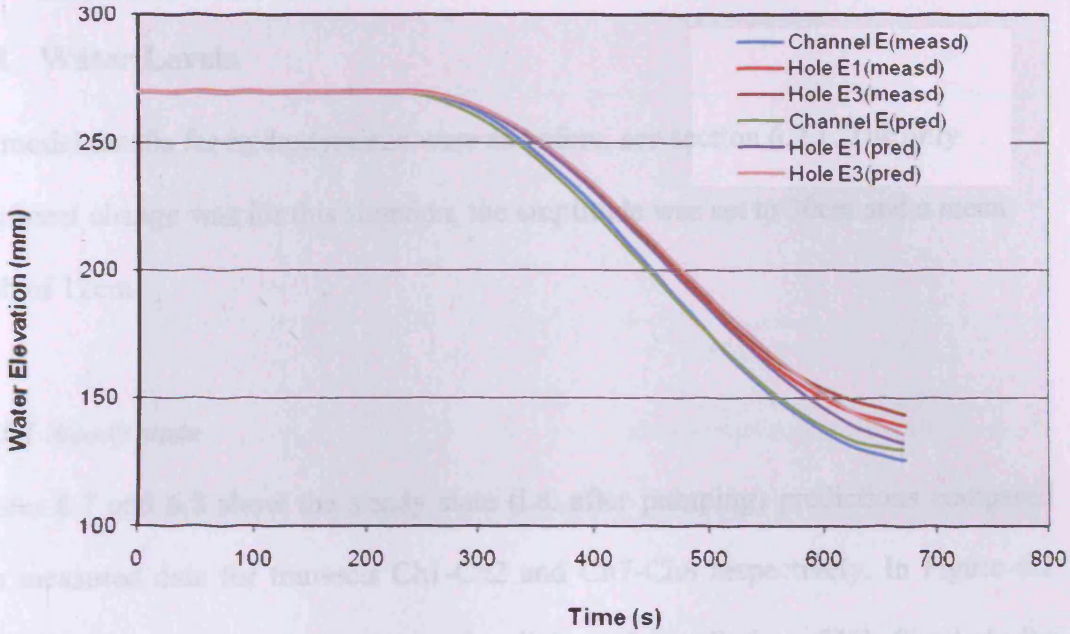

Figure 6.5: Comparison of measured and predicted elevations for 15min step-change at transect E

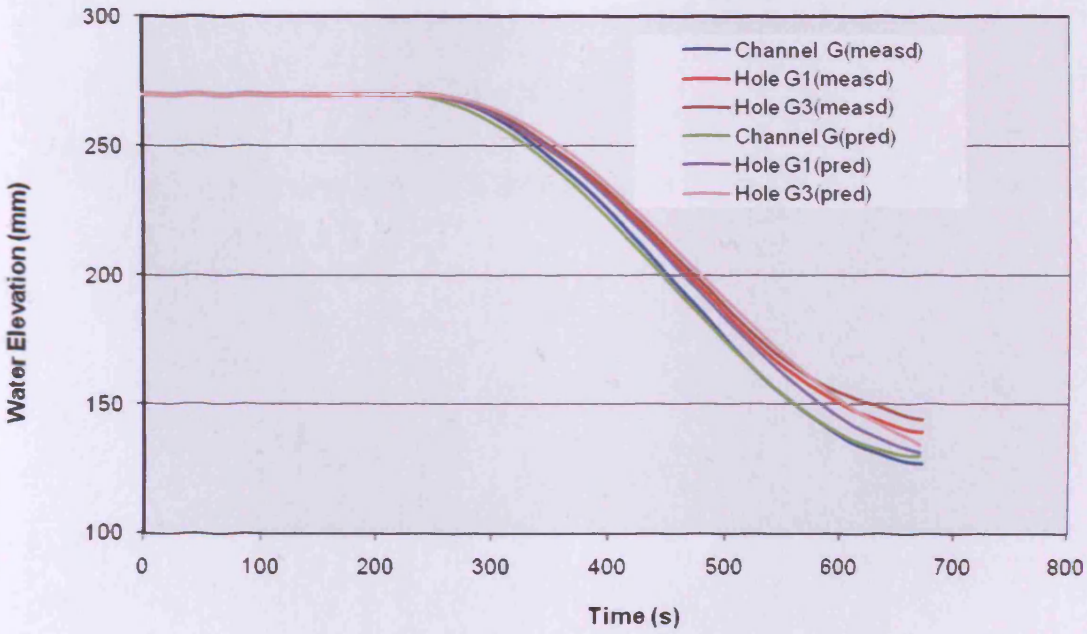

Figure 6.6: Comparison of measured and predicted elevations for 15min step-change at transect G

6.3 Sand Embankment

6.3.1 Water Levels

The model details for hydrodynamic were as before, see section 6.2.1. The only significant change was for this situation, the amplitude was set to 30cm and a mean depth of 12cm.

6.3.1.1 Steady state

Figures 6.7 and 6.8 show the steady state (i.e. after pumping) predictions compared with measured data for transects Ch1-Ch2 and Ch7-Ch8 respectively. In Figure 6.7 the predictions are encouraging except for slight underprediction of H1. Similarly for transect Ch7-Ch8 (see Figure 6.8); the predictions compare favourably with the measured data. Although the model slightly overpredicted H7, the results are particularly encouraging for Ch7, H8 and Ch8.

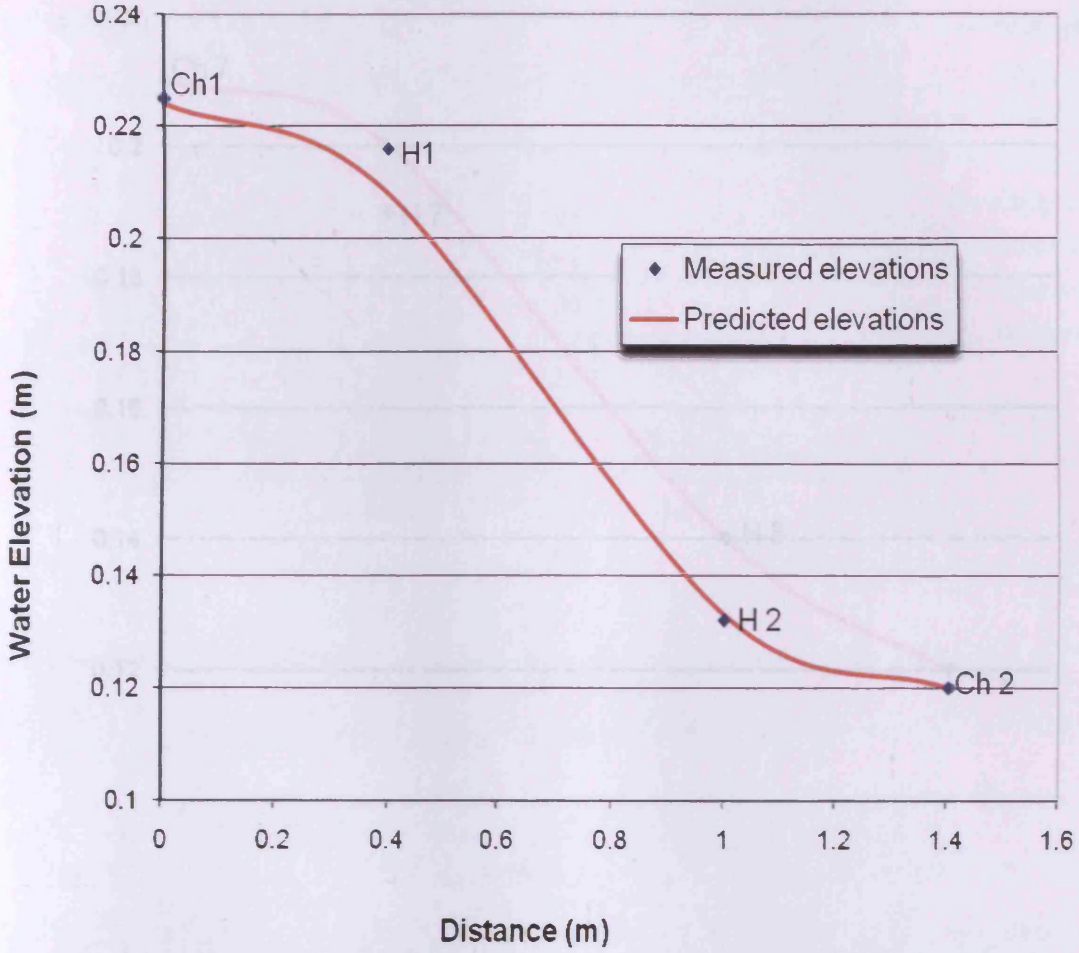

Figure 6.7: Measured and predicted elevations for steady state after pumping (Ch1-Ch2)

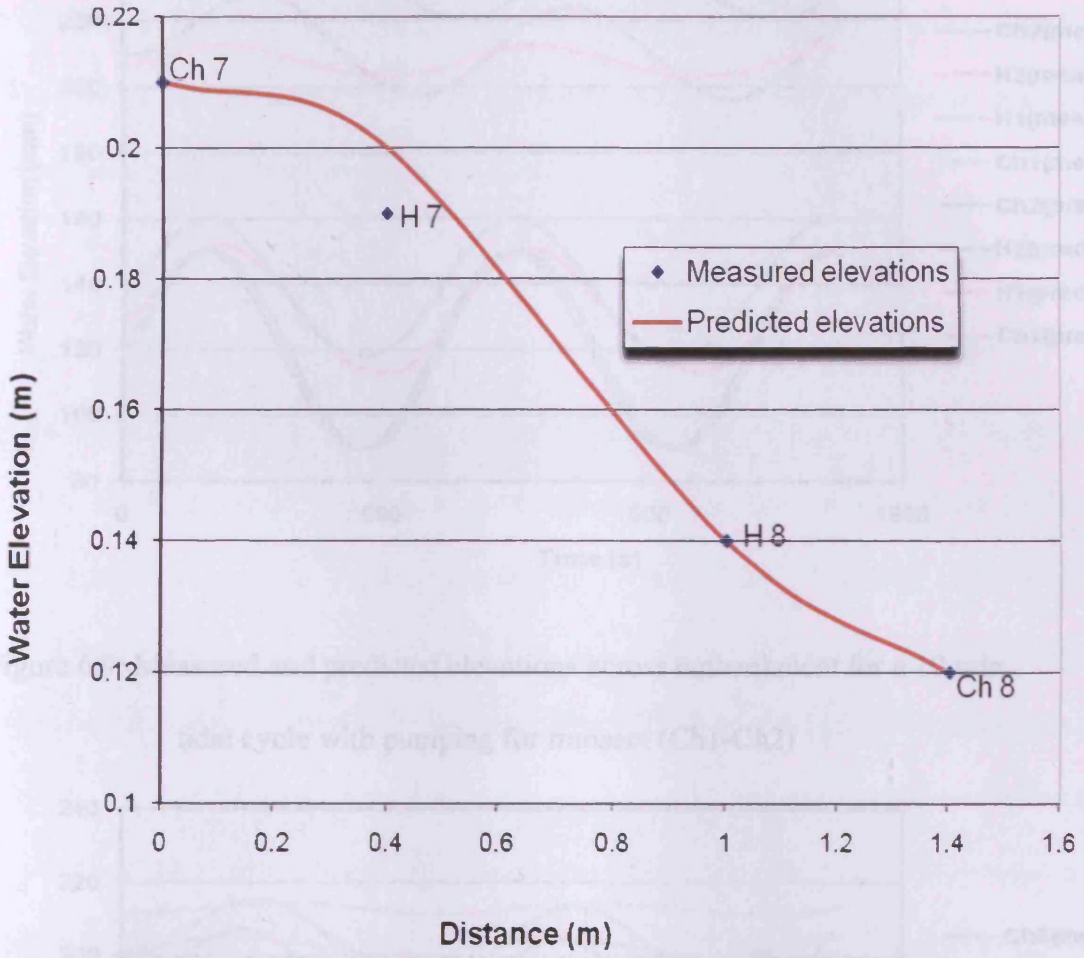

Figure 6.8: Measured and predicted elevations for steady state after pumping (Ch7-Ch8)

6.3.1.2 Tidal cycles

Figures 6.9 and 6.10 show the measured and predicted elevations in front of and behind the embankment for transects Ch1-Ch2 and Ch7-Ch8 after pumping and with a 10 min tidal cycle. Ch2 and Ch8 are in front of the embankment, whereas Ch1 and Ch7 are behind the embankment. H1 and H7 are the injection holes and H2 and H8 are the monitoring holes. As can be seen from the results, the numerical model is able to predict the elevations in front of the embankment very accurately, but under predicts elevations behind the embankment. The phase difference between the

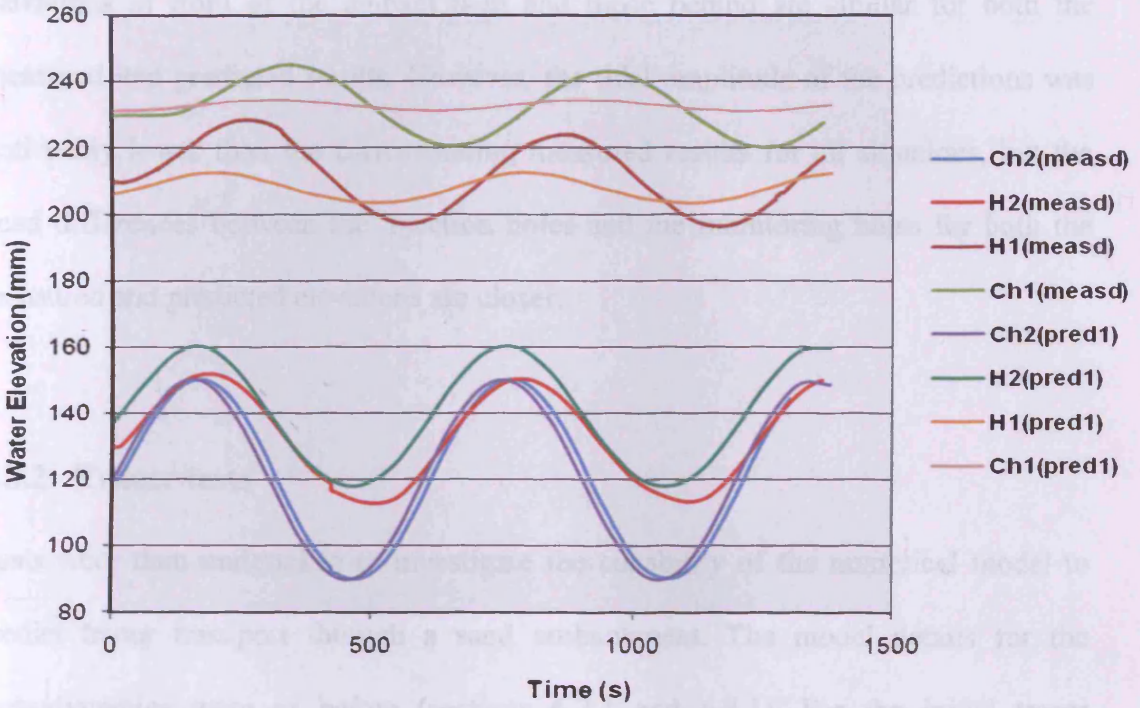

Figure 6.9: Measured and predicted elevations across embankment for a 10 min tidal cycle with pumping for transect (Ch1-Ch2)

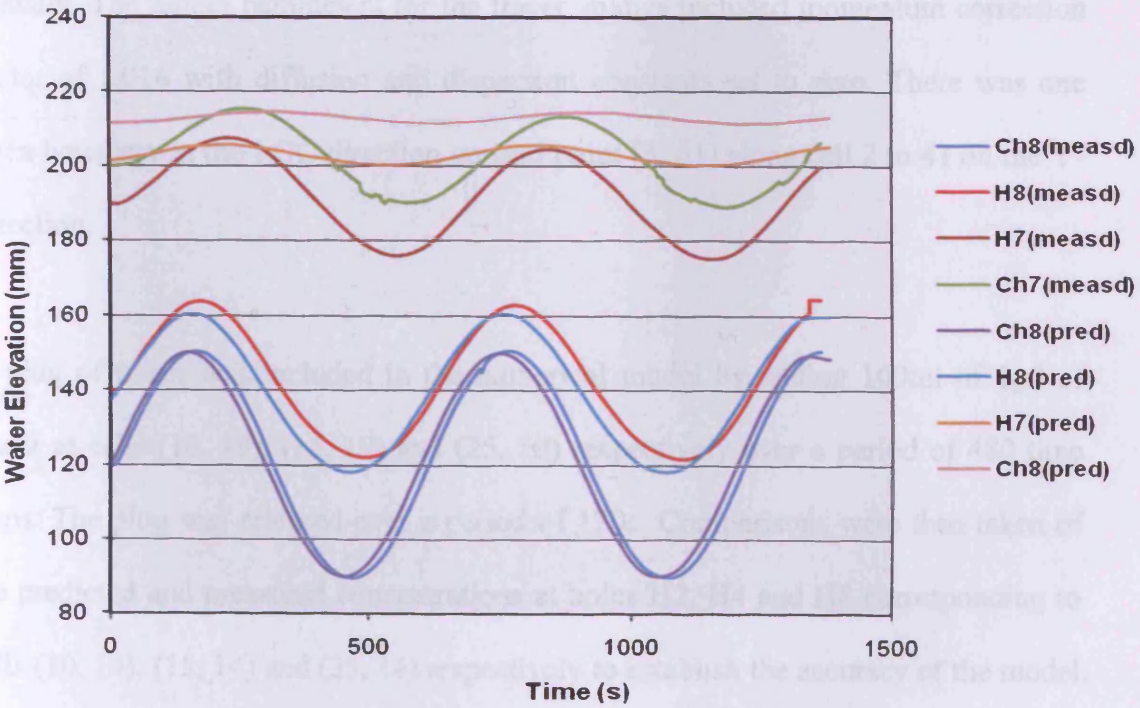

Figure 6.10: Measured and predicted elevations across embankment for a 10 min tidal cycle with pumping for transect (Ch7-Ch8)

elevations in front of the embankment and those behind are similar for both the measured and predicted results. However, the tidal amplitude of the predictions was noticeably lower than the corresponding measured results for all situations, but the head differences between the injection holes and the monitoring holes for both the measured and predicted elevations are closer.

6.3.2 Tracer tests

Tests were then undertaken to investigate the capability of the numerical model to predict tracer transport through a sand embankment. The model details for the hydrodynamics were as before (sections 6.2.1 and 6.3.1). For the initial tracer conditions, a uniform concentration of 1g/l was assumed to exist in the outfall cells and retained on these cells for the first time step; all other cells had zero concentration initially. The model parameters for the tracer studies included momentum correction factor of 1.016 with diffusion and dispersion constants set to zero. There was one open boundary in the I (X) direction on grid point (3, 61) along cell 2 to 41 on the Y-direction.

A plug of tracer was included in the numerical model by adding 100ml of 1g/l of tracer at cells (10, 19), (15, 19) and (25, 19) respectively over a period of 480 time steps. The plug was released over a period of 120s. Comparisons were then taken of the predicted and measured concentrations at holes H2, H4 and H8 corresponding to cells (10, 14), (15, 14) and (25, 14) respectively to establish the accuracy of the model. The corresponding results are shown in Figures 6.11 to 6.16.

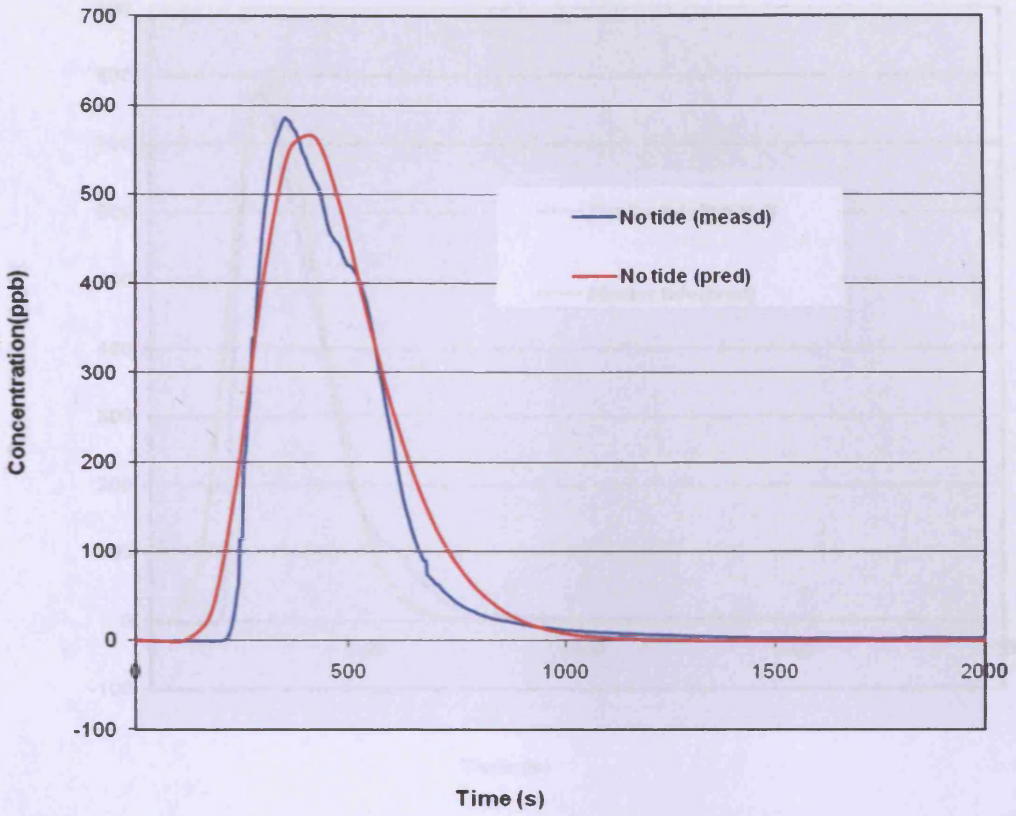

Figure 6.11: Measured and predicted concentration distribution in H2

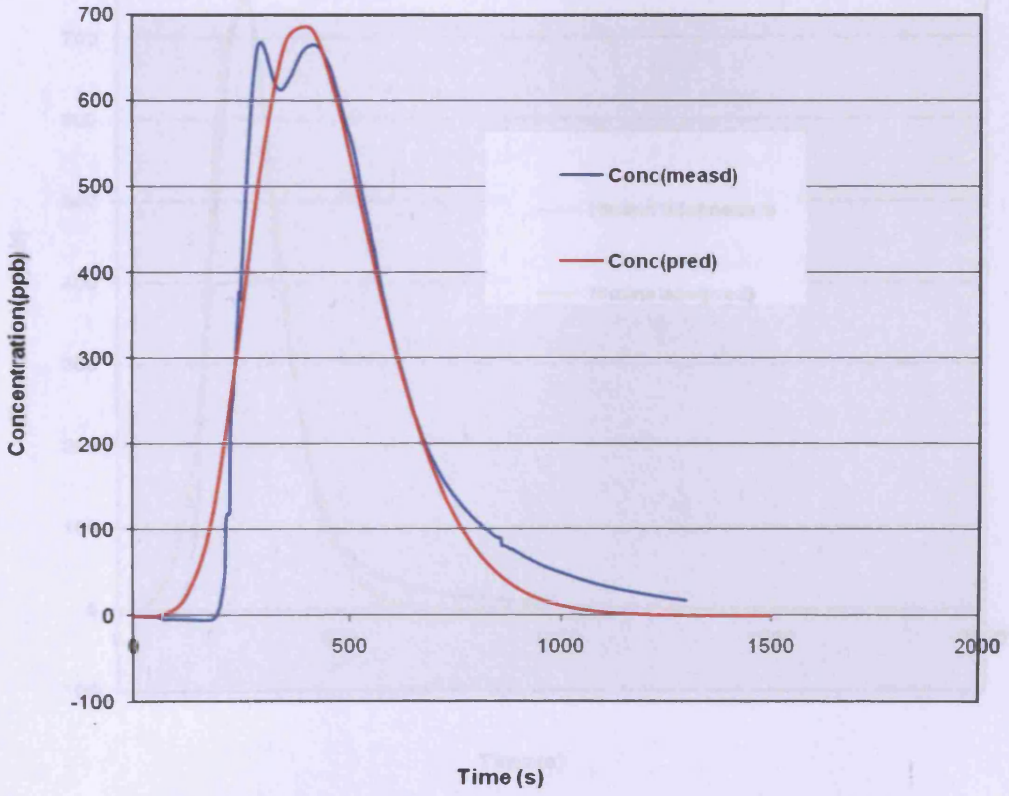

Figure 6.12: Measured and predicted concentration distribution in H4

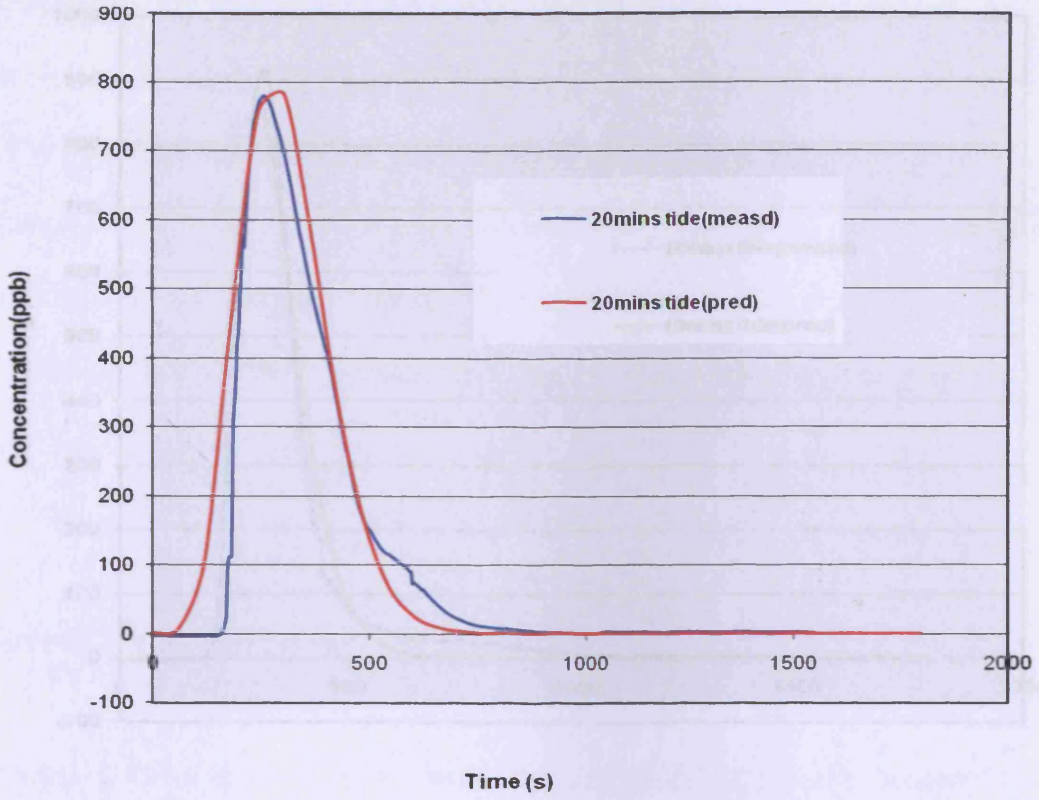

Figure 6.13: Measured and predicted concentration for 20 min tidal forcing at H2

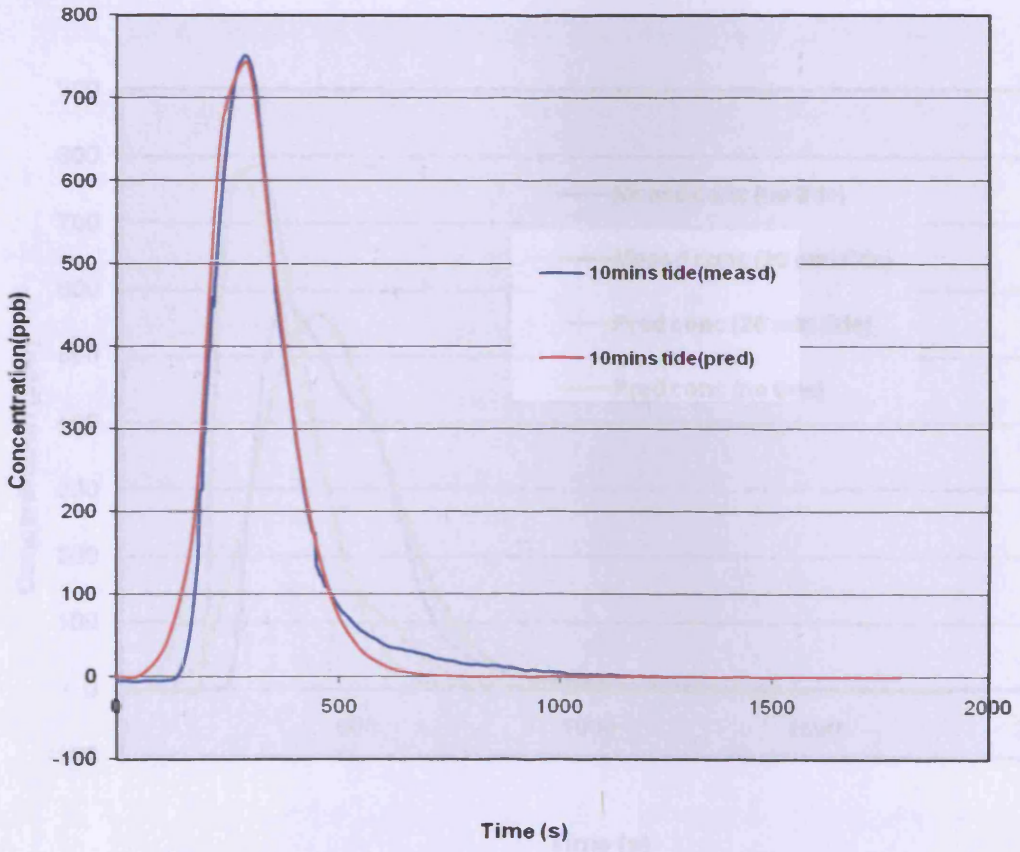

Figure 6.14: Measured and predicted concentration for 10 min tidal forcing at H4

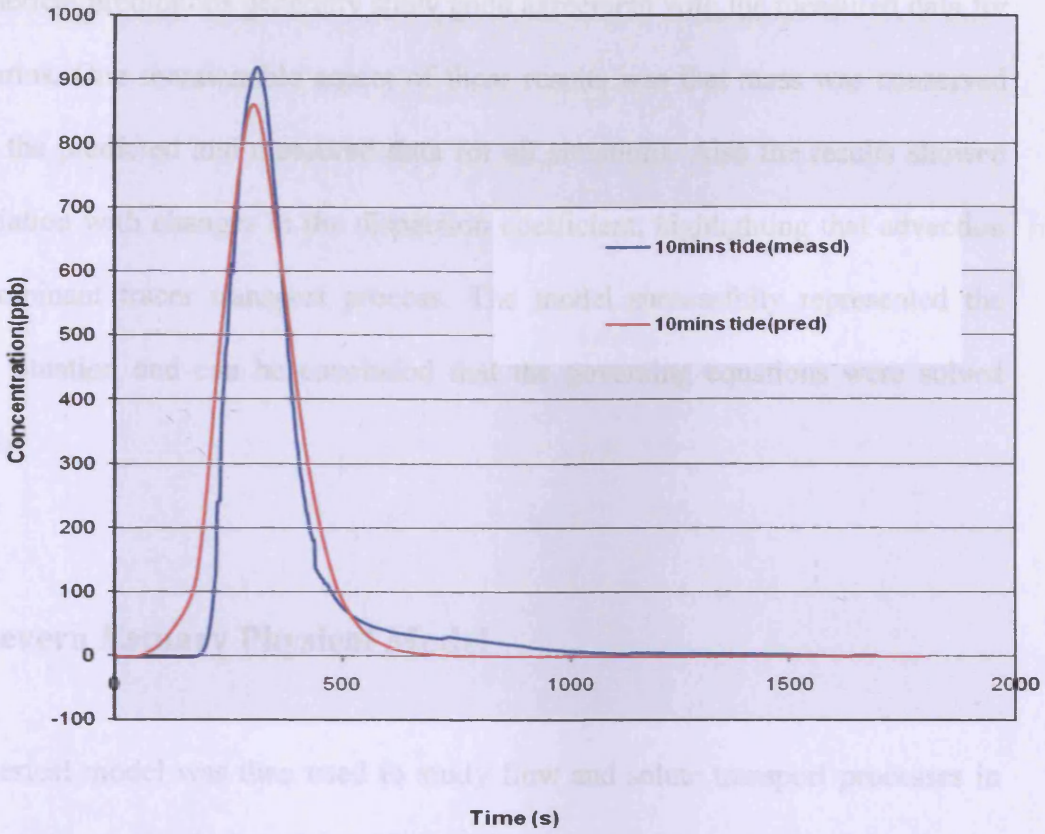

Figure 6.15: Measured and predicted concentration for 10 min tidal forcing at H8

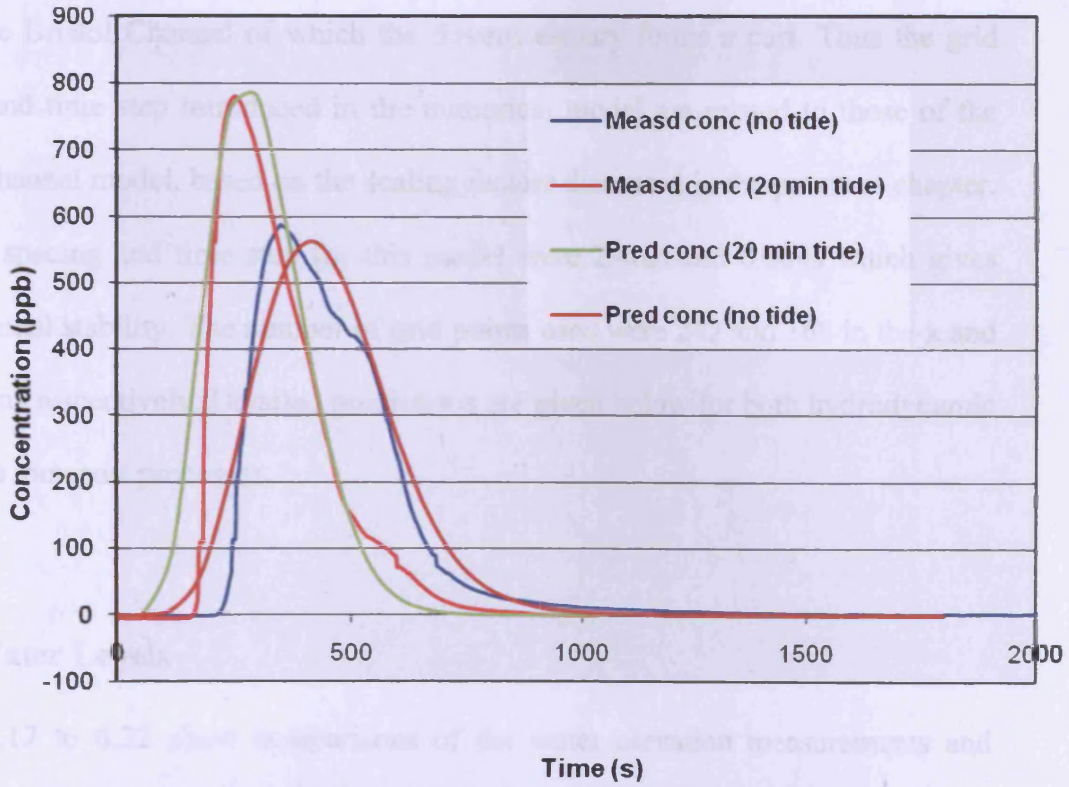

Figure 6.16: Measured and predicted concentrations for both with 20 min tide and without tidal forcing at H2

The numerical predictions generally show good agreement with the measured data for all scenarios. One mentionable aspect of these results was that mass was conserved for both the predicted and measured data for all situations. Also the results showed little variation with changes in the dispersion coefficient, highlighting that advection is the dominant tracer transport process. The model successfully represented the physical situation and can be concluded that the governing equations were solved efficiently.

6.4 Severn Estuary Physical Model

The numerical model was then used to study flow and solute transport processes in the Severn estuary physical model, with the laboratory model placed in the same tidal basin. The numerical model for the Severn estuary is related to an existing model set up for the Bristol Channel of which the Severn estuary forms a part. Thus the grid spacing and time step introduced in the numerical model are related to those of the Bristol Channel model, based on the scaling factors discussed in the previous chapter. The grid spacing and time step for this model were 2.4cm and 0.004s which gives unconditional stability. The number of grid points used were 242 and 168 in the x and y directions respectively. Detailed predictions are given below for both hydrodynamic and solute transport processes.

6.4.1 Water Levels

Figures 6.17 to 6.22 show comparisons of the water elevation measurements and numerical predictions at selected sites along the estuary. As can be seen the

numerical model gives good agreement between both sets of results at all of the sites shown. In characterising roughness height, either Manning's n or Chezy's C is used in the hydraulics industry (Lavedrine, 2002), so for this study the Manning's coefficient used was 0.0350 and eddy viscosity coefficient of 0.15.

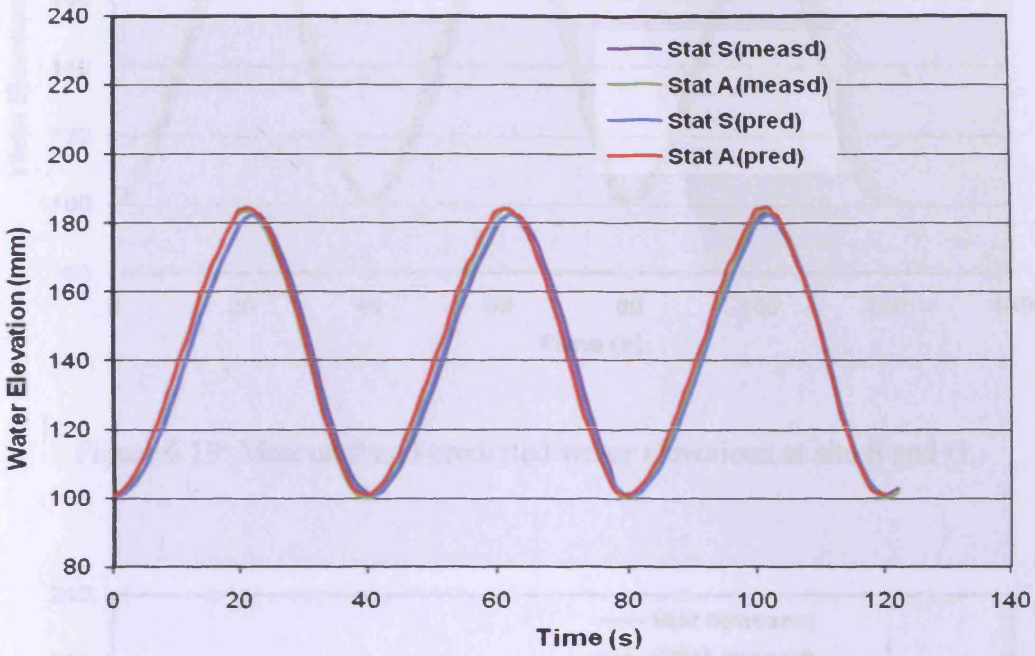

Figure 6.17: Measured and predicted water elevations at site S and A

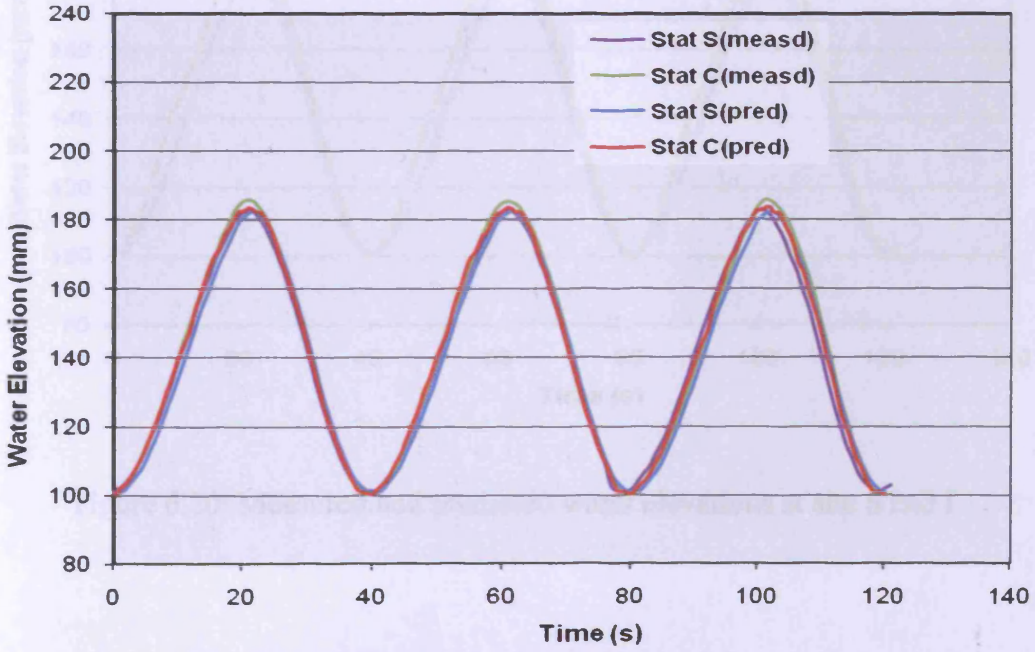

Figure 6.18: Measured and predicted water elevations at site S and C

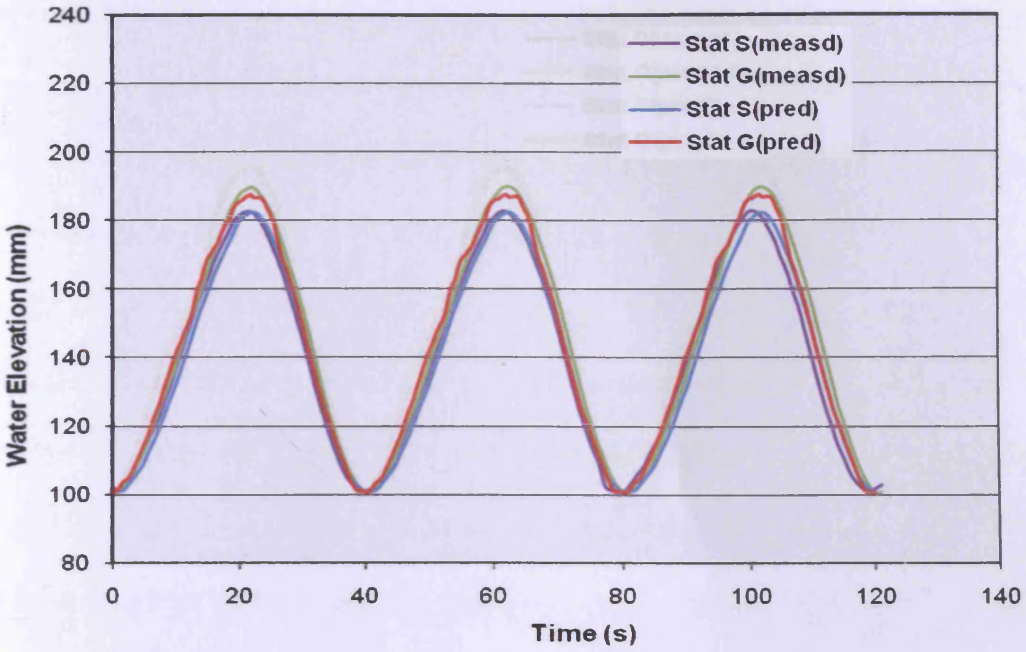

Figure 6.19: Measured and predicted water elevations at site S and G

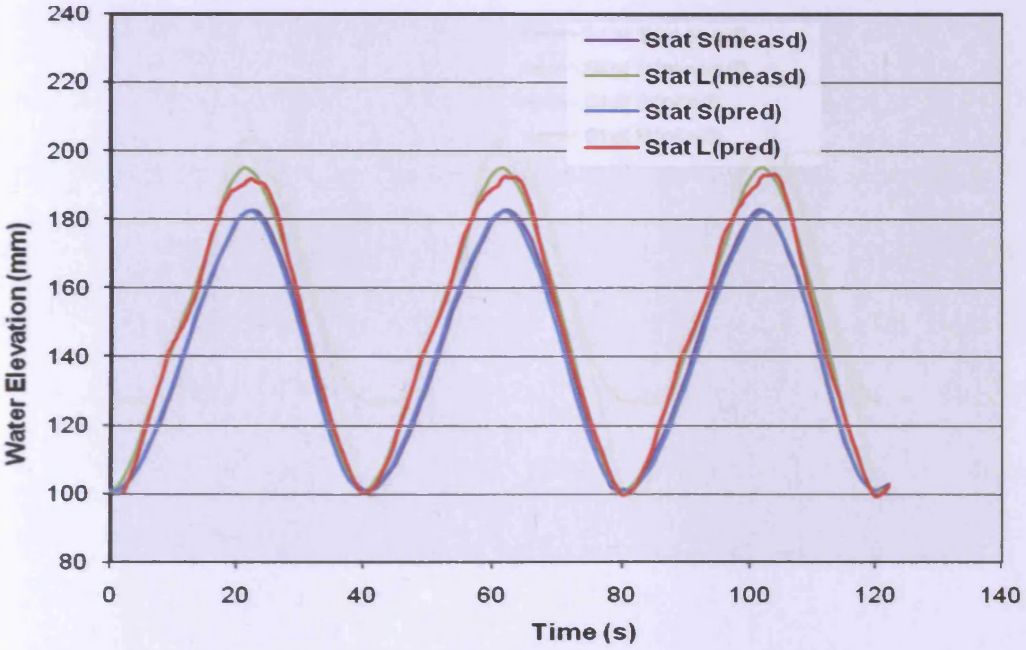

Figure 6.20: Measured and predicted water elevations at site S and L

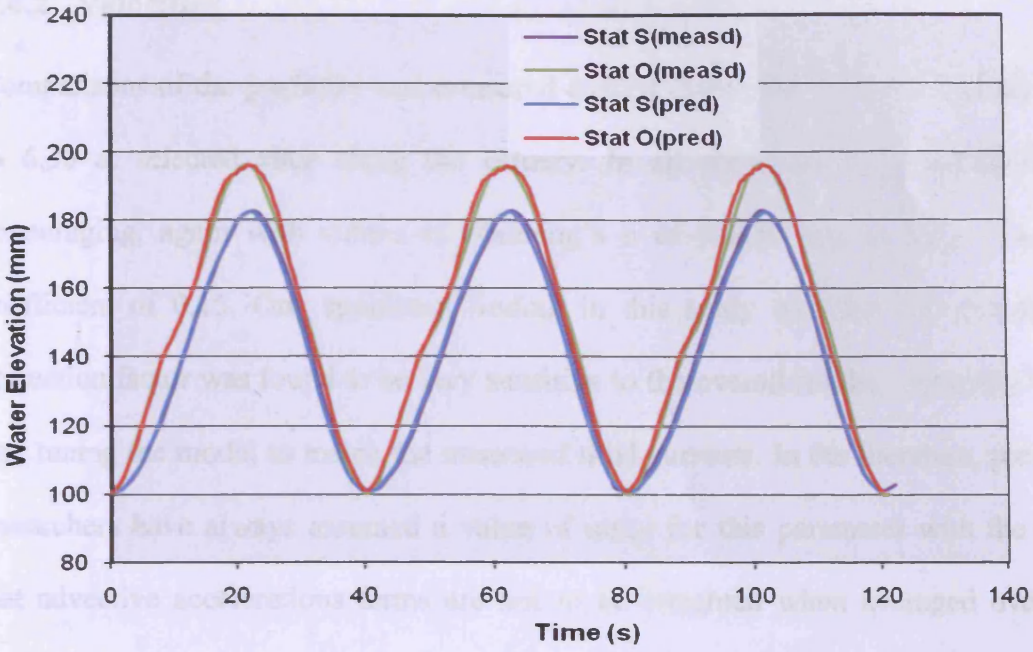

Figure 6.21: Measured and predicted water elevations at site S and O

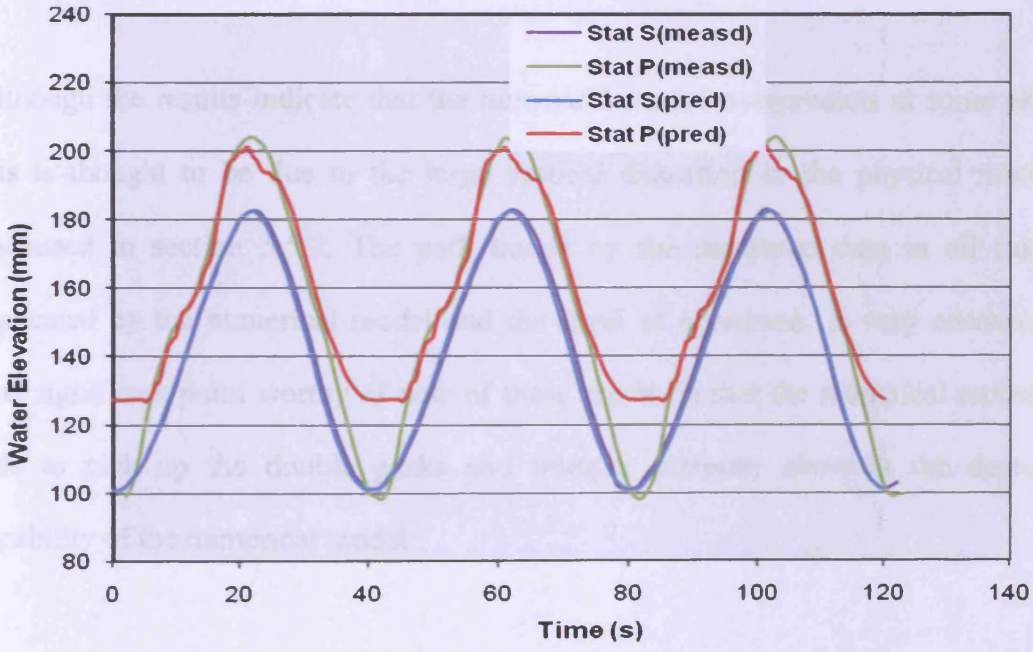

Figure 6.22: Measured and predicted water elevations at site S and P

6.4.2 Velocities

Comparisons of the predicted and measured current speeds are shown in Figures 6.23 to 6.30 at selected sites along the estuary. In all the cases the predictions are encouraging, again with values of Manning's n of 0.0350 and an eddy viscosity coefficient of 0.15. One sgnificant finding in this study was that the momentum correction factor was found to be very sensitive to the overall results, especially when fine tuning the model to match the measured tidal currents. In the literature, previous researchers have always assumed a value of unity for this parameter with the view that advective accelerations terms are not to be weighted when averaged over the depth or area. In this particular case, the optimum value of this parameter was found to be 0.70 after 4 trials, which had been reduced by a third of what is commonly assumed.

Although the results indicate that the numerical model overpredicts at some phases, this is thought to be due to the large vertical distortion in the physical model as discussed in section 5.5.2. The path traced by the measured data in all cases is replicated by the numerical model and the level of agreement is very encouraging. One significant point worthy of note of these results is that the numerical model was able to pick up the double peaks and troughs correctly showing the degree of capability of the numerical model.

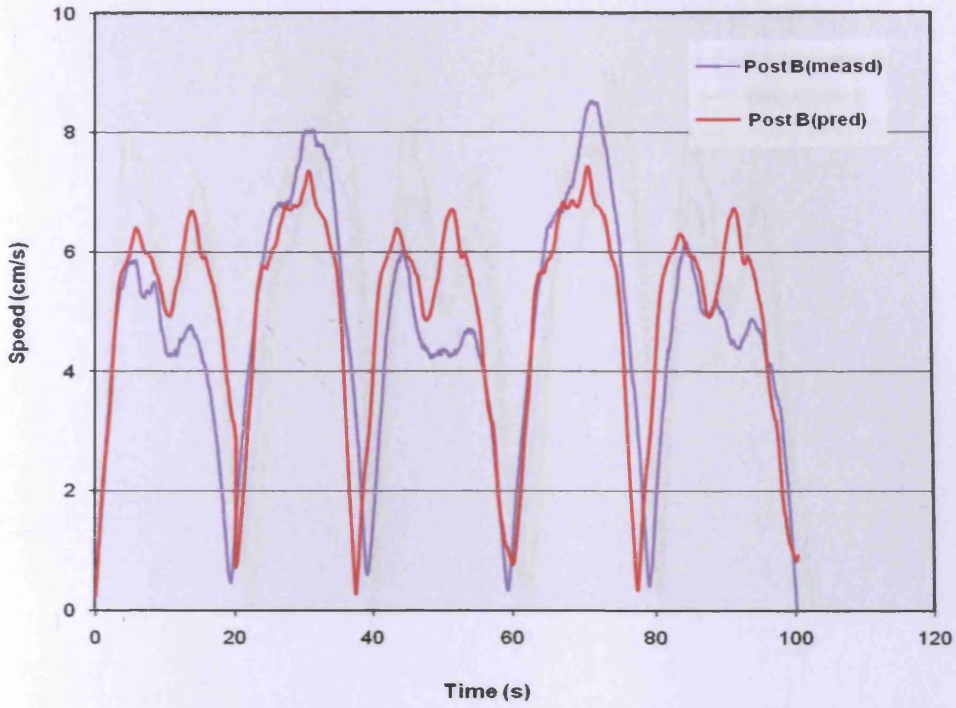

Figure 6.23: Comparison of measured and predicted current speed at station B

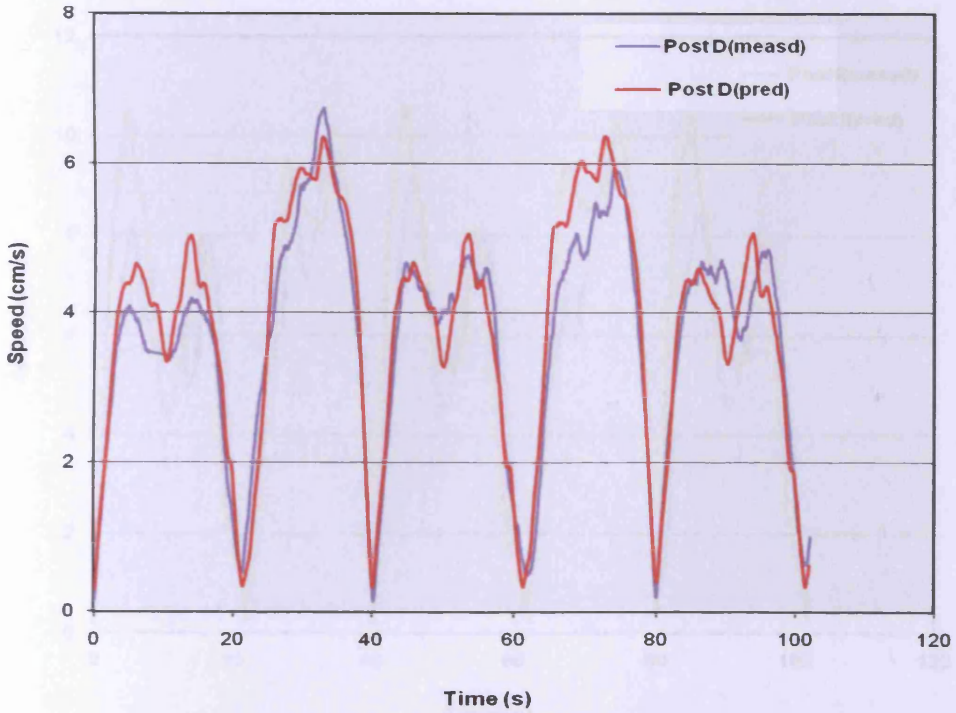

Figure 6.24: Comparison of measured and predicted current speed at station D

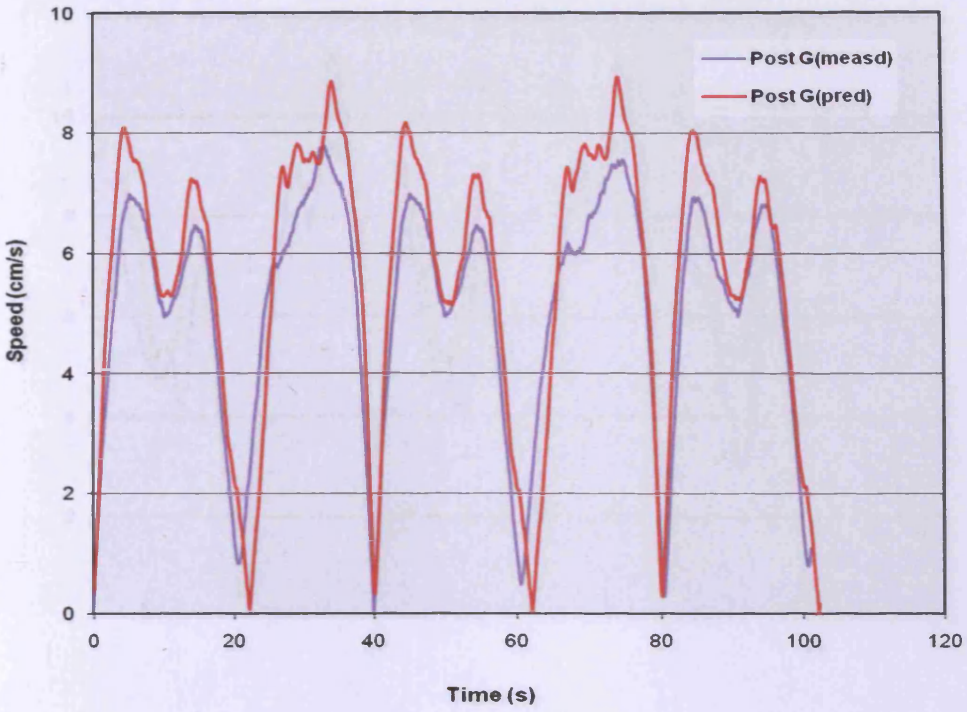

Figure 6.25: Comparison of measured and predicted current speed at station G

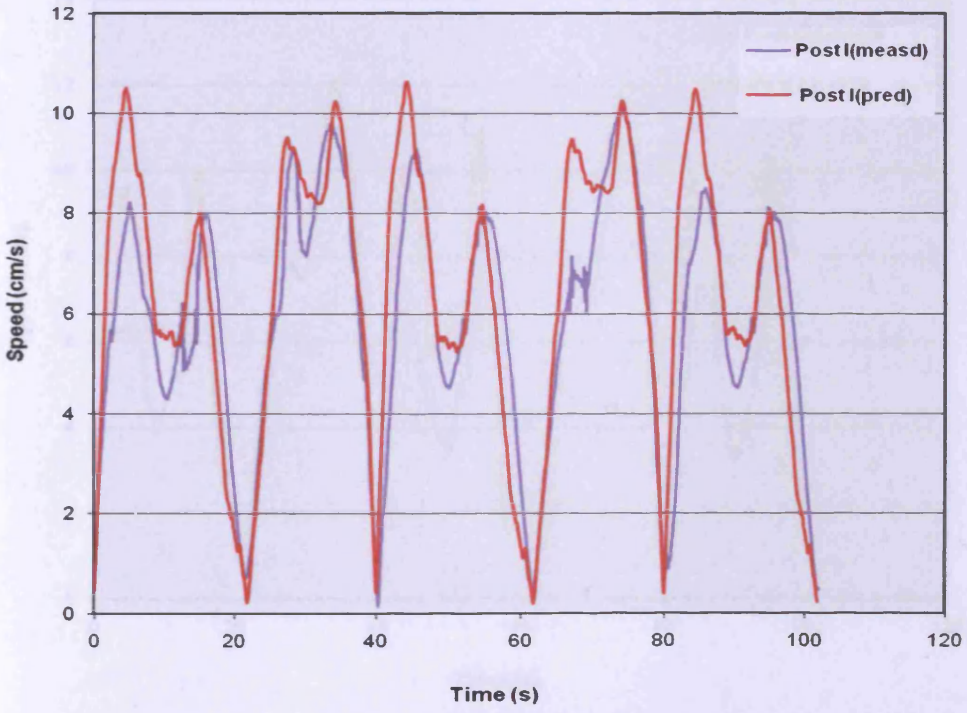

Figure 6.26: Comparison of measured and predicted current speed at station I

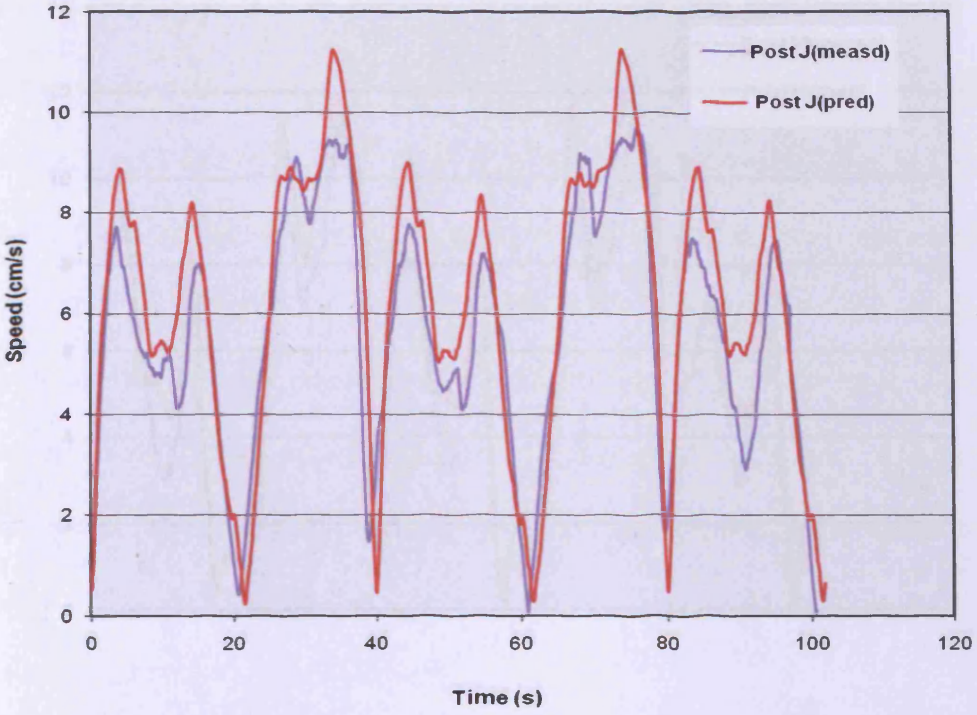

Figure 6.27: Comparison of measured and predicted current speed at station J

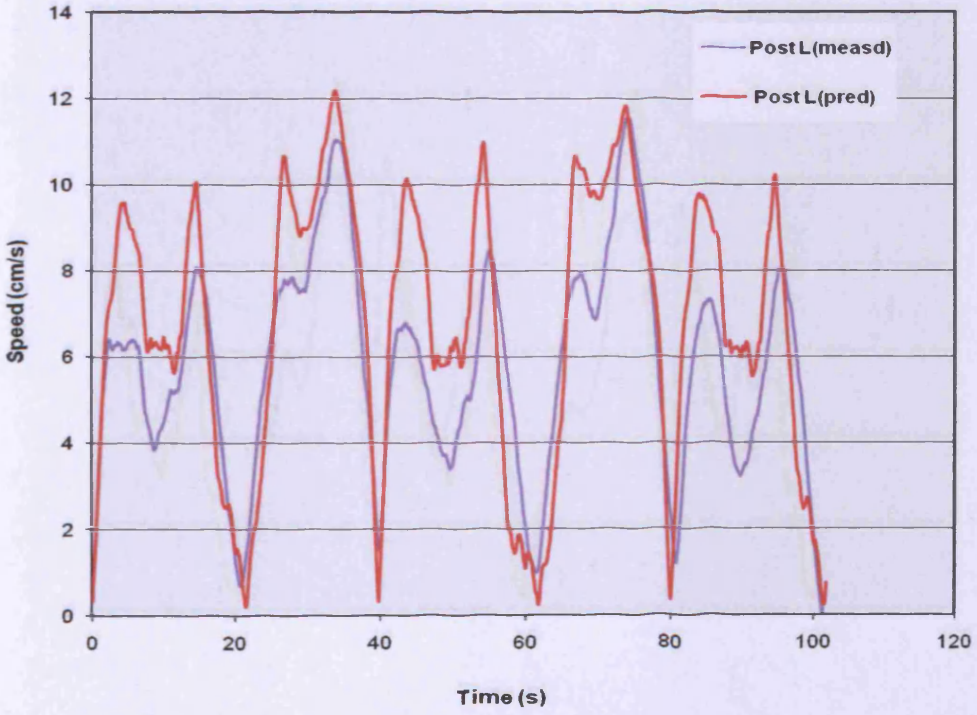

Figure 6.28: Comparison of measured and predicted current speed at station L

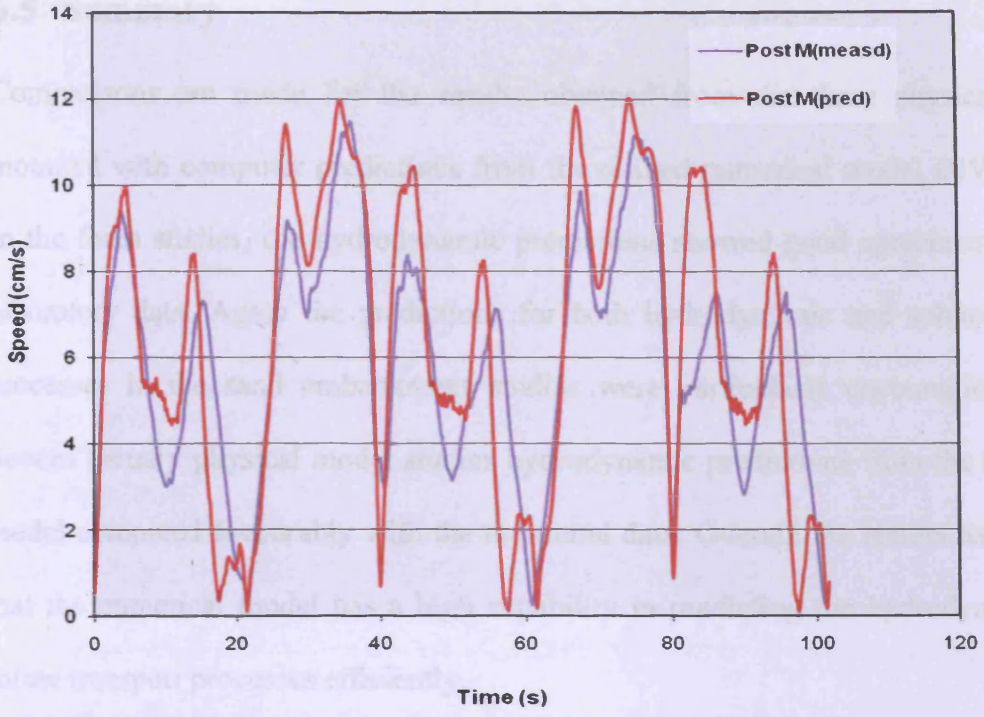

Figure 6.29: Comparison of measured and predicted current speed at station M

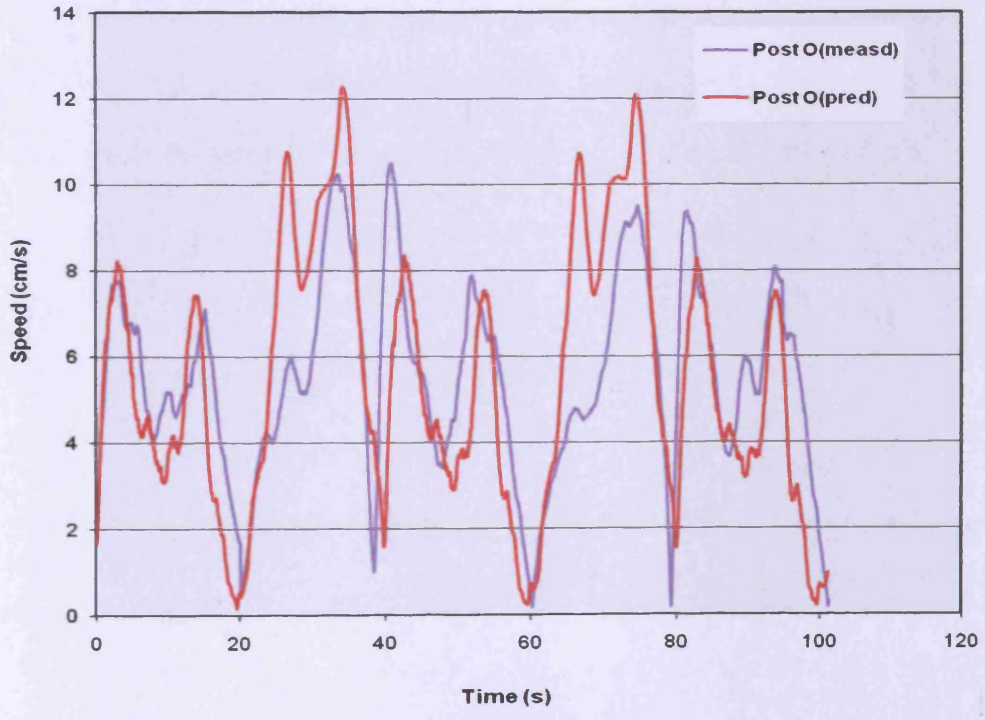

Figure 6.30: Comparison of measured and predicted current speed at station O

6.5 Summary

Comparisons are made for the results obtained from the three physical models mounted with computer predictions from the refined numerical model DIVAST-SG. In the foam studies, the hydrodynamic predictions showed good agreement with the laboratory data. Again the predictions for both hydrodynamic and solute transport processes in the sand embankment studies were particularly encouraging. In the Severn Estuary physical model studies hydrodynamic predictions from the numerical model compared favourably with the measured data. Overall, the results have shown that the numerical model has a high capability in predicting the hydrodynamic and solute transport processes efficiently.

CHAPTER 7 CONCLUSIONS AND RECOMMENDATIONS

7.1 Conclusions

7.1.1 Reviews

There has been extensive work undertaken by previous researchers on the coupling of surface and sub-surface flows. Most of these studies have linked either 1-D surface to 3-D subsurface flows or 3-D surface flows to 1-D subsurface flows in an iterative or non-iterative manner. There are only a few studies that have linked 2-D surface flows to 2-D sub-surface flows which has formed the main focus of this study. Even for the few model studies that have linked 2-D surface water to 2-D groundwater models, in most cases they have only looked at piezometric heads (i.e. water levels) of the surface water-groundwater system. In this study, however, apart from the water levels or piezometric heads, the research has also focused on solute transport processes in the surface water and groundwater including estuarine systems which is thought to be unique in comparison with studies undertaken by previous researchers.

The following conclusions are drawn from the study outlined in the text:

In this study, an existing 1-D and 2-D linked surface water model, which has been extended to include 2-D groundwater flows, has been refined and deployed for implementation for the following laboratory studies.

7.1.2 Foam studies:

As outlined in the text, a surface water – groundwater system was created with two foam material blocks acting as groundwater material, and with a flowing river in between the two foam blocks. River flow in the form of a channel became possible with the aid of an oscillating weir at the lower boundary of the system. Water levels in the form of tidal waves in the channel were compared with the piezometric heads of the adjacent boreholes in the foam for different tidal periods. The piezometric water levels decreased as permeability increased in conformity with work done by previous researchers like Darcy (1856). The results from this laboratory studies were compared with predictions from the refined numerical model and they showed good comparison.

One of the main objectives of this study was to investigate solute transport processes in surface water-groundwater system and look at the influence that the processes of advection, diffusion and dispersion have on the transportation processes. This has normally been achieved with the use of dye studies by conducting tracer tests. Consequently a Rhodamine WT tracer test studies were mounted for the surface water-groundwater system set up with the foam material. It was observed that the tracer could not move through the foam material after injection to the detection point for it to be picked by the monitoring equipment.

Polyurethane foams are thought to be good absorbents and adsorbents of dyes including families of Rhodamine and other organic phenols (Robaina et al., 2009; Baldex et al., 2008; El-Shahawi and Aldhaheri, 1996; El-Shahawi, 1994; Fong and Chow, 1992). They are able to retain different classes of substances because of the presence of polar and non-polar groups in their structures (Baldex et al., 2008). In

discussing the transport of sorbing solutes in homogeneous porous media, Abulaban et al. (1998), observed that as local dispersion tends to spread the plume and dilute the concentration, there is an increase in a retardation coefficient that tends to slow its progress. They argued that, this phenomenon can be construed as self-restraining process imposed by the plume itself and thus the plume tends to resist hydrodynamic dispersion. In the process, according to Abulaban et al. (1998), the concentration approaches zero as the retardation coefficient tends to infinity and consequently the solute can hardly move at such low concentrations. This may be one of the plausible reasons why the dye could not move in the foam.

Another observation by Dawson et al. (2007) suggests that saturating polyurethane foam with a polar fluid (like water) reduces the strength and stiffness of the foam. This could create surface tension forces which would impede the movement of the solute from one point to the other. The inability of the dye to move therefore was thought of as due to sorption and surface tension forces.

This idea of using foam blocks to replicate groundwater material was thought to be the novel and the first time that foam had been considered as a means of replicating groundwater flow in controlled laboratory conditions.

7.1.3 Sand embankment studies

In view of the fact that the tracer studies through the foam material failed to model realistically solute transport in ground water systems, the foam material was replaced with a more traditional sand embankment in the same tidal basin, as used for the foam material. The set-up has been described in Chapter Five. In this part of the study,

extensive data were collected for both the hydrodynamic parameters, in terms of water elevations and flow paths, and solute transport processes with the use of dye tracer studies. Water elevations in the channel were compared with water elevations in the adjacent boreholes and again they showed consistency, with changes in permeability as found for previous researchers. Comparison of numerical model predictions with results of the laboratory data were particularly encouraging, confirming that the 2-D linked surface flow and sub-surface flow model was accurately predicting the hydrodynamic processes.

The tracer tests studies were conducted for two scenarios: with the influence of tidal forcing and without tidal forcing. Studies were also undertaken of mass solute injection for each of the two scenarios. For the two scenarios and for different mass solute injection levels, the concentration distribution curves (or flowthrough curves) showed that mass was conserved for all cases. However, for the same mass of solute injected, there were peak and temporal differences between the two scenarios. Whereas for the same mass of solute injected, the flowthrough curve peaked early with tidal forcing, whereas the peak was delayed without tidal forcing. More so, the maximum concentration with tidal forcing was greater than for the situation without tidal forcing. This was consistent with simulations from the numerical model and also with simulations from a box model used by Li et al, (2004). The tide provided a source of increasing turbulence and for that matter the mixing process was enhanced thereby enhancing the solute transport processes. Also, increased mixing meant that more solute would be detached from the sediments and would arrive at the monitoring station than for the case of no tidal forcing, as was observed in this study.

In furtherance to the effect of tidal forcing on solute transport, another situation was created where for the same mass of solute injected tides of different period were forced on the transport process and comparisons were then made for the results obtained. It was observed that the concentration distributions peaked earlier with low tidal periods than for those with high tidal periods. Lower tidal periods meant higher frequency waves and thereby leading to increased turbulence and enhanced mixing and consequently greater maximum peak concentrations with lower arrival times.

One significant finding worth highlighting is that when the mass of solute was doubled during injection, the concentration distribution showed similar trends in terms of peak concentrations, but no difference in temporal distribution. Based on the results and findings the following conclusions can be drawn:

1. Pollution from wetlands to marine environments via groundwater flow paths is more pronounced with the tides from adjacent coastal waters. The impact is higher with higher frequency tides or long period waves, such as surges.
2. The level of pollution in the aquatic environment is dependent upon the amount of contamination at the source.

Comparisons of the results from the laboratory studies and numerical model predictions showed good agreement. It was found that advection was the most significant transport phenomenon for both surface and sub-surface flows, particularly in comparison with dispersion and diffusion. The numerical model simulations also confirmed these findings, since changes in dispersion/diffusion coefficients in the numerical model did not noticeably affect the numerical model predictions.

7.1.4 Severn Estuary Physical model

A Severn Estuary physical model was constructed in the same tidal basin. As far as this author is aware, this physical model study of the Severn Estuary is the first of its kind to have been undertaken. It is significant because in recent years the estuary has attracted a lot of attention, especially with the potential of alternative energy generation. Thus any studies that can help mimic the situation and conditions as in the prototype would help address the many concerns that the estuary is currently attracting.

The model could not match the prototype because of scaling difficulties and space constraints. However, some conclusions are worthy of note.

- It was shown from the physical model results that the tidal amplitude reduces from the head of the estuary as the tide moves seawards. Thus for this funnel-shaped estuary, the tidal amplitude increased as the width of the estuary becomes constricted towards the landward limit. This phenomenon was in agreement with field studies as reported in Xia et al.(2010).
- Extensive tidal current data were collected at various sites along the physical model estuary. It was shown that these tidal currents are ebb-dominated and were consistent with studies undertaken in the main Severn Estuary by previous researchers, such as (Uncles 1983; Xia et al., 2010).
- It was shown from the physical model results that for a semi-diurnal tidal estuary like the Severn, tides have lesser effect on the transport of solutes than from catchments. Thus the impact of pollution from diffuse sources to marine environments from catchments could be higher in less tidally dominated coastal waters than a tidal one. This conclusion is consistent with simulations

from Robinson et al (2007). Also the spatial extent of pollution is minimised within the estuary as the tide tends to push the pollutants back and forth along the estuary or coastal zone.

- The capability of the numerical model was tested and verified with the results from the data collected from the physical model. It was shown that water elevations compared favourably and a comparison with field data were also very encouraging. Tidal current predictions from the numerical model also showed good agreement with the physical model results. These results were achieved with a Manning roughness coefficient of 0.035 and eddy viscosity constant of 0.15.
- One of the significant findings from this study was the choice of the momentum correction factor and how it influenced the outcome of the hydrodynamic results. In the literature the momentum correction parameter is generally disregarded or inherently assumed to be close to unity and hence it is assumed that the advective acceleration terms are not weighted when averaged either over the area or depth in a 1-D or 2-D model respectively. However, in this study, the momentum correction factor was found to be very sensitive to the overall results, especially when fine tuning the model to match the measured tidal currents. In this particular case, the optimum value of this parameter was found to be 0.70 after 4 trials. The implication of this result is that the momentum correction factor term is not necessarily insignificant in 2-D modelling and it can reduce the effect of the advective acceleration terms by up to a third relative to the normal assumed value. This is thought to be a significant finding that future researchers must take into consideration in coastal model studies of macro-tidal estuarine modelling.

The purpose of these experiments was to investigate the manner in which flow and a conservative tracer interacted between surface and sub-surface flows for simulated riverine and tidal conditions. These experiments and the corresponding datasets are thought to be unique.

7.2 Recommendations

Following the outcomes of the results and findings from this study, the following are recommended for future studies:

- Surface and subsurface flows are three dimensional in nature. Thus, in real situations, apart from horizontal flows, transport of fluids and solutes also occur in the vertical. In this study, however, the focus has been on hydrodynamic and solute transport processes in the two dimensional plane only. It is therefore recommended that for a complete understanding of the system, a 3-D groundwater model should be linked with a 3-D surface water (estuary or coastal water) model, to be deployed for the processes outlined in this study.
- The model has been verified and tested against laboratory data in this study. Field situations, however, are different from laboratory situations in terms of both spatial and temporal extent. It is therefore recommended that further testing of the model should be carried out for field studies, with particular emphasis on diffusion and advection for the groundwater model.
- The solute transport processes focused on using conservative dye in the tracer studies. Such studies give an idea about the diffusion/dispersion processes without looking at how decay can affect the solute transport processes. It is recommended that further controlled laboratory testing be undertaken, ideally

for non-conservative tracers to investigate effects of decay relative to diffusion/dispersion processes under controlled conditions.

- The purpose of the sand box with sediments attached to the Severn Estuary physical model was to look at the impact of diffuse source pollution from catchments on the marine environment and under controlled laboratory conditions. In this study, however, a one dimensional pollution pathway was created to link the sediments to the estuary for the studies to be conducted. This may not mimic the real situation on the ground. It is therefore recommended that a catchment model, such as HSPF, be linked to the existing 1D-2D DIVAST estuary model for detailed knowledge and analysis of the impact of pollution from such sources on coastal waters.

REFERENCES

Abesser, C., P. Shand, D. Goody and D. Peach, 2008. The role of alluvial valley deposits in groundwater-surface water exchange in a Chalk river. In: Abesser, C., T. Wagener and G. Nuetzmann (eds): Groundwater-Surface Water Interaction: Process Understanding, Conceptualization and Modelling Oxford: IAHS

Abulaban, A., J. L. Nieber and D. Misra, 1998. Modelling plume behaviour for nonlinearly sorbing solutes in saturated homogeneous porous media. *Advances In Water Resources 21, 487-498.*

Ahmad, Z., U. C. Kothyari and K. G. Ranga Raju, 2004. Longitudinal dispersion in sediment-laden open channel flows. *International Journal of Sediment Research 19(1), 1-14.*

Ahn, J. H., S. B. Grant, C. Q. Surbeck, P. M. Digiacomo, N. P. Nezlin and S. Anderson, Jiang (2005). Coastal Water Quality Impact of Stormwater Runoff from Urban Watershed in Southern California. *Environ. Sci. Technol. 39, 5940-5953*

Alley, W. M. and P. E Smith, 1982. Multi-event urban runoff quality model (DR3M-QUAL), US Geological Survey, Open File Report 82–724, Reston VA, U.S.A.

Alley, W. M., R. W. Healy, J. W. Labaugh and T. E. Reilly, 2002. Flow and storage in groundwater systems. Science 296, 1985-1990.

Argent R. M., G. M. Podger., R. B. Grayson., K. Fowler. and N. Murray, 2006. E2 catchment modelling software: user guide. Australia: eWater Cooperative Research Centre, 111p.

Auer, M.T., and S.L. Niehaus, 1993 Modelling Faecal Coliform Bacteria-I. Field and Laboratory Determination of Loss Kinetics. *Water Research*, IAWQ 27(4), 693-701.

Atkinson, T. C. and P. M. Davis, 2000. Longitudinal dispersion in natural channels: 1. Experimental results from the River Severn, U.K. *Hydrology and Earth System Sciences 4(3), 345-353.*

Anderson, M.L., J. E. Whitlock and V. J. Harwood, 2005. Persistence and differential survival of fecal indicator bacteria in subtropical waters and sediments. *Applied Environmental Microbiology 71, 3041–3048*

Anderson, P. F. and G. W. Council, 2008. Practical tools for calibration of transient groundwater models. In: Refsgaard, J. C., K. Kovar, E. Harder and E. Nygaard (eds). Calibration and Reliability in Groundwater Modelling: Credibility of Modelling (ModelCARE2007). Oxford UK.: Intenational Association of Hydrological Sciences 320, 305-309.

Ataie-Ashtiani, B, 2007. MODSharp: Regional-scale numerical model for quantifying Groundwater flux and contaminant discharge into the coastal zone. *Environmental Modelling & Software 22, 1307-1315.*

Auld, H., D. MacIver, J. Klaassen, 2004: Heavy rainfall and waterborne disease outbreaks: the Walkerton example. *Journal of Toxicology and Environmental Health Part A* 67, 1879–87.

Baldez, E. E., N. F. Robaina, R. J. Cassella, 2008. Employment of polyurethane foam for the adsorption of Methylene Blue in aqueous medium. *Journal of Hazardous Materials 159, 580–586*

Banhart, J., 2001. Manufacture, characterisation and application of cellular metals and metal foams. *Progress in Materials Science 46, 559–632*

Bethge E. and U. Mohrlok, 2008. Uncertainty assessment for contaminant leaching from flood water retention areas. In: Refsgaard, J. C., K. Kovar, E. Harder and E. Nygaard (eds). Calibration and Reliability in Groundwater Modelling: Credibility of Modelling (ModelCARE2007). Oxford UK.: International Association of Hydrological Sciences 320

Bianchi, M., C. Zheng, G. R. Tick and S. M. Gorelick (2008). Evaluation of Fickian and non-Fickian models for solute transport in porous media containing decimetre-scale preferential flow paths. In: Refsgaard, J. C., K. Kovar, E. Harder and E. Nygaard (eds). Calibration and Reliability in Groundwater Modelling: Credibility of Modelling (ModelCARE2007). Oxford UK: International Association of Hydrological Sciences 320

Bicknell, B. R., J. C. Imhoff, A. S. Donigian and R. C. Johanson, 1997. Hydrological

simulation program—FORTRAN (HSPF). User's Manual for release 11. EPA—600/R-97/080. Athens, GA: United States Environmental Protection Agency.

Boehm, A. B., J. A. Fuhrman, R. D. Mrse and S. B. Grant (2003). Tiered Approach for Identification of a Human Faecal Pollution Source at a Recreational Beach: Case Study at Avalon Bay, Catalina Island, California. Environ. Sci. Technol. 37: 673-680.

Bordalo, A. A., 1993. Effects of salinity of bacterioplankton: field and microcosm experiments. *Journal of Applied Bacteriology 75: 393-398.*

Bradford, S.F.and N. D Katopodes, 1998. Nonhydrostatic model for surface irrigation. *Journal of Irrigation and Drainage Engineering 124 (4), 200–212.*

Broda, S., C. Paniconi and M. Larocque 2008. Evaluation of the hillslope-storage Boussinesq model with leakage. In: Refsgaard, J. C., K. Kovar, E. Harder and E. Nygaard (eds). Calibration and Reliability in Groundwater Modelling: Credibility of Modelling (ModelCARE2007). Oxford UK.: International Association of Hydrological Sciences 320, 182-187.

Brookes, J. D., J. A. M. Hipsey, M. D. Burch, N. J. Ashbolt and C. Ferguson, 2004. Fate and transport of pathogens in lakes and reservoirs. *Environment International 30(5), 741-759*

Bruce, M. G., M. B. Curtis, M. M. Payne, R. K. Gautom, E. C. Thompson, A. L. Bennett and J. I. Kobayashi, 2003: Lake-associated outbreak of Escherichia coli O157:H7 in Clark County, Washington, August 1999. *Archives of Pediatric and Adolescent Medicine* 157, 1016–21.

BS1377, 1990. BS 1377 : Part 5 : 1990 Determination of permeability by the constant-head method. British Standards.

Bureau of Economic Geology 2005. Groundwater-Surface Water Interactions in Texas. Bureau of Economic Geology Report, University of Texas, Austin.

Burton, D. J., J. R. West, R. W. Horsington and K. Randle 1995. Modelling Transport Processes in the Ribble Estuary. *Environmental International 21(2), 141-1995.*

Carrol, S. P., L. Dawes, M. Hargreaves and A. Goonetilleke, 2009. Faecal pollution

source identification in an urbanising catchment using antibiotic resistance profiling, discriminant analysis and partial least squares regression. *Water Research 43, 1237-1246.*

Cartwright, N., O. Z. Jessen and P. Nielsen, 2006. Application of a coupled ground-surface water flow model to simulate periodic groundwater flow influenced by a sloping boundary, capillarity and vertical flows. *Environmental Modelling & Software 21: 770-778.*

Casulli, V.and R.T Cheng, 1992. Semi-implicit finite difference methods for three dimensional shallow water flow. *International Journal for Numerical Methods in Fluids 15 (6), 629–648*

Castor, M. L. and M. J. Beach, 2004. Reducing illness transmission from disinfected recreational water venues – swimming, diarrhea and the emergence of a new public health concern. *Paediatric Infectious Diseases Journal* 23, *866–70.*

Causon, D. M., D. M. Ingram and C. G. Mingham, 2001. A Cartesian cut cell method for shallow water flows with moving boundaries. *Advances in WaterResources 24: 899-911.*

Chatwin, P. C., 1971. On the interpretation of some longitudinal dispersion experiments. *Journal of Fluid Mechanics 48(4), 689–702.*

Cooper, H. H. J. and M. I. Rorabaugh, 1963. Ground-water Movements and Bank Storage due to Flood stages in Surface Streams. U.S. Geological Survey.

Cotruvo, J.A., A. Dufour, G. Rees, J. Bartram, R. Carr, D.O. Cliver et al.,(eds.), 2004. Waterborne Zoonoses – Identification, Causes and Control. London, UK: IWA Publishing.

Crowther, J., D. Kay and M. D. Wyer, 2002. Faecal-indicator concentrations in waters draining lowland pastoral catchments in the UK: relationships with land use and farming practices. *Water Research 36, 1725–1734.*

Crowther, J., M. D.Wyer, M. Bradford, D. Kay and C.A. Francis, 2003. Modelling faecal indicator concentrations in large rural catchments using land use and topographic data. *Journal of Applied Microbiology 94, 962–973.*

Culliton, T. J., 1998. Population, distribution, density and growth; A state of the coast report, NOAA's state of the coast report; Natl. Oceanic and Atmos. Admin., Silver Spring, Md.

Cunge, J.A., F.M. Holly, Jr and A. Verwey, 1980. Practical Aspects of Computational River Hydraulics. London: Pitman Publishing Limited, 420pp.

Czernuszenko, W.,1990. Dispersion of pollutants in flowing surface waters. *Encyclopedia of fluid mechanics*, 119–169.

Danon-Schaffer, M.N. ,2001. Walkerton's contaminated water supply system: a forensic approach to identifying the source. *Environmental Forensics 2, 197–200*

Darcy, H. (1856). Les Fontaines Publiques de la Ville de Dijon. Dalmont, Paris.

Dagan, G and S. C. Lessoff, 2008. Application of stochastic modelling to numerical flow: transmissivity upscaling In: Refsgaard, J. C., K. Kovar, E. Harder and E. Nygaard (eds). Calibration and Reliability in Groundwater Modelling: Credibility of Modelling (ModelCARE2007). Oxford UK: International Association of Hydrological Sciences 320

Davis, P. M., T. C. Atkinson and T. M. L. Wigley, 2000. Longitudinal dispersion in natural channels: 2. The roles of shear flow dispersion and dead zones in the River Severn, U.K. *Hydrology and Earth Systems Sciences 4(3), 355-371.*

Davis, P. M. and T. C. Atkinson 2000. Longitudinal dispersion in natural channels: 3. The roles of shear flow dispersion and dead zones in the River Severn, U.K. *Hydrology and Earth Systems Sciences 4(3), 355-371.*

Deng, Z.-Q. and H.-S. Jung, 2009. Scaling dispersion model for pollutant transport in Rivers. *Environmental Modelling & Software 24, 627-631.*

Deng, Z.-Q., L. Bengtsson, V. P. Singh and D. D. Adrian, 2002. Longitudinal Dispersion Coefficient in Single-Channel Streams. *Journal of Hydraulic Engineering 128 (10), 901-916.*

Deng, Z.-Q., V. P. Singh and L. Bengtsson, 2001. Longitudinal Dispersion Coefficient in Straight Rivers. *Journal of Hydraulic Engineering 127 (11), 919-927.*

DHI, 1995. MIKE 21 short description, Danish Hydraulic Institute, Hørsholm, Denmark.

DHI Water and Environment, 2005. MIKE SHE – integrated surface water and groundwater.http://www.dhigroup.com/Software/WaterResources/MIKESHE.asp x

Dronkers, J.J., 1964. Tidal Computations in Rivers and Coastal Waters. Amsterdam: North Holland Publishing Co..

Dupuit, J., 1863. Études théoriques et pratiques sur le mouvement des eaux. Paris: Dunod.

Earle, J.R., 2003. The three rivers project—water quality monitoring and management systems in the Boyne, Liffey and Suir Catchments in Ireland, *Water Scence. Technology* **47** (7-8), 217–225

Easton, J. H., M. Lalor, J. J. Gauthier and R. Pitt, 2004. In-situ die-off of indicator bacteria and pathogens. In: Proceedings of the National Beach Conference, October 13–15, San Diego, CA.

Ebrahimi, K., 2004 Development of an Integrated Free Surface and Groundwater Flow Model. PhD thesis, Cardiff University.

Ebrahimi, K., R. A. Falconer and B. Lin 2007. Flow and solute fluxes in integrated Wetland and coastal systems. *Environmental Modelling & Software 22, 1337-1348.*

EC, 2000. DIRECTIVE 2000/60/EC OF THE EUROPEAN PARLIAMENT AND OF THE COUNCIL of 23 October 2000 establishing a framework for Community action in the field of water policy. European Parliament and Council 2000/60/EC.

Elder, J.W., 1959. The Dispersion of Marked Fluid in a Turbulent Shear Flow. *Journal of Fluid Mechanics 5(4), 544-560.*

Elfeki, A. M. M., G. J. M. Uffink and S. Lebreton, 2007. Simulation of solute transport under oscillating groundwater flow in homogeneous aquifers. *Journal of Hydraulic Research 45(2), 254-260.*

El-Shahawi, M. S., 1994. Retention and separation of some organic water pollutants with unloaded and tri-n-octylamine loaded polyester-based polyurethane foams. *Talanta 41(9), 1481-1488.*

El-Shahawi, M. S.and S. M. Aldhaheri, 1996. Preconcentration and separation of acaricides by polyurethane foam. *Analytica Chimica Acta 320, 277-287*

Environment Agency, 2007. The unseen threat to water quality. Diffuse water pollution in England and Wales Report. Bristol: Environment Agency.

EPA, 2004. Potential Environmental Impacts of Animal Feeding Operations. http://www.epa.gov/agriculture/ag101/ impacts.html.

Esposito, G., H. G. B. Allersma, K. Soga, C. Kechavarzi and H. Coumoulos, 2000. Centrifuge simulation of LNAPL infiltration in partially saturated porous granular medium. In : Garnier, J.et al (eds), Proceedings of the International Symposium on Physical Modelling and Testing in Environmental Geotechnics. NECER, France: 277-284.

Evison, L. M., 1989. Comparative studies on the survival of indicator organisms and pathogens in fresh and sea water. *Water Science Technology **20**, 309–315*

Fairbanks, J., S. Panday and P. Huyakorn, 2001. Comparisons of Linked and fully coupled Approaches to Simulating Conjunctive Surface/Subsurface Flow and their Interactions. MODFLOW 2001 and other Modeling Odysseys.

Falconer, R. A., 1974. Tidal Circulation Effects in Rectangular Harbors. MSc. Thesis, University of Washington, USA.

Falconer, R. A., 1977. Mathematical Modelling of Jet-Forced Circulation in Reservoirs and Harbours. PhD Thesis, University of London, London England.

Falconer, R. A., 1986. Water quality simulation study of a natural harbour. *Journal of Waterway, Port, Coastal and Ocean Engineering, ACSE 112(1), 15-34*

Falconer, R. A., 1992. Coastal Pollution modelling, why we need modelling: an introduction. Proceedings of the Institution of the Civil Engineers. Water Maritme and Energy 96: 121-123.

Falconer, R. A., 2007. M. Sc. Lecture Notes on Environmental Hydraulics, Cardiff University.

Falconer, R. A., 1993. An Introduction to Nearly Horizontal Flows. Coastal, Estuarial and Harbour Engineers' Reference Book. M. B. Abbott and W. A. Price, E. & F. N.Spon Ltd, 27-36.

Falconer, R. A. and Y. Chen, 1991. An Improved Representation of Flooding and Drying and Wind Stress Effects in a Two-Dimensional Tidal Numerical Model. Proceedings of Institution of Civil Engineers, Part 2, 91, 659-678.

Falconer, R. A. and Y. Chen, 1996. Modelling sediment transport and water quality

processes on tidal floodplains. In: Anderson, M. G., D. E. Walling and P. D. Bates (eds). Floodplain Processes. Chichester: John Wiley and Sons Ltd, 361-398.

Falconer, R. A. and B. Lin, 2003. Hydro-environmental modelling of riverine basins using dynamic rate and partitioning coefficients. International Journal of River Basin Management 1(1), 81-89.

Falconer, R.A., B. Lin and S.M. Kashefipour, 2000. Modelling Water Quality Processes in Riverine Systems, Cardiff University.

Falconer, R. A., B. Lin, Y. Wu and E. Harris ,2001a. DIVAST Reference Manual. Cardiff, Hydroenvironmental Research Centre, Cardiff School of Engineering, Cardiff University.

Falconer, R.A., B. Lin and S.M. Kashefipour, 2001b, Modelling water Quality Processes in Riverine System. In: Anderson, M. G. and P. D. Bates (eds). Model Validation: Perspectives in Hydrological Science. John Wiley & Sons, Ltd., 357-387

Falconer, R. A., B. Lin, Y. Wu and E. Harris ,2001c. DIVAST User Manual. Cardiff, Hydroenvironmental Research Centre, Cardiff School of Engineering, Cardiff University.

Falconer, R.A., E. Wolanski and L. Mardapitta-Hadjipandeli, 1986. Modeling Tidal Circulation in an Island's Wake. Journal of Waterway, Port, Coastal and Ocean Engineering 112 (2).

Farrel, R., M. Whiteman and P. Gijsbergs, 2008. The National Groundwater Modelling System for England and Wales. In: Refsgaard, J. C., K. Kovar, E. Harder and E. Nygaard (eds). Calibration and Reliability in Groundwater Modelling: Credibility of Modelling (ModelCARE2007). Oxford UK.: International Association of Hydrological Sciences 320,

Fayer, R.and J. M. Trout, 2005. Zoonotic protists in the marine environment. In: Belkin, S. S. and R. Cowell (Eds.). Oceans and Health: Pathogens in Marine Environment. Dordrecht: Kluwer Academic Publishers, 143–163.

Ferguson, C., A. Husman and D. AltavillaDeere, 2003. Fate and transport of surface

water pathogens in watersheds. *Critical Reviews in Environmental Science and Technology 33(3), 299-361.*

Fischer, H. B., 1967. The mechanics of dispersion in natural streams. *Journal of Hydraulics Division,* ASCE, 93(6), 187-216.

Fischer, H. B., 1968. Dispersion predictions in natural streams. *Journal of Sanitary Engineering,* ASCE 94(5), 927-943.

Fischer, H. B., 1973. Longitudinal Dispersion and Turbulent Mixing in Open Channel Flow. *Annual Review of Fluid Mechanics* 5, 59-78.

Fischer, H. B, 1975. Discussion of "Simple method for predicting dispersion in streams" by R. S. McQuivey and T. N. Keefer. *Journal of Environmental Engineering Division,* ASCE 101(3), 453-455.

Fischer, H. B., E. J. List, R. C. Y. Koh, J. Imberger and N. H. Brooks, 1979. Mixing in inland and coastal waters. New York: Academic Press.

Fong, P.and A. Chow, 1992. Extraction of aromatic acids and phenols by polyurethane foam. *Talanta 39(5), 497-503.*

Freeze, R. and J. A. Cherry, 1979. Groundwater. Prentice-Hall, Inc.

Freeze, R. A., 1972. Role of Subsurface Flow in Generating Surface Runoff 1. Base flow Contributions to Channel Flow. *Water Resources Research 8(3), 609-623.*

Frick, W. E., T. Khangaonkar, A. C. Sigleo and Z. Yang 2007. Estuarine-ocean exchange in a North Pacific estuary: Comparison of steady state and dynamic models. *Estuarine, Coastal and Shelf Science 74, 1-11.*

Friedrichs, C. T. and D. G.Aubrey. 1994. Tidal propagation in strongly convergent channels. *Journal of Geophysical Research 99, 3321–3336.*

Froehlich, D.C., 1989, HW031.D - Finite Element Surface-Water Modeling System: Two-Dimensional Flow in a Horizontal Plane-Users Manual: Federal Highway Administration Report FHWA-RD-88-177, 285 p.

Fryar, A. E., S. A. Macko, W. F. Mullican, III, K. D. Romanak, and P. C. Bennett. 2000. Nitrate reduction during ground-water recharge, Southern High Plains, Texas. Journal of Contaminant Hydrology 40:335-363.

Galbiati, L., F. Bouraoui, F. J. Elorza and G. Bidoglio, 2006. Modelling diffuse pollution loading into a Mediterranean lagoon: Development and application of an integrated surface-subsurface model tool. *Eological Modelling, 193, 4-18.*

Gerbaux, O., T. Vercueil, A. Memponteil and B Bador, 2009. Experimental characterization of single and two-phase flow through nickel foams. *Chemical Engineering Science 64, 4186-4195.*

Giudici, M., T. R. Ginn, C. Vassena, H. Haeri and L. Fogla 2008. A critical review of the Properties of forward and inverse problems in groundwater hydrology. In: Refsgaard, J. C., K. Kovar, E. Harder and E. Nygaard (eds). Calibration and Reliability in Groundwater Modelling: Credibility of Modelling (ModelCARE2007). Oxford UK.: International Association of Hydrological Sciences 320, 240-244.

Gleizon, P., A. G. Punt and M. G. Lyons, 2003. Modelling hydrodynamics and sediment flux within a macrotidal estuary: problems and solutions. *The Science of the Total Environment 314-316, 589-597.*

Godfrey, R. G., and B. J. Fredrick, 1970. Stream dispersion at selected sites. *Professional Rep. No. 433-K*, U.S. Geological Survey.

Goldstein, S., 1938. Modern Development in Fluid Dynamics. Oxford: Oxford University Press 1.

Götzinger, J., R. Barthel, J. Jagelke and A. Bardossy, 2008. The role of groundwater recharge and baseflow in integrated models. In: Abesser, C., T. Wagener and G. Nuetzmann (eds): Groundwater-Surface Water Interaction: Process Understanding, Conceptualization and Modelling Oxford: IAHS

Gunduz, O. and M. M. Aral, 2005. River networks and groundwater flow: a simultaneous solution of a coupled system. *Journal of Hydrology 301: 216-234.*

Haack, S. K., L. R. Fogarty and C. Wright, 2003. Escherichia coli and Enterococci at Beaches in the Grand Traverse Bay, Lake Michigan: Sources, Characteristics, and Environmental Pathways. *Environ. Sci. Technol. 37, 3275-3282.*

Haitjema H.M., 1995. Analytic element modeling of groundwater flow. San Diego: Academic Press 394 p.

Harbaugh, A.W., 2005. MODFLOW-2005, The U.S. Geological Survey modular ground-water model—the Ground-Water Flow Process: U.S. Geological Survey Techniques and Methods 6-A16,

Harbaugh, A.W., Banta, E.R., Hill, M.C., and McDonald, M.G., 2000, MODFLOW-2000, the U.S. Geological Survey modular ground-water model -- User guide to modularization concepts and the Ground-Water Flow Process: U.S. Geological Survey Open-File Report 00-92, 121 p.

Harris, C., M. C. R. Davies and N. Depountis 2000. Development of a miniaturised electrical imaging apparatus for monitoring contaminant plume evolution during centrifuge modelling. In : Garnier, J.et al (eds), Proceedings of the International Symposium on Physical Modelling and Testing in Environmental Geotechnics. NECER, France: 277-284.

Harris, E. L., R. A. Falconer and B. Lin, 2004. Modelling hydroenvironmental and health risk assessment parameters along the South Wales Coast. *Journal of Environmental Management 73, 61-70.*

Hashemi, M. R., M. J. Abedini, S. P. Neill and P. Malekzadeh, 2008. Tidal and surge modelling using differential quadrature: A case study in the Bristol Channel. *Coastal Engineering 55, 811–819*

Havnø, K., Madsen, M.N. and Dørge, J., 1995. MIKE11—a generalized river modelling package. In: Singh, V.P., (Ed). Computer Models of Watershed Hydrology. Englewood, USA: Water Resources Publications, 733–782.

Haydon, S. and. A. Deletic, 2009. Model output uncertainty of a coupled pathogen indicator-hydrologic catchment model due to input data uncertainty. *Environmental Modelling & Software, 24: 322-328.*

He, L-M. and Z-L. He, 2008. Water quality prediction of marine recreational beaches receiving watershed baseflow and stormwater runoff in southern California, USA. *Water Research 42, 2563-2573.*

HEC 1995. HEC-RAS River Analysis System, Hydraulic Reference Manual, Davis,

CA. Henderson, D. R. F., 1966. Open Channel Flow. London: Collier-Macmillan Publishers, 522pp

Henriksen, H. J. and A. L. Højberg, 2008. Model peer reviews and modeller-manager

dialogues as an avenue to improved model credibility. In: Refsgaard, J. C., K. Kovar, E. Harder and E. Nygaard (eds). Calibration and Reliability in Groundwater Modelling: Credibility of Modelling (ModelCARE2007). Oxford UK.: International Association of Hydrological Sciences 320, 101-107

Hoebe, C., Vennema, H., Husman, A.M.D. and van Duynhoven, Y. 2004: Norovirus outbreak among primary schoolchildren who had played in a recreational water fountain. *Journal of Infectious Diseases* 189, 699–705.

Holme, R. 2003: Drinking water contamination in Walkerton, Ontario: positive resolutions from a tragic event. *Water Science and Technology* 47, 1–6.

Hsieh PA, Wingle W, Healy RW. 2000. *VS2DI* – a Graphical Software Package for Simulating Fluid Flow and Solute or Energy Transport in Variably Saturated Porous Media, US Geological Survey Water-Resources Investigations Report 99-4130.

Hughes, S. A., 1995. Physical Modelling and Laboratory Techniques in Coastal Engineering. Singapore: World Scientific Publishing Co. Pte. Ltd.

Hunt, R., 2003. Ground Water-Lake Interaction Modelling Using the LAK3 Package for Modflow 2000. *Ground Water 41(2), 114 -118.*

Hussein, M. and F. W. Schwartz, 2003. Modeling of Flow and Contaminant Transport in coupled stream-aquifer systems. *Journal of Contaminant Hydrology 65, 41-64.*

Huysmans, M. and A. Dassargues, 2006. Stochastic analysis of the effect of spatial variability of diffusion parameters on radionuclide transport in a low permeability clay layer. *Hydrogeology Journal 14, 1094-1106.*

Jamieson, R., R. Gordon, D. Joy and H. Lee, 2004. Assessing microbial pollution of rural surface waters: A review of current watershed scale modeling approaches. *Agricultural Water Management 70, 1-17.*

Jobson, H. E. and A. W. Harbaugh, 1999. Modifications to the Diffusion Analogy Surface-Water Flow model (DAFLOW) for coupling to the Modular Finite-Difference Ground-Water Flow model (MODFLOW). Reston, Virginia: U.S. Geological Survey 59.

Kalbus, E., F. Reinstorf and M. Schirmer, 2006. Measuring methods for groundwater, surface water and their interactions: a review. *Hydrological Earth System Science Discussions(3), 1809-1850*

Kashefipour, S. M., B. Lin, E. Harris and R. A. Falconer ,2006. Hydro-environmental modelling for bathing compliance of an estuarine basin. *Water Research 36, 1854-1868.*

Kashefipour, S. M., B. Lin and R. A. Falconer, 2006. Modelling the fate of faecal indicators in a coastal basin. *Water Research 40, 1413-1425.*

Kashefipour, S. M. and R. A. Falconer 2002. Longitudinal dispersion coefficients in natural channels. *Water Research 36, 1596-1608.*

Kay, D., C. M. Stapleton, M. D. Wyer, A. T. McDonald, J. Crowther, N. Paul et al., 2005a. Decay of intestinal enterococci concentrations in high energy estuarine and coastal waters: towards real-time T-90 values for modelling faecal indicators in recreational waters. *Water Research 39, 655–667.*

Kay, D., M. D. Wyer., J. Crowther, C.M. Stapleton, M. Bradford, A. T. McDonald et al., 2005b. Predicting faecal indicator fluxes using digital land use data in the UK's sentinel Water Framework Directive catchment: the Ribble study. *Water Research 39, 655–667.*

Kay, D., J Crowther, C. M. Stapleton, M. D. Wyer, L. Fewtrell, S. Anthony et al., 2008. Faecal Indicator organism concentrations and catchment export coefficients in the UK. *Water Research 42: 2649-2661.*

Kay, D., M. Aitken, J. Crowther, I. Dickson, A. C. Edwards, C. Francis et al., 2007a. Reducing fluxes of faecal indicator compliance parameters to bathing waters from diffuse agricultural sources: The Brighouse Bay study, Scotland. *Environmental Pollution 147, 138–149.*

Kay, D., A. C. Edwards, R. C. Ferrier, C. Francis, C. Kay, L. Rushby et al., 2007b. Catchment microbial dynamics: the emergence of a research agenda. *Progress in Physical Geography, 31(1), 59-76.*

Koch, H., K. Mazur and U. Grunewald ,2008. Coupling of surface water management and Groundwater dynamics for mining pit lakes: In: Abesser, C., T. Wagener and G. Nuetzmann (eds): Groundwater-Surface Water Interaction: Process Understanding, Conceptualization and Modelling Oxford: IAHS

Kollet, S.J. and R.M. Maxwell, 2006. Integrated surface-groundwater flow modeling:

A free surface overland flow boundary condition in a parallel groundwater flow model. *Advances in Water Resources 29: 945–958.*

Konikow, L. F., D. J. Goode and G. Z. Hornberger, 1996. A Three-Dimensional Method-of-Characteristics Solute-Transport Model (MOC3D).

Konikow, L. F., G. Z. Hornberger, L. D. Putnam, A. M. Shapiro and B. A. Zinn, 2008. The use of groundwater age as a calibration target. In: Refsgaard, J. C., K. Kovar, E. Harder and E. Nygaard (eds). Calibration and Reliability in Groundwater Modelling: Credibility of Modelling (ModelCARE2007). Oxford UK.: International Association of Hydrological Sciences 320

Koussis, A. D., and J. Rodriguez-Mirasol, 1998. Hydraulic estimation of dispersion coefficient for streams. Technical Note, *Journal of Hydraulic Engineering,* ASCE, 124(3), 317-320.

Langevin, C., E. Swain and M. Wolfert, 2005. Simulation of integrated surface-water/ground-water flow and salinity for a coastal wetland and adjacent estuary. *Journal of Hydrology 314, 212-234.*

Lanzoni, S. and G. Seminara, 1998. On tide propagation in convergent estuaries. *Journal of Geophysical Research 103(C13), 30793-30812.*

Lapen, D. R., J. S. Price and R. Gilbert, 2005. Modelling two-dimensional steady-state Groundwater flow and flow sensitivity to boundary conditions in blanket peat complexes. *Hydrological. Processes. 19, 371-386*

Lane, S. N. 1998. Hydraulic modelling in hydrology and geomorphology: A review of high resolution approaches. *Hydrological Processes 12, 1131-1150.*

Lavedrine, I. A., 2002. Modelling of reservoir flows using Computational Fluid Dynamics. In: Falconer, R. A., B. Lin, E. L. Harris and C. A. M. E. Wilson (eds). Hydroinformatics: Model Development and Data Management. Proceedings of the Fifth International Conference on Hydroinformatics, Cardiff, UK: IWA Publishing 1, 340-345.

Lee, C. M., T. Y. Lin, C-C. Lin, G. A. Kohbodi, A. Bhatt, R. Lee and J. A. Jay, 2006. Persistence of fecal indicator bacterial in Santa Monica Bay beach sediments. *Water Research 40: 2593-2602.*

Legout, C., J. Molenat, L. Aquilina, C. Gascuel-Odoux, M. Faucheux, Y. Fauvel and T. Bariac 2007. Solute transfer in the unsaturated zone-groundwater continuum of a headwater catchment. *Journal of Hydrology 332, 427-441.*

Lewandowski J and G. Nutzmann, 2008. Surface water-groundwater interactions: hydrological and biogeochemical processes at the lowland River Spree (Germany). In: Abesser, C., T. Wagener and G. Nuetzmann (eds). Groundwater-Surface Water Interaction: Process Understanding, Conceptualization and Modelling Oxford: IAHS.

Li, L., D. A. Barry, D.-S. Jeng and H. Prommer, 2004. Tidal dynamics of groundwater flow and contaminat transport in coastal aquifers. In: Cheng, A. H.-D and D. Quazar.(eds). Coastal aquifer management : monitoring, modelling, and case studies. United States: Lewis Publishers.

Liang, D., R. A. Falconer and B. Lin, 2007. Coupling surface and subsurface flows in a depth averaged flood wave model. *Journal of Hydrology 337, 147-158.*

Lim, L.S., Varkey, P., Giesen, P. and Edmonson, L. 2004: Cryptosporidiosis outbreak in a recreational swimming pool in Minnesota. *Journal of Environmental Health* 67, 16 20.

Lin, B. and R. A. Falconer, 2001. Numerical modelling of 3-d tidal currents and water quality indicators in the Bristol Channel. Proceedings of the Institution of Civil Engineers: Water & Maritime Engineering 148 (3). Institution of Civil Engineers, London, September, 2001: 155-166

Lin, B. and R. A. Falconer 2005. Integrated 1-D and 2-D models for flow and water quality Modelling. XXXI IAHR Congress 543. Seoul, Korea: September 11-16, 2005.

Lin, B., M. Syed, and R. A. Falconer, 2008. Predicting faecal indicator levels in estuarine receiving.waters.-.An integrated hydrodynamic and ANN modelling approach. *Environment Modelling &. Software 23, 729-740.*

Lin, Y.-C. and M. A. Medina Jr, 2003. Incorporating transient storage in conjunctive stream-aquifer modeling. *Advances in Water Resources 26(9), 1001-1020.*

Liu, H., 1977. Predicting dispersion coefficient of streams. *Journal of Environmental Engineering Division, ASCE 103(1), 59–69.*

Llerar-Meza, G., D. Fernàndez-Garcia and J. J. Gómez-Hernández, 2008. Upscaling of solute transport based on the concept of memory function. In: Refsgaard, J. C., K. Kovar, E. Harder and E. Nygaard (eds). Calibration and Reliability in Groundwater Modelling: Credibility of Modelling (ModelCARE2007). Oxford UK: International Association of Hydrological Sciences 320, 210-213

Lowe, S. A. and T. J. Groninger 2005. Discussions and Closures: Discussion of

"Estimation of the Longitudinal Dispersion Coefficient Using the Velocity Profile in Natural Streams" by Il Won Seo and Kyong Oh Baek. *Journal of Hydraulic Engineering, 927-928.*

Lutterodt, G., M. Basnet, J.W.A Foppen and S Uhlenbrook, 2009.The effect of surface characteristics on the transport of multiple Escherichia coli isolates in large scale columns ofquartz sand. Water Research 43, 595–604

Madsen, H., R.-S. Blasone and D. Rosbjerg 2008. Recnt advances in parameter Estmation and uncertainty assessment in integrated hydrological modelling. In: Refsgaard, J. C., K. Kovar, E. Harder and E. Nygaard (eds). Calibration and Reliability in Groundwater Modelling: Credibility of Modelling (ModelCARE2007). Oxford UK.: International Association of Hydrological Sciences 320

Manoj, N. T., 2008. Numerical modelling of tidal circulation and studies on salinity distribution in Mandovi and Zuari estuaries. Ph.D. Thesis, Goa University, Goa, India

Martin, J. L., and S. McCutcheon, 1999. Hydrodynamics and transport for water quality modeling. Florida : CRC Press, Inc.

Martin-Vide, J. P., P. J. M. Moreta and S. Lopez-Querol, 2008. Improved 1-D modelling in compound meandering channels with vegetated floodplains. *Journal of Hydraulic Research 46(2), 265-276.*

Markstrom, S.L., R.G. Niswonger, R.S. Regan, D.E. Prudic, and P.M. Barlow, 2008. GSFLOW-coupled ground-water and surface-water FLOW model based on the integration of the precipitation-runoff modeling system (PRMS) and the modular ground-water flow model (MODFLOW-2005). United States

Mantovanelli, A., E. Marone, E.T. da Silva, L.F. Lautert, M.S. Klingenfuss, V.P. Prata Jr.et al., 2004. Combined tidal velocity and duration asymmetries as a determinant of water transport and residual flow in Paranaguá Bay estuary. *Estuarine, Coastal and Shelf Science* 59, 523–537.

McCarthy, R., 1993. Residual currents in tidally dominated, well-mixed estuaries. Tellus 45A, 325-340.

McCutcheon, S. C. 1989 *Water quality modeling*, Vol. I, CRC, Boca Raton, Fla., 27–171.

McDonald, M. G. and A. W. Harbaugh, 1988. A Modular Three-dimensional Finite

Difference Ground-water Flow Model. U. S. Geological Survey. Techniques ofWater-Resources Investigations of the United States Geological Survey, Book 6,Chapter A1

Merrit, M. L. and L. F. Konikow ,2000. Documentation of a Computer Program to Simulate Lake-Aquifer Interaction using the MODFLOW Ground-Water flow model and the MOC3D Solute-Transport Model. Tallahassee, Florida: U.S. Geological Survey, 146p.

Mitchell, S. B., H. M. Burgess, D. J. Pope and A. Theodoridou, 2008. Field studies of velocity, salinity and suspended solids concentration in a shallow tidal channel near tidal flap gates. *Estuarine, Coastal and Shelf Science 78, 385-395.*

Monninkhoff, B., 2002. Coupling of the groundwater model FEFLOW with the hydrodynamic model MIKE11 German-Chinese Conference 'Modern methods and instruments for water management and flood protection. IWU-Tagungsberichte, p. 161–173.

Morita, M., Yen, B.C., 2002. Modelling of conjunctive two-dimensional surface three dimensional subsurface flows. *Journal of Hydraulic Engineering 128 (2), 184–200*

Nguyen, K. D. and A. Quahsine, 1997. 2D Numerical Study on Tidal Circulation in Strait of Dover. *Journal of Waterway, Port, Coastal, and Ocean Engineering, 8-15.*

Niswonger, R.G., Prudic, D.E., Markstrom, S.L., Regan, R.S., and Viger, R.J. (2006). GSFLOW—A basin-scale model for coupled simulation of ground-water and surfacewater flow—Part B. Concepts for modeling ground-water flow with the U.S. GeologicalSurvey MODFLOW model, this issue.

Noat, D. and W. Rodi, 1984. Numerical simulations of secondary currents in channel flow. *Journal of Hydraulic Engineering 108(HY8), 948-968.*

Nordin, C. F. and G. V Sabol, 1974. Empirical data on longitudinal dispersion in rivers. Water Resources Investigations Rep. *No. 20–74*, U.S. Geological Survey

Obiri-Danso, K. and K. Jones 2000. Intertidal Sediments as Reservoirs for Hippurate

Negative Campylobacters, Salmonellae and Faecal Indicators in the EU Recognised Bathing Waters in North West England. *Water Research 34(2), 519-527.*

Ogden, I.D., N. F. Hepburn, M. MacRae, N. J. C.Strachan, D. R. Fenlon, S. M. Rusbridge and T. H. Pennington, 2002. Long-term survival of Escherichia coli O157 on pasture following an outbreak associated with sheep at a scout camp. *Letters in Applied Microbiology 34, 100–104*

Oliver, D.M. P.M. Haygarth, C.D. Clegg and A.L. Heathwaite, 2006. Differential E. coli die-off patterns associated with agricultural matrices. *Environmental Science and Technology* 40, 5710–5716.

Ongley, E. D. and W. G. Booty 1999. Pollution Remediation Planning in Developing Countries: Conventional Modelling versus Knowledge-Based Prediction. *Water International (in press).*

Pachepsky,Y.A.,Sadeghi, A.M.,Bradford, S.A.,Shelton,D.R.,Guber, A. K., Dao, T., 2006. Transport and fate of manure-borne pathogens: modeling perspective. *Agricultural Water Management 86, 81–92.*

Painchaud, J., D. Lefaivre and J.-C. Therriault, 1987. Box model analysis of bacterial fluxes in the St. Lawrence Estuary. *Marine Ecology Progress Series 41, 241-252.*

Panday, S. and P. S. Huyakorn, 2004. A fully coupled physically-based spatially distributed model for evaluating surface/subsurface flow. *Advances in Water Resources 27, 361-382.*

Parsons, R, 2008. Quantify groundwater's role in sustaining Groenvlei, a shallow lake in the Southern Cape region of South Africa. In: Abesser, C., T. Wagener and G. Nuetzmann (eds): Groundwater-Surface Water Interaction: Process Understanding, Conceptualization and Modelling Oxford: IAHS

Peaceman, D. W. and H. H. Rachford-Jr., 1955. The numerical solution of parabolic and elliptic differential equations. *Journal of the Society for Industrial and Applied Mathematics 3, 28–41.*

Peyrard D., S. Sauvage., P. Vervier., J. M. Sanchez-Perez and M. Quintard, 2008. A coupled vertically integrated model to describe lateral exchanges between surface and subsurface in large alluvial floodplain with a fully penetrating river. *Hydrological Processes 22, 4257-4273.*

Pfingstein, W., 2008. The influence of the experimental set-up and the model approach on the determination of diffusion coefficients for radionuclides in laboratory colum experiments. In: Refsgaard, J. C., K. Kovar, E. Harder and E. Nygaard (eds). Calibration and Reliability in Groundwater Modelling: Credibility of Modelling (ModelCARE2007). Oxford UK: International Association of Hydrological Sciences 320, 278-283.

Piasecki, M., and N. D Katopodes, 1999. Identification of stream dispersion coefficients by adjoint sensitivity method. *Journal of Hydraulic Engineering, 125(7), 714–724.*

Pinder, G. F. and S. P. Sauer, 1971. Numerical Simulation of Flood Wave Modification Due to Bank Storage Effects. *Water Resources Research 7(1), 63-70.*

Popescu, I. C., N. Gardin, S. Brouyère and A. Dassargues, 2008. Groundwater vulnerability Assessment using physically-based modelling: from challenges to pragmatic solutions. In: Refsgaard, J. C., K. Kovar, E. Harder and E. Nygaard (eds). Calibration and Reliability in Groundwater Modelling: Credibility of Modelling (ModelCARE2007). Oxford UK: International Association of Hydrological Sciences 320

Punt, A. G., G. E. Millward and J. R. W. Harris, 2003. Modelling solute transport in the Tweed Estuary, UK using ECos. *The Science of the Total Environment 314-316: 715-725.*

Preston, R.W., 1985. The Representation of Dispersion in Two-Dimensional Shallow Water Flow. Central Electricity Research Laboratories, Report No. TPRD/U278333/N84, May, 13pp.

Prickett T. A., and C. G. Lonnquist, 1971. Selected Digital computer techniques for groundwater resource evaluation. Champaign, Illinois: Illinois State Water Survey Bulletin 55.

Prudic, D. E. 1989. Documentation of a computer program to simulate stream aquifer relations using a modular, finite difference, ground-water flow model. 113.

Prudic, D. E., L. F. Konikow and E. R. Banta, 2004. A new Streamflow-Routing (SFR1) Package to simulate stream-aquifer interaction with MODFLOW-2000. Carson City, Nevada: USGS, 95.

Querner, E. P., 1997. Description and application of the combined surface and groundwater flow model MOGROW. *Journal of Hydrology 192, 158-188.*

Rassam, D. W. and A. D. Werner, 2008. Review of groundwater–surface water interaction modelling approaches and their suitability for Australian conditions. eWater Technical Report. Canberra: eWater Cooperative Research Centre.

Reeves, R. L., S. B. Grant, R. B. Mrse, C. M. C. Oancea, B. F. Sanders and A. B. Boehm (2004). Scaling and Management of Fecal Indicator Bacteria in Runoff from a Coastal Urban Watershed in Southern California. Environment Science and Technology 38, 2637-2648.

Refsgaard, J.C. and Sørensen, H.R., 1997. Water management of the Gabcikovo Scheme for balancing the interest of hydropower and environment. In: Refsgaard, J. C. and E. A. Karalis (eds). Operational Water Management. Rotterdam, The Netherlands: Balkema, 365–372

Refsgaard, J.C. and Storm, B., 1995. In: Singh, V.P. (Ed). Computer Models of Watershed Hydrology. Englewood, USA: Water Resources Publications, 809–846.

Restrepo, J. I., A. M. Montoya and J. Obeysekera, 1998. A Wetland Simulation Module for the MODFLOW Ground Water Model. *Ground Water 36(5), 764-770.*

Rethati, L, 1983. Groundwater in Civil Engineering. Amsterdam, The Netherlands: Elsevier

Robaina, N. F., S. Soriano and R. J. Cassella, 2009. Polyurethane foam loaded with SDS for the adsorption of cationic dyes from aqueous medium: Multivariate optimization of the loading process. *Journal of Hazardous Materials 167, 653–659*

Robinson, C., L. Li and D. A. Barry 2007. Effect of tidal forcing on a subterranean estuary. *Advances in Water Resources 30, 851-865.*

Rodi, W., 1984. Turbulence Models and their Applications in Hydraulics. Delft: IAHR Publication.

Rodi, W., 1987. Turbulence Models and their Applications in Hydraulics-A state of the art review. Rotterdam: IAHR Publication.

Rodi, W., 2000. Turbulence Models and their Applications in Hydraulics. 3rd ed. Rotterdam: A. A. Balkema.

Ross, M. A., P. D. Tara, J. S. Geurink, and M. T. Stewart, 1997. FIPR Hydrological

Model. Tampa, Florida: Center for Modeling Hydrologic and Aquatic Systems, Department of Civil and Environmental Engineering and Department of Geological, University of South Florida.

Runkel, R. L. 2000. Using OTIS to Model Solute Transport in Streams and Rivers. U.S. Geological Survey: Fact Sheet FS-138-99.

Rushton, K. R. and S. C. Redshaw, 1979. Seepage and Groundwater Flow. Wiley.

Rushton, K. R., 2007. Representation in regional models of saturated river-aquifer interaction for gaining/losing rivers. *Journal of Hydrology 334(1-2), 262-281*

Rutherford, J. C.,1994. River mixing. Chichester, U.K.: Wiley 102–200.

Saied, U and I. K. Tsanis, 2008. A coastal area morphodynamics model. *EnvironmentalModelling & Software 23, 35-49.*

Savenije, H. H. G., 2005. Salinity and Tides in Alluvial Estuaries. 1st Ed. Amsterdam, The Netherlands: Elsevier, 197 pp.

Scanlon, B.R. and Goldsmith, R.S., 1997. Field study of spatial variability in unsaturated flow beneath and adjacent to playas. *Water Resources Research 33(10), 2239–2252*

Scott, C. F. 1994. A Numerical Study of the Interaction of Tidal Oscillations and Non-Liniarities in an Estuary. *Estuarine, Coastal and Shelf Science 39, 477-496.*

Schaffranek R.W., Baltzer R.A. and Goldberg D.E. 1981. A Model For Simulation of Flow in Singular and Interconnected Channels. Techniques of Water Resources Investigations of the United States Geological Survey. Book 7, Chapter C3. Washington: US Government Printing Office.

Schlichting, H., 1979. Boundary Layer Theory. New York: McGraw-Hill Book Co.

Schmalz, B., P. Springer and N. Fohrer, 2008: Interactions between near-surface groundwater and surface water in a drained riparian wetland. In: Abesser, C., T. Wagener and G. Nuetzmann (eds). Groundwater-Surface Water Interaction: Process Understanding, Conceptualization and Modelling Oxford: IAHS.

Schnauder, I., B. Bockelmann-Evans and B. Lin, (2007). Modelling faecal bacteria pathways in receiving waters. Proceedings of the Institution of Civil Engineers, Maritime Engineering, 160 (MA4), 143-153.

Seo, I. W., and T. S. Cheong, 1998. Predicting longitudinal dispersion coefficient in natural streams. *Journal of Hydraulic Engineering, 124(1), 25-32.*

Sherman, J.O. 1990. User's manual for WSPRO. A computer model for water surface

profile computation. Report No. FHWA-IP-89–027. Reston, Va.: U.S. Geological Survey

Šimůnek J., M. Sejna and M. T. van Genuchten, 1999. The HYDRUS-2D software package for simulating two-dimensional movement of water, heat, and multiple solutes in variably saturated media. Version 2.0. IGWMC-TPS-53. Colorado: International Ground Water Modelling Centre, Colorado School of Mines Golden.

Sinclair, A., D. Hebb, R. Jamieson, R. Gordon, K. Benedict, K. Fuller, G. W. Stratton and A. Madani, 2009. Growing season surface water loading of fecal indicator organisms within a rural watershed. *Water Research 43, 1199-1206*

Singh, S., Z. Ahmad and U. C. Kothyari, 2009. Two-dimensional mixing of pollutants in streams with transverse line source. *Journal Hydraul. Res. 47(1), 90-99.*

Sinton, L. W., C. H. Hall, P. A. Lynch and R. J. Davies-Colley, 2002. Sunlight inactivation of fecal indicator bacteria and bacteriophages from waste stabilization pond effluent in fresh and saline waters. *Applied Environmental Microbiology 68(3), 1122-1131.*

Sleigh, P.A., P.H. Gaskell, M. Berzins, and N.G. Wright, 1998. An Unstructured Finite-Volume Algorithm for Predicting Flow in Rivers and Estuaries. *Computers and Fluids* 27(4), 479-508.

Smith, E., S. Hegazy and N. El-Aassar, 2003. Pond treatment and effluent reuse of sewage from an oil production site in an arid coastal environment. *Water Science Technology. 48, 45–52.*

Smith, R. E. and D. A. Woolhiser, 1971. Overland flow on an Infiltrating Surface. *Water Resources Research 7(4), 899-913.*

Sokrut, N., 2001. A distributed coupled model of surface and subsurface dynamics as a tool for catchment management. Stockholm, Sweden: Royal Institute of Technology.

Sokrut, N., J. Motovilov and R. Thunvik, 2001. ECOMAG-MODFLOW: An example of the integration of surface and groundwater hydrological models. MODFLOW 2001 and Other Modeling Odysseys, IGWMC, Colorado School of Mines and the U.S. Geological Survey 1, 404.

Sooky, A. A., 1969. Longitudinal dispersion in open channels. *Journal of Hydraulic Division, American. Society of Civil Engineering 95(4), 1327–1346.*

Sophocleous, M.A., J.K. Koelliker, R.S. Govindaraju, T. Birdie, S.R. Ramireddygari and S.P. Perkins, 1999. Integrated Numerical Modeling for Basin-wide Water Management: The Case of the Rattlesnake Creek Basin in South-central Kansas. *Journal of Hydrology 214(1-4), 179-196.*

Sophocleous, M., 2002. Interactions between groundwater and surface water: the state of the science. *Hydrogeology Journal 10(1), 52–67*

Sørensen, H.R., Klucovska, J., Topolska, J., Clausen, T. and Refsgaard, J.C., 1996. An engineering case study—modelling the influences of Gabcikovo hydropower plant on the hydrology and ecology in the Slovakian part of the river branch system of Zitny Ostrov. In: Refsgaard, J.C., (Ed). Distributed Hydrological Modelling. Kluwer, Dordrecht, The Netherlands, 233–253.

Sparks, T., 2007. Integrated Surface Water-Groundwater Modelling: Linking Surface Water and Groundwater using DIVAST-SG. PhD Thesis, Cardiff University.

Spanoudaki, K., A. Nanou, A. I. Stamou, G. Christodoulou, T. Sparks, B. Bockelmann and R. A. Falconer 2005. Integrated surface water-groundwater modelling. 9th International Conference on Environmental Science and Technology (9CEST2005), Rhodes island, Greece 1-3 September, 2005. *Global NEST Journal 7(3)*

Spanoudaki, K., A. I Stamou and A. Nanou-Giannarou ,2009. Development and verification of a 3-D integrated surface water–groundwater model. *Journal of Hydrology 375, 410–427*

Stauffer, F., Doppler, T. and H-J. H. Franssen 2008. How successful are standard models of groundwater-river interactions. In: Refsgaard, J. C., K. Kovar, E. Harder and E. Nygaard (eds). Calibration and Reliability in Groundwater Modelling: Credibility of Modelling (ModelCARE2007). Oxford UK: International Association of Hydrological Sciences 320,163-168

Steets, B. M. and P. A Holden, 2003. A mechanistic model of runoff associated fecal coliform fate and transport through a coastal lagoon. *Water Research 37, 589–608.*

Stelling, G. S., A. K. Wiersma and J. B. T. M. Willemse, 1986. Practical Aspects of Accurate Tidal Computations. *Journal of Hydraulic Engineering 112, 802-817.*

Streeter, V. L., E.B. Wylie and K.W. Bedford, 1998. Fluid Mechanics. 9th Ed.

Singapore: McGraw-Hill Book Co., 740pp.

Swain, E. D. and E. J. Wexler, 1996. A Coupled Surface-water and Ground-water flow model (Modbranch) for simulation of stream-aquifer interaction.

Tannehill, J.C., D.A. Anderson and R.H. Pletcher, 1997. Computational Fluid Mechanics and Heat Transfer. 2nd Ed. USA: Taylor & Francis 792pp.

Taylor, G. I., 1953. Dispersion of soluble matter in solvent flowing slowly through a tube. London: Proceedings of the Royal Society A219, 186–203.

Taylor, G. I., 1954. The dispersion of matter in turbulent flow through a pipe. London: Proceedings of the Royal Society A223, 446-468.

Taylor, R., A. Cronin, S. Pedley, J. Barker and T. Atkinson 2004. The implications of Groundwater velocity variations on microbial transport and wellhead protection-review of field evidence. *FEMS Microbiology Ecology 49, 17-26.*

Therrien R., R. G. Mclaren, E. A. Sudicky and S. M. Panday 2007. Hydrogeosphere: a three-dimensional numerical model describing fully-integrated subsurface and surface flow and solute transport. Waterloo, Ontario, Canada: Groundwater Simulations Group. Techniques of Water-Resources Investigations of the United States GeologicalSurvey Book 6, Chapter A6.

Thomann R.V. and J.A. Muller, 1987. Principles of Surface Water Quality Modelling Control. New York: Harper Collins Publishers Inc., 644pp.

Thoms, M. C. 2003. Flood-plain river ecosystems:lateral connections and the implications of human interference. *Geomorphology* 56, 335-349.

Thorbjarnarson, K.W., J. Inami and G. Girty, 2002. Visual solute transport: a computer code for use in hydrogeology classes. *Journal of Geoscience Education 5, 287-291*

Traini, C., D. Menier and J-N. Proust, 2008. The Vilaine River estuary in the Bay of Biscay: Insight int geomorphologic controls on estuarine sedimentation. Geophysical Research Abstracts 10, EGU2008-A-05586, EGU General Assembly.

Turner_Designs, 2006a. Application Support Bulletin 103: Fluorescein and a Fluorometer. http://www.turnerdesigns.com/t2/doc/appnotes/998_5103.html.

Turner_Designs, 2006b). Application Support Bulletin 104: Fluorescent Tracer Dyes http://www.turnerdesigns.com/t2/doc/appnotes/998_5104.html.

White, L. and E. Wolanski, 2008. Flow separation and vertical motions in a tidal flow. interacting with a shallow-water island. *Estuarine, Coastal and Shelf Science 77, 457-466.*

Uchiyama, Y., 1999. Coastal Groundwater Flow and Associated Nutrient Transport into the Sea. 2nd UJNR/CEST Panel, Charleston, Maryland; Oct. 1999.

Uncles, R. J., 1983. Hydrodynamics of the Bristol Channel. *Marine Pollution Bulletin 15(2), 47-53*

Urbano, L., B. Waldron, D. Larsen and H. Shook, 2006. Groundwater-surface water interactions at the transition of an aquifer from unconfined to confined. *Journal of Hydrology 321, 200-212.*

USEPA. 2000. Proceedings of the ground-water/surface-water interactions workshop. U.S. Environmental Protection Agency Report 542/R-00, 1-200 p.

Vanderkwaak, J. E., 1999. Numerical simulation of flow and chemical transport in integrated surface–subsurface hydrologic systems. Ph.D. Thesis, University of Waterloo, Waterloo, Ontario.

van Elburg H., G. B. Engelen and C. J. Hemker, 1993. FLOWNET manual. Version 5.4. FreeUniversity of Amsterdam

Verburg K., P. J. Ross. and K. L Bristow, 1996. SWIM v2.1 user manual. Divisional Report 130. CSIRO Division of Soils, Australia

Vieira, J. K., 1993. Dispersive processes in two-dimensional models. In: Abott, M. B. and W. A. Price (eds). Coastal, Estuarial and Harbour Engineers' Reference Book. London: E. & F. N. Spon Ltd, 179-190.

Weare, T. J., 1976. Instability in Tidal Flow Computational Schemes. *Journal of Hydraulic Division, ASCE 102, 569-580.*

Wijeratne, E. M. S., and L. Rydberg, 2007. Modelling and observations of tidal wave propagation, circulation and residence times in Puttalam Lagoon, Sri Lanka. *Estuarine Coastal and Shelf Science, 74: 697-708.*

Winter, T. C., J. W Harvey, O. L Franke and W. M. Alley, 1998. Groundwater and surface water – a single resource. United States Geological Survey, Circular 1139.

Woessner, W. W., 2000. Stream and fluvial plain ground water interactions: Rescaling hydrogeologic thought. *Ground Water 38(3), 423-429.*

Workman, S. R., S. E. Serrano and K. Liberty, 1997. Development and application of

an analytical model of stream/aquifer interaction. *Journal of Hydrology 200, 149-163.*

Wu, J., 1969. Wind Stress and Surface Roughness at Air-Sea Interface. *Journal of Geophysical Research* 74, 444-455

Xia, J., R. A. Falconer and B. Lin, 2010. Impact of different tidal renewable energy projects on the hydrodynamic processes in the Severn Estuary, UK. *Ocean Modelling 32, 86–104*

Xu, P., F. Brissaud and A. Fazio, 2002. Non-steady-state modelling of faecal coliform removal in deep tertiary lagoons. *Water Research 36, 3074-3082.*

Xu, H., J. Lin and D. Wang, 2008. Numerical study on salinity stratification in the Pamlico River Estuary. *Estuarine, Coastal and Shelf Science 80*

Yuan, D., B. Lin and R. A. Falconer, 2008. Simulating moving boundary using a linked Groundwater and surface water model. *Journal of Hydrology 349, 524-535.*

Yuan, D., B. Lin, R. A. Falconer and J. Tao, 2007. Development of an integrated model for assessing the impact of diffuse and point source pollution on coastal waters. *Environmental Modelling & Software 22, 871-879.*

Zheng, L., C. Chen and F. Y. Zhang, 2004. Development of water quality model in the Satilla River Estuary, Georgia. *Ecological Modelling, 178, 457-482.*

APPENDIX

Appendix 1 Definition of Terms for a Typical Input File for DIVAST-SG

The attached text file is a typical data input file for the sand embankment for simulation of DIVAST-SG.

The following are some of the terms defined as Falconer et al (2001c) and Sparks (2007) that describe the parameters used in the modelling domain.

IMAX number of grid cells in the x-direction

JMAX number of grid cells in the y-direction

JSPACE number of characters for each output item. The output is in integer format. For example the value of JSPACE can be 3, 4 or 5. If JSPACE = 3 then the output is set to 38I3 and if the value is 4, the output is 29I4 and if the value is 5, the output is 23I5 resulting in the output page of 114, 116 and 115 characters for output blocks corresponding to 3, 4 and 5 respectively.

NADVIT number of iterations for the advective acceleration terms to be time centred. It is a counter for the number of iterations and currently set to 2. It may need no changing.

NFLRUF logical flag for rough turbulent flow or smooth laminar flow (rough=0, smooth=1). If NFLRUF = 1, then Manning equation is assumed and if

NFLRUF = 0, then Chezy co-efficient is assumed by solving Darcy-Weisbachs equation, refer to main text.

TECTIM gives the interval that Tecplot and point data is collected

TECOUT switches output to a Tecplot file on and off.

NUMPRT number of times calculations are written to the output files (a maximum of 50 is allowed by the present version of DIVAST, the maximum of NUMPRT can be increased by altering the dimension of the array TPRINT). i. e. NUMPRT ≤ Array size for TPRINT.

NWEPRN logical flag for printouts of water elevations at each grid cell (Yes = 1; No = 0)

NVEPRN logical flag for printouts of velocities at each grid cell (Yes = 1; No = 0)

NDEPRN logical flag for printouts of depths at each grid cell (Yes = 1; No = 0)

NCHPRN logical flag for printouts of CHEZY value at each grid cell (Yes = 1; No = 0)

NEDPRN logical flag for printouts of depth mean eddy viscosity at each grid cell (Yes = 1; No = 0)

NDIPRN logical flag for printouts of dispersion-diffusion coefficients at each grid cell (Yes = 1; No = 0)

NSOPRN logical flag for printouts of solute concentrations at each grid cell (Yes = 1; No = 0)

NFLWIN logical flag for inclusion of surface wind stress effects (Yes = 1; No = 0). If there is no wind then NFLWIN is set to 0 especially for a typical laboratory situation like this study.

NFLDRY logical flag for enabling the flooding and drying checks (Yes = 1; No = 0).

NFLSOL logical flag for enabling solute transport computation (Yes = 1; No = 0). In this study the fag was set to 1. If NFLSOL = 0, then only hydrodynamic processes are modelled.

NOSECT maximum permitted number of reaches of integration in either the first dimension of IROW & JCOL. If NOSECT is too high, it wastes computer memory and if it's too small, the program fails. It is advised that the values be obtained from the .OUT file after a test run. Typical, one may start with 200 for NOSECT.

IENDOB number of open boundaries in the x-direction or along the I-row.

JENDOB number of open boundaries in the y-direction or along the J-column

IOBD open boundary types and locations for IENDOB. The number of lines used to IOBD values must be the same as the value of IENDOB. If IENDOB = 0, no input data for IOBD.

JOBD similar for IOBD.

Typically, open boundaries are specified with 0, 1, 2, and 3 with the description as :

0 = flow or velocity at lower boundary; 1 = flow or velocity at upper boundary, 2 = water elevation at lower boundary, and 3 = water elevation at upper boundary. Each open boundary consists of four elements. The first element stored in the IOBD(n, I) or JOBD(n, I). For example if IENDOB = 2 and JENDOB = 1 then IOBD and JOBD may be represented by the following as typical examples:

IOBD (1) = 0 27 62 100

IOBD (2) = 2 13 36 55

JOBD (1) = 3 102 116 140

The interpretations are for IOBD (1), the open boundary is flow or velocity at the lower boundary at cell 27 on I and starts from cell 62 on J up to 100; for IOBD (2), the boundary is a water elevation at lower boundary at cell 13 on the I row and starts at 36 on the J column and ends at 55 on the J column. The JOBD (1) is a water elevation at upper boundary on cell 102 on the J column and starts at 116 on the I row and ends at 140 on the I row. It must be noted that the reference of lower and upper boundaries does not mean the downstream or upstream of a traditional river reach but the direction a boundary faces. A lower boundary faces the direction of increasing I or J, whilst an upper boundary faces the direction of decreasing I or J. In DIVAST the details of boundary conditions are stored in subroutine BOUND.

TIMESM total time of simulation in hours. For example if 10 tides are to be run at 12.5 hours per tide, then TIMESM = 125hours.

HFDT half time step i.e. $\frac{\Delta t}{2}$

DELX grid cell size in metres Δx

ANGLAT angle of latitude (in degrees) of the centre of the model. It is to be used for Coriolis calculation. In this study there was no Coriolis effect so ANGLAT was set to 0.

RUFFMM bed roughness height in millimetres

VISCMM kinematic viscosity of the fluid in (mm^2s^{-1}). For sea water =1.31mm^2s^{-1}

REMIN minimum value of the Reynolds number (usually for natural flow = 1000)

TCHEZY time in hours at which Chezy values are recalculated.

TEDDY time in hours at which eddy viscosities are updated

TDISP time in hours at which the dispersion-diffusion coefficients are updated

BETA momentum correction factor for non-uniform vertical velocity distribution. Typically the value = 1.016 for seventh power law profile. It is just about unity and has always been assumed as that but in this study has been proven to be sensitive to the overall results.

COED coefficient of eddy viscosity for non-uniform velocity distribution. Typical values are between 0.23 and 1.00. In DIVAST, the depth-integrated eddy viscosity is calculated from:

$\bar{\varepsilon} = C_e \frac{H}{C}\sqrt{g(U^2+V^2)}$, C_e = eddy viscosity coefficient $\approx$ 0.15 in the model, C = Chezy, H = depth, and U, V are the depth averaged velocities in x and y directions respectively and g is gravity.

GAMMA longitudinal dispersion coefficient (assumed to be between 5.93 and 13.0)

DELTA lateral turbulent diffusion coefficient

ADDIS option to include additional dispersion-diffusion term; assumed zero but in areas where dispersion diffusion is likely to be higher then a value can be included.

WINDIS option to include extra dispersion and diffusion if wind is included.

PRESET preset minimum depth for performance calculations

ANGNOR clockwise angle from North to positive x-direction in degrees. Set to zero in this study because of the laboratory situation.

WINSPD wind speed in m/s. Again in this study it was assumed zero

WINANG	surface wind direction in degrees (coming from) clockwise angle from North.
DENAIR	density of air $\approx 1.25 kg/m^3$
DENWAT	density of water $\approx 1000 kg/m^3$ and for sea water $\approx 1026 kg/m^3$
WATEMP	water temperature
NUMOUT	number of outfalls across the domain, currently must be wet.
OUTFALL	three values per line giving the outfall location (in terms of grid cell location) and outfall discharge (m^3/s). If NUMOUT = 0, no outfall data be included.

In DIVAST SG, the domain block cells are represented by 0, 1 and 7 which define dry, wet and groundwater cells respectively. The porosity and the permeability of the groundwater material come at the bottom of the input file after the depth data.

For more details of the other terms, see Falconer et al, (2001) and Sparks (2007)

Typical Input file for DIVAST-SG (in this case for the sand embankment)

```
----------------General Data-------------------------
IMAX     =        61          MAXIMUM NO. OF GRID POINTS IN I (OR X) DIRECTION
JMAX     =        42          MAXIMUM NO. OF GRID POINTS IN J (OR Y) DIRECTION
JSPACE   =         4          INTEGER SPACE BETWEEN PRINTOUT VALUES
NADVIT   =         2          NO. OF ITERATIONS FOR ADVECTIVE ACCELERATIONS
NDFORM   =         0          FORM OF DEPTH DATA: SIDE CENTRES = 0 & CORNERS = 1
NFLRUF   =         0          ROUGH TURBULENT FLOW ASSUMED: NO=0 & YES=1
TECTIM   =        60          interval (secs) to output tecplot data
TECOUT   =         1          Output to tecplot data file? (LARGE FILES!) no=0 & yes=1
NUMPRT   =         4          NUMBER OF PRINTOUT TIMES SPECIFIED AS DATA
NWEPRN   =         1          FLAG FOR WATER ELEVATION PRINTOUT: NO=0 & YES=1
NVEPRN   =         1          FLAG FOR VELOCITY COMPONENT PRINTOUT: NO=0 & YES=1
NDEPRN   =         1          FLAG FOR DEPTHS AT CENTRE PRINTOUT: NO=0 & YES=1
NRFPRN   =         0          FLAG FOR ROUGHNESS NO=0, CHEZY=1, MAN.=2 & DARCY=3
NEDPRN   =         0          FLAG FOR EDDY VISCOSITY PRINTOUT: NO=0 & YES=1
NRNPRN   =         0          FLAG FOR REYNOLDS NUMBER PRINTOUT: NO=0 & YES=1
NDIPRN   =         0          FLAG FOR DISPERSION-DIFF. PRINTOUT: NO=0 & YES=1
NSOPRN   =         1          FLAG FOR SOLUTE LEVEL PRINTOUT: NO=0 & YES=1
NTAPRN   =         0          FLAG FOR BED SHEAR STRESS PRINTOUT: NO=0 & YES=1
NERPRN   =         0          FLAG FOR CALCULATING & PRINTING EROSION: NO=0 & YES=1
NRDPRN   =         0          FLAG FOR RESIDUAL COMPONENTS PRINTOUT: NO=0 & YES=1
NFLWIN   =         0          FLAG FOR INCLUDING A SURFACE WIND STRESS: NO=0 & YES=1
NFLDRY   =         0          FLAG FOR INCLUDING FLOODING & DRYING: NO=0 & YES=1
NFLSOL   =         1          FLAG FOR INCLUDING SOLUTE PREDICTIONS: NO=0 & YES=1
NFLSGI   =         1          FLAG FOR INCLUDING SURFACE-GROUNDWATER INTERACTIONS: NO=0 & YES=1
------------Point Data Collection----------------
NUMPNT   =        33          NUMBER OF POINTS TO RECORD DATA FROM
channel1 =   10   27
hole 1   =   10   21          i-coord, j-coord
hole 2   =   10   15
channel2 =   10   10
channel3 =   15   27
hole 3   =   15   21
hole 4   =   15   15
channel4 =   15   10
channel5 =   20   27
hole 5   =   20   21
hole 6   =   20   15
channel6 =   20   10
channel7 =   25   27
hole 7   =   25   21
hole 8   =   25   15
channel8 =   25   10
weir     =   60   22
channel9 =   35   27          i-coord, j-coord
hole9    =   35   21
hole 10  =   35   15
channel10=   35   10
hole 11  =   38   10
hole 12a =   35   39
hole 13  =   25   29
hole 13a =   25   32
hole 14  =   25   34
hole 14m =   25   37
hole 14a =   25   39
hole 15  =   15   29
hole 15m =   20   29
hole 16  =   15   34
hole 16a =   15   39
hole 16m =   15   37
------------Boundary Conditions------------------
IENDOB   =         1          NO. OF OPEN BOUNDARY REACHES IN I DIRECTION
JENDOB   =         0          NO. OF OPEN BOUNDARY REACHES IN J DIRECTION
IOBD 1   =    3   61    2   41
------------Model Data---------------------------
TIMESM   =      2.00          TIME OF SIMULATION (HOURS)
HFDT     =    0.1250          HALF TIME STEP (S)
DELX     =      0.10          GRID SPACING (M)
ANGLAT   =      0.00          ANGLE OF LATITUDE OF DOMAIN IN DEGREES
RUFFMM   =      1.00          ROUGHNESS LENGTH K (MM)
VISCMM   =      1.31          KINEMATIC VISCOSITY OF FLUID (MM^2/S)
REMIN    =     100.0          MINIMUM REYNOLDS NUMBER
TCHEZY   =      0.01          TIME AT WHICH ROUGHNESS COEFF. IS CHANGED (HRS)
TEDDY    =      0.01          TIME AT WHICH EDDY VISCOSITY IS CHANGED (HRS)
TDISP    =      0.01          TIME AT WHICH DISPERSION COEFF. IS CHANGED (HRS)
ALPHA    =    0.7143          SLIP BOUND COEFF NO =-1.0 FREE =1.0 PARTIAL =0.7143
BETA     =     1.016          MOMENTUM CORRECTION FACTOR
COED     =      0.15          EDDY VISCOSITY COEFFICIENT
GAMMA    =     0.000          LONGITUDINAL DISPERSION COEFFICIENT
DELTA    =     0.000          LATERAL TURBULENT DIFFUSION COEFFICIENT
ADDIS    =     0.000          ADDITIONAL DISPERSION-DIFFUSION (M^2/S)
```

```
WINDIS   =     0.000          WIND INDUCED DISPERSION (M^2/S)
PRESET   =     0.005          MINIMUM DEPTH FOR FLOODING & DRYING (M)
ANGNOR   =      0.00          CLOCKWISE ANGLE FROM NORTH TO X-DIRECTION IN DEG.
WINSPD   =      0.00          WIND SPEED (M/S)
WINANG   =      0.00          WIND ANGLE - CLOCKWISE FROM NORTH IN DEGREES
DENAIR   =      1.25          DENSITY OF AIR (KG/M^3)
DENWAT   =   1000.00          DENSITY OF WATER (KG/M^3)
WATEMP   =     10.00          WATER TEMPERATURE IN DEG. CENTIGRADE
-------------Outfall and Solute Data---------------------
NUMOUT   =         2          NUMBER OF OUTFALLS
OUTFALL1 =    3    7          river flow
OUTFALL2 =   10   19          dye injection point
NUMTME   =         7          NUMBER OF TIME VARIATIONS OF OUTFALL DISCHARGE
OUTFALL DISCHARGES m^3/s (time,discharge for outfall 1, discharge for outfall 2 etc)
0.0000  0.0000  0.000
0.0001  0.0005  0.000
0.0049  0.0005  0.000
1.0500  0.0005  1.11E-6              currently set up as 100ml injected over 2 min
1.0750  0.0005  1.11E-6              concentration is set below in SAL OUTS:
0.0751  0.0005  0.000
10.000  0.0005  0.000
NFLSAL   =         1          FLAG FOR SALINITY INPUT NO=0 & YES=1
NFLTMP   =         0          FLAG FOR TEMPERATURE INPUT NO=0 & YES=1
NFLTCL   =         0          FLAG FOR T. COLI INPUT NO=0 & YES=1
NFLFCL   =         0          FLAG FOR F. COLI INPUT NO=0 & YES=1
NFLBOD   =         0          FLAG FOR B.O.D. INPUT NO=0 & YES=1
NBOD5D   =         0          CONVERT ULTIMATE BOD TO 5-DAY BOD NO=0 & YES=1
NFLORG   =         0          FLAG FOR ORGANIC NIT. NO=0 & YES=1
NFLAMN   =         0          FLAG FOR AMMONIA NIT. NO=0 & YES=1
NFLNTA   =         0          FLAG FOR NITRATE NIT. NO=0 & YES=1
NFLDOX   =         0          FLAG FOR DISSOLVED OXYG. NO=0 & YES=1
NFLALG   =         0          FLAG FOR ALGAL BIOMASS NO=0 & YES=1
NFLPHS   =         0          FLAG FOR PHOSPHORUS NO=0 & YES=1
NFLSED   =         0          FLAG FOR SEDIMENT TRANSPORT NO=0 & YES=1
NSFORM   =         0          SEDIMENT FORMULA TYPE: ENG-HAN = 0 & VAN RIJN = 1
NFLCHS   =         0          FLAG FOR COHESIVE SEDIMENT TRANSPORT NO=0 & YES=1
FACWAT   =    1.0E+2          FACTOR FOR SCALING LEVELS PRINTOUT (<0-VARIABLE SCALING)
FACVEL   =    -1.E+0          FACTOR FOR SCALING VELOCITY PRINTOUT
FACDEP   =    1.0E+2          FACTOR FOR SCALING WATER DEPTH PRINTOUT
FACRUF   =    -1.E+0          FACTOR FOR SCALING CHEZY, MANNING OR DARCY PRINTOUT
FACEDD   =    -1.E+0          FACTOR FOR SCALING EDDY VISCOSITY PRINTOUT
FACRNO   =    -1.E+0          FACTOR FOR SCALING REYNOLDS NO. PRINTOUT
FACDIS   =    -1.E+0          FACTOR FOR SCALING DISPERSION PRINTOUT
FACSAL   =    1.0E+1          FACTOR FOR SCALING SALINITY PRINTOUT
FACTEM   =    -1.E+0          FACTOR FOR SCALING TEMPERATURE PRINTOUT
FACTCL   =    -1.E+0          FACTOR FOR SCALING TOTAL COLIFORM PRINTOUT
FACFCL   =    -1.E+0          FACTOR FOR SCALING FAECAL COLIFORM PRINTOUT
FACBOD   =    -1.E+0          FACTOR FOR SCALING BIOCHEM OXYG DEM PRINTOUT
FACORG   =    -1.E+0          FACTOR FOR SCALING ORGANIC NITROGEN PRINTOUT
FACAMN   =    -1.E+0          FACTOR FOR SCALING AMMONIA NITROGEN PRINTOUT
FACNTA   =    -1.E+0          FACTOR FOR SCALING NITRATE NITROGEN PRINTOUT
FACDOX   =    -1.E+0          FACTOR FOR SCALING DISSOLVED OXYGEN PRINTOUT
FACALG   =    -1.E+0          FACTOR FOR SCALING ALGAL BIOMASS PRINTOUT
FACPHS   =    -1.E+0          FACTOR FOR SCALING PHOSPHORUS PRINTOUT
FACSED   =    -1.E+0          FACTOR FOR SCALING NON-COHESIVE SEDIMENT PRINTOUT
FACCHS   =    -1.E+0          FACTOR FOR SCALING SUSP. COHESIVE SEDIMENT PRINTOUT
FACCHB   =    -1.E+0          FACTOR FOR SCALING DEPO. COHESIVE SEDIMENT PRINTOUT
FACNSD   =    -1.E+0          FACTOR FOR SCALING NET SEDIMENT FLUX PRINTOUT
FACSTR   =    -1.E+0          FACTOR FOR SCALING BED SHEAR STRESS PRINTOUT
FACRVL   =    -1.E+0          FACTOR FOR SCALING RESIDUAL VELOCITY PRINTOUT
FACRST   =    -1.E+0          FACTOR FOR SCALING RESIDUAL BED SHEAR PRINTOUT
FACRER   =    -1.E+0          FACTOR FOR SCALING RESIDUAL EROSION PRINTOUT
SALINT   =      0.00          INITIAL SALINITY LEVELS ACROSS DOMAIN (PPT)
SAL OUTS:-      0.00     1.00   OUTFALL SALINITY LEVELS (PPT)
TMPINT   =      0.00          INITIAL TEMPERATURE LEVELS ACROSS DOMAIN (DEG C)
TMP OUTS:-      0.00          OUTFALL TEMPERATURE LEVELS (DEG C)
TCLINT   =      0.00          INITIAL TOTAL COL. LEVELS ACROSS DOMAIN (CTS/100ML)
TCL OUTS:-      0.00          OUTFALL TOTAL COLIFORM LEVELS (CTS/100ML)
FCLINT   =      0.00          INITIAL FAECAL COL LEVELS ACROSS DOMAIN (CTS/100ML)
FCL OUTS:-      0.00          OUTFALL FAECAL COLIFORM LEVELS (CTS/100ML)
BODINT   =      0.00          INITIAL BOD LEVELS ACROSS DOMAIN (MG/L)
BOD OUTS:-      0.00          OUTFALL BOD LEVELS (MG/L)
ORGINT   =      0.00          INITIAL ORGANIC NIT. LEVELS ACROSS DOMAIN (MG/L)
ORG OUTS:-      0.00          OUTFALL ORGANIC NITROGEN LEVELS (MG/L)
AMNINT   =      0.00          INITIAL AMMONIA NIT. LEVELS ACROSS DOMAIN (MG/L)
AMN OUTS:-      0.00          OUTFALL AMMONIA NITROGEN LEVELS (MG/L)
TRAINT   =      0.00          INITIAL NITRATE NIT. LEVELS ACROSS DOMAIN (MG/L)
TRA OUTS:-      0.00          OUTFALL NITRATE NITROGEN LEVELS (MG/L)
SALFDO   =      0.00          SALINITY LEVEL FOR SATURATION DO CALCULATION (PPT)
DOX OUTS:-      0.00          OUTFALL DISSOLVED OXYGEN LEVELS (MG/L)
ALGINT   =      0.00          INITIAL ALGAL BIOMASS LEVELS ACROSS DOMAIN (MG/L)
ALG OUTS:-      0.00          OUTFALL ALGAL BIOMASS LEVELS (MG/L)
PS1INT   =      0.00          INITIAL ORGANIC PHOS. LEVELS ACROSS DOMAIN (MG/L)
PS1 OUTS:-      0.00          OUTFALL ORGANIC PHOSPHORUS LEVELS (MG/L)
PS2INT   =      0.00          INITIAL DISSOLVED PHOS. LEVELS ACROSS DOMAIN (MG/L)
PS2 OUTS:-      0.00          OUTFALL DISSOLVED PHOSPHORUS LEVELS (MG/L)
```

```
SEDINT   =      0.00          INITIAL SUSPENDED SED. LEVELS ACROSS DOMAIN (MG/L)
GAMSUS   =      5.00          GAMMA FOR SUSPENDED SEDIMENTS
SPGRAV   =      2.65          SPECIFIC GRAVITY OF SUSPENDED SEDIMENTS
D16MMS   =      0.00          SEDIMENT DIAMETER WITH 16% FINER (MM)
D50MMS   =      0.00          SEDIMENT DIAMETER WITH 50% FINER (MM)
D84MMS   =      0.00          SEDIMENT DIAMETER WITH 84% FINER (MM)
D90MMS   =      0.00          SEDIMENT DIAMETER WITH 90% FINER (MM)
CHSINT   =      0.00          INITIAL COHESIVE SUSP. SED. CONCENTRATION (KG/M^3)
CSGRAV   =      2.65          SPECIFIC GRAVITY OF SUSPENDED COHESIVE SEDIMENTS
C50MMS   =     0.063          AVERAGE SIZE OF COHESIVE FLOCS (MM)
COFERO   =    0.0015          EMPIRICAL EROSION COEFFICIENT (KG/N/S)
CRTDEP   =     0.100          CRITICAL STRESS FOR DEPOSITION (N/M^2)
CRTERO   =     0.300          CRITICAL STRESS FOR RE-SUSPENSION (N/M^2)
WSFIDX   =       4.0          EXPONENT INDEX FOR HINDERED SETTLING VELOCITY
WSFGAM   =       1.0          COEFFICIENT FOR HINDERED SETTLING VELOCITY
CHS OUTS:-     100.1          OUTFALL COHESIVE SEDIMEBNT CONCENTRATIONS
SPHTEC   =     0.000          SURFACE HEAT EXCHANGE COEFFICIENT (WATTS/M^2/DEG C)
SPTMCF   =     4.200          SPECIFIC THERMAL CAP. OF FLUID (JOULES/M^3/DEG C)
TCLK5D   =     2.400          DECAY RATE FOR T. COLI (1/DAY)
TH5TCL   =     1.047          TEMPERATURE CORRECTION FOR T. COLI
FCLK5D   =     2.400          DECAY RATE FOR F. COLI (1/DAY)
TH5FCL   =     1.047          TEMPERATURE CORRECTION FOR F. COLI
BODK1D   =     5.000          DECAY RATE FOR BOD VIA DEOXYGENATION (1/DAY)
TH1BOD   =     1.000          TEMPERATURE CORRECTION FOR BOD VIA DEOXYGENATION
BODK3D   =     0.000          DECAY RATE FOR BOD VIA SETTLING LOSS (1/DAY)
TH3BOD   =     1.000          TEMPERATURE CORRECTION FOR BOD VIA SETTLING LOSS
ORGB3D   =     0.400          DECAY RATE FOR ORG NIT TO CONVERT TO NH3 (1/DAY)
TH3ORG   =     1.047          TEMPERATURE CORRECTION FOR ORG NIT VIA CONVERSION
ORGS4D   =     0.100          DECAY RATE FOR ORG NIT VIA SETTLING (1/DAY)
TH4ORG   =     1.024          TEMPERATURE CORRECTION FOR ORG. NIT. VIA SETTLING
AMNB1D   =     1.000          DECAY RATE FOR BIOL. OXIDATION OF NH3 (1/DAY)
TH1AMN   =     1.083          TEMPERATURE CORRECTION FOR BIOL. OXIDATION OF NH3
TH2DOX   =     1.024          TEMPERATURE CORRECTION FOR REAERATION RATE
DOXK4D   =     5.000          SEDIMENT OXYGEN DEMAND RATE (MG/M^2 PER DAY)
TH4DOX   =     1.060          TEMPERATURE CORRECTION FOR SEDIMENT OXYGEN DEMAND
DOXA5C   =     3.500          RATE OF OXYGEN UPTAKE PER UNIT OF AMMONIA NITROGEN
DOFMMH   =     5.000          DO EXCHANGE COEFF. FOR STAGNANT WATER (MM/HOUR)
DOLMT2   =     2.000          HALF-SATURATION DO LIMITING CONSTANT (MG/L)
DOXA3C   =     0.133          DO PRODUCTION / UNIT OF CHLOROPHYLL (MG-DO/MG-CHLA)
DOXA4C   =     0.100          DO UPTAKE / UNIT OF CHLOROPHYLL (MG-DO/MG-CHLA)
ALGMAX   =     2.000          MAX. ALGAE GROWTH RATE AT REFERENCE TEMP. (1/DAY)
THMALG   =     1.047          TEMPERATURE CORRECTION FOR MAX. ALGAE GROWTH RATE
ALGRSP   =     0.060          RATE OF RESPIRATION PLUS EXCRETION (1/DAY)
THARSP   =     1.047          TEMPERATURE CORRECTION FOR RESPIRATION & EXCRETION
VELALG   =     0.050          ALGAE (CHLOROPHYLL) SETTLING VELOCITY (M/DAY)
ALGNPM   =     0.010          NON-PREDATORY MORTALITY RATE FOR ALGAE (1/DAY)
ALGLGZ   =     0.020          RATE OF ALGAL LOSSES DUE TO GRAZING (1/DAY)
FPHOTP   =     0.500          PHOTOPERIOD (EXPRESSED AS FRACTION OF THE DAY)
EXTLT0   =     0.090          LIGHT EXT COEF FOR ALL ABSORPT COMPS BUT PHYT (1/M)
EXTLT1   =    0.0088          LIGHT EXT COEF FOR PHYTOPLANKTON (1/M)
EXTLT2   =     0.054          LIGHT EXT COEF FOR PHYTOPLANKTON (1/M)
EXTLT3   =     0.667          LIGHT EXT COEF FOR PHYTOPLANKTON (1/M)
SURFLT   =     250.1          LIGHT INTENSITY AT WATER SURFACE
HFSATL   =       6.0          LIGHT LEVEL AT WHICH GROWTH IS HALF OF  MAX. RATE
HFSATN   =     0.060          HALF-SATURATION CONSTANT FOR NITROGEN (MG/L)
HFSATP   =     0.010          HALF-SATURATION CONSTANT FOR PHOSPHORUS (MG/L)
ALGA1C   =     7.000          NIT. FRACTION OF ALGAL CHLOROPHYLL (MG-N/MG-CHLA)
FRCORG   =     0.100          FRACTION OF DEAD & RESPIRED PHYTOPLANKTON RECYCLED
FRCPHS   =     0.100          FRACTION OF DEAD & RESPIRED PHYTOPLANKTON RECYCLED
PHSA2C   =     1.000          PHOS FRACTION OF ALGAL CHLOROPHYLL (MG-P/MG-CHLA)
PHSB4D   =     0.085          HYDROLYSIS RATE FOR ORG. PH TO INORG. PH (1/DAY)
THPSB4   =     1.047          TEMPERATURE CORRECTION FOR ORG. P TO INORG. P
PHSS5D   =     0.010          SETTLING RATE CONST OF ORGANIC PHOSPHORUS (1/DAY)
THPSS5   =     1.047          TEMPERATURE CORRECTION FOR ORG. P SETTLING RATE
PHSF2D   =     0.010          SETTLING RATE CONST OF INORG. PHOSPHORUS (1/DAY)
THPSF2   =     1.047          TEMPERATURE CORRECTION FOR INORG. P SETTLING RATE
NFLDOF   =         1          0 (FT UNIT); 1 (OWENS RELATION); 2 (BANKS FOR LAKE)
   0.00000   0.00100   0.25000   0.50000        (PRINTOUT TIMES)
----------Tidal boundary (water elevation) Data--------------
SINTIDE  =      1        I6      Sinusoidal tide, 1= yes, 0= no
TIDEAMP  =    0.0325     F10.4   Tidal Amplitude (only used if SINTIDE=1)
TIDEMWL  =    0.1425     F10.4   Tidal Mean Water Level (only used if SINTIDE=1)
TIDEHR   =   10.0000     F10.4   Tidal period (wavelength for sinusoidal tide, length of cycle to
repeat for non-sinusoidal tide) (hours)
TIDESTART=MWL+           A4      Start sinusoidal tidal cycle at: high tide (HIGH), Rising Mean Water
Level (MWL+), Falling Mean Water Level (MWL-) or low tide (LOW )
PRETIDE  =    1.0000     F10.4   Time before tidal boundary cycle is started. (hours)
NOPTS    =      2        I6      Number of points specified for non-sinusoidal tide
NUMTDS   =   10.0000     F10.4   Number of tidal cycles
  time  elevation (non-sinusoidal tide points on NOPTS lines below here F6.3 F8.3)
 0.000  +0.100
10.000  +0.100
----------Flow or velocity boundary data:--------------------
FLOWTYPE =      0        I6      Type of Boundaries (0=Flow 1=Velocity )
FPHASE   =    0.0500     F10.4   Time over which flow at boundary is introduced
CDWEIR   =    0.6100     F10.4   Weir coefficient-----First flow Boundary------IBNDPTS 1=    2
```

```
I4      Number of flow changes for flow boundary 1 - (minimum 2)   time(F10.4)  flow/velocity(F10.4)
(flow change points on NOFPTS lines below here)     0.000    0.0300     3.000    0.0300
---------------Layer Domain Specification--------------
Layer1
00000000000000000000000000000000000000000000000 1
01111111111111111111111111111111111111111111110 2
01111111111111111111111111111111111111111111110 3
01111111111111111111111111111111111111111111110 4
00000000000000000000000000000000000001111111110 5
01111111111117777777711111111111111111111111110 6
01111111111117777777711111111111111111111111110 7
01111111111117777777711111111111111111111111110 8
01111111111117777777711111111111111111111111110 9
01111111111117777777711111111111111111111111110 10
01111111111117777777711111111111111111111111110 11
01111111111117777777711111111111111111111111110 12
01111111111117777777711111111111111111111111110 13
01111111111117777777711111111111111111111111110 14
01111111111117777777711111111111111111111111110 15
01111111111117777777711111111111111111111111110 16
01111111111117777777711111111111111111111111110 17
01111111111117777777711111111111111111111111110 18
01111111111117777777711111111111111111111111110 19
01111111111117777777711111111111111111111111110 20
01111111111117777777711111111111111111111111110 21
01111111111117777777711111111111111111111111110 22
01111111111117777777711111111111111111111111110 23
01111111111117777777711111111111111111111111110 24
01111111111117777777711111111111111111111111110 25
01111111111117777777711111111111111111111111110 26
01111111111117777777711111111111111111111111110 27
01111111111117777777711111111111111111111111110 28
01111111111117777777711111111111111111111111110 29
01111111111117777777711111111111111111111111110 30
01111111111117777777711111111111111111111111110 31
01111111111117777777711111111111111111111111110 32
01111111111117777777711111111111111111111111110 33
01111111111117777777711111111111111111111111110 34
01111111111117777777711111111111111111111111110 35
01111111111117777777711111111111111111111111110 36
01111111111117777777711111111111111111111111110 37
01111111111117777777777777777777777777777777038
01111111111117777777777777777777777777777777039
01111111111117777777777777777777777777777777040
01111111111117777777777777777777777777777777041
01111111111100000000000000000000000000000000042
01111111111117777777777777777777777777777777043
01111111111117777777777777777777777777777777044
01111111111117777777777777777777777777777777045
01111111111111111111111111111111111111111111046
01111111111111111111111111111111111111111111047
01111111111111111111111111111111111111111111048
01111111111111111111111111111111111111111111049
01111111111111111111111111111111111111111111050
01111111111111111111111111111111111111111111051
01111111111111111111111111111111111111111111052
01111111111111111111111111111111111111111111053
01111111111111111111111111111111111111111111054
01111111111111111111111111111111111111111111055
01111111111111111111111111111111111111111111056
01111111111111111111111111111111111111111111057
01111111111111111111111111111111111111111111058
01111111111111111111111111111111111111111111059
01111111111111111111111111111111111111111111060
00000000000000000000000000000000000000000000061
---------------Elevation Data for surface and Groundwater Layers-------------------
22      JNUM number of columns of depth data in each block
X-direction Surface Elevations BELOW Datum
     1     2     3     4     5     6     7     8     9    10    11    12    13    14    15    16
17    18    19    20    21
  0.00  0.00  0.00  0.00  0.00  0.00  0.00  0.00  0.00  0.00  0.00  0.00  0.00  0.00  0.00  0.00
0.00  0.00  0.00  0.00  0.00     1
  0.00  0.00  0.00  0.00  0.00  0.00  0.00  0.00  0.00  0.00  0.00  0.00  0.00  0.00  0.00  0.00
0.00  0.00  0.00  0.00  0.00     2
  0.00  0.00  0.00  0.00  0.00  0.00  0.00  0.00  0.00  0.00  0.00  0.00  0.00  0.00  0.00  0.00
0.00  0.00  0.00  0.00  0.00     3
  0.00  0.00  0.00  0.00  0.00  0.00  0.00  0.00  0.00  0.00  0.00  0.00  0.00  0.00  0.00  0.00
0.00  0.00  0.00  0.00  0.00     4
  0.00  0.00  0.00  0.00  0.00  0.00  0.00  0.00  0.00  0.00  0.00  0.00  0.00  0.00  0.00  0.00
0.00  0.00  0.00  0.00  0.00     5
  0.00  0.00  0.00  0.00  0.00  0.00  0.00  0.00  0.00  0.00  0.00  0.00  0.00  0.00  0.00  0.00
0.00  0.00  0.00  0.00  0.00     6
  0.00  0.00  0.00  0.00  0.00  0.00  0.00  0.00  0.00  0.00  0.00  0.00  0.00  0.00  0.00  0.00
0.00  0.00  0.00  0.00  0.00     7
  0.00  0.00  0.00  0.00  0.00  0.00  0.00  0.00  0.00  0.00  0.00  0.00  0.00  0.00  0.00  0.00
0.00  0.00  0.00  0.00  0.00     8
```

0.00	0.00	0.00	0.00	0.00	0.00	0.00	0.00	0.00	0.00	0.00	0.00	0.00	0.00	0.00	0.00	9
0.00	0.00	0.00	0.00	0.00	0.00	0.00	0.00	0.00	0.00	0.00	0.00	0.00	0.00	0.00	0.00	10
0.00	0.00	0.00	0.00	0.00	0.00	0.00	0.00	0.00	0.00	0.00	0.00	0.00	0.00	0.00	0.00	11
0.00	0.00	0.00	0.00	0.00	0.00	0.00	0.00	0.00	0.00	0.00	0.00	0.00	0.00	0.00	0.00	12
0.00	0.00	0.00	0.00	0.00	0.00	0.00	0.00	0.00	0.00	0.00	0.00	0.00	0.00	0.00	0.00	13
0.00	0.00	0.00	0.00	0.00	0.00	0.00	0.00	0.00	0.00	0.00	0.00	0.00	0.00	0.00	0.00	14
0.00	0.00	0.00	0.00	0.00	0.00	0.00	0.00	0.00	0.00	0.00	0.00	0.00	0.00	0.00	0.00	15
0.00	0.00	0.00	0.00	0.00	0.00	0.00	0.00	0.00	0.00	0.00	0.00	0.00	0.00	0.00	0.00	16
0.00	0.00	0.00	0.00	0.00	0.00	0.00	0.00	0.00	0.00	0.00	0.00	0.00	0.00	0.00	0.00	17
0.00	0.00	0.00	0.00	0.00	0.00	0.00	0.00	0.00	0.00	0.00	0.00	0.00	0.00	0.00	0.00	18
0.00	0.00	0.00	0.00	0.00	0.00	0.00	0.00	0.00	0.00	0.00	0.00	0.00	0.00	0.00	0.00	19
0.00	0.00	0.00	0.00	0.00	0.00	0.00	0.00	0.00	0.00	0.00	0.00	0.00	0.00	0.00	0.00	20
0.00	0.00	0.00	0.00	0.00	0.00	0.00	0.00	0.00	0.00	0.00	0.00	0.00	0.00	0.00	0.00	21
0.00	0.00	0.00	0.00	0.00	0.00	0.00	0.00	0.00	0.00	0.00	0.00	0.00	0.00	0.00	0.00	22
0.00	0.00	0.00	0.00	0.00	0.00	0.00	0.00	0.00	0.00	0.00	0.00	0.00	0.00	0.00	0.00	23
0.00	0.00	0.00	0.00	0.00	0.00	0.00	0.00	0.00	0.00	0.00	0.00	0.00	0.00	0.00	0.00	24
0.00	0.00	0.00	0.00	0.00	0.00	0.00	0.00	0.00	0.00	0.00	0.00	0.00	0.00	0.00	0.00	25
0.00	0.00	0.00	0.00	0.00	0.00	0.00	0.00	0.00	0.00	0.00	0.00	0.00	0.00	0.00	0.00	26
0.00	0.00	0.00	0.00	0.00	0.00	0.00	0.00	0.00	0.00	0.00	0.00	0.00	0.00	0.00	0.00	27
0.00	0.00	0.00	0.00	0.00	0.00	0.00	0.00	0.00	0.00	0.00	0.00	0.00	0.00	0.00	0.00	28
0.00	0.00	0.00	0.00	0.00	0.00	0.00	0.00	0.00	0.00	0.00	0.00	0.00	0.00	0.00	0.00	29
0.00	0.00	0.00	0.00	0.00	0.00	0.00	0.00	0.00	0.00	0.00	0.00	0.00	0.00	0.00	0.00	30
0.00	0.00	0.00	0.00	0.00	0.00	0.00	0.00	0.00	0.00	0.00	0.00	0.00	0.00	0.00	0.00	31
0.00	0.00	0.00	0.00	0.00	0.00	0.00	0.00	0.00	0.00	0.00	0.00	0.00	0.00	0.00	0.00	32
0.00	0.00	0.00	0.00	0.00	0.00	0.00	0.00	0.00	0.00	0.00	0.00	0.00	0.00	0.00	0.00	33
0.00	0.00	0.00	0.00	0.00	0.00	0.00	0.00	0.00	0.00	0.00	0.00	0.00	0.00	0.00	0.00	34
0.00	0.00	0.00	0.00	0.00	0.00	0.00	0.00	0.00	0.00	0.00	0.00	0.00	0.00	0.00	0.00	35
0.00	0.00	0.00	0.00	0.00	0.00	0.00	0.00	0.00	0.00	0.00	0.00	0.00	0.00	0.00	0.00	36
0.00	0.00	0.00	0.00	0.00	0.00	0.00	0.00	0.00	0.00	0.00	0.00	0.00	0.00	0.00	0.00	37
0.00	0.00	0.00	0.00	0.00	0.00	0.00	0.00	0.00	0.00	0.00	0.00	0.00	0.00	0.00	0.00	38
0.00	0.00	0.00	0.00	0.00	0.00	0.00	0.00	0.00	0.00	0.00	0.00	0.00	0.00	0.00	0.00	39
0.00	0.00	0.00	0.00	0.00	0.00	0.00	0.00	0.00	0.00	0.00	0.00	0.00	0.00	0.00	0.00	40
0.00	0.00	0.00	0.00	0.00	0.00	0.00	0.00	0.00	0.00	0.00	0.00	0.00	0.00	0.00	0.00	41
0.00	0.00	0.00	0.00	0.00	0.00	0.00	0.00	0.00	0.00	0.00	0.00	0.00	0.00	0.00	0.00	42
0.00	0.00	0.00	0.00	0.00	0.00	0.00	0.00	0.00	0.00	0.00	0.00	0.00	0.00	0.00	0.00	43
0.00	0.00	0.00	0.00	0.00	0.00	0.00	0.00	0.00	0.00	0.00	0.00	0.00	0.00	0.00	0.00	44
0.00	0.00	0.00	0.00	0.00	0.00	0.00	0.00	0.00	0.00	0.00	0.00	0.00	0.00	0.00	0.00	45
0.00	0.00	0.00	0.00	0.00	0.00	0.00	0.00	0.00	0.00	0.00	0.00	0.00	0.00	0.00	0.00	46
0.00	0.00	0.00	0.00	0.00	0.00	0.00	0.00	0.00	0.00	0.00	0.00	0.00	0.00	0.00	0.00	47
0.00	0.00	0.00	0.00	0.00	0.00	0.00	0.00	0.00	0.00	0.00	0.00	0.00	0.00	0.00	0.00	48
0.00	0.00	0.00	0.00	0.00	0.00	0.00	0.00	0.00	0.00	0.00	0.00	0.00	0.00	0.00	0.00	49
0.00	0.00	0.00	0.00	0.00	0.00	0.00	0.00	0.00	0.00	0.00	0.00	0.00	0.00	0.00	0.00	50
0.00	0.00	0.00	0.00	0.00	0.00	0.00	0.00	0.00	0.00	0.00	0.00	0.00	0.00	0.00	0.00	51

```
0.00  0.00  0.00  0.00  0.00    46
  0.00  0.00  0.00  0.00  0.00  0.00  0.00  0.00  0.00  0.00  0.00  0.00  0.00  0.00  0.00  0.00
0.00  0.00  0.00  0.00  0.00    47
  0.00  0.00  0.00  0.00  0.00  0.00  0.00  0.00  0.00  0.00  0.00  0.00  0.00  0.00  0.00  0.00
0.00  0.00  0.00  0.00  0.00    48
  0.00  0.00  0.00  0.00  0.00  0.00  0.00  0.00  0.00  0.00  0.00  0.00  0.00  0.00  0.00  0.00
0.00  0.00  0.00  0.00  0.00    49
  0.00  0.00  0.00  0.00  0.00  0.00  0.00  0.00  0.00  0.00  0.00  0.00  0.00  0.00  0.00  0.00
0.00  0.00  0.00  0.00  0.00    50
  0.00  0.00  0.00  0.00  0.00  0.00  0.00  0.00  0.00  0.00  0.00  0.00  0.00  0.00  0.00  0.00
0.00  0.00  0.00  0.00  0.00    51
  0.00  0.00  0.00  0.00  0.00  0.00  0.00  0.00  0.00  0.00  0.00  0.00  0.00  0.00  0.00  0.00
0.00  0.00  0.00  0.00  0.00    52
  0.00  0.00  0.00  0.00  0.00  0.00  0.00  0.00  0.00  0.00  0.00  0.00  0.00  0.00  0.00  0.00
0.00  0.00  0.00  0.00  0.00    53
  0.00  0.00  0.00  0.00  0.00  0.00  0.00  0.00  0.00  0.00  0.00  0.00  0.00  0.00  0.00  0.00
0.00  0.00  0.00  0.00  0.00    54
  0.00  0.00  0.00  0.00  0.00  0.00  0.00  0.00  0.00  0.00  0.00  0.00  0.00  0.00  0.00  0.00
0.00  0.00  0.00  0.00  0.00    55
  0.00  0.00  0.00  0.00  0.00  0.00  0.00  0.00  0.00  0.00  0.00  0.00  0.00  0.00  0.00  0.00
0.00  0.00  0.00  0.00  0.00    56
  0.00  0.00  0.00  0.00  0.00  0.00  0.00  0.00  0.00  0.00  0.00  0.00  0.00  0.00  0.00  0.00
0.00  0.00  0.00  0.00  0.00    57
  0.00  0.00  0.00  0.00  0.00  0.00  0.00  0.00  0.00  0.00  0.00  0.00  0.00  0.00  0.00  0.00
0.00  0.00  0.00  0.00  0.00    58
  0.00  0.00  0.00  0.00  0.00  0.00  0.00  0.00  0.00  0.00  0.00  0.00  0.00  0.00  0.00  0.00
0.00  0.00  0.00  0.00  0.00    59
  0.00  0.00  0.00  0.00  0.00  0.00  0.00  0.00  0.00  0.00  0.00  0.00  0.00  0.00  0.00  0.00
0.00  0.00  0.00  0.00  0.00    60
  0.00  0.00  0.00  0.00  0.00  0.00  0.00  0.00  0.00  0.00  0.00  0.00  0.00  0.00  0.00  0.00
0.00  0.00  0.00  0.00  0.00    61
----------------Porosity data:------------------------------
number of variations in x and y directions respectively (ni, nj - 1 line)
j column nos. where those variations occur (jcont(j),...jcont(nj) - 1 line)
i row nos. where variations occur, and value of porosity at each point
(icont(i),porosity(j),porosity(nj) - ni lines)
2, 2
1,42
1,0.41,0.41
61,0.41,0.41
----------------Permeability data:--------------------------
number of variations in x and y directions respectively (ni, nj - 1 line)
j column nos. where those variations occur (jcont(j),...jcont(nj) - 1 line)
i row nos. where variations occur, and value of permeability at each point
(icont(i),porosity(j),porosity(nj) - ni lines)
2,2
1,42
1,0.01,0.01
61,0.01,0.01
```